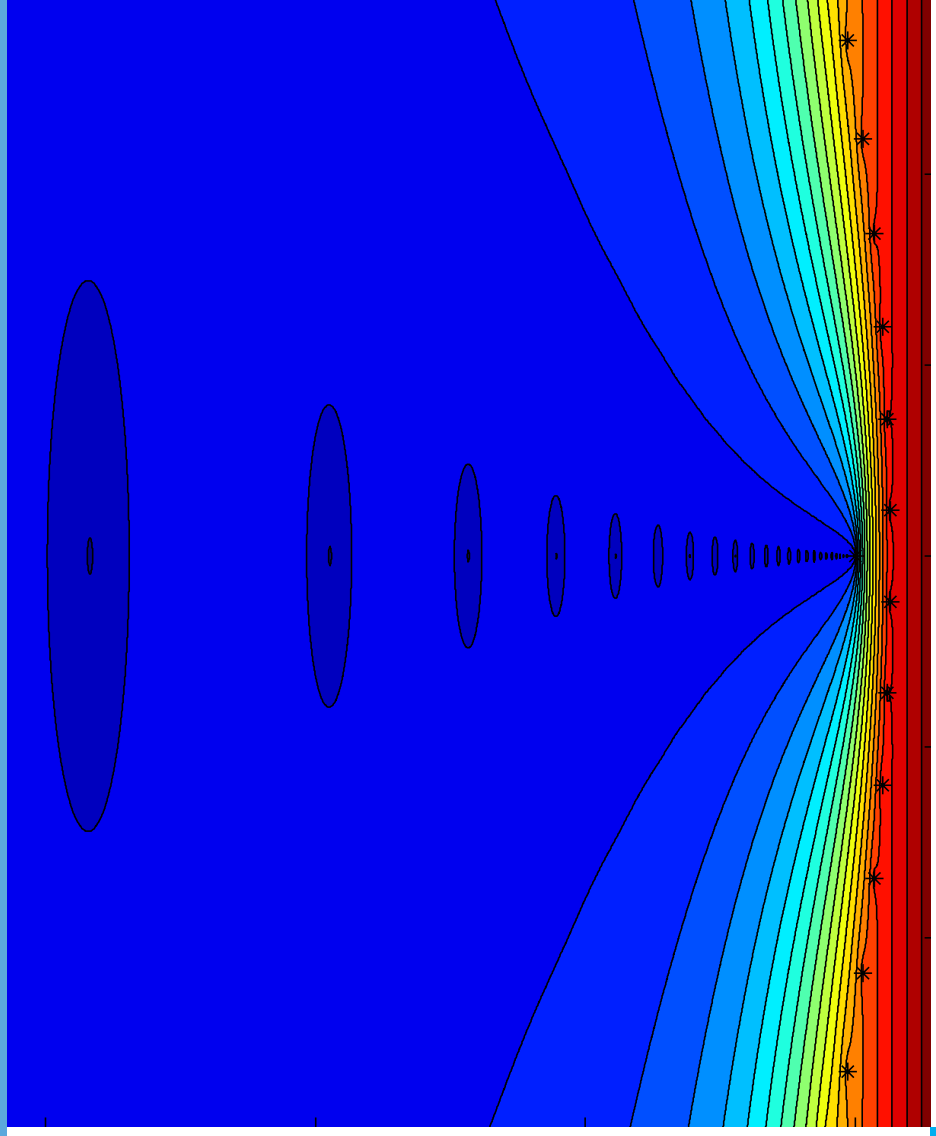

SCIENCE • TECHNOLOGY • RESEARCH HIGHLIGHTS • VISIONS

Dissertation
32

Numerical methods for nuclear fuel burnup calculations

Maria Pusa

VTT

VTT SCIENCE 32

Numerical methods for nuclear fuel burnup calculations

Maria Pusa

Thesis for the degree of Doctor of Science in Technology to be presented with due permission for public examination and criticism in Auditorium N at Aalto University (Otakaari 1 M, Espoo, Finland), on the 24th of May, 2013, at 12 noon.

ISBN 978-951-38-7999-0 (Soft back ed.)
ISBN 978-951-38-8000-2 (URL: http://www.vtt.fi/publications/index.jsp)

VTT Science 32

ISSN-L 2242-119X
ISSN 2242-119X (Print)
ISSN 2242-1203 (Online)

JULKAISIJA – UTGIVARE – PUBLISHER

VTT
PL 1000 (Tekniikantie 4 A, Espoo)
02044 VTT
Puh. 020 722 111, faksi 020 722 7001

VTT
PB 1000 (Teknikvägen 4 A, Esbo)
FI-02044 VTT
Tfn. +358 20 722 111, telefax +358 20 722 7001

VTT Technical Research Centre of Finland
P.O. Box 1000 (Tekniikantie 4 A, Espoo)
FI-02044 VTT, Finland
Tel. +358 20 722 111, fax +358 20 722 7001

Kopijyvä Oy, Kuopio 2013

Numerical methods for nuclear fuel burnup calculations

Maria Pusa. Espoo 2013. VTT Science 32. 86 p. + app. 78 p.

Abstract

The material composition of nuclear fuel changes constantly due to nuclides transforming to other nuclides via neutron-induced transmutation reactions and spontaneous radioactive decay. The objective of burnup calculations is to simulate these changes over time. This thesis considers two essential topics of burnup calculations: the numerical solution of burnup equations based on computing the burnup matrix exponential, and the uncertainty analysis of neutron transport criticality equation based on perturbation theory.

The burnup equations govern the changes in nuclide concentrations over time. They form a system of first order differential equations that can be formally solved by computing the matrix exponential of the burnup matrix. Due to the dramatic variation in the half-lives of different nuclides, the system is extremely stiff and the problem is complicated by vast variations in the time steps used in burnup calculations. In this thesis, the mathematical properties of burnup matrices are studied. It is deduced that their eigenvalues are generally confined to a region near the negative real axis. Rational approximations that are accurate near the negative real axis, and the Chebyshev rational approximation method (CRAM) in particular, are proposed as a novel method for solving the burnup equations. The results suggest that the proposed approach is capable of providing a robust and accurate solution to the burnup equations with a very short computation time.

When a mathematical model contains uncertain parameters, this uncertainty is propagated to responses dependent on the model. This thesis studies the propagation of neutron interaction data uncertainty through the criticality equation on a fuel assembly level. The considered approach is based on perturbation theory, which allows computing the sensitivity profiles of a response with respect to any number of parameters in an efficient manner by solving an adjoint system in addition to the original forward problem. The uncertainty related to these parameters can then be propagated deterministically to the response by linearizing the response.

Keywords burnup equations, Chebyshev rational approximation, CRAM, matrix exponential, sensitivity analysis, uncertainty analysis

Academic dissertation

Supervisor	Prof. Olavi Nevanlinna Department of Mathematics and Systems Analysis Aalto University, Finland
Instructor	Dr. Jaakko Leppänen Nuclear Energy VTT Technical Research Centre of Finland
Preliminary examiners	Dr. Ivan Kodeli Jožef Stefan Institute, Slovenia
	Prof. Jukka Tuomela Department of Mathematics University of Eastern Finland
Opponent	Prof. Antonella Zanna Munthe-Kaas Department of Mathematics University of Bergen, Norway

Contents

Acknowledgments

I wish to express my sincere gratitude to my instructor at VTT, Dr. Jaakko Leppänen, for his support and insight during this entire process and especially for the unique opportunity to be a part of developing Serpent. Working together has been a lot of fun during these years.

I am obliged to our Group Manager, Dr. Petri Kotiluoto, and our Technology Manager, Dr. Timo Vanttola, for their support and for giving me the freedom in my research work. I'd also like to thank my colleagues at VTT, especially my team members and everyone in our office.

I'm grateful to Prof. Olavi Nevanlinna of the Department of Mathematics and Systems Analysis, Aalto University, for acting as my supervisor and for his mathematical insight and ideas that helped me to improve this dissertation, and to Prof. Antonella Zanna Munthe-Kaas of the Department of Mathematics, University of Bergen, Norway, for acting as my opponent in the defense of this thesis. I wish to thank the preliminary examiners of my dissertation, Dr. Ivan Kodeli of Jožef Stefan Institute, Slovenia and Prof. Jukka Tuomela of University of Eastern Finland, for their careful work. In addition, I'm grateful to Dr. Kodeli for his kind help over the years related to the UAM benchmark.

Above all, I want to thank my dear husband Mikko, not only for his constant love and support, but also for his practical help in every aspect of the process.

This work has been funded through the Finnish Research Programme on Nuclear Power Plant Safety SAFIR and the Academy of Finland research programmes NETNUC and NUMPS.

List of publications

This thesis consists of the present article and the following six publications.

I M. Pusa and J. Leppänen, "Computing the matrix exponential in burnup calculations", *Nucl. Sci. Eng.*, **164**, 2, 140–150 (2010).

II M. Pusa, "Rational approximations to the matrix exponential in burnup calculations", *Nucl. Sci. Eng.*, **169**, 2, 155–167 (2011).

III M. Pusa, "Correction to partial fraction decomposition coefficients for Chebyshev rational approximation on the negative real axis", `arXiv:1206.2880v1[math.NA]` (2012).

IV M. Pusa and J. Leppänen, "Solving linear systems with sparse Gaussian elimination in the Chebyshev rational approximation method (CRAM)", accepted for publication in *Nucl. Sci. Eng.* (Nov 2013).

V M. Pusa, "Incorporating sensitivity and uncertainty analysis to a lattice physics code with application to CASMO-4", *Ann. Nucl. Energy*, **40**, 1, 153–162 (2012).

VI M. Pusa, "Perturbation-theory-based sensitivity and uncertainty analysis with CASMO-4", *Sci. Technol. Nucl. Install.*, **2012**, 157029 (2012).

Author's contribution

Publications II, III, V, VI and the present article, which contains also new considerations, were written solely by the author. The author had a major role in Publications I and IV. A detailed description on the author's contribution in these two publications is given below.

Publication I: Computing the matrix exponential in burnup calculations

The author was responsible for the theoretical considerations, selecting the matrix exponential methods to be studied, implementing the Krylov-based matrix exponential method and the Chebyshev rational approximation method, and performing the computations. The article was written by the author, apart from the introduction section, which was written in collaboration by the two authors.

The second author designed the interface for the matrix exponential solver and added the implemented CRAM solution method to the reactor physics code Serpent. The second author also chose the test cases to be studied, calculated the burnup matrices with Serpent, and performed the calculation that compared the efficiency of the matrix exponential solution against the TTA method in a full assembly burnup calculation with Serpent.

Publication IV: Solving linear systems with sparse Gaussian elimination in the Chebyshev rational approximation method (CRAM)

The author was responsible for the theoretical considerations, selecting the solution method and implementing it to the reactor physics code Serpent, performing the computations and writing the article.

The second author selected the test case to be studied and provided the input file for Serpent.

1. Introduction

1.1 Background

In an operating nuclear reactor, the material composition of a nuclear fuel changes constantly. In nuclear fission, the original nucleus splits into lighter nuclides, releasing secondary particles and energy. In addition, nuclides transform to other nuclides through other neutron-induced transmutation reactions and spontaneous radioactive decay. The radioactive decay process continues even when nuclear fuel is removed from the reactor.

In many applications, it is essential to be able to predict the changes in the nuclear fuel composition. For example, the safety and economy of a reactor core loading depend heavily on the changes in nuclide concentrations and how these changes are compensated for. This is relevant when designing new reactor concepts and when optimizing the reactor core loading of existing reactors alike. Also, it is important to assess the material decomposition of spent fuel after removing it from the reactor and at any time afterwards. Final deposition applications necessitate predicting the nuclide concentrations at time steps of the order of thousands of years.

In practice, the changes in nuclear fuel material composition are evaluated by dedicated burnup calculation codes. Unfortunately, it is extremely difficult to simulate the problem in the true time-dependent form, due to the coupling between nuclide concentrations and neutron density distribution—the transmutation rates of neutron-induced reactions depend on the neutron density distribution in the system, and the neutron density distribution, on the other hand, is strongly dependent on the isotopic compositions of the fissile material.

Burnup calculations are based upon the assumption that nuclide concentrations can be assumed constant when solving the neutron density distribution. They are formulated around two central equations in reactor physics, which are the *neutron transport equation* and the *burnup equations*. The neutron transport equation is essentially a balance equation for the neutron density. In burnup calculations, it is modeled as a time-independent eigenvalue problem, called the *criticality equation*, in which case the solution comprises of neutron density distribution and the multiplication factor, which characterizes the time dependence of the system. Based on the neutron density distribution solution, it is possible to compute the rates at which

nuclides transform to other nuclides. These reaction rates can be used to form the burnup equations, which govern the changes in nuclide concentrations over time. Burnup calculations form a cyclic process, where the system is modeled forward in time by solving the criticality equation and the burnup equations in a sequential manner.

1.2 Research objectives

Due to the special demands related to the target of application, it is crucial that the computational methods related to burnup calculations are constantly developed and refined, and that their accuracy and efficiency are improved. In addition, uncertainty analysis methods are needed for evaluating the reliability of the calculation results.

1.2.1 Numerical solution of burnup equations

There are generally various numerical methods for solving the neutron transport equation. However, notably little interest and research effort has been previously shown towards the solution of burnup equations. The burnup equations form a system of first order differential equations, which can be formally solved by computing the matrix exponential of the burnup matrix. Since the half-lives of different nuclides vary dramatically, the system is extremely stiff. It is also difficult that the time steps used in burnup calculations generally vary from less than a day at the beginning of the irradiation cycle to a few hundred days at the end. For these reasons, the computation of the matrix exponential has been previously considered impossible for the full burnup system. Instead, simplified burnup chains have been used, or the most short-lived nuclides have been treated separately when computing a matrix exponential solution.

The focus of this thesis was to examine if it is possible to solve a detailed burnup system containing over a thousand nuclides by a single matrix exponential method. The motivation for this was the development of the burnup calculation routines in the Serpent Monte Carlo reactor physics code developed at VTT. [1]

In this thesis, the mathematical properties of burnup matrices are studied systematically for the first time. It turns out that the eigenvalues of burnup matrices are confined to a region near the negative real axis and that they are connected with the class of M-matrices. These properties can be utilized in solving the burnup equations by employing rational approximations that are accurate near the negative real axis. The Chebyshev rational approximation method (CRAM), defined as the best rational approximation on the negative real axis, is proposed as a novel method for solving the burnup equations. In addition, rational approximation based on quadrature formulas derived from complex contour integrals is proposed. The proposed methods are compared to established numerical methods and highly accurate reference solutions.

[1] A complete and up-to-date description of the Serpent code is found at the project website. (`http://montecarlo.vtt.fi`)

1.2.2 Propagation of uncertainty through criticality equation

In addition to numerical error, the reliability of calculation results is affected by uncertain parameter values utilized in the computations. In particular, reactor physics calculations employ large nuclear data libraries containing the interaction data between neutrons and nuclei. These nuclear data libraries are believed to be one of the most significant sources of uncertainty in all reactor physics calculations, including burnup calculations. In order to evaluate the reliability of the calculation results, this parameter uncertainty needs to be propagated through the calculations. Since the libraries typically contain at least tens of thousands of uncertain parameters, calculation times often inhibit the use of statistical approaches in practical applications.

In this thesis, uncertainty analysis is applied to the criticality equation, which is one of the two equations that are solved sequentially during burnup calculations. The considered uncertainty analysis method is based on perturbation theory, which allows efficiently propagating the uncertainty related to a nuclear data library to the response of interest by solving an adjoint system in addition to the original forward problem. The described work was done in a context other than burnup calculations, but it forms a theoretical background for propagating nuclear data uncertainty through the criticality equation to parameters needed in burnup equations.

2. Burnup calculations

The objective of burnup calculations is to simulate the long-term time behavior of a nuclear reactor. The neutronic properties of nuclear fuel depend strongly on the isotopic composition of the fissile materials. In an operating reactor, these material compositions change constantly due to neutron-induced reactions and spontaneous radioactive decay. The rates of the former reactions depend on the neutron density distribution in the system. Unfortunately, it is not possible to solve the coupled problem for neutron density distribution and nuclide concentrations in a truly time-dependent form, and approximations are required.

Burnup calculations are based on the assumption that the neutron density distribution and the changes in the nuclide concentrations can be solved sequentially in a cyclic manner by alternating the two computation steps, and using results from the previous step. During the first step, the neutron density distribution is computed assuming that the nuclide concentrations are fixed. This requires solving the *neutron transport equation*, which is essentially a balance equation for neutrons. Based on the neutron density distribution, the rates of the neutron-induced reactions can be computed. During the second step, the changes in the nuclide concentrations are solved from the *burnup equations* assuming constant reaction rates. This calculational strategy can be further refined by means of predictor–corrector methods, which aim at predicting the most representative averages for the reaction rates approximated as constants during the solution of burnup equations.[2] The following subsections introduce the two basic equations—the criticality equation and the burnup equations—on which burnup calculations are based.

2.1 Neutron transport and criticality equation

The neutron transport equation is a balance equation for the neutron density distribution $N(\boldsymbol{r}, \boldsymbol{\Omega}, E, t)$, defined in a six-dimensional phase space as the expected number of neutrons in a volume dV about the point $\boldsymbol{r}$, traveling in the cone of directions $d\boldsymbol{\Omega}$ about the direction $\boldsymbol{\Omega}$, with energies in the interval $[E, E + dE]$ at the time instant t. In nuclear reactors, neutron–neutron interactions can be neglected, and the neutron

[2] The use of predictor–corrector methods does not affect the solution of the criticality equation nor the burnup equations.

density distribution depends solely on the interactions between neutrons and matter.

The interaction probabilities between neutrons and matter are described by quantities called *neutron cross-sections*. These probabilities depend on the target nucleus, the type of the interaction, and the energy of the neutron. The microscopic cross-section $\sigma_{i,\mathrm{x}}(E)$ characterizes the probability that a neutron with energy E interacts with nuclide i through reaction x. It has the dimensions of area and it can be interpreted as the effective cross-sectional area per nucleus seen by a neutron. The macroscopic cross-section is defined as the microscopic cross-section multiplied by nuclide density. In a medium consisting of several nuclides, the macroscopic cross-section for reaction x may be written

$$\Sigma_{\mathrm{x}}(\boldsymbol{r}, E) = \sum_{i=1}^{n} n_i(\boldsymbol{r})\, \sigma_{i,\mathrm{x}}(E) \;, \tag{2.1}$$

where n_i denotes the concentration of nuclide i. A macroscopic cross-section can be interpreted physically as the interaction probability per path length traversed by a neutron.

There are various reactions through which neutrons and nuclides may interact. These reactions can be divided into fission, capture and scattering reactions. Capture reactions include all of the reactions, where no secondary neutrons are emitted. It is customary to include both fission and capture reactions in absorption. The total cross-section $\Sigma_{\mathrm{t}}(\boldsymbol{r}, E)$ corresponds to the probability of any type of reaction.

In scattering reactions, it is necessary to specify the probability distributions for the energy and direction of the scattered neutron. The differential scattering cross-section

$$\Sigma_{\mathrm{s}}(\boldsymbol{r}, E \to E', \boldsymbol{\Omega} \cdot \boldsymbol{\Omega}')$$

corresponds to the probability that the scattered neutron will have the direction $\boldsymbol{\Omega}'$ and energy E'. Scattering collisions can be divided into elastic and inelastic reactions. The latter may result in the emission of multiple secondary neutrons.

In fission, it can be approximated that secondary neutrons are produced isotropically and that their energy spectrum is independent of the energy of the neutron causing the fission. Therefore, only two additional quantities need to be specified in addition to the fission cross-section $\Sigma_{\mathrm{f}}(\boldsymbol{r}, E)$. These quantities are the mean number of fission neutrons produced in a fission caused by a neutron with energy E, denoted by $\nu(E)$, and the fission neutron energy spectrum, denoted by $\chi(E)$.

Neutron transport problems are most often formulated in terms of the *neutron flux* Φ, which is defined

$$\Phi(\boldsymbol{r}, \boldsymbol{\Omega}, E, t) = v\, N(\boldsymbol{r}, \boldsymbol{\Omega}, E, t) \;,$$

where v is the neutron velocity. The *scalar flux* is obtained by integrating the angular flux Φ over all directions:

$$\phi(\boldsymbol{r}, E) = \int d\boldsymbol{\Omega}\, \Phi(\boldsymbol{r}, \boldsymbol{\Omega}, E) \;. \tag{2.2}$$

The time-dependent transport equation for the neutron flux can now be written

$$\frac{1}{v}\frac{\partial \Phi}{\partial t} + \boldsymbol{\Omega} \cdot \nabla_r \Phi + \Sigma_{\mathrm{t}} \Phi = \int dE' \int d\boldsymbol{\Omega}'\, \Sigma'_{\mathrm{s}}\, \Phi' + \frac{\chi(E)}{4\pi} \int dE'\, \nu(E')\, \Sigma'_{\mathrm{f}}\, \phi' \;, \tag{2.3}$$

where

- $\Phi = \Phi(\boldsymbol{r}, \boldsymbol{\Omega}, E, t)$
- $\Phi' = \Phi(\boldsymbol{r}, \boldsymbol{\Omega}', E', t)$
- $\phi' = \phi(\boldsymbol{r}, E')$
- $\Sigma_\mathrm{t} = \Sigma_\mathrm{t}(\boldsymbol{r}, E)$
- $\Sigma_\mathrm{s}' = \Sigma_\mathrm{s}(\boldsymbol{r}, E' \rightarrow E, \boldsymbol{\Omega}' \cdot \boldsymbol{\Omega})$
- $\Sigma_\mathrm{f}' = \Sigma_\mathrm{f}(\boldsymbol{r}, E')$

Equation (2.3) can be written in operator form as

$$\frac{1}{v}\frac{\partial \Phi}{\partial t} + A\Phi = B\Phi \,, \tag{2.4}$$

where $A\Phi$ includes all terms, except for the time derivative and the fission source term $B\Phi$.

In most cases the time-dependence of the neutron transport equation is not treated explicitly, but the problem is solved as a criticality eigenvalue problem. Physically it is clear that by adjusting the number of fission neutrons emitted, it is possible to obtain a system in which the rate of neutron production is equal to the losses by absorption and leakage. Therefore, Eq. (2.3) can be written as an eigenvalue problem called the *criticality equation*

$$A\Phi = \frac{1}{k}B\Phi \,, \tag{2.5}$$

to which a non-negative solution is guaranteed to exist, corresponding to the largest eigenvalue k. This eigenvalue is called the multiplication factor and it characterizes the time behavior of the system. If $k > 1$, the neutron flux will increase with time, and the system is called supercritical. The case $k = 1$ corresponds to a truly time-independent solution, in which case the system is called critical. Finally, if $k < 1$, the neutron flux will decrease with time, and the system is called subcritical. Since Eq. (2.5) is homogeneous, it allows an arbitrary normalization of the solution. In burnup calculations the flux solution is typically normalized to coincide with the power of the system.

There exists a variety of computational methods for solving the criticality equation and they can be divided into deterministic methods and Monte Carlo simulation. Traditionally, burnup calculations have been performed in two dimensions using deterministic methods. A review of the different methods falls outside the scope of this thesis, but practically all deterministic methods use similar strategies for dealing with the energy and angular dependence of the criticality equation, and these techniques are explained briefly in the following.

The angular dependence of the scattering source in Eq. (2.5) is most often handled by expanding it as a truncated series of spherical harmonics. In this case, the truncation order zero corresponds to isotropic scattering. After this, there are two

established practices to deal with the angular dependence of the neutron flux. In the discrete ordinates method, the criticality equation is evaluated and solved in discrete angular directions $\{\boldsymbol{\Omega}_j\}_{j=1}^{N}$. In the spherical harmonics method, on the other hand, the angular flux is expanded as a truncated series of spherical harmonics.

The energy discretization procedure is virtually always based on the *multi-group approximation*. In this approach, the considered energy interval $[E_{\min}, E_{\max}]$ is divided into groups, $[E_g, E_{g-1}]$, $g = 1, \ldots, G$, with $E_0 = E_{\max}$ and $E_G = E_{\min}$. After expanding the scattering source in the base of spherical harmonics, the multi-group criticality equation for group g may be obtained by integrating Eq. (2.5) over the interval $[E_g, E_{g-1}]$. Assuming isotropic scattering, this leads to a system of the form

$$\begin{aligned}&\boldsymbol{\Omega} \cdot \nabla \Phi^g(\boldsymbol{r}, \boldsymbol{\Omega}) + \Sigma^g \Phi^g(\boldsymbol{r}, \boldsymbol{\Omega}) \\ &\quad = \frac{1}{4\pi} \sum_{h=1}^{G} \Sigma_{\mathrm{s}}^{h \to g} \phi^h(\boldsymbol{r}) + \frac{\chi_g}{4\pi k} \sum_{h=1}^{G} \bar{\nu}\, \Sigma_{\mathrm{f}}^h \phi^h(\boldsymbol{r}) \,, \quad g = 1, \ldots, G \,,\end{aligned} \tag{2.6}$$

where the multi-group quantities are defined as

$$\Sigma^g(\boldsymbol{r}) = \frac{\int_g \Sigma(\boldsymbol{r}, E)\, \phi(\boldsymbol{r}, E)\, dE}{\int_g \phi(\boldsymbol{r}, E)\, dE} \,, \tag{2.7}$$

$$\Sigma_{\mathrm{s}}^{g' \to g}(\boldsymbol{r}) = \frac{\int_{g'} \int_g \Sigma_{\mathrm{s}}(\boldsymbol{r}, E' \to E)\, \phi(\boldsymbol{r}, E')\, dE'\, dE}{\int_{g'} \phi(\boldsymbol{r}, E')\, dE'} \,, \tag{2.8}$$

$$\chi^g = \int_g \chi(E)\, dE \,, \tag{2.9}$$

and the multi-group flux as

$$\Phi^g(\boldsymbol{r}, \boldsymbol{\Omega}) = \int_g \Phi(\boldsymbol{r}, \boldsymbol{\Omega}, E)\, dE \,. \tag{2.10}$$

Of course, solving the multi-group flux from Eq. (2.6) requires that the multi-group cross-sections are known. In practice, this requires computing the multi-group cross-sections approximatively before the actual transport calculation in the true geometry has been carried out. Depending on the number of energy groups used in the transport calculation, this may require a series of calculations based on different computational strategies.

The Monte Carlo method is a stochastic solution scheme, in which the random walk of individual neutrons is simulated by drawing samples from probability distributions. In a simple Monte Carlo simulation, neutrons are tracked through geometries by sampling their free path lengths. If the sampled free path length does not cross material boundaries, it determines the next collision site for the neutron. In this case, also the interaction nuclide and type are sampled from appropriate probability distributions. The interaction between the neutron and the nuclide can either be an absorption or a scattering reaction. If the neutron is absorbed, its history is terminated. In case of a scattering reaction, the energy and direction of the scattered neutron are sampled from appropriate distributions. When a material boundary is crossed, the simulation proceeds by sampling a new free path length in the entered material,

starting from the boundary. The history of a neutron consists of these tracks from the initial emission to the final absorption or escape from the system. The simulation results can then be used to compute statistical estimates for reaction rates and other quantities of interest, without the need to explicitly solve the flux distribution. The main advantage of the Monte Carlo approach is that it can easily deal with complex three dimensional geometries. It is also useful that the latest available knowledge on neutron interactions can readily be utilized in Monte Carlo calculations. The drawback of the method, on the other hand, is the high computational cost, which often becomes a practical limitation.

2.2 Burnup equations

Burnup equations describe the changes in the concentrations of the nuclides considered in a burnup calculation. They form a system of first order linear differential equations that can be written

$$n_i'(t) = -r_i\, n_i(t) + \sum_{j \neq i} r_{j\to i}\, n_j(t)\ , \quad n_i(0) = n_0^i\ , \quad i = 1\ \ldots, n\ , \tag{2.11}$$

where r_i is the total rate density at which nuclide i is transformed to other nuclides, $r_{j\to i}$ is the rate density at which nuclide $j \neq i$ is transformed to nuclide i, and n_0^i is the initial concentration of nuclide i. Equation (2.11) can be written in matrix form as

$$\boldsymbol{n}' = \boldsymbol{A}\boldsymbol{n}\ , \quad \boldsymbol{n}(0) = \boldsymbol{n}_0\ , \tag{2.12}$$

where $\boldsymbol{A} \in \mathbb{R}^{n\times n}$ is called the *burnup matrix* and $\boldsymbol{n} \in \mathbb{R}^n$ is the nuclide concentration vector. The diagonal elements $a_{ii} = -r_i$ of the burnup matrix correspond to the total loss rates, and the off-diagonal elements $a_{ij} = r_{j\to i}$ to the production rates.

Nuclides can transform to other nuclides through neutron-induced reactions and spontaneous radioactive decay. As previously explained, burnup equations are formed based on the assumption that the reaction rates of the neutron-induced reactions can be approximated as fixed constants. After solving the neutron flux, the rate for a particular neutron reaction can be computed by integrating the flux multiplied by the corresponding microscopic cross-section over space and energy.

Let us first consider reactions other than fission, and let σ_{ji} denote the microscopic cross-section for the neutron reactions that transform nuclide j to nuclide i. The corresponding average transmutation rate density can be computed as

$$V^{-1} \int_{E_{\min}}^{E_{\max}} dE \int_V dV\, \sigma_{ji}(E)\, \phi(\boldsymbol{r}, E) = \overline{\sigma}_{ij}\, \overline{\phi}\ , \tag{2.13}$$

where

$$\overline{\sigma}_{ji} = \frac{\int_{E_{\min}}^{E_{\max}} dE \int_V dV\, \sigma_{ji}(E)\, \phi(\boldsymbol{r}, E)}{\int_{E_{\min}}^{E_{\max}} dE \int_V dV \phi(\boldsymbol{r}, E)} \tag{2.14}$$

and

$$\overline{\phi} = V^{-1} \int_{E_{\min}}^{E_{\max}} dE \int_V dV\, \phi(\boldsymbol{r}, E) \tag{2.15}$$

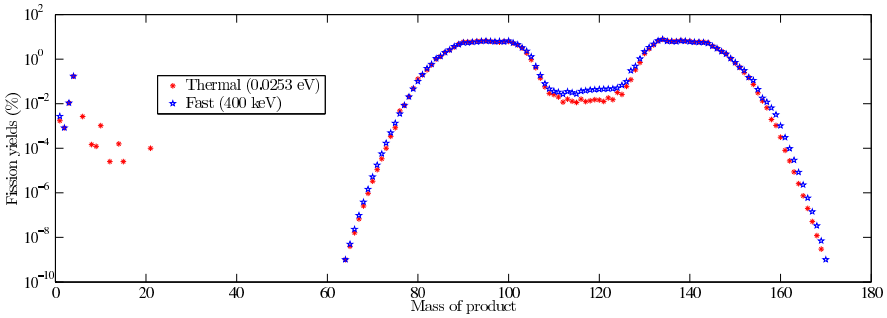

Figure 2.1. Independent fission product yields for ^{235}U.

is the energy and region averaged flux, normalized to coincide with the power of the system.

In the case of fission, the transmutation rate $j \to i$ can written

$$V^{-1} \int_{E_{\min}}^{E_{\max}} dE \int_V dV \, \gamma_{ji}(E)\, \sigma_{j,\mathrm{f}}(\boldsymbol{r}, E)\, \phi(\boldsymbol{r}, E) = \gamma_{ji}\, \overline{\sigma}_{j,\mathrm{f}}\, \overline{\phi} \,, \tag{2.16}$$

where γ_{ji} is the yield of the fission product nuclide i.

In addition to neutron reactions, nuclides can transform to other nuclides via spontaneous radioactive decay. Let λ_{ji} denote the decay constant corresponding to radioactive decay $j \to i$. The total rate at which nuclide j is transformed to nuclide i can now be written

$$r_{j\to i} = \overline{\sigma}_{ji}\overline{\phi} + \gamma_{ji}\overline{\sigma}_{j,\mathrm{f}}\overline{\phi} + \lambda_{ji} \,, \tag{2.17}$$

and the total loss rate correspondingly

$$r_j = \sum_{k\neq j} \overline{\sigma}_{jk} + \overline{\sigma}_{j,\mathrm{f}} + \sum_{k\neq j} \lambda_{jk} \,. \tag{2.18}$$

Let Z denote the atomic number and A the mass number of a nuclide. Table 2.1 lists the most relevant decay and neutron-induced reactions in burnup calculations. Figure 2.1 shows a plot of the fission product yields for ^{235}U.

When forming the burnup equations, it is possible to take into account the production of by-product nuclides. In this case, for example, the reaction rate for each (n,p) reaction contributes to the production rate of ^{1}H. Traditionally, the production of nuclides as by-products has been ignored [1, 2]. Therefore, the term *augmented burnup matrix* will be used to refer to the case, where the production of by-product nuclides has been taken into account when constructing the burnup matrix.

Definition 2.2.1 (Augmented burnup matrix)**.** *A burnup matrix* $\boldsymbol{A} \in \mathbb{R}^{n\times n}$ *is called* augmented*, when it has been constructed such that the reactions, in which by-products are emitted, also contribute to the production rates of the by-product nuclides.*

In the absence of neutron irradiation, nuclides transform only through radioactive decay, and the burnup equations reduce to decay equations. In this case, the burnup matrix is called a *decay matrix*.

Table 2.1. The most relevant decay and neutron-induced reactions in burnup calculations for a nuclide with atomic number Z and mass number A.

Mode of decay	Daughter nuclide	By-product nuclide
α decay	$(Z-2, A-4)$	^{4}He
Proton emission	$(Z-1, A-1)$	^{1}H
Neutron emission	$(Z, A-1)$	-
β^- decay	$(Z+1, A)$	-
β^+ decay	$(Z-1, A)$	-
(n, 2n)	$(Z, A-1)$	-
(n, 3n)	$(Z, A-2)$	-
(n, 4n)	$(Z, A-3)$	-
(n, γ)	$(Z, A+1)$	-
(n, p)	$(Z-1, A)$	^{1}H
(n, d)	$(Z-1, A-1)$	^{2}H
(n, t)	$(Z-1, A-2)$	^{3}H
(n,^{3}He)	$(Z-2, A-2)$	^{3}He
(n, α)	$(Z-2, A-3)$	^{4}He
Fission	fission product nuclides	-

3. Matrix exponential solution of burnup equations

The burnup equations according to Eq. (2.12) can be formally solved by the matrix exponential method yielding the simple solution

$$\boldsymbol{n}(t) = e^{\boldsymbol{A}t}\,\boldsymbol{n}_0 \;, \tag{3.1}$$

where the exponential of the matrix $\boldsymbol{A}t$ can be defined as the power series expression

$$e^{\boldsymbol{A}t} = \sum_{k=0}^{\infty} \frac{1}{k!}\,(\boldsymbol{A}t)^k \;, \tag{3.2}$$

with the additional definition $\boldsymbol{A}^0 = \boldsymbol{I}$. There are generally various numerical methods for computing the matrix exponential. However, the suitability of a particular method depends substantially on the characteristics of the problem at hand. The mathematical properties of (augmented) burnup matrices are studied systematically in Section 3.1. The characteristics and numerical computation of the burnup matrix exponential are then considered in Section 3.2. Rational approximations accurate near the negative real axis are proposed as a novel method for solving the burnup equations and this framework is considered in Section 3.3.

3.1 Mathematical properties of burnup matrices

In order to select a well-suited method for computing the matrix exponential solution, it is necessary to consider the mathematical characteristics of burnup matrices.

First of all, burnup matrices are relatively large and sparse. The total number of nuclides depends both on the employed nuclear data library and the criterion for selecting the nuclides. The evaluated nuclear data library `JEFF-3.1` [3], for example, contains neutron interaction data for 381 nuclides and decay data for 3852 nuclides. The nuclides to be considered in a burnup calculation are chosen based on the transmutation chains originating from the initial nuclides, possibly accompanied with a probabilistic criterion, the resulting total number of nuclides typically being between 1200 and 1700.

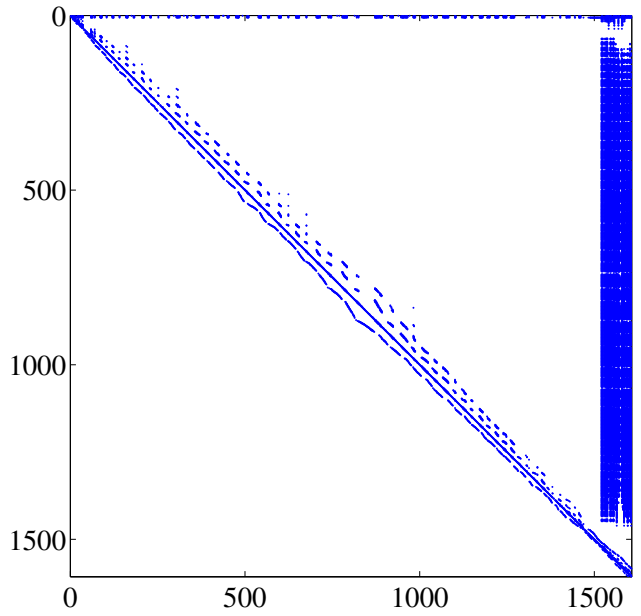

Figure 3.1. Sparsity pattern of an augmented burnup matrix corresponding to a system with 1606 nuclides.

When constructing the burnup matrix, the nuclides can be indexed arbitrarily. The burnup matrix becomes nearly upper triangular if the nuclides are indexed in an ascending order with respect to their ZAI index, defined as ZAI = $10\,000\,Z + 10\,A + I$, where Z is the atomic number, A is the mass number of the nuclide and I is the isomeric state number. In this case, the non-zero elements are concentrated around the diagonal, and fission product distributions on the right hand side. The matrix elements below the diagonal correspond to reactions where the ZAI index increases, the only considered reactions being β^- decay and the (n,γ) reaction. Figure 3.1 shows the sparsity pattern of a typical burnup matrix for a system with 1606 nuclides. The matrix elements on the first subdiagonal correspond to the (n,γ) reaction, in which the mass number of the nuclide increases by one. The non-zeros below the first subdiagonal, on the other hand, correspond to β^- decay with each arc corresponding to the isotopes of a single element. The sparsity pattern follows from that β^- decay generally occurs in neutron-rich nuclides only. Empty columns in the matrix correspond to nuclides which are stable and do not elicit any neutron reactions.

As explained in Section 2.2, the diagonal elements of the burnup matrix are non-positive, and the element $-a_{ii}$ characterizes the total rate at which nuclide i is transformed to other nuclides. The off-diagonal elements, on the other hand, are non-negative, and the element a_{ij} describes the rate by which nuclide j is transformed to nuclide i. This simple sign pattern connects the burnup matrices with the class of *Z-matrices*.

Definition 3.1.1. *A matrix $\boldsymbol{Z} \in \mathbb{R}^{n\times n}$ is called a Z-matrix if its off-diagonal elements are non-positive, i.e. $z_{ij} \leq 0$ for $i \neq j$. The class of Z-matrices is denoted by*

$$Z_n = \{\boldsymbol{Z} \in \mathbb{R}^n |\, z_{ij} \leq 0, \quad i \neq j\} \,. \tag{3.3}$$

Based on this definition, it is evident that the negatives of burnup matrices belong to Z-matrices. This observation is interesting, because it suggests connections with the theory of non-negative matrices. Especially, every $\boldsymbol{Z} \in Z_n$ can be expressed in the form

$$\boldsymbol{Z} = s\boldsymbol{I} - \boldsymbol{B} \,, \quad s > 0 \,, \quad \boldsymbol{B} \geq 0 \,, \tag{3.4}$$

where $\boldsymbol{B} \geq 0$ denotes $B_{ij} \geq 0$ for $i, j = 1, \ldots, n$. This is further discussed in Section 3.1.2, where the spectral properties of burnup matrices are considered.

Nuclides may transform to other nuclides through spontaneous radioactive decay and neutron-induced reactions. The measured nuclide half-lives corresponding to radioactive decay can vary from 10^{-24} seconds to billions of years, which introduces elements of both extremely small and large magnitude to the burnup matrix, making the system numerically extremely stiff. The highly unstable nuclides, whose decay constants can be of the order of 10^{21} s^{-1}, are numerically the most difficult. An example of such nuclide is the boron isotope ^{7}B, which decays to the beryllium isotope ^{6}Be by proton emission with a half-live of the order of 10^{-22} s. Since

$$\|\boldsymbol{A}\|_1 \geq \max_{i,j} |a_{ij}| \,,$$

this reaction alone increases the burnup matrix norm to be at least of the order of 10^{21}.

The magnitudes of neutron-induced reaction rates vary significantly less. In accordance with Eqs. (2.13) and (2.16), their values are bounded by the maximum values of the cross-sections and the normalization of the neutron flux by power. One of the largest known cross-sections is the capture cross-section of ^{135}Xe, whose maximum value is of the order of 10^{-16} cm^2. The highest ever measured neutron fluxes are of the order $\sim 10^{16}/(\text{cm}^2\,\text{s})$, the record being $\sim 3 \times 10^{16}$ neutrons/(cm^2 s) achieved in the High Flux Isotope Reactor at Oak Ridge National Laboratory. Therefore, the magnitudes of neutron-induced reactions can be conservatively bounded from above by unity in reactor conditions.

To illustrate the extensive variations in the decay and transmutation rates, Fig. 3.2 shows a plot of the absolute values of a 1606×1606 augmented burnup matrix. Figure 3.3 is a close-up from Fig. 3.2, showing $\boldsymbol{A}(1:36, 1:30)$ and corresponding to the 36 lightest nuclides, ranging from the hydrogen isotope ^{1}H to the oxygen isotope ^{18}O.

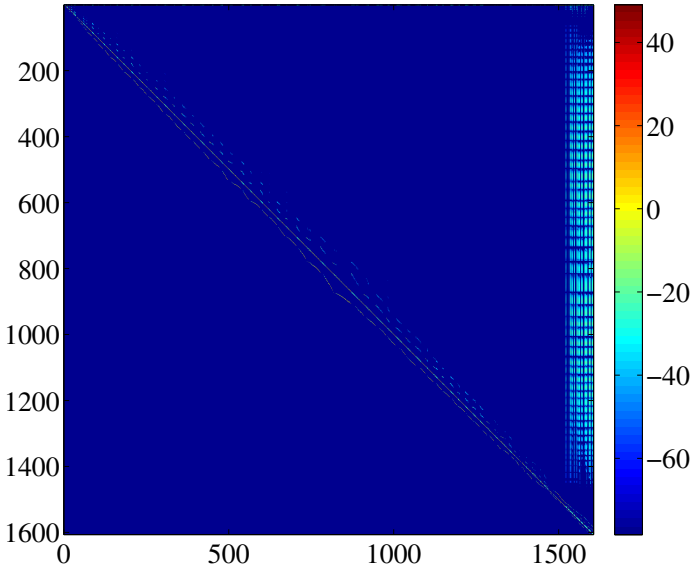

Figure 3.2. A plot illustrating the (10-base) logarithmic variations in the absolute values of burnup matrix elements for a test case with 1606 nuclides.

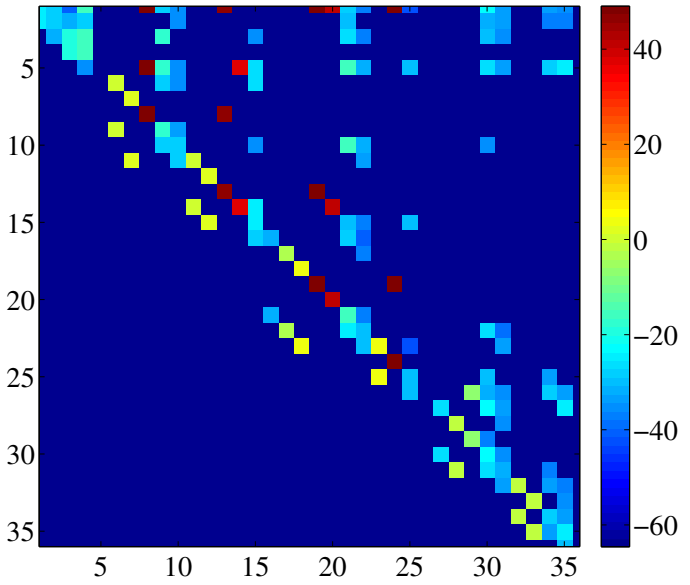

Figure 3.3. A close-up of the matrix in Fig. 3.2 corresponding to the 36 lightest nuclides ranging from ^{1}H to ^{18}O.

3.1.1 Graph-theoretical approach

Some insight into the numerical properties of burnup matrices can be gained by considering their graphs. In this context, the column and row indices of $\boldsymbol{A}$ are referred to as vertices. When $a_{ij} \neq 0$, there exists an *edge* from vertex i to vertex j, and the notation $i \rightarrow j$ is used. A *path* of length m from node i to node k is defined as a sequence of non-zero vertices $[i = i_1, i_2, i_3 \ldots, i_m, i_{m+1} = k]$, such that $i_n \rightarrow i_{n+1}$ for $n = 1, \ldots, m+1$. The physical interpretation for this is that there exists a transmutation path of length m from nuclide k to nuclide i.

A graph is called acyclic, if the paths related to it do not form closed cycles. In this case, the vertices can be ordered topologically, meaning that if $i \rightarrow j$, the vertex i appears before j in the ordering. An acyclic graph corresponds to a matrix that can be permuted to lower triangular form. When a graph is not acyclic, it can be divided into *strongly connected components* (SCCs). A strongly connected component is defined as a set of vertices, for which there exists a path from each vertex to every other vertex. After dividing a graph into strongly connected components, these components can be ordered topologically in the same manner as the vertices of an acyclic graph, after which the corresponding systems of differential equations can be solved independently in this order. This corresponds to permuting the matrix to lower block triangular form with irreducible diagonal blocks.

In the case of a burnup matrix, a strongly connected component corresponds to a set of nuclides for which there exists a transmutation path from every nuclide to every other nuclide. In this context, it should be noted that measured nuclear data does not exist for all reactions that are unlikely but possible in theory. The considerations in this section are based on evaluated nuclear data libraries and the library `JEFF-3.1` [3] in particular. Some general conclusions can be drawn from studying the transmutation paths of nuclides. First of all, the only reactions increasing the ZAI index are the (n, γ) reaction and β^- decay. Therefore, a closed cycle must necessarily contain at least one of these reactions. Nuclides that do not undergo either of these reactions, form SCCs whose size is one. It can also be deduced that fissile nuclides and fission product nuclides belong to different SCCs, since transmutation paths from fission products to fissile nuclides are extremely unlikely under reactor conditions. [3]

Interestingly, the nuclides produced as by-products, i.e. ^{1}H, ^{2}H, ^{3}H, ^{3}He and ^{4}He, always form a *sink* in the augmented burnup matrix, meaning that there is no outbound edge from this set of vertices. This is due to the fact that these nuclides do not elicit any reactions that would produce nuclides outside this group. The nuclide ^{4}He is stable and elicits no neutron reactions corresponding to a zero column in the burnup matrix, whereas the rest of the by-product nuclides form a single SCC.

Let us again consider the augmented burnup matrix plotted in Figures 3.1 and 3.2. This matrix corresponds to a burnup system with 1606 nuclides, ranging from

[3] Interestingly, these paths are theoretically possible if data based on nuclear models rather than measurements is considered. For example, the nuclear data library `TENDL-2011` [4] produced with the nuclear reaction program Talys [4] contains data that enables paths from fission products to fissile nuclides. However, since these transmutation paths are extremely unlikely, they are not further considered here.

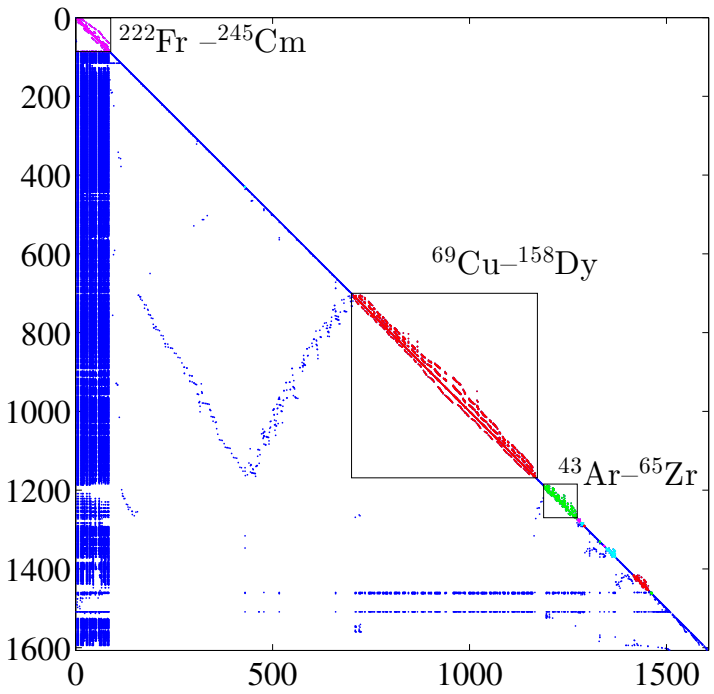

Figure 3.4. Burnup matrix permuted to lower block triangular form. The diagonal blocks with size greater than one have been plotted with magenta, red, green or cyan. For the three largest blocks, the nuclides with the smallest and the greatest ZAI indices in the SCC have been indicated.

^{1}H to ^{245}Cm when ordered according to their ZAI index. For this matrix, the number of SCCs is 896. However, only twelve of these components include more than a single nuclide. The *source* SCC, i.e. a SCC without any inbound edges, consists 83 nuclides ranging from ^{222}Fr to ^{245}Cm. The largest SCC comprises 463 nuclides ranging from ^{69}Cu to ^{159}Dy. Figure 3.4 depicts the SCCs of the test case burnup matrix by showing a plot of the matrix permuted to block lower triangular form.

3.1.2 Spectrum

Real parts of eigenvalues

When considering the spectral properties of burnup matrices, it is important to distinguish between classically defined and augmented burnup matrices. In the case of conventional burnup matrices, the number of nuclides does not increase in all reactions except fission. As explained in Section 3.1.1, there are generally no transmutation chains from fission product nuclides to fissile nuclides. Therefore, the con-

Table 3.1. Possible decay and neutron reactions for the by-product nuclides.

Nuclide	Possible reactions		
^{1}H	(n,γ)		
^{2}H	(n,γ)	(n,2n)	
^{3}H	β^-	(n,2n)	
^{3}He	(n,p)	(n,d)	(n,t)
^{4}He			

centrations of all nuclides must remain bounded at all times [l]. In this case, the following theorem ([5], p. 165) gives a useful characterization of the real parts of the burnup matrix eigenvalues.

Theorem 3.1.2. *Every solution* $\boldsymbol{n}$ *of system (2.12) remains bounded as* $t \to \infty$ *if and only if the following holds*

(i) $\mathrm{Re}\,(\lambda) \leq 0 \quad \forall\, \lambda \in \Lambda(\boldsymbol{A})$

(ii) Every $\lambda \in \Lambda(\boldsymbol{A})$ *with Re* $(\lambda) = 0$ *is a semisimple eigenvalue, i.e. the geometric and algebraic multiplicities agree.*

Here $\Lambda(\boldsymbol{A})$ *denotes the set of the eigenvalues of* $\boldsymbol{A}$.

However, the situation changes slightly for the augmented burnup matrix. In this case, the number of nuclides increases in all reactions that produce a by-product nuclide in addition to the daughter nuclide. In this context, it is not evident that all nuclide concentrations remain bounded as $t \to \infty$. This follows from that neutrons are not assumed to be part of the burnup system but they are supposed to be added constantly to the system. However, as discussed in Section 3.1.1, the only nuclides produced as by-products are ^{1}H, ^{2}H, ^{3}H, ^{3}He and ^{4}He. The vertices corresponding to these nuclides always form a sink in the burnup matrix graph. It follows that no nuclides are produced from these nuclides, and that *the concentrations of all nuclides except for these by-product nuclides must remain bounded at all times.*

Fortunately, the eigenvalues related to the by-product nuclides can be separated from the rest of the eigenvalues of the augmented burnup matrix, remembering that the spectrum of a block triangular matrix is the union of the spectra of the diagonal blocks, i.e.

$$\Lambda(\boldsymbol{A}) = \bigcup_j \Lambda(\boldsymbol{A}_{jj}) \,, \tag{3.5}$$

where $\boldsymbol{A}_{jj}$ are the irreducible diagonal blocks. Here each diagonal block corresponds to the set of nuclides forming a SCC. Therefore, it can be concluded that Theorem 3.1.2 applies to all eigenvalues of an augmented burnup matrix except for the ones related to the diagonal block corresponding to the nuclides ^{1}H, ^{2}H, ^{3}H and ^{3}He. This submatrix, denoted by $\widetilde{\boldsymbol{A}} \in \mathbb{R}^{4\times 4}$, and its spectrum are considered in the following.

Table 3.1 lists the reactions that are possible for the by-product nuclides. From the perspective of eigenvalues, it is noteworthy that ^{3}He elicits (n, p), (n, d), and (n, t)

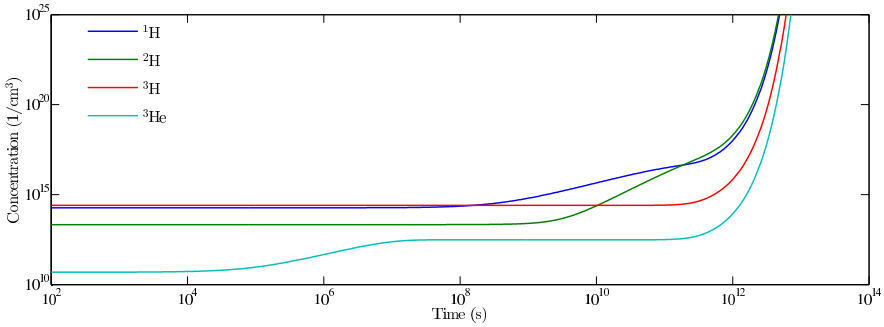

Figure 3.5. Nuclide concentrations corresponding the solution of $\boldsymbol{x}' = \widetilde{\boldsymbol{A}}\boldsymbol{x}$.

reactions (in this case, (n, p) and (n, t) are actually the same reaction) producing either one ^{3}H and one ^{1}H nuclide or two ^{2}H nuclides Therefore, the number of nuclides increases in both of these reactions. As can be seen from Table 3.1, there are transmutation paths from ^{1}H, ^{2}H and ^{3}H to ^{3}He, meaning that also the number of ^{3}He nuclides increases as a function of time. Considering this, it is evident that the nuclide concentrations of the by-product nuclides grow unboundedly when $t \to \infty$. This clearly unphysical behavior stems from the assumption of constant rates for the neutron-induced reactions during the burnup step. According to this assumption, neutrons are added to the system constantly and, in the β^- decay of ^{3}H to ^{3}He, neutrons are converted to protons, increasing the amount of matter as a function of time. Therefore, the eigenvalues related to $\widetilde{\boldsymbol{A}}$ can have positive real parts.

In reality, of course, all nuclide concentrations remain bounded at all times. Therefore, the dynamical behavior of the subsystem $\boldsymbol{x}' = \widetilde{\boldsymbol{A}}\boldsymbol{x}$ reflects the validity of the assumption of constant reaction rates during the burnup step. Therefore, $\lambda t \gg 1$ for any $\lambda \in \Lambda(\widetilde{\boldsymbol{A}})$ would indicate the invalidity of this assumption for the time step t. Figure 3.5 shows the nuclide concentrations as a function of time for a PWR pin-cell test problem. In this test case, $\widetilde{\boldsymbol{A}}$ has a single positive eigenvalue which is of the order of 10^{-12}. It can be seen from this figure that the nuclide concentrations begin to increase unrealistically when $\lambda t \to 1$. It should also be noted that although the rate for the β^- decay is constant, the magnitudes of the neutron reactions are ultimately determined by the normalization of the neutron flux by power. Increasing the power by a factor of 10 000, for example, increases the sole positive eigenvalue from the order of 10^{-12} only to the order of 10^{-10}. This extreme example illustrates that the theoretical mathematical instability of this subsystem does not pose a problem in practice.

Imaginary parts of eigenvalues

The characterization of the imaginary parts of the burnup eigenvalues is more difficult. It is again useful to consider the SCCs separately. It is evident, that the eigenvalues corresponding to SCCs consisting of a single vertex coincide with the respective

diagonal elements of the matrix.

From a physical standpoint, the imaginary part ω of an eigenvalue corresponds to an oscillation with period $T = 2\pi/\omega$. Some insight on the interactions' underlying oscillatory behavior can be gained by considering a small system that can be solved analytically. First of all, it is easy to show that a system consisting of two nuclides cannot have non-real eigenvalues. Therefore, the following closed-cycle system consisting of three nuclides can be regarded as a model problem in this context:

$$\begin{bmatrix} n_1' \\ n_2' \\ n_3' \end{bmatrix} = \begin{bmatrix} -\mu_1 & 0 & \mu_3 \\ \mu_1 & -\mu_2 & 0 \\ 0 & \mu_2 & -\mu_3 \end{bmatrix} \begin{bmatrix} n_1 \\ n_2 \\ n_3 \end{bmatrix} . \tag{3.6}$$

For this system, a necessary condition for the existence of a non-real eigenvalue is that the constants μ_i satisfy

$$\sqrt{\mu_1} - \sqrt{\mu_2} < \sqrt{\mu_3} < \sqrt{\mu_1} + \sqrt{\mu_2} . \tag{3.7}$$

Furthermore, the absolute value of the imaginary part ω attains its maximum value

$$\omega_{\max} = \sqrt{\mu_1 \mu_2} \tag{3.8}$$

when $\mu_3 = \mu_1 + \mu_2$. When $\mu_1 \gg \mu_2$, the left-hand and right-hand sides of the inequality (3.7) approach $\sqrt{\mu_1}$, and μ_3 must be arbitrarily close to μ_1 in order to induce a complex eigenvalue. Assuming, for example, $\mu_1 \sim 10^{-2}$ and $\mu_2 \sim 10^{-8}$, the first 4 decimals of μ_1 and μ_3 must coincide in order for this system to have non-real eigenvalues.

The principles related to this model problem can be generalized to more complex closed-cycle systems. Non-real eigenvalues are most likely to occur, when the rates of the reactions forming a closed cycle are of the same magnitude. When some of the reactions are significantly more likely than others, they can be considered instant. Physically, it is intuitive that the imaginary parts must be of the same order as the rates for the least likely reactions in the cycle.

As discussed in the beginning of Section 3.1, the values of the decay constants vary extensively, whereas the rates for neutron reactions are relatively slow. In a thermal reactor operating at full power, most of the transmutation coefficients are of order $\leq 10^{-8}$ s^{-1}. In a fast reactor, the flux is higher but most of the neutron reactions are less likely, which results in most of the reaction rates being even smaller than in a thermal reactor. Based on computing the eigenvalues for a wide range of burnup matrices, it seems that they are generally confined to a region near the negative real axis. For every burnup matrix that we have considered, this has also been the case. When the power level is decreased, the transmutation coefficients become smaller. In this case the absolute values of the imaginary parts of the eigenvalues decrease as well. It seems that the oscillations are most likely to occur for reduced power cases where the greatest transmutation coefficients are of order $\leq 10^{-12}$. In

general, the eigenvalues of the burnup matrix appear to remain bounded near the negative real axis in all conceivable burnup calculation cases with imaginary parts at the most of the order of 10^{-8}.

It was stated previously that the negatives of burnup matrices belong to Z-matrices. This property can be exploited in deriving a wedge condition for the burnup matrix eigenvalues. Let $\boldsymbol{Z} \in Z_n$, in which case we can write $\boldsymbol{Z} = s\boldsymbol{I} - \boldsymbol{B}$ with $s > 0$ and $\boldsymbol{B} \geq 0$. Since $\boldsymbol{B} \geq 0$, it follows from the Perron–Frobenius theorem that $\boldsymbol{B}$ has a real eigenvalue $\lambda \geq 0$ such that $|\mu| \leq \lambda \; \forall \; \mu \in \Lambda(\boldsymbol{B})$. Therefore, λ corresponds to the spectral radius of $\boldsymbol{B}$, denoted by $\rho(\boldsymbol{B})$.

Definition 3.1.3 (M-matrix)**.** *Let $\boldsymbol{Z} \in Z_n$ so that it can be written in the form $\boldsymbol{Z} = s\boldsymbol{I} - \boldsymbol{B}$ with $s > 0$ and $\boldsymbol{B} \geq 0$. If $s \geq \rho(\boldsymbol{B})$, $\boldsymbol{Z}$ is called an M-matrix. If $s = \rho(\boldsymbol{B})$, the M-matrix is singular, and if $s > \rho(\boldsymbol{B})$, it is non-singular.*

M-matrices can be characterized by various equivalent properties (see Theorem 2.3 in [6]), of which the following three are of special interest:

Theorem 3.1.4. *Let $\boldsymbol{A} \in Z_n$ Then the following properties are equivalent*

1. *$\boldsymbol{A}$ is an M-matrix*
2. *$\boldsymbol{A} + \varepsilon\boldsymbol{I}$ is a non-singular M-matrix for any $\varepsilon > 0$*
3. *Every eigenvalue of the matrix $\boldsymbol{A}$ has a non-negative real part*

From the third property we directly obtain the following theorem.

Theorem 3.1.5. *The negatives of (conventional) burnup matrices belong to the class of M-matrices.*

The connection between burnup matrices and M-matrices is interesting because it gives a wedge condition to the non-real eigenvalues of burnup matrices.

Theorem 3.1.6 (Eigenvalues of singular M-matrix)**.** *Let $\boldsymbol{M} \in \mathbb{R}^{n \times n}$ be a singular M-matrix with $n \geq 2$. Then its eigenvalues are confined to the closed wedge*

$$\overline{W}_n = \left\{ z = re^{i\theta} \mid r > 0 \, , |\theta| \leq \frac{\pi}{2} - \frac{\pi}{n} \right\} . \tag{3.9}$$

Proof. It has been proven that the eigenvalues of non-singular M-matrices belong to the open wedge

$$W_n = \left\{ z = re^{i\theta} \mid r > 0 \, , |\theta| < \frac{\pi}{2} - \frac{\pi}{n} \right\} \tag{3.10}$$

if $n > 2$ and in $(0, \infty)$ if $n = 2$ [7]. Based on property 2 in Theorem 3.1.4, for any $\varepsilon > 0$, the matrix $\boldsymbol{M} + \varepsilon\boldsymbol{I}$ is a non-singular M-matrix whose eigenvalues are confined to the region W_n. However, since the eigenvalues of a matrix depend continuously on the matrix, it follows that the eigenvalues of the singular matrix $\boldsymbol{M}$ must be confined to the wedge $\overline{W}_n$. □

Notice that Theorem 3.1.6 can also be applied to the irreducible diagonal blocks corresponding to the SCCs of a burnup matrix. In this case, the wedge W_n can be narrowed to correspond to the size of the largest SCC of the matrix. When considering augmented burnup matrices, it is evident that all diagonal blocks—apart from the one corresponding to the by-product nuclides—are M-matrices to which these wedge conditions can be applied. The block matrix $\widetilde{\boldsymbol{A}} \in \mathbb{R}^{4\times 4}$ corresponding to the by-product nuclides may have eigenvalues with a positive real part. However, any of its 2×2 principal submatrix is an M-matrix. This can be attributed to the fact that removing any two nuclides from the respective burnup chain cuts off the feedback mechanism necessary for the nuclide concentrations to increase as a function of time. Therefore, we can identify $\widetilde{\boldsymbol{A}}$ with the following class of matrices [8]:

Definition 3.1.7. *$\boldsymbol{A} \in L_0^k$ if and only if $\boldsymbol{A}$ is a Z-matrix and each $k \times k$ principal sub-matrix of $\boldsymbol{A}$ is an M-matrix, but there is at least one $(k+1) \times (k+1)$ principal sub-matrix that is not an M-matrix.*

Based on this definition, $-\widetilde{\boldsymbol{A}} \in L_0^{n-2} = L_0^2$. From [8] we now obtain the following characterization: $\widetilde{\boldsymbol{A}}$ has exactly one eigenvalue on the positive real axis with all the other eigenvalues having non-positive real parts.

We can now summarize the estimates obtained for the eigenvalues of augmented burnup matrices:

Theorem 3.1.8. *(Eigenvalues of augmented burnup matrices) Let $\boldsymbol{A} \in \mathbb{R}^{n\times n}$ be an augmented burnup matrix. If $n = 2$,*

$$\Lambda(\boldsymbol{A}) \subset (-\infty, 0] \, .$$

Otherwise, if the nuclides ^{1}H, ^{2}H, ^{3}H, and ^{3}He are included to the burnup system, $\boldsymbol{A}$ has four eigenvalues corresponding to them. Exactly one of these eigenvalues is real-valued and positive, while the other three eigenvalues have non-positive real parts. The remaining eigenvalues of $\boldsymbol{A}$ are confined to the wedge

$$W_n = \left\{ z = re^{i\theta} \,\middle|\, r > 0 \, , |\theta| \geq \frac{\pi}{2} + \frac{\pi}{n} \right\} \tag{3.11}$$

around the negative real axis.

Figure 3.6 shows an example of the spectrum of an augmented burnup matrix for a system with 1606 nuclides. This is the same matrix that was plotted in Figures 3.1 and 3.2. Figure 3.7 shows a close-up from Figure 3.6 together with the wedge estimate from Theorem 3.1.8.

Eigenvalue decomposition

A matrix $\boldsymbol{A} \in \mathbb{R}^{n\times n}$ is called diagonalizable, if it has the eigenvalue decomposition

$$\boldsymbol{A} = \boldsymbol{T}\boldsymbol{\Lambda}\boldsymbol{T}^{-1} \, , \tag{3.12}$$

where $\boldsymbol{\Lambda}$ is a diagonal matrix containing the eigenvalues of $\boldsymbol{A}$, and $\boldsymbol{T}$ is an invertible matrix containing the respective eigenvectors. Therefore, in order for the matrix $\boldsymbol{A}$

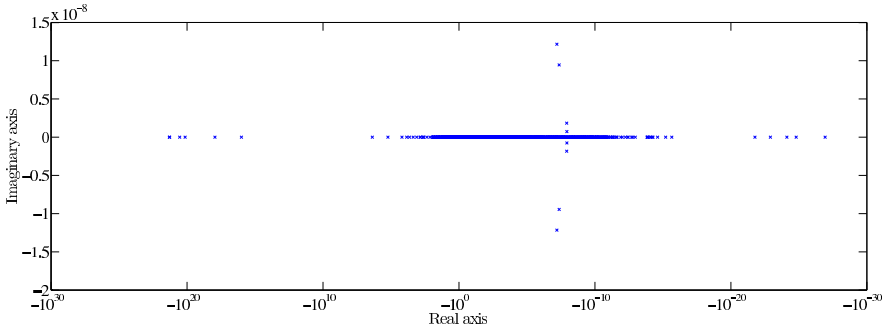

Figure 3.6. Plot of the eigenvalues $z \in \{z \in \mathbb{C} \,|\, z \in \Lambda(\boldsymbol{A}), \operatorname{Re} z < 0\}$ of an augmented burnup matrix $\boldsymbol{A}$ for a system with 1606 nuclides. In addition, the matrix has a single positive eigenvalue $z_+ \approx 4.15 \times 10^{-12}$ and zero as a 29-fold eigenvalue.

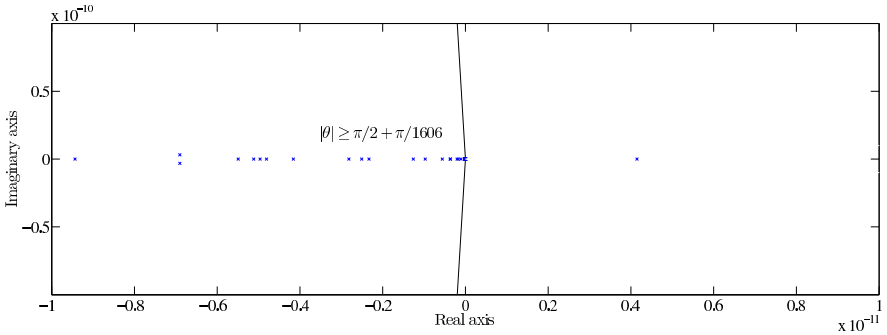

Figure 3.7. Close-up of the eigenvalues plotted in Fig. 3.6 near the origin, together with the wedge estimate from Theorem 3.1.8.

to be diagonalizable, it must have n linearly independent eigenvectors that span the space $\mathbb{C}^n$. This happens especially if the matrix has n distinct eigenvalues.

If a nuclide is stable and does not elicit any neutron reactions, it always induces a zero eigenvalue to the burnup matrix. For this reason, burnup matrices are nearly always singular with zero as a multiple eigenvalue. However, according to Theorem 3.1.2, the eigenvalue zero is semi-simple meaning that its geometric and algebraic multiplicities agree. Therefore, in order for a burnup matrix to be defective, it should have a non-zero eigenvalue, whose geometric multiplicity is smaller than its algebraic multiplicity.

For a single nuclide forming a SCC of unit size, the respective eigenvalue coincides with its removal rate. When considering a SCC consisting of several nuclides, an eigenvalue can no longer be connected with a particular nuclide but they all represent the set of nuclides and their effective removal rates taking the feedback mechanisms (i.e. closed cycles) into consideration. Since the decay and transmutation constants of different nuclides are never *precisely* equal, a repeated non-zero eigenvalue is

theoretically extremely unlikely. Therefore, burnup matrices should ideally be diagonalizable with zero as the only multiple eigenvalue. Nonetheless, as recently noted in [9], the half-lives of some short-lived nuclides have not been measured accurately, which results in identical estimates for some of them. [4] This imprecision of the decay data may cause a burnup matrix to have multiple eigenvalues in practise. In addition to these multiple eigenvalues resulting from inaccurate decay data, burnup matrices typically have many nearly confluent eigenvalues, which complicates their numerical computation. [5]

In some cases, the condition of an eigenvalue problem may be a sign of that the eigenvalues are not meaningful, and the pseudospectra of the matrix should be studied instead [10]. The ε-pseudospectrum $\sigma_\varepsilon(\boldsymbol{A})$ of $\boldsymbol{A}$ is defined as the set $z \in \mathbb{C}$ such that

$$\| (z\boldsymbol{I} - \boldsymbol{A})^{-1} \| > 1/\varepsilon \,, \tag{3.13}$$

where the matrix $(z\boldsymbol{I} - \boldsymbol{A})^{-1}$ is called the *resolvent* of $\boldsymbol{A}$ at z. In the previous definition, it is assumed that $\| (z\boldsymbol{I} - \boldsymbol{A})^{-1} \| = \infty$ when $z \in \Lambda(\boldsymbol{A})$ so that the spectrum of $\boldsymbol{A}$ is contained in the ε-pseudospectrum for every $\varepsilon > 0$. It can be shown that when matrix $\boldsymbol{A}$ is perturbed by a matrix $\boldsymbol{E}$ such that $\|\boldsymbol{E}\| < \varepsilon$, the eigenvalues of $\boldsymbol{A} + \boldsymbol{E}$ are confined to $\sigma_\varepsilon(\boldsymbol{A})$ [10]. Therefore, the ε-pseudospectrum characterizes the sensitivity of the eigenvalue problem to perturbations.

When computing the eigenvalues of a burnup matrix, problems are typically faced due to the algorithm not being able to distinguish between the nearly confluent eigenvalues. Also, round-off errors may induce small positive eigenvalues, which are clearly nonphysical. From a practical point of view, these errors are not acceptable since they change the character of the problem. However, the absolute magnitudes of the errors are generally of the order of the arithmetic precision used in the computation, suggesting that the eigenvalue problem is not especially sensitive to perturbations. The study of the pseudospectra of burnup matrices supports this conclusion. Figure 3.8 shows the boundaries of the 2-norm ε-pseudospectra for a burnup matrix that was formed by selecting only the most important actinides and fission products, totalling in 219 nuclides. The norm of the respective burnup matrix is of the order of 10^{-4}. It can be seen from Fig. 3.8 that at distance δ from the eigenvalues, the norm $\| (z\boldsymbol{I} - \boldsymbol{A})^{-1} \|$ is of the order of δ^{-1}.

3.2 Matrix exponential

3.2.1 Definitions of matrix functions

There are many equivalent ways to define the matrix exponential $e^{\boldsymbol{A}t}$ in addition to the power series definition of Eq. (3.2). In this context, it is useful to consider definitions for general matrix functions first. Two definitions of particular interest are presented

[4] It should be noted that in [9] the focus is on the identical eigenvalues resulting from linearizing the closed cycles in the burnup chain rather than identical eigenvalues of burnup matrices.

[5] The computation of the eigenvalues becomes significantly better-conditioned if the SCCs of the matrix are formed first and the eigenvalues are then computed for each diagonal block corresponding a SCC.

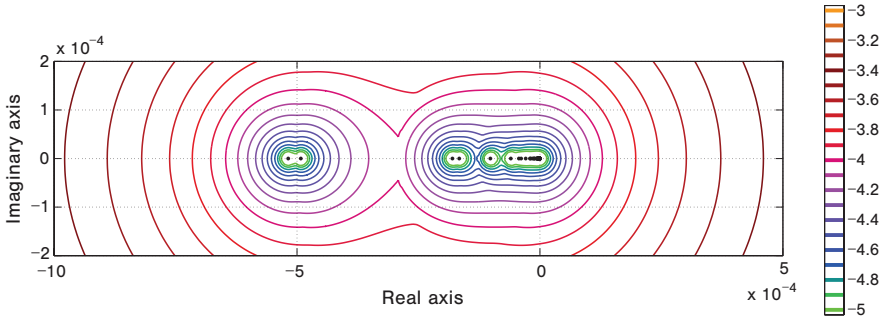

Figure 3.8. Pseudospectra of a small burnup matrix corresponding to a system with 219 nuclides. The outer boundaries of $\sigma_\varepsilon(\boldsymbol{A})$ are plotted for selected values between $\varepsilon = 10^{-5}$ and $\varepsilon = 10^{-3}$. The eigenvalues of the matrix are marked with black dots. The plot was computed with the Eigtool package for MATLAB [11].

here—the definition based on Jordan canonical form, and the definition based on the Cauchy integral formula.

It is well-known that any matrix $\boldsymbol{A} \in \mathbb{C}^{n\times n}$ can be written in the Jordan canonical form

$$\boldsymbol{A} = \boldsymbol{T}\,\boldsymbol{J}\,\boldsymbol{T}^{-1}\,, \tag{3.14}$$

where $\boldsymbol{J}$ is a diagonal block matrix

$$\boldsymbol{J} = \operatorname{diag}\left[\boldsymbol{J}_{m_1}(\lambda_1), \ldots, \boldsymbol{J}_{m_p}(\lambda_p)\right]$$

and $\lambda_1, \ldots, \lambda_p$ are eigenvalues of $\boldsymbol{A}$. The matrix $\boldsymbol{J}$ is unique up to the order of the diagonal blocks, whereas the transformation matrix $\boldsymbol{T}$ is in general not unique. The diagonal blocks are of the form

$$\boldsymbol{J}_{m_j}(\lambda_j) = \begin{bmatrix} \lambda_j & 1 & 0 & \cdots & 0 \\ & \lambda_j & 1 & \ddots & \vdots \\ & & \lambda_j & \ddots & 0 \\ & \boldsymbol{0} & & \ddots & 1 \\ & & & & \lambda_j \end{bmatrix} = \lambda_j \boldsymbol{I} + \boldsymbol{S}_{m_j} \in \mathbb{C}^{m_j\times m_j} \tag{3.15}$$

with $\sum_{j=1}^{p} m_j = n$. The number of Jordan blocks corresponding to λ_j is equal to the number of linearly independent eigenvectors related to that eigenvalue. Let l_j denote the *index* of λ_j, defined as the size of the largest Jordan block corresponding to λ_j. In order to define the matrix function $f(\boldsymbol{A}t)$ based on Jordan canonical form, we need the following definition [12].

Definition 3.2.1. *A function f is defined on the spectrum of $\boldsymbol{A}t$ if the values*

$$f^{(i)}(t\lambda_j)\,, \quad i = 0 \ldots, l_j - 1\,, \quad j = 1, \ldots, s \tag{3.16}$$

exist. Here $\{\lambda_1, \ldots, \lambda_s\}$ are the distinct eigenvalues of $\boldsymbol{A}$.

We can now formulate the following definition for the matrix function $f(\boldsymbol{A}t)$.

Definition 3.2.2. *Let the function f be defined on the spectrum of* $\boldsymbol{A}t \in \mathbb{C}^{n\times n}$ *and let* $\boldsymbol{A} = \boldsymbol{T}\,\boldsymbol{J}\,\boldsymbol{T}^{-1}$ *denote the Jordan decomposition of* $\boldsymbol{A}$*. Then*

$$f(\boldsymbol{A}t) = \boldsymbol{T}\,\mathrm{diag}\left[f(\boldsymbol{J}_{m_1}(t\lambda_1)),\cdots,f(\boldsymbol{J}_{m_p}(t\lambda_p))\right]\boldsymbol{T}^{-1}\,, \tag{3.17}$$

where

$$f\left(\boldsymbol{J}_{m_j}(t\lambda_j)\right) = \sum_{\nu=0}^{m_j-1}\frac{f^{(\nu)}(t\lambda_j)}{\nu!}\boldsymbol{S}_{m_j}^{\nu}\,. \tag{3.18}$$

Notice that when the matrix $\boldsymbol{A}$ is diagonalizable, the Jordan decomposition reduces to the eigenvalue decomposition and $f(\boldsymbol{A}t)$ can be computed simply as

$$f(\boldsymbol{A}t) = \boldsymbol{T}\,f(\boldsymbol{\Lambda}t)\,\boldsymbol{T}^{-1}\,. \tag{3.19}$$

Definition 3.2.2 and Eq. (3.19) are useful because they directly show the connection between the eigenvalues and the exponential of a matrix. It should be noticed that since the exponential function is analytic everywhere in the complex plane, the matrix function $e^{\boldsymbol{A}t}$ is defined for all $\boldsymbol{A}t \in \mathbb{C}^{n\times n}$.

Another interesting definition for the matrix function $f(\boldsymbol{A}t)$ is based on a generalization of the Cauchy integral theorem.

Definition 3.2.3. *Let* $\boldsymbol{A} \in \mathbb{C}^{n\times n}$ *and let f be analytic inside the closed contour* Γ *that winds once around the spectrum of* $\boldsymbol{A}t$*. Then*

$$f(\boldsymbol{A}t) = \frac{1}{2\pi i}\int_{\Gamma} f(z)\,(z\boldsymbol{I}-\boldsymbol{A}t)^{-1}\,dz\,. \tag{3.20}$$

In the previous definition, the resolvent of $\boldsymbol{A}t$ can be written in the form

$$(z\boldsymbol{I}-\boldsymbol{A}t)^{-1} = \frac{\boldsymbol{B}(z)}{\det(z\boldsymbol{I}-\boldsymbol{A}t)}\,, \tag{3.21}$$

where

$$\boldsymbol{B}(z) = z^{n-1}\boldsymbol{B}_0 + z^{n-2}\boldsymbol{B}_1 + \ldots + z\boldsymbol{B}_{n-2} + \boldsymbol{B}_{n-1} \tag{3.22}$$

with $\boldsymbol{B}_0, \boldsymbol{B}_1, \ldots, \boldsymbol{B}_{n-1}$ matrices with constant elements [13].

3.2.2 Application to burnup matrices

Some interesting properties of the burnup matrix exponential $\boldsymbol{E}(t) = e^{\boldsymbol{A}t}$ can be deduced based on physical considerations. First of all, for each value of t, the element $E_{ij}(t)$ characterizes the contribution from nuclide j to nuclide i during time step t. Therefore, it is clear that all elements of $\boldsymbol{E}(t)$ must be non-negative at all times. Interestingly, this same conclusion follows directly from the fact that the negatives of (augmented) burnup matrices are Z-matrices. The following theorem is from [12]:

Theorem 3.2.4. $e^{\boldsymbol{A}t} \geq 0$ *for all* $t \geq 0$ *if and only if* $-\boldsymbol{A}$ *is a Z-matrix.*

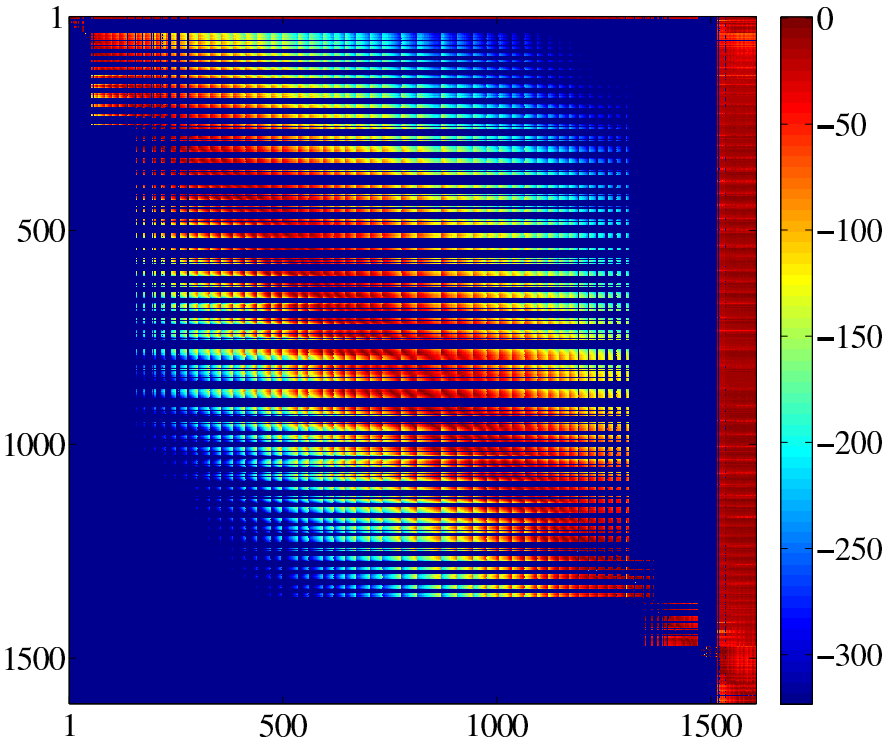

Figure 3.9. Plot of the matrix elements $\boldsymbol{E} = e^{\boldsymbol{A}t}$ with $t \approx 8.64 \times 10^5$ s on a logarithmic scale. The matrix $\boldsymbol{E}$ was computed with MATLAB's Symbolic toolbox using high-precision arithmetics.

Due to the previous theorem, the negatives of Z-matrices are sometimes called *essentially non-negative*. Figure 3.9 shows a plot of the matrix exponential for an augmented burnup system with 1606 nuclides. Notice that a zero element $E_{ij} = 0$ in the figure means that there is no transmutation path from nuclide j to nuclide i. Especially, the rows $2, \ldots, 6$ corresponding to the by-product nuclides have zero elements, since no nuclides are produced from these nuclides. It can also be seen from the figure that the elements with the greatest magnitude are gathered around the diagonal. This in accordance with the reasoning that the longer and more complex a particular transmutation path, the less likely it is to contribute to the respective nuclide concentration.

In some cases, it is useful to consider the norm $\|e^{\boldsymbol{A}t}\|$ as a function of time. For non-normal matrices, it is possible that the transient behavior of the system differs from the behavior at $t \to \infty$. The following theorem from [10] gives a useful relationship between $e^{\boldsymbol{A}t}$ and the resolvent $(z\boldsymbol{I} - \boldsymbol{A})^{-1}$.

Theorem 3.2.5. *Let $\boldsymbol{A} \in \mathbb{C}^{n\times n}$ and let $\omega \in \mathbb{R}$ and $M \geq 1$ be such that*

$$\|e^{\boldsymbol{A}t}\| \leq Me^{\omega t} \quad \forall\, t \geq 0\,. \tag{3.23}$$

For any $z \in \mathbb{C}$ with $\mathrm{Re}\, z > \omega$ in the resolvent set of $\boldsymbol{A}$ it holds

$$(z\boldsymbol{I} - \boldsymbol{A})^{-1} = \int_0^\infty e^{-zs} e^{s\boldsymbol{A}}\, ds\,, \tag{3.24}$$

and

$$\| (z\boldsymbol{I} - \boldsymbol{A})^{-1} \| \leq \frac{M}{\mathrm{Re}\, z - \omega}\,. \tag{3.25}$$

In the case of conventional burnup matrices, the number of nuclides increases only through fission. As explained in Section 3.1.1, there are generally no transmutation paths from fission product nuclides back to fissionable nuclides. Therefore, the total number of nuclides in the system is bounded. The element $E_{ij}(t)$ of $\boldsymbol{E}(t) = e^{\boldsymbol{A}t}$ is equal to the concentration of nuclide i at time t, assuming nuclide j is the only nuclide with a non-zero initial concentration and that this concentration is equal to unity. The column sum, $\sum_{i=1}^{n} E_{ij}(t)$, on the other hand, corresponds to the total number of nuclides in the system at time t, assuming an initial condition consisting of a single nuclide j. The norm $\|e^{\boldsymbol{A}t}\|_1$ is defined as the maximum absolute column sum of the matrix. Therefore, we can state that

$$\|e^{\boldsymbol{A}t}\|_1 \leq C\,, \tag{3.26}$$

where C is a constant equal to the maximum number of nuclides that can result from an initial state consisting of a single nuclide. In practise, there are always reactions competing with fission, for which reason the previous inequality holds for C smaller than the maximum number of fission product nuclides. However, C can always be chosen as the maximum number of nuclides produced in a fission.

Based on Theorem 3.2.5, we now obtain the following bound for the resolvent in 1-norm:

Theorem 3.2.6. *Let $\boldsymbol{A} \in \mathbb{R}^{n\times n}$ be a (conventional) burnup matrix. Then for any $\mathrm{Re}\, z > 0$*

$$\| (z\boldsymbol{I} - \boldsymbol{A})^{-1} \|_1 \leq \frac{C}{\mathrm{Re}\, z}\,. \tag{3.27}$$

3.2.3 Numerical computation

In general, there are various numerical methods for computing the matrix exponential. However, the suitability of a particular method depends on the characteristics of the problem under consideration. When considering the efficiency of a particular method, there are a few cases that should be distinguished. First of all, computing $e^{\boldsymbol{A}t}$ for a single value of t is different from computing it for several values of t. Also, the case where the full matrix $e^{\boldsymbol{A}t}$ is required differs from the case where only the action of the matrix exponential on a vector is needed, i.e. $e^{\boldsymbol{A}t}\boldsymbol{y}$ for some $\boldsymbol{y} \in \mathbb{R}^n$.

In burnup calculations, the objective is generally to compute the nuclide concentrations at time step t, i.e. the product $e^{\boldsymbol{A}t}\boldsymbol{n}_0$ for a single value of t and a single nuclide initial concentration vector $\boldsymbol{n}_0$. The full matrix exponential is occasionally needed in special applications, where it is important to know the contributions from individual

nuclides. As mentioned previously, the time steps used in burnup calculations typically vary from a few days at the beginning of the irradiation cycle to a few hundred days at the end. When considering nuclear fuel outside the reactor, the burnup equations reduce to equations describing radio-active decay, and the time steps can in principle extend to thousands of years.

Due to the extensive variations in the magnitudes of the burnup matrix elements, the computation of matrix exponential has previously been considered infeasible for entire burnup systems. Instead, simplified burnup chains have been used, or the most short-lived nuclides have been treated separately when computing a matrix exponential solution. For example, in the ORIGEN [14] code, the matrix exponential is computed with the truncated Taylor series method with scaling and squaring, after excluding short-lived nuclides from the burnup matrix to be treated separately. In the AEGIS code, a Krylov subspace method is applied to a simplified burnup chain with 221 nuclides, in which case the burnup matrix norm is of the order of 10^{-2} [15]. These frameworks are considered briefly in the following.

Truncated Taylor series is perhaps the most obvious numerical method for computing the matrix exponential. The main limitation of this approach is related to round-off errors. In some cases, even increasing the number of terms does not improve accuracy due to the accuracy limitations in the computer arithmetics. The applicability range of the method can be extended by the method of *scaling and squaring*, which is based on the identity

$$e^{\boldsymbol{A}t} = \left(e^{\boldsymbol{A}t/m}\right)^m \quad , \tag{3.28}$$

where m can be taken as a power of two, $m = 2^k$, so that the norm $\|\boldsymbol{A}/m\|$ becomes sufficiently small. In this context is should be pointed out that the method of scaling and squaring is only applicable to computing the full matrix $e^{\boldsymbol{A}t}$ and it cannot be applied, when only the vector $e^{\boldsymbol{A}t}\boldsymbol{y}$ is desired.[6] Unfortunately, the squaring phase of the scaling and squaring method may lead to a loss of accuracy due to round-off errors in the canceling of large elements [16]. In ORIGEN [14], the fastest transitions are removed from the burnup system in order for the matrix norm to meet the criterion

$$\min\left\{\|\boldsymbol{A}t\|_1,\ \|\boldsymbol{A}t\|_\infty\right\} < -2\,\log(0.001) \approx 13.8155$$

before the computation of the matrix exponential. This corresponds to removing nuclides i for which $e^{a_{ii}t} < 0.001$ [14].

In Krylov methods, the computation of the product $e^{\boldsymbol{A}t}\boldsymbol{n}_0$ is made more affordable by projecting the matrix $\boldsymbol{A}$ to a lower-dimensional Krylov subspace. The projection can be carried out with the Arnoldi iteration, which results in m iteration steps to the partial Hessenberg reduction

$$\boldsymbol{A}\,\boldsymbol{Q}_m = \boldsymbol{Q}_m\,\boldsymbol{H}_m + h_{m+1,m}\,\boldsymbol{q}_{m+1}\,\boldsymbol{e}_m^{\mathsf{T}} \ , \tag{3.29}$$

[6] When computing $e^{\boldsymbol{A}t}\boldsymbol{y}$, the norm of $\boldsymbol{A}t$ can only be reduced by dividing the time step t into smaller sub-steps and by repeating the computation for each sub-step.

where $\boldsymbol{Q}_m \in \mathbb{R}^{n\times m}$ is orthogonal, $\boldsymbol{H}_m \in \mathbb{R}^{m\times m}$ is a Hessenberg matrix, and $m < n$. The matrix exponential solution can then be approximated as

$$e^{\boldsymbol{A}t}\boldsymbol{n}_0 \approx \|\boldsymbol{n}_0\|\,\boldsymbol{Q}_m\, e^{\boldsymbol{H}_m t}\boldsymbol{e}_1 \,, \tag{3.30}$$

where the product $e^{\boldsymbol{H}_m t}\boldsymbol{e}_1$ for the small and dense matrix $\boldsymbol{H}_m$ can be computed by any suitable algorithm. The eigenvalues of $\boldsymbol{H}_m$, called the Ritz values, are typically close to the eigenvalues of $\boldsymbol{A}$ near the edge of the spectrum. The accuracy of the Krylov approximation may be compromised if these extreme eigenvalues are not representative of the original problem, which clearly is the case with burnup matrices. Besides, Krylov subspace methods are generally motivated by the original problem being too large to be solved directly, the typical applications including matrices arising from the discretization of a differential equation. In this context, burnup matrices can be regarded relatively small considering that polynomial or rational approximations can easily be applied directly to them. Therefore, the solution of burnup equations falls out of the scope of the application area of Krylov subspace methods.

The methods described above have been previously used for solving the burnup equations. In addition to these, another method worth mentioning is the rational Padé approximation of the exponential function. Padé approximation with scaling and squaring can be considered the most established matrix exponential method, and it is the method implemented in MATLAB's matrix exponential function `expm` [17]. The (k, m) Padé approximant of the exponential function is defined as the rational function $r_{km}(x) = p_{km}(x)/q_{km}(x)$ such that

$$p_{km} = \sum_{j=0}^{k} \frac{(k+m-j)!\,k!}{(k+m)!\,(k-j)!}\,\frac{x^j}{j!} \tag{3.31}$$

and

$$q_{km} = \sum_{j=0}^{m} \frac{(k+m-j)!\,m!}{(k+m)!\,(m-j)!}\,\frac{(-x)^j}{j!} \,. \tag{3.32}$$

This approximation can be shown to fit the exponential function e^x to the order $(m+n)$ at the origin, i.e.

$$\left(\frac{d^j r_{km}(x)}{dx^j}\right)_{x=0} = 1 \,, \quad j = 0, 1, \ldots, m+n \,. \tag{3.33}$$

The accuracy of the approximant is restricted near the origin, and for this reason it is generally applied together with the method of scaling and squaring. When the matrix $\boldsymbol{A}$ is not diagonalizable and the matrix exponential is defined based on the Jordan decomposition according to Eq. (3.2.2), it is advantageous that the accuracy of the Padé approximation extends to the derivatives in the vicinity of the origin. However, without scaling and squaring the method yields poor results for matrices with eigenvalues far from the origin, and therefore this approach is not well-suited for solving the burnup equations, where the matrix norm is large and only the vector $e^{\boldsymbol{A}t}\,\boldsymbol{n}_0$ is desired.

3.3 Solution based on rational approximations near the negative real axis

The matrix exponential can be computed based on a rational function $r(z)$ that is known to be a good approximation to the function e^z in some region in the complex plane $\mathbb{C}$. According to Definition 3.2.3, the matrix exponential can be defined as a contour integral, with the integration path winding around the spectrum of the matrix. Therefore, calculating $e^{\boldsymbol{A}t}$ is essentially equivalent to evaluating contour integrals of the form

$$(e^{\boldsymbol{A}t})_{kl} = \frac{1}{2\pi i} \int_{\Gamma} e^z R_{kl}(z)\, dz \,, \tag{3.34}$$

where $\boldsymbol{R} = (z\boldsymbol{I} - \boldsymbol{A}t)^{-1}$, $R_{kl} = \mathcal{O}(1)$ when $z \to -\infty$, and the singularities of R_{kl} are the eigenvalues of $\boldsymbol{A}t$. Since the eigenvalues of (augmented) burnup matrices are confined to a region near the negative real axis, the integration contour can be extended to a parabolic or hyperbolic shape in the left complex plane. Because the integrand will decrease exponentially, these contour integrals can be approximated efficiently using quadrature formulas [18]. Interestingly, the quadrature formulas can be associated with rational functions, whose poles and residues are the nodes and weights of the numerical integration formula, respectively [18]. In addition, every rational function can be correspondingly interpreted as a quadrature formula applied to a contour integral in the left complex plane. This interpretation gives the following expression for the approximation error [18]:

$$I - I_N = \frac{1}{2\pi i} \int_{\Gamma'} \left(e^z - r(z)\right) R_{kl}(z)\, dz \,, \tag{3.35}$$

where Γ' is a contour that extends from $-\infty$ towards the origin, encircles the origin while remaining to the left of the poles of r, and then extends back to $-\infty$ without crossing the negative real axis at any point.

In Eq. (3.35), I_N denotes the integral of Eq. (3.34) approximated by some quadrature rule with N points. When deriving Eq. (3.35), the integration contour Γ is assumed to encircle the eigenvalues of $\boldsymbol{A}t$. Therefore, the accuracy of the rational approximation may suffer a break-down if the eigenvalues of $\boldsymbol{A}t$ fall outside the contour defined by the poles of the rational function. Interestingly, this phenomenon is not visible when only Definition 3.2.2 is considered.

The framework based on Cauchy integral formula has been considered in detail in the context of burnup equations [I, II]. This has drawn attention to the non-real eigenvalues of burnup matrices. Especially, the accuracy of a rational approximation optimal on the negative real axis is expected to be affected by the magnitudes of the eigenvalues' imaginary parts. Also, the method may suffer a break-down if some of the eigenvalues fall outside the integration contour implicitly defined by the rational approximation.

3.3.1 Partial fraction decomposition form

When approximating the matrix exponential, it is usually advantageous to employ the partial fraction decomposition (PFD) form of the rational function. Let $\pi_{k,l}$ denote the set of rational functions $r_{k,l}(x) = p_k(x)/q_l(x)$, where p_k is a polynomial of order k and q_k is a polynomial of order l. For a rational function $r_{k,k}$ with simple poles, the partial fraction decomposition is of the form

$$r_{k,k}(z) = \alpha_0 + \sum_{j=1}^{k} \frac{\alpha_j}{z - \theta_j} \,, \tag{3.36}$$

where α_0 is the limit of the function $r_{k,k}$ at infinity, and α_j are the residues at the poles θ_j:

$$\alpha_j = \frac{p_k(\theta_j)}{q_k'(\theta_j)} \,. \tag{3.37}$$

Also, rational functions in $\pi_{k-1,k}$ that have simple poles can be written in this form with $\alpha_0 = 0$.

When the coefficients of $r_{k,k}$ are real, its poles form conjugate pairs, so that the computational cost can be reduced to half for a real variable x:

$$r_{k,k}(x) = \alpha_0 + 2\,\mathrm{Re}\left(\sum_{j=1}^{k/2} \frac{\alpha_j}{x - \theta_j}\right) \tag{3.38}$$

and for a real matrix $\boldsymbol{A} \in \mathbb{R}^{n\times n}$, the rational function may be computed as

$$r_{k,k}(\boldsymbol{A}t)\boldsymbol{n}_0 = \alpha_0 \boldsymbol{n}_0 + 2\,\mathrm{Re}\left(\sum_{j=1}^{k/2} \alpha_j (\boldsymbol{A}t - \theta_j \boldsymbol{I})^{-1} \boldsymbol{n}_0\right) . \tag{3.39}$$

It can be seen from Eq. (3.39) that computing a rational approximation $r_{k,k}(\boldsymbol{A}t)$ requires solving $k/2$ linear systems.

When no nuclides are excluded from the burnup computation, the dimensions of the burnup matrix are generally between 1200 and 1700, making the linear systems relatively large. The numerical characteristics of burnup matrices, discussed in Section 3.1, may compromise the accuracy of widely used iterative solvers, many of which are based on Krylov subspace techniques whose convergence is ultimately related to the spectral properties of the matrix at hand. Luckily, the nearly upper triangular sparsity pattern of burnup matrices, depicted in Fig. 3.1 for example, can be utilized by employing a direct method. A method based on sparse Gaussian elimination has been implemented to the reactor physics code Serpent. The suitability and characteristics of this method in the context of burnup equations are analyzed in detail in [IV].

3.3.2 Chebyshev rational approximation method (CRAM)

In Chebyshev Rational Approximation Method (CRAM), the rational function $\hat{r}(z)$ is chosen as the best rational approximation of the exponential function on the negative

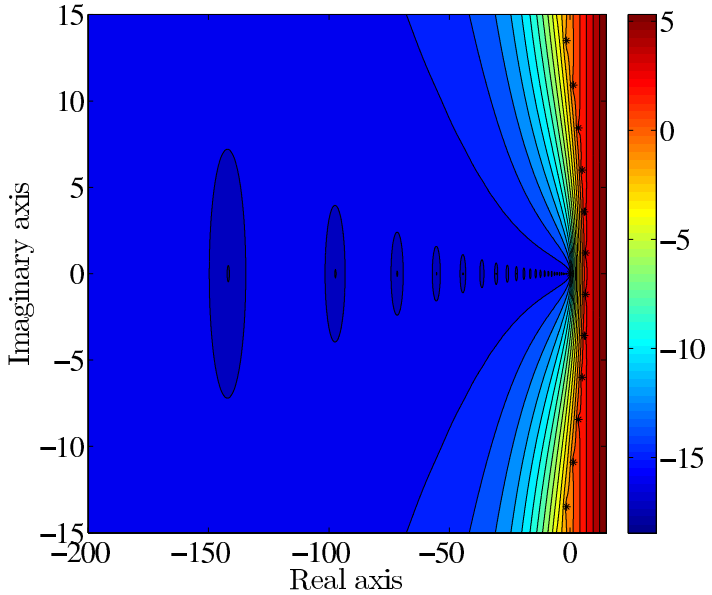

Figure 3.10. Plot of $\log_{10}|e^z - \hat{r}_{16,16}(z)|$ illustrating the accuracy of CRAM of order 16 in the complex plane. The poles of $\hat{r}_{16,16}$ have been marked with black asterisks.

real axis $\mathbb{R}_-$. Let π denote the set of rational functions $r_{k,k}(x) = p_k(x)/q_k(x)$, where p_k and q_k are polynomials of order k. The CRAM approximation of order k is defined as the unique rational function $\hat{r}_{k,k} = \hat{p}_k(x)/\hat{q}_k(x)$ satisfying

$$\hat{\varepsilon}_{k,k} \equiv \sup_{x\in\mathbb{R}_-} |\hat{r}_{k,k}(x) - e^x| = \inf_{r_{k,k}\in\pi_{k,k}} \left\{ \sup_{x\in\mathbb{R}_-} |r_{k,k}(x) - e^x| \right\}. \tag{3.40}$$

The asymptotic convergence of this approximation on the negative real axis is remarkably fast, with the convergence rate $\mathcal{O}(H^{-k})$, where $H = 9.289\,025\,49\ldots$ is called the Halphen constant [19]. It was recently discovered by Stahl and Schmelzer [20] that this convergence extends to compact subsets on the complex plane and also to Hankel contours in $\mathbb{C}\setminus\mathbb{R}_-$, i.e. to contours that extend from $-\infty$ around the origin clockwise back to $-\infty$ without crossing the negative real axis. Figure 3.10 illustrates the accuracy of CRAM of order 16 in the left complex plane. It should be noticed that the accuracy of the approximation is not confined merely to the negative real axis, but extends to a wide region near it. Also, the function is relatively flat in the direction of the imaginary axis.

On the negative real axis, the deviation between the approximation $\hat{r}_{k,k}$ and the exponential function equioscillates between $-\hat{\varepsilon}_{k,k}$ and $\hat{\varepsilon}_{k,k}$. As $x \to -\infty$, the exponential function tends to zero, whereas CRAM of order k stabilizes to $\hat{\varepsilon}_{k,k}$. This is illustrated in Figure 3.11 which shows a plot of $\hat{r}_{16,16}$ on the negative real axis. Therefore, as $x \to -\infty$, the *relative* accuracy of $\hat{r}_{k,k}$ deteriorates. This is illustrated in Figure 3.12, which shows the relative error of CRAM of order 16 on the negative

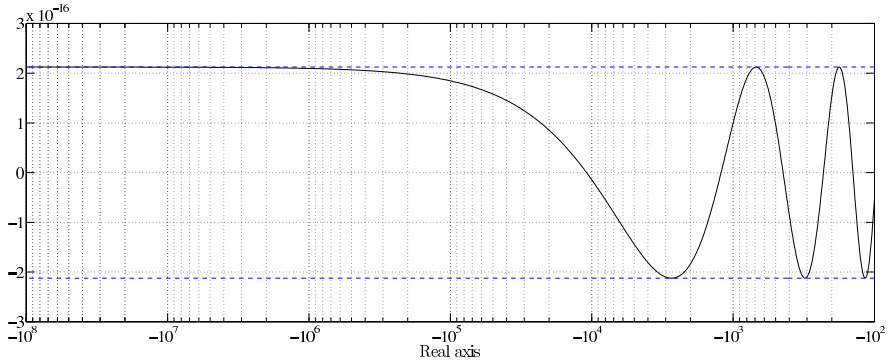

Figure 3.11. Plot of $\hat{r}_{16,16}(x)$ on the negative real axis.

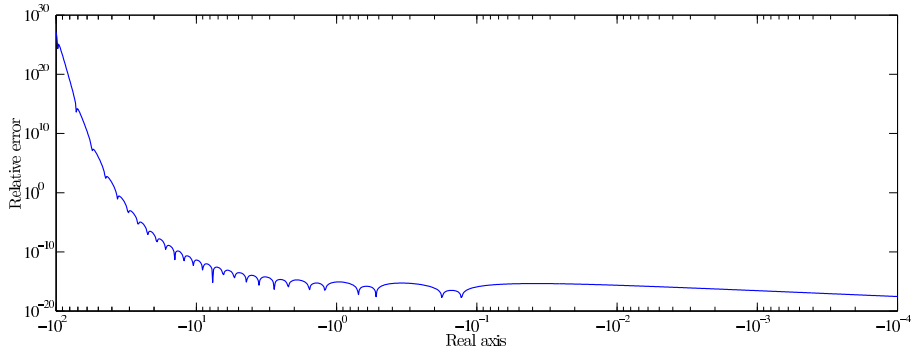

Figure 3.12. Plot of $|e^x - \hat{r}_{16,16}(x)|\, e^{-x}$ illustrating the relative accuracy of CRAM of order 16 on the negative real axis.

real axis. In this context, it should be mentioned that it is generally impossible to derive best approximations with respect to relative error.

The main difficulty in using CRAM is determining the coefficients of the rational function for a given k. In principle, the polynomial coefficients of $\hat{p}_k$ and $\hat{q}_k$ can be computed with Remez-type methods, but this requires delicate algorithms combined with high-precision arithmetics. Fortunately, these coefficients have been computed to a high accuracy by Carpenter et al. for approximation orders $k = 0, 1, \ldots, 30$, and they are provided in [21]. Although the PFD coefficients can in principle be computed from the polynomial coefficients, the computation of the polynomial roots may be ill-conditioned and requires great care. The PFD coefficients for approximation orders 10 and 14 have been provided in [22], and the given coefficients for $k = 14$ have been used in several applications, including the matrix exponential computing package EXPOKIT [23]. However, it was recently observed that the coefficients reported in [22] contain errors and do not correspond to the true best approximation [II]. After discovering the erroneous behavior induced by the coefficients from [22], partial fraction coefficients for approximation orders $k = 14$ and $k = 16$ were computed from

the polynomial coefficients provided in [21] and subsequently reported in [II] and [III].

The application of CRAM to computing the matrix exponential was originally made famous by Cody, Meinardus, and Varga in 1969 in the context of rational approximation of e^{-x} on $[0, \infty)$, and it was recently resurfaced by Trefethen, Weideman, and Schmelzer [18]. The application of CRAM to burnup equations was first considered in [I] and [II] and it was later compared to other depletion algorithms in [24]. The main conclusions are briefly summarized here. Overall, CRAM has been shown to give a robust and accurate solution to burnup equations with high computational efficiency. In contrast to other matrix exponential methods considered previously, CRAM can be applied to large burnup problems containing over thousand nuclides and with the matrix norm being of the order of 10^{21}. In this context, CRAM has been demonstrated to allow time steps of the order of 10^7 s, which can be considered to be the maximum feasible time step in burnup calculations. The convergence rate of CRAM, when applied to burnup equations, has been close to the asymptotic convergence rate on the negative real axis. [II]

It has been observed that the accuracy of CRAM depends relatively little on the characteristics of the problem at hand, such as the nuclear fuel or the neutron spectrum in the system [24]. However, it has been noticed that CRAM gives less accurate results for fresh fuel cases compared to depleted fuel cases [24]. It has been suggested that the reduced relative accuracy is related to the longer and more complex burnup chains being computed less accurately with CRAM [24]. When the fuel is fresh, only a few elements of $\boldsymbol{n}_0$ are nonzero, and all the nuclides are produced solely from these initial nuclides. For a large part of nuclides, this means both long and complex transmutation chains being emphasized in the result. This reasoning was later supported based on computing the full matrix $\hat{r}_{16,16}(\boldsymbol{A}t)$ explicitly [II].

As discussed in Section 3.1.2, burnup matrices are generally diagonalizable, although the imprecision of decay data may compromise this property in some cases. It is nonetheless fruitful to study the approximation error of CRAM from this perspective. Assuming a diagonal decomposition according to Eq. (3.19), we obtain the following expression for the approximation error of CRAM of order k, when applied to burnup equations:

$$\varepsilon_{k,k}(t) = \boldsymbol{T}\left(e^{\boldsymbol{\Lambda}t} - \hat{r}_{k,k}(\boldsymbol{\Lambda}t)\right)\beta\,, \tag{3.41}$$

where $\beta = \boldsymbol{T}^{-1}\boldsymbol{n}_0$. Let us consider this error as a function of time. When the eigenvalues of $\boldsymbol{A}$ are located strictly on the negative real axis, the elements of $\varepsilon_{k,k}$ are expected to oscillate until $\hat{r}_{k,k}(\lambda_j t)$ has stabilized to $\hat{\varepsilon}_{k,k}$ for all the eigenvalues λ_j. Otherwise, as t increases, the non-real eigenvalues of $\boldsymbol{A}t$ shift along lines, whose slopes are determined by the ratio of their real and imaginary parts. In theory, the error according to Eq. (3.41) may increase as a function of time if the eigenvalues shift to a region where the accuracy of the approximation $\hat{r}_{k,k}$ is notably worse than on the negative real axis. In particular, in accordance with Definition 3.2.3, the approximation error increases significantly when the contour implicitly defined by the rational approximation is crossed. However, based on discussion in Section 3.1.2, this scenario seems highly unlikely. Therefore, it can be deduced that the absolute error related to a CRAM solution to burnup equations is not expected to increase as

a function of time.

If the burnup matrix is not diagonalizable due to a multiple eigenvalue $\tilde{\lambda}$ with index l, the error related to this eigenvalue can be traced back to the deviation between the exponential function and the derivatives $\hat{r}_{k,k}(\tilde{\lambda}), \hat{r}'_{k,k}(\tilde{\lambda}), \ldots, \hat{r}^{(l-1)}_{k,k}(\tilde{\lambda})$. However, the previous reasoning still applies in the sense that the absolute approximation error is not expected to increase as a function of time.

We are usually interested in the *relative* accuracy of the solution, i.e. we want to know how many of its digits are correct. Based on previous discussion, the absolute error of the solution is not expected to increase, but oscillate as a function of time. Therefore, the time behavior of the relative error depends mainly on the nuclide concentration $n_i(t)$. It is clear that if a nuclide concentration diminishes significantly during the time step considered, the relative accuracy of the CRAM solution may be compromised.

To further study the accuracy of CRAM in the context of burnup equations, CRAM of order 16 was applied to two test cases, which are considered in the following. The first test case considers a small burnup system, which allows the approximation error to be analyzed in more detail. The second test case considers a decay system, i.e. burnup equations in the absence of neutron irradiation.

Application to a small test problem

In this section CRAM is applied to a small burnup system, which was formed by selecting the 36 lightest nuclides (from ^{1}H to ^{18}O) from the burnup chain of 1606 nuclides corresponding to a PWR pin-cell with fuel irradiated to 0.1 MWd/kgU burnup. The corresponding burnup matrix is shown in Fig. 3.3. For this test case, the burnup matrix norm is of the order of 10^{21}, the shortest transition being the decay of of ^{7}B whose half-life is of the order of 10^{-24} seconds.

The spectrum of this small test case matrix captures well the relevant properties of burnup matrices. The matrix has a single positive eigenvalue, $z_+ \approx 4.15 \times 10^{-12}$, and zero as a threefold eigenvalue. The rest of the eigenvalues are plotted in Figure 3.13. The two eigenvalues with non-zero imaginary parts are related to the submatrix $\tilde{\boldsymbol{A}} \in \mathbb{R}^{4\times 4}$ corresponding to the by-product nuclides ^{1}H, ^{2}H, ^{3}H, and ^{3}He. In accordance with Theorem 3.1.8, the eigenvalue zero is semisimple and the matrix is diagonalizable.

The exponential of the burnup matrix is depicted in Fig. 3.14, and the relative error of CRAM of order 16 applied to the same matrix is shown in Fig. 3.15 on a logarithmic scale. It can be seen from Fig. 3.15 that the approximation is very accurate for almost all matrix elements. The three greatest errors, ($D_{23,23} \approx 2.44 \times 10^{-1}$, $D_{18,18} \approx 4.11 \times 10^{-2}$ and $D_{23,18} \approx 3.76 \times 10^{-4}$), plotted in red, correspond to nuclides ^{12}Be (index 23) and ^{12}B (index 18) that are both short-lived, with half-lives of the order of milliseconds.

In this test case, the nuclide ^{12}B is not formed from any other nuclide and it forms its own strongly connected component. The relative accuracy of the matrix element $\widehat{E}_{18,18}$ is determined solely by the relative accuracy of $\hat{r}_{16,16}$ at the corresponding

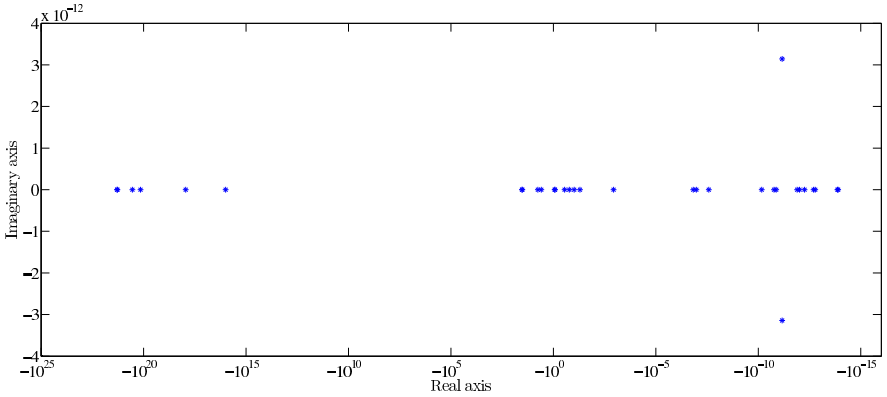

Figure 3.13. A plot of the eigenvalues $z \in \{z \in \mathbb{C} \,|\, z \in \Lambda(\boldsymbol{A}), \text{Re}\, z < 0\}$ for the test case with 36 nuclides. In addition, the matrix has a single positive eigenvalue, $z_+ \approx 4.15 \times 10^{-12}$, and zero as a threefold eigenvalue.

eigenvalue $z_1 = A_{18,18} \approx -32.5$. The nuclide ^{12}Be forms a SCC with 6 other nuclides, and the matrix element $E_{23,18}$ is a linear combination of eight different modes, 7 of them corresponding to the SCC, and one to the decay of ^{12}B to ^{12}Be. When considering the element $E_{23,18}$, the eigenvalues corresponding to the transition $^{12}\text{B}\rightarrow{}^{12}\text{Be}$ and the effective removal rate of the nuclide are the most important. Therefore, the accuracy of the $\widehat{E}_{23,18}$ is dominated by the relative accuracy of $\hat{r}_{16,16}$ at these two eigenvalues $z_1 \approx -32.5$ and $z_2 \approx -34.3$. The same reasoning applies to the element $\widehat{E}_{23,23}$, for which the most significant mode corresponds to the eigenvalue $z_2 \approx -34.3$.

As can be seen from Figs. 3.14 and 3.15, there is a clear trend in that the relative errors tend to be greater for the matrix elements with smaller values. However, even arbitrarily small matrix elements can be captured with amazing accuracy by CRAM, if the relative accuracy of the approximation is good at the eigenvalues corresponding to the relevant modes. For example, the matrix element $E_{17,23} \approx 1.73 \times 10^{-69}$ is computed to 8 correct digits with CRAM of order 16. The index 17 corresponds to the nuclide ^{10}Be which belongs to the same SCC as ^{12}Be. For this matrix element, the most significant modes correspond to eigenvalues $z \in [-10^{-13}, -10^{-14}]$.

Figure 3.16 shows the test case nuclide concentrations and Fig. 3.17 the respective approximation error of $\hat{r}_{16,16}$ as a function of time between 10 s and 10^{12} s $\approx$ 32 000 years. The reference solutions were computed with MATLAB's Symbolic Toolbox using high-precision arithmetics. As can be seen from the the figure, for $t \in [10,\ 10^{10}]$ s, the approximation error is the greatest for nuclides, whose concentrations diminish the most rapidly. The trend that these errors begin to diminish for time steps greater than 10^6 s is explained by the fact that after this time the respective nuclide concentrations begin to increase as a function of time. It should be pointed out that the concentration of ^{12}Be falls to zero so rapidly that its concentration and the respective approximation error were not included in the plots. It is interesting that

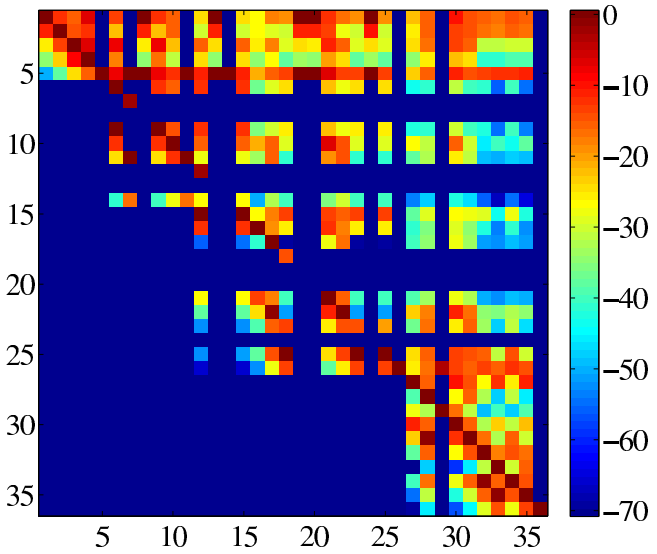

Figure 3.14. Plot of the matrix elements $\boldsymbol{E} = e^{\boldsymbol{A}}$ on a logarithmic scale. The matrix $\boldsymbol{E}$ was computed with MATLAB's Symbolic Toolbox with high-precision arithmetics.

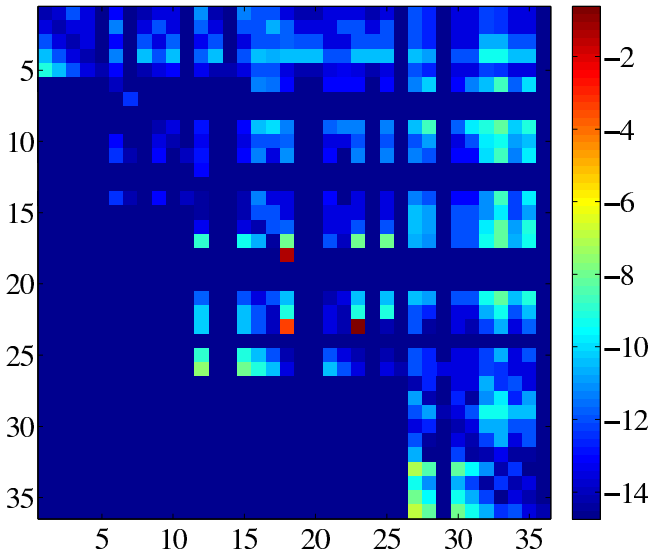

Figure 3.15. Relative error of CRAM of order 16 when applied to the burnup matrix corresponding the test case with 36 nuclides, i.e. plot of matrix $\boldsymbol{D}$ defined as $D_{ij} = \log_{10}\left(\frac{E_{ij}(1)-\widehat{E}_{i,j}(1)}{E_{ij}(1)}\right)$, where $\widehat{\boldsymbol{E}} = \hat{r}_{16,16}(\boldsymbol{A})$.

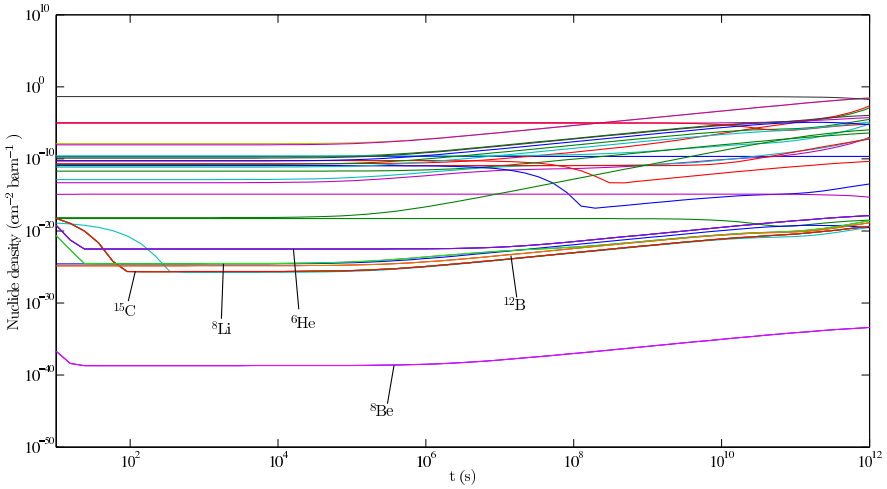

Figure 3.16. Nuclide concentrations corresponding the small test case with 36 nuclides.

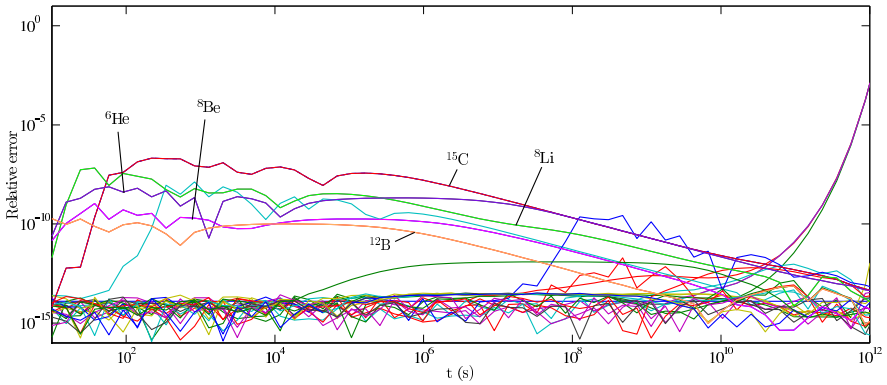

Figure 3.17. The relative errors of CRAM solution of order 16 for the nuclide concentrations corresponding to the small test case with 36 nuclides.

although the approximation error is comparatively large for the matrix element $\widehat{E}_{18,23}$, corresponding the transition ^{12}Be$\rightarrow{}^{12}$B, the error is much smaller for the concentration of ^{12}B. This is due to the accuracy of the solution being dominated by the matrix elements corresponding to the greatest initial nuclide densities. When $t \rightarrow 10^{12}$ s, $z_+ t \rightarrow 1$, and the accuracy of the approximation begins to deteriorate for the by-product nuclides ^{1}H, ^{2}H, ^{3}H, and ^{3}He corresponding to the positive eigenvalue z_+. This results from the accuracy of $\hat{r}_{16,16}$ quickly deteriorating on the positive real axis.

The test case nuclide concentrations and the approximation error of CRAM of order 16 for time steps between $t = 10^{12}$ s $\approx$ 32 000 years and $t = 10^{20}$ s $\approx 3.2 \times 10^{12}$ years

are shown in Figures 3.20 and 3.21. Time steps of this magnitude are clearly not feasible in burnup calculations, but they are considered here to further study the characteristics of the approximation. As can be seen from Figure 3.20, the concentrations of the by-product nuclides begin to increase very rapidly for time steps greater than 10^{12} s. This increase is not captured by the CRAM approximation that virtually breaks down on the positive real axis. Therefore, the relative error of the by-product nuclide concentrations quickly stabilizes to unity. For time steps greater than 10^{14} s, these concentrations are rounded off to infinity in computer arithmetics, after which the respective relative errors are no longer well-defined. Large oscillations in the error curves after $t = 10^{15}$ s $\approx 7.6 \times 10^8$ years are explained by the oscillation of $\hat{r}_{16,16}$ around the negative real axis. The stabilized nuclide concentrations, plotted in green and blue, correspond to ^{12}C and ^{18}O, which do not elicit any neutron nor decay reactions based on the data used in the test case.

Application to a decay system

In the absence of neutron irradiation, nuclides transform to other nuclides merely through radioactive decay and the burnup equations reduce to decay equations. The decay paths do not form closed cycles and therefore the decay matrix can be permuted to upper triangular form. It follows that the eigenvalues of decay matrices are known to be strictly confined to the negative real axis. The lack of closed loops causes a great part of the nuclide concentrations to diminish rapidly in comparison to burnup cases. Based on the previous discussion, this is expected to affect the relative accuracy of the CRAM solution.

In this section, CRAM is applied to a decay system consisting of 1531 nuclides. Compared to the burnup cases considered previously, the decay matrix is significantly sparser. Figure 3.20 shows the nuclide concentrations of the test case actinides as a function of time. The reference solutions were computed with MATLAB's Symbolic Toolbox using high-precision arithmetics. As can be seen from the figure, several of the nuclide concentrations fall quickly to zero after the time step $t \sim 10^4$ s, and this trend becomes stronger as t increases. Figure 3.21 shows the relative error of CRAM of order 16 for the respective nuclide concentrations. By comparing these figures, it is evident that the relative accuracy of the CRAM solution deteriorates as the nuclide concentrations diminish.

Let us consider the approximation error of CRAM as a function of time assuming the diagonalizability of the decay matrix in which case the error satisfies Eq. (3.41). As explained previously, the CRAM approximation of order k approaches $\hat{\varepsilon}_{k,k}$ as $x \to -\infty$, whereas the exponential function falls to zero. If a nuclide concentration $n_i(t)$ diminishes drastically during the time step t, it can be anticipated that $-\lambda_j t \gg 1$ for all the relevant eigenvalues. In this case, it can be approximated $e^{\lambda_j t} - \hat{r}_{16,16}(\lambda_j t) \approx \hat{\varepsilon}_{k,k}$ for all these eigenvalues (see also Figure 3.12), and the following estimate can be

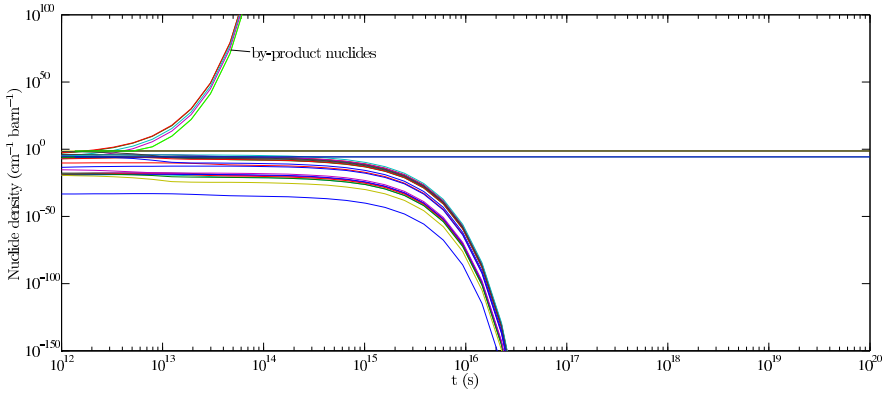

Figure 3.18. Nuclide concentrations corresponding the small test case with 36 nuclides for time steps greater than $t = 10^{12}$ s.

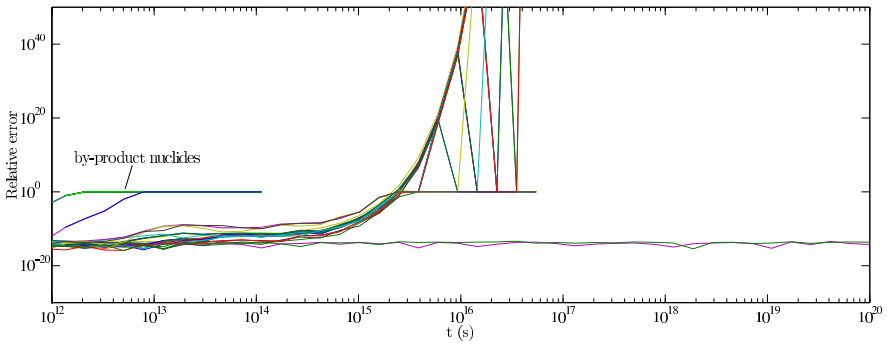

Figure 3.19. The relative errors of CRAM solution of order 16 for the nuclide concentrations corresponding to the small test case with 36 nuclides for time steps greater than $t = 10^{12}$ s.

derived for the approximation error:

$$\begin{aligned}\frac{\varepsilon_i(t)}{n_i(t)} &= \frac{|\sum_{j=1}^{n} T_{ij}\left(e^{\lambda_j t} - \hat{r}_{k,k}(\lambda_j t)\right)\beta_j|}{n_i(t)} \\ &= \frac{|\sum_{j=1}^{n}\sum_{m=1}^{n} T_{ij}\left(e^{\lambda_j t} - \hat{r}_{k,k}(\lambda_j t)\right) T_{jm}^{-1} n_m(0)|}{n_i(t)} \\ &\approx \frac{|-\hat{\varepsilon}_{k,k}\sum_{m=1}^{n}\sum_{j=1}^{n} T_{ij}\, T_{jm}^{-1} n_m(0)|}{n_i(t)} = \hat{\varepsilon}_{k,k}\frac{n_i(0)}{n_i(t)}\,. \end{aligned} \tag{3.42}$$

Equation (3.42) suggests that the relative accuracy of the CRAM solution deteriorates significantly if $n_i(t)$ becomes smaller than $\hat{\varepsilon}_{k,k}\, n_i(0)$. In other words, the value $\hat{\varepsilon}_{k,k}$ implicitly defines a numerical cut-off for the results. Therefore, concentrations $\hat{n}_i(t)$ smaller than $\hat{\varepsilon}_{k,k}\, n_j(0)$ (as given by CRAM of order k) should be treated as zero. How-

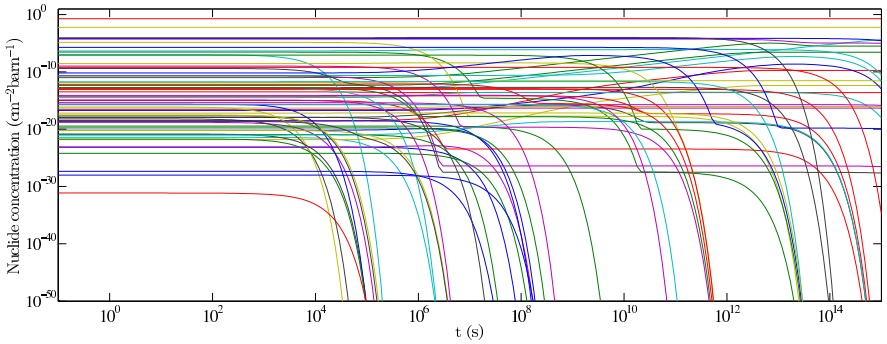

Figure 3.20. Concentrations of the actinides corresponding the decay system test case with 1531 nuclides.

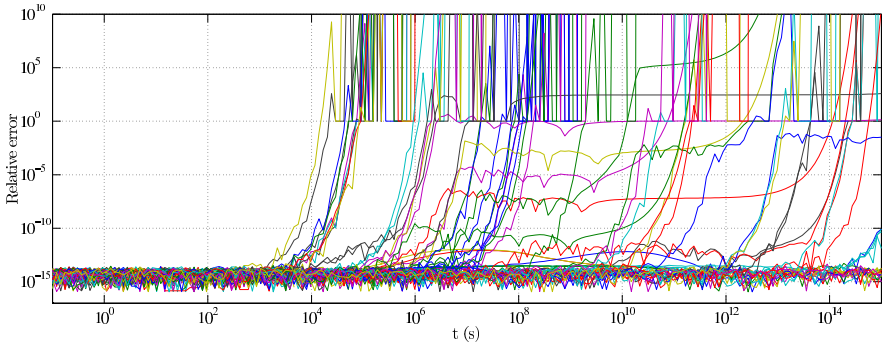

Figure 3.21. Relative error of the CRAM of order 16 solution for the actinides corresponding the decay system test case with 1531 nuclides.

ever, it should be emphasized that CRAM may also yield a reduced relative accuracy for the solution in other situations. Nonetheless, it is clear that nuclide concentrations smaller than $\hat{\varepsilon}_{k,k}\, n_j(0)$ have a poor relative accuracy when computed with CRAM of order k.

Figure 3.22 shows the nuclide concentrations for the time step $t = 10^7$ s $\approx$ 116 days, together with the concentrations given by CRAM of order 16. At this time, 1007 of the 1531 nuclides have concentrations smaller than $\hat{\varepsilon}_{16,16}$ times their initial concentrations. Let $\hat{\boldsymbol{n}}$ denote the solution given by CRAM of order 16. It can be clearly seen from the figure that the values of $\hat{n}_j$ saturate to $\hat{\varepsilon}_{16,16} n_j(0)$ when the reference solution n_j becomes smaller than this value.

Compared to the burnup cases considered previously in [I, II] and in [24], CRAM yields significantly less accurate results for this decay system. This clearly results from the nuclide concentrations diminishing faster than in burnup cases, where the nuclide chains contain more closed cycles. This supports the conclusion that the non-real eigenvalues of burnup matrices are not as relevant to the accuracy of CRAM

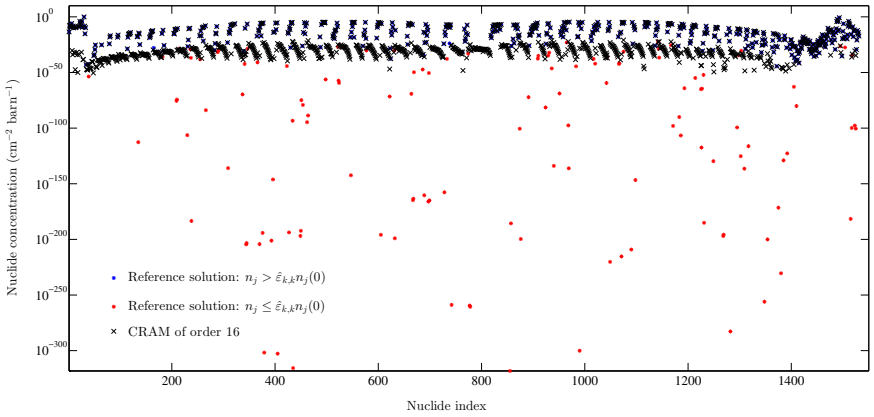

Figure 3.22. Test case nuclide concentrations for the time step $t = 10^7$ s given by a highly accurate reference solution and CRAM of order 16.

after all. Furthermore, CRAM should be used with caution in conjunction with decay systems. It should also be noted that the decay equations can be solved analytically by the linear chain method [25, 26]. In the development version of Serpent 2, the analytical method is used by default in the absence of neutron irradiation. Of course, problems can be encountered in reduced power cases, where an analytical solution cannot be found, but the nuclide concentrations diminish rather rapidly due to the neutron reactions being unlikely. In these applications, the length of the time step should be kept sufficiently small in order to guarantee the accuracy of the solution.

3.3.3 Rational approximations from contour integrals

As explained previously, the burnup matrix exponential can be defined as an integral along a contour with, for example, a parabolic or hyperbolic shape in the left complex plane. Because the integrand will decrease exponentially, these contour integrals can be approximated efficiently using quadrature formulas. These quadrature formulas can furthermore be interpreted as rational approximations that can be used to approximate the matrix exponential, the poles and residues of the function being the nodes and weights of the numerical integration formula [18]. This approach was first applied to the solution of burnup equations in [II].

As discussed previously, the application of these numerical integration schemes requires that the singularities of the integrand lie inside the contour. Therefore, the respective rational approximation is expected to give poorer results when the eigenvalues of $\boldsymbol{A}t$ fall outside the contour. This phenomenon is studied more closely in the context of burnup equations in the following subsection.

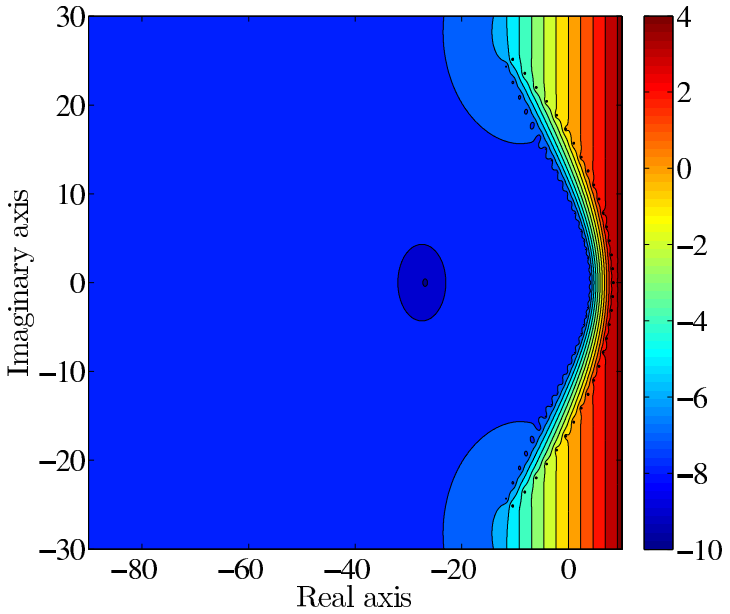

Figure 3.23. A plot of $\log_{10}|r_{31,32}(z) - e^z|$ in the complex plane. The 32 quadrature points (i.e. poles of $r_{31,32}$) have been marked with black dots in the plot.

Application to a test problem with 219 nuclides

In this section, a quadrature-based rational approximation is applied to a small burnup test case formed by selecting only the most important actinides and fission products, totalling in 219 nuclides. The test case represents a PWR pin-cell lattice in which the fuel has been irradiated to 25 MWd/kgU burnup. The chosen rational approximation is based on the following contour, suggested by Weideman [27] and later considered in [II]:

$$\phi : \mathbb{R} \to \mathbb{C}\,, \quad \phi(x) = N(0.1309 - 0.1149\,x^2 + i\,0.2500\,x)\,. \tag{3.43}$$

This contour is asymptotically optimal with the convergence rate of $\mathcal{O}(2.85^{-N})$, when singularities are located on the negative real axis. In this study, $N = 32$ quadrature points were chosen, which resulted in the rational function $r_{31,32} \in \pi_{31,32}$. The approximation error related to this rational function is shown in Figure 3.23.

The spectrum of the (conventional) burnup matrix corresponding to this test case is plotted in Figure 3.24. The burnup matrix has four pairs of eigenvalues with nonzero imaginary parts, the smallest of them being of the order of 10^{-13} and the largest of the order of 10^{-8}. As t increases, the eigenvalues of $\boldsymbol{A}t$ shift along lines, whose slopes are determined by the ratio of their real and imaginary parts. This is illustrated in Figure 3.25, which shows the lines corresponding to the four complex eigenvalues of $\boldsymbol{A}$ together with the parabolic contour for $N = 32$. As can be seen from the figure,

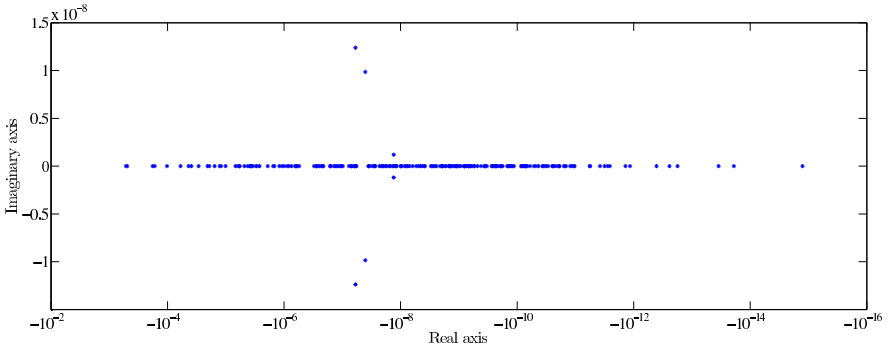

Figure 3.24. A plot of the eigenvalues $z \in \{z \in \mathbb{C} \,|\, z \in \Lambda(\boldsymbol{A}), \text{Re}\, z < 0\}$ for the test case with 219 nuclides. In addition, the matrix has zero as a twofold eigenvalue.

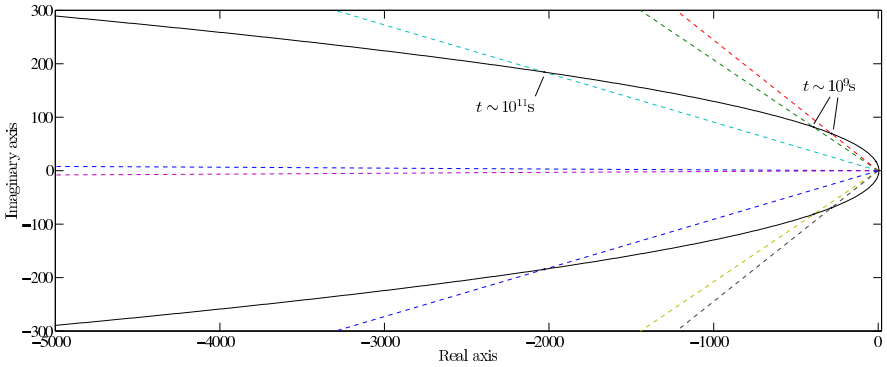

Figure 3.25. A plot of the lines $z = \lambda t$ (dashed line) for the four complex eigenvalues $\lambda \in \Lambda(\boldsymbol{A})$ and the parabolic contour of Eq. (3.43) (solid line) for $N = 32$.

two of the eigenvalues cross the contour when t is of the order of 10^9 s $\approx$ 32 years and one when t is of the order of 10^{11} s $\approx$ 3200 years. The eigenvalue with the smallest imaginary part crosses the contour when $t \sim 10^{13}$ s $\approx$ 0.32 million years.

Figure 3.26 shows the matrix exponential $e^{\boldsymbol{A}t}$ and the relative error related to $r_{31,32}(\boldsymbol{A}t)$ for $t = 10^8$ s $\approx$ 3.2 years, and Figure 3.27 the mean and maximum relative errors of the nuclide concentrations as a function of time. The error begins to increase notably when $t \to 10^{11}$ s. Figure 3.28 shows the relative errors plotted against the reference nuclide concentrations for the values $t \sim 10^8$ s and $t \sim 10^{11}$ s. Based on this figure, it appears that the increase in the relative error is again due to some of the nuclide concentrations tending to zero when $t \to \infty$. The impact of the eigenvalues shifting over the integration contour could not be detected by studying the error related to the elements of the matrix $r_{31,32}(\boldsymbol{A}t)$ at different time steps.

The fact that the complex eigenvalues are not manifested in the accuracy of the solution can be explained by investigating the rational approximation more closely.

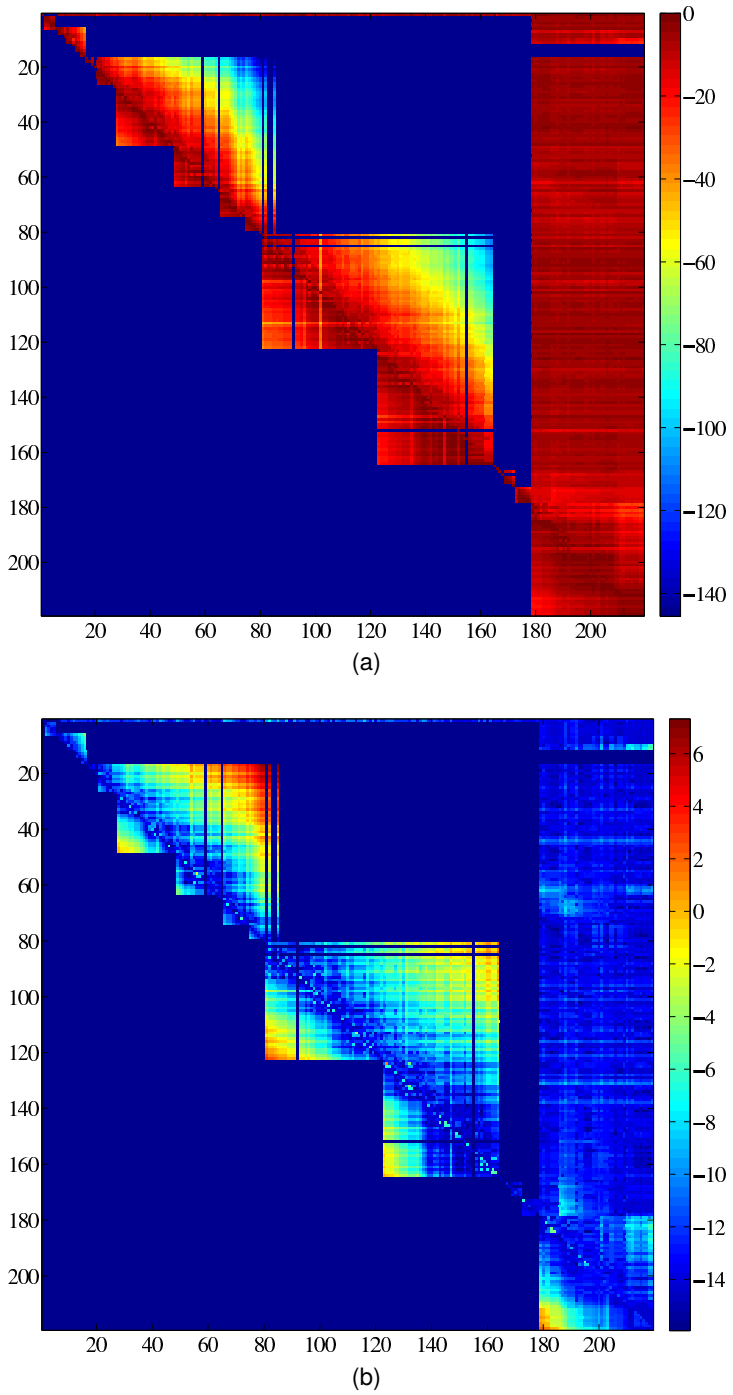

Figure 3.26. Plot of (a) the matrix elements $\boldsymbol{E} = e^{\boldsymbol{A}t}$, and (b) the relative error related to $r_{32,31}(\boldsymbol{A}t)$ for $t = 10^8$ s ≈ 3.2 years on a logarithmic scale.

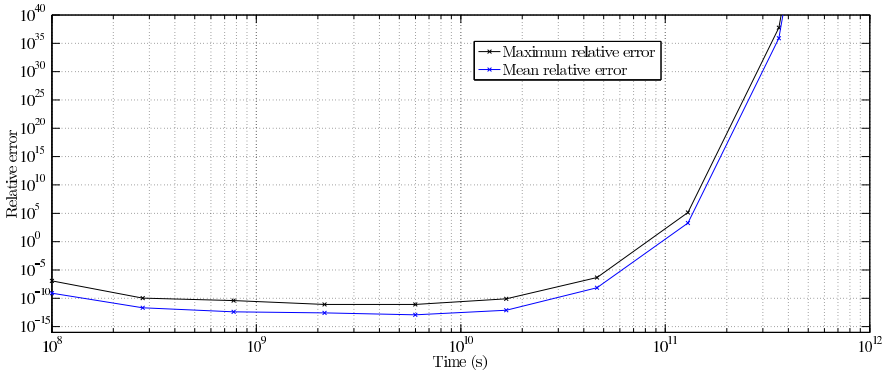

Figure 3.27. Mean and maximum relative errors of the quadrature-based solution as a function of time for the small test case with 219 nuclides.

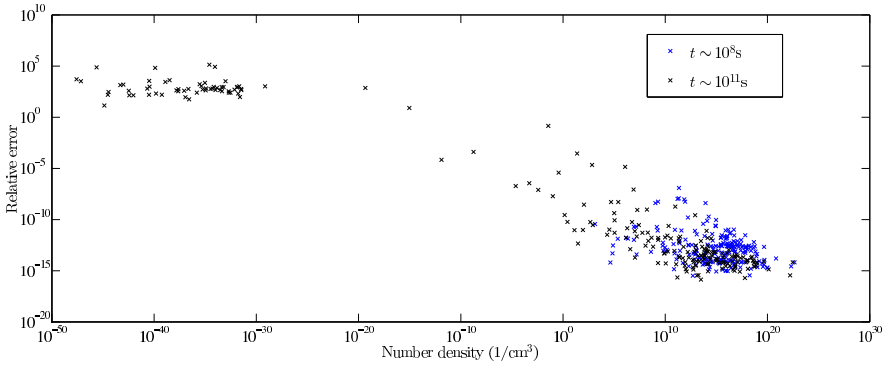

Figure 3.28. Plot of the relative error of the quadrature-based solution for time steps $t \approx 10^8$ s and $t \approx 10^{11}$ s for the small test case with 219 nuclides.

In accordance with Definition 3.2.3, it is clear that the integral along the contour of Eq. (3.43) no longer represents the matrix exponential, if some of the eigenvalues are located outside the contour. However, after applying the quadrature rule, the part of the contour extending beyond the quadrature points becomes irrelevant. Therefore, if the eigenvalues lying outside the contour are located far from the quadrature points (in the direction of the negative real axis), they are not expected to affect the accuracy of the solution. It can also be seen from Figure 3.23 that the accuracy of the approximation diminishes rapidly outside the contour near the quadrature points. However, on the left of the quadrature points the error function is basically flat. In this test case, the eigenvalues of $\boldsymbol{A}t$ fall outside the contour of Eq. (3.43) so far from the quadrature points that it is clear that this is not significant to the accuracy of the solution.

When the approximation order is increased, the part of the contour spanned by the quadrature points becomes greater. However, also the contour becomes broader

according to Eq. (3.43). For this test case, there is actually no approximation order for which the eigenvalues cross the contour in the part spanned by the respective quadrature points. It follows that the quadrature-based method does not break down due to the complex eigenvalues at any time step. However, as discussed previously, the relative accuracy of the solution diminishes as t increases. The complex eigenvalues of this small burnup matrix are very representative of the spectrum of burnup matrices in general. Therefore, this study supports the previous observation of the complex eigenvalues with small imaginary parts not being relevant to the accuracy of the quadrature-based solution in the context of burnup equations [II].

4. Perturbation theory based sensitivity and uncertainty analysis applied to criticality equation

When uncertain parameters are utilized in computations, also the calculation results contain uncertainty. In order to estimate the reliability of these calculations, it is necessary to develop uncertainty analysis methods enabling the propagation of parameter uncertainty through the calculations.

In recent years, the interest towards sensitivity and uncertainty analysis has increased notably in the field of nuclear engineering. In 2006, the OECD/NEA expert group on Uncertainty Analysis in Modelling decided to prepare a benchmark titled *Uncertainty Analysis in Best-Estimate Modelling (UAM) for Design, Operation and Safety Analysis of LWRs* [28] to establish the current state and needs of sensitivity and uncertainty analysis. The goal of the benchmark is to propagate uncertainty through all stages of coupled neutronics/thermal hydraulics calculations. The imprecision of neutron interaction data is likely one of the most significant sources of uncertainty in these calculations, and therefore the propagation of this uncertainty is considered to be the main priority at the moment. As a first step, this requires developing sensitivity and uncertainty analysis methods for fuel assembly codes that are used to produce homogenized data for coupled neutronics/thermal-hydraulics calculations.

This chapter describes the implementation of uncertainty analysis capability to the fuel assembly burnup calculation code CASMO-4 [29] in the context of the UAM benchmark. The developed uncertainty analysis methodology is deterministic, meaning that the uncertainties are computed based on the sensitivity profiles and covariance matrices for the uncertain nuclear data parameters. Sensitivity analysis studies the changes in system responses due to perturbations in the parameters. Perturbation theory provides an efficient technique to compute sensitivity profiles by utilizing the adjoint system of the original forward problem. At the time of launching the benchmark, the generally employed reactor physics codes did not have uncertainty analysis capabilities, and the modified CASMO-4 was one of the first fuel assembly programs that enabled sensitivity and uncertainty analysis based on perturbation theory.

4.1 Background for sensitivity and uncertainty analysis

Let us consider a mathematical model containing uncertain parameters. The objective of uncertainty analysis is to estimate how the uncertainty in these parameters is propagated to a response dependent on the solution of the problem under consideration. In this thesis the considered mathematical model is the neutron transport eigenvalue problem called the criticality equation, i.e. Eq. (2.5), which can be written in operator form as

$$\boldsymbol{A}\boldsymbol{\Phi} = \frac{1}{k}\boldsymbol{B}\boldsymbol{\Phi} \,, \tag{4.1}$$

where $\boldsymbol{\Phi} \in H_\Phi$ is the neutron flux, H_Φ is a Hilbert space, and k is the multiplication factor. The uncertain parameters consist of neutron cross-section data and they are denoted by the vector $\boldsymbol{\sigma} \in E_\sigma$, where E_σ is a normed linear space. It should be noted that both the continuous-energy criticality equation and the various systems derived from it in numerical computations can be written in the form of Eq. (4.1). For continuous-energy criticality equation, the Hilbert space under consideration is L^2. The considered responses are the critical eigenvalue k and ratios of the form

$$R(\boldsymbol{e}) = \frac{\langle \boldsymbol{\Phi}, \boldsymbol{\Sigma}_1 \rangle}{\langle \boldsymbol{\Phi}, \boldsymbol{\Sigma}_2 \rangle} \,, \tag{4.2}$$

where $\boldsymbol{\Sigma}_1, \boldsymbol{\Sigma}_2 \in H_\Phi$. Therefore, only functional responses are considered in this thesis. For example, few-group cross-sections homogenized over a geometry can be written in the form of Eq. (4.2).

The uncertainty of the parameters $\boldsymbol{\sigma}$ should be understood in terms of the Bayesian probability interpretation [30]. In this framework, probability is defined as a subjective measure that characterizes the plausibility of various hypotheses. When estimating parameters, all knowledge about a parameter σ_j is assumed to be incorporated into its marginal probability distribution $p(\sigma_j)$. This distribution is defined so that the integral $\int_a^b p(\sigma_j)\, d\sigma_j$ corresponds to the (Bayesian) probability that the value of σ_j belongs to the interval $[a, b]$. The distribution $p(\boldsymbol{\sigma})$ can then be used to form an estimate $\hat{\sigma}$ for the parameters and their associated uncertainties. In most cases either the mean value or the mode are chosen as $\hat{\sigma}$. Typically, the variance of the distribution is chosen to give a numerical value to the related uncertainty. When several parameters are considered simultaneously, the probability distribution under consideration is their joint distribution $p(\boldsymbol{\sigma})$, and the covariance matrix of this distribution may be chosen as the descriptive statistic for the uncertainty.

In Bayesian formalism, the outcome of the uncertainty analysis should ideally be the full posterior distribution $p(\boldsymbol{R})$ for the response vector $\boldsymbol{R} \in \mathbb{R}^J$. However, determining $p(\boldsymbol{R})$ analytically is usually not feasible, and therefore approximations need to be made. Uncertainty analysis methods can be divided into statistical and deterministic methods according to the chosen strategy. In statistical methods, the values of the uncertain parameters are sampled from their probability distribution, after which these values are used to compute a set of values for the responses. In this manner, the distribution $p(\boldsymbol{R})$ is simulated point-wise. In deterministic uncertainty analysis, the objective is not to form the entire distribution $p(\boldsymbol{R})$, but to compute an estimate

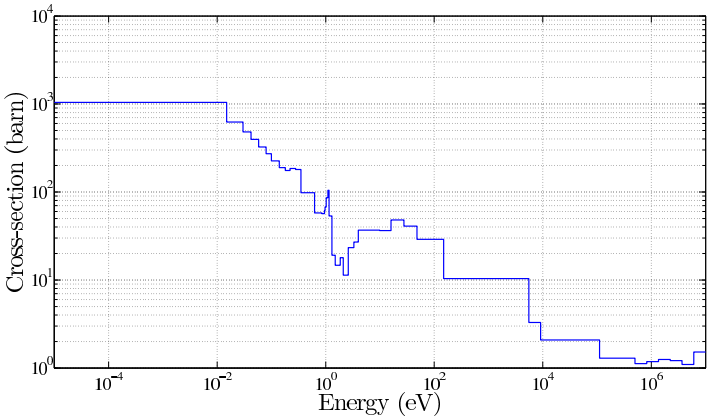

Figure 4.1. The self-shielded 40-group fission cross-section of ^{235}U for a BWR fuel assembly test problem.

for the covariance matrix Cov[$\boldsymbol{R}$], after which the distribution can be assumed to be Gaussian. Most often this is based on the linearization of the responses with respect to the uncertain parameters. This requires computing the *local sensitivities* of the responses at the parameters' best-estimate values.

The local sensitivity of response R is defined as the directional derivative in the direction of the perturbation $\delta\boldsymbol{\sigma}$. When considering the continuous-energy eigenvalue problem, the cross-sections are functions of energy and location, and the appropriate derivative is the functional directional derivative called the Gâteaux-variation [31]. It follows that the sensitivity of R with respect to the perturbation $\boldsymbol{h} = [\delta\boldsymbol{\Phi}, \delta\boldsymbol{\sigma}] \in D = H_\Phi \times E_\sigma$ at the point $\hat{\boldsymbol{e}} = [\hat{\boldsymbol{\Phi}}, \hat{\sigma}] \in D$ may be defined as:

$$\delta R(\hat{\boldsymbol{e}}; \boldsymbol{h}) = \lim_{t \to 0} \frac{R(\hat{\boldsymbol{e}} + t\boldsymbol{h}) - R(\hat{\boldsymbol{e}})}{t} \,. \tag{4.3}$$

The *local relative sensitivity* is defined as $S(\hat{\boldsymbol{e}}; \boldsymbol{h}) = \delta R(\hat{\boldsymbol{e}}; \boldsymbol{h})/R(\hat{\boldsymbol{e}})$, respectively.

The objective of sensitivity analysis is to compute these derivatives with respect to all uncertain parameters in the mathematical model. When solving the criticality equation, the utilized nuclear data typically contains tens of thousands of uncertain parameters. Since neutron cross-sections are functions of energy and position, the local sensitivities need to be computed with respect to cross-section values at each energy and mesh point in the calculation. In reactor physics applications, the number of responses is typically small compared to the number of uncertain parameters. For example, the fuel assembly burnup calculation program CASMO-4 [29], utilized in this work, computes by default a few dozen responses that are passed on to subsequent codes simulating the full core. These responses include the following assembly homogenized two-group cross-sections: transport, absorption, production, fission, scattering and κ-fission. The two-group homogenized cross-sections can be written in the form of Eq. (4.2) and they have been considered as responses in this thesis. To illustrate the uncertainty related to nuclear data parameters, Figure 4.1

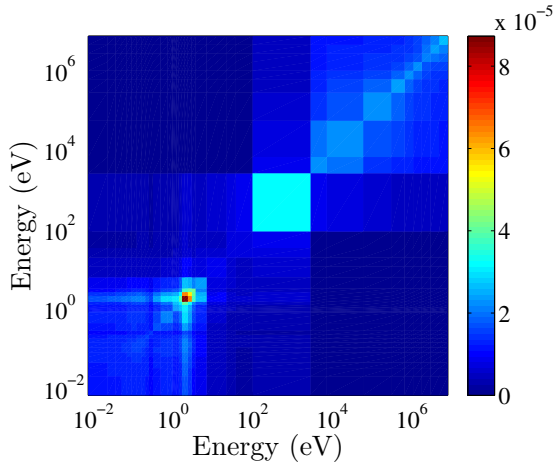

Figure 4.2. The relative covariance matrix of the ^{235}U fission cross-section taken from the SCALE 6.1 covariance library and modified to the 40 energy group structure of CASMO-4.

shows the 40-group fission cross-section of ^{235}U for a BWR fuel assembly test problem as computed with CASMO-4. The corresponding multi-group covariance matrix is shown in Figure 4.2.

The large number of uncertain parameters in reactor physics applications usually inhibits statistical uncertainty analysis in practise. Fortunately, the sensitivities can be computed deterministically in an efficient manner by exploiting the adjoint of the eigenvalue problem. This framework, referred to as *perturbation theory* in the context of reactor physics, is considered in Section 4.2.

After computing the sensitivities and linearizing the response vector, $\boldsymbol{R} \approx \boldsymbol{R}(\hat{\sigma}) + \boldsymbol{S}\sigma$, where $\boldsymbol{S} \in \mathbb{R}^{J\times K}$ is the sensitivity matrix containing the derivatives with respect to all considered uncertain parameters, the covariance matrix of the response can be simply computed using the identity

$$\mathrm{Cov}\,[\boldsymbol{R}] \approx \mathrm{Cov}\,[\boldsymbol{R}(\hat{\sigma}) + \boldsymbol{S}\sigma] = \boldsymbol{S}\,\mathrm{Cov}\,[\sigma]\,\boldsymbol{S}^{\mathsf{T}} \tag{4.4}$$

known as the first-order uncertainty propagation formula or the *Sandwich rule*. It is noteworthy that in the case where $\boldsymbol{R}$ depends linearly on the parameters and $p(\sigma)$ is a Gaussian distribution, the Sandwich rule yields the exact posterior distribution, i.e.

$$\eta = \boldsymbol{c} + \boldsymbol{S}\sigma \sim \mathrm{N}(\,\boldsymbol{c} + \boldsymbol{S}\hat{\sigma},\ \boldsymbol{S}\,\mathrm{Cov}\,[\sigma]\,\boldsymbol{S}^{\mathsf{T}}\,)\,, \tag{4.5}$$

where $\boldsymbol{c} \in \mathbb{R}^{K}$ is a constant vector.

4.2 Perturbation theory

The objective of sensitivity analysis is to compute the derivatives of system responses with respect to all uncertain parameters in the mathematical model. In perturbation theory, these derivatives are computed in an efficient manner by utilizing the adjoint system of the original forward problem. This approach was first considered in reactor analysis in [32, 33].

Consider the eigenvalue system given by Eq. (4.1). When the parameters $\boldsymbol{\sigma}$ are perturbed, also the solution $\boldsymbol{\Phi}$ changes, and therefore the computation of the sensitivity $\delta R(\hat{\boldsymbol{e}}; \boldsymbol{h})$ according to Eq. (4.3) requires that the perturbation $\delta\boldsymbol{\Phi}$ is known. In principle, $\delta\boldsymbol{\Phi}$ can be computed to first order from the following *forward sensitivity system*:

$$\begin{aligned} \delta\boldsymbol{A}(\hat{\boldsymbol{e}}; \boldsymbol{h}) &= -\frac{1}{k^2}\,\delta k(\hat{\boldsymbol{e}}; \boldsymbol{h})\,\boldsymbol{B}\boldsymbol{\Phi} + \frac{1}{k}\,\delta\boldsymbol{B}(\hat{\boldsymbol{e}}; \boldsymbol{h}) \\ \Leftrightarrow\ \boldsymbol{A}'_\sigma(\hat{\boldsymbol{e}})\,\delta\boldsymbol{\sigma} + \boldsymbol{A}(\hat{\boldsymbol{e}})\,\delta\boldsymbol{\Phi} &= -\frac{1}{k^2}\,\delta k(\hat{\boldsymbol{e}}; \boldsymbol{h})\,\boldsymbol{B}\boldsymbol{\Phi} + \frac{1}{k}\,\boldsymbol{B}'_\sigma(\hat{\boldsymbol{e}})\,\delta\boldsymbol{\sigma} + \frac{1}{k}\,\boldsymbol{B}(\hat{\boldsymbol{e}})\,\delta\boldsymbol{\Phi}\,, \end{aligned} \tag{4.6}$$

which can be derived by taking the Gâteaux variation of system (4.1) with respect to a perturbation $\boldsymbol{h}$ on both sides. However, when computing several sensitivities, this approach would require the repetitive solving of Eq. (4.6). The adjoint system of Eq. (4.1) is defined as the system that satisfies the following relation: [7]

$$\left\langle \boldsymbol{A}\boldsymbol{\Phi} - \frac{1}{k}\boldsymbol{B}\boldsymbol{\Phi},\ \boldsymbol{\Psi} \right\rangle = \left\langle \boldsymbol{\Phi},\ \boldsymbol{A}^*\boldsymbol{\Psi} - \frac{1}{k}\boldsymbol{B}^*\boldsymbol{\Psi} \right\rangle\,, \tag{4.7}$$

where the brackets $\langle \cdot, \cdot \rangle$ denote an inner product. When considering the continuous-energy criticality equation, it is customary to employ the L^2 inner product [34, 35]. The solution to the adjoint problem

$$\left(\boldsymbol{A}^* - \frac{1}{k}\boldsymbol{B}^* \right) \boldsymbol{\Psi} = 0 \tag{4.8}$$

is called the *fundamental adjoint*. Physically, the solution to this system can be interpreted to represent the average contribution, i.e. importance of a neutron to the multiplication factor. Interestingly, the adjoint system of Eq. (4.8) can be derived solely based on this physical interpretation [36].

By utilizing Eqs. (4.7) and (4.8), it is straightforward to obtain the following expression for the relative sensitivity of the multiplication factor with respect to a perturbation $\delta\boldsymbol{\sigma}$ (For derivation, see e.g. [37] or [V]):

$$\frac{\delta k(\hat{\boldsymbol{e}}; \boldsymbol{h})}{k} = -\frac{\left\langle (\boldsymbol{A}'_\sigma(\hat{\sigma})\boldsymbol{\Phi} - \frac{1}{k}\boldsymbol{B}'_\sigma(\hat{\sigma})\boldsymbol{\Phi})\,\delta\boldsymbol{\sigma},\ \boldsymbol{\Psi} \right\rangle}{\left\langle \frac{1}{k}\boldsymbol{B}\boldsymbol{\Phi},\ \boldsymbol{\Psi} \right\rangle}\,. \tag{4.9}$$

Sensitivity analysis of the critical eigenvalue based on Eq. (4.9) is known as *classical perturbation theory* in reactor physics.

[7] In some cases the adjoint relation needs to be written in the form $\langle \boldsymbol{A}\boldsymbol{\Phi} - \frac{1}{k}\boldsymbol{B}\boldsymbol{\Phi},\ \boldsymbol{\Psi} \rangle = \langle \boldsymbol{\Phi},\ \boldsymbol{A}^*\boldsymbol{\Psi} - \frac{1}{k}\boldsymbol{B}^*\boldsymbol{\Psi} \rangle + \left[\boldsymbol{P}(\boldsymbol{\Psi}, \boldsymbol{\Phi})\right]_{\boldsymbol{x}\in\partial\Omega}$, where $\left[\boldsymbol{P}(\boldsymbol{\Psi}, \boldsymbol{\Phi})\right]_{\boldsymbol{x}\in\partial\Omega}$ is a bilinear form associated with the system. We will only consider cases where it is straightforward to force this term to vanish.

For responses of the form of Eq. (4.2), the *generalized adjoint* can be defined as the solution to the following inhomogeneous system

$$\left(\boldsymbol{A}^* - \frac{1}{k}\boldsymbol{B}^*\right)\boldsymbol{\Gamma} = \frac{\nabla_\Phi R}{R} , \tag{4.10}$$

where $\nabla_\Phi R$ is the Fréchet derivative of R, also called the gradient. The generalized adjoint $\boldsymbol{\Gamma}(\boldsymbol{r}, \boldsymbol{\Omega}, E)$ can be physically interpreted as the average contribution of an additional neutron at the phase space point $[\boldsymbol{r}, \boldsymbol{\Omega}, E]$ to the response under consideration. It is noteworthy that when considering the generalized adjoint problem, the eigenvalue k is fixed to correspond to the solution of Eq. (4.1), and the operator $\boldsymbol{A}^* - \frac{1}{k}\boldsymbol{B}^*$ is singular. Therefore, in order for the solution $\boldsymbol{\Gamma}$ to exist, the gradient $\nabla_\Phi R$ needs to be orthogonal to the forward solution

$$\langle \nabla_\Phi R,\ \boldsymbol{\Phi} \rangle = 0 . \tag{4.11}$$

Responses satisfying Eq. (4.11) are called allowable for generalized perturbation theory [37]. It is easy to show that for responses of the form of Eq. (4.2), the relative gradient becomes

$$\frac{\nabla_\Phi R}{R} = \frac{\boldsymbol{\Sigma}_1}{\langle \boldsymbol{\Phi},\ \boldsymbol{\Sigma}_1 \rangle} - \frac{\boldsymbol{\Sigma}_2}{\langle \boldsymbol{\Phi},\ \boldsymbol{\Sigma}_2 \rangle} . \tag{4.12}$$

and that Eq. (4.11) is satisfied. Also, when a solution $\boldsymbol{\Gamma}_0$ to Eq. (4.10) exists, there exists an infinite amount of solutions of the form

$$\boldsymbol{\Gamma} = \boldsymbol{\Gamma}_0 + a\boldsymbol{\Psi} , \quad a \in \mathbb{R} . \tag{4.13}$$

In this case, it is possible to choose a solution orthogonal to the (forward) fission source. This particular solution can be written

$$\begin{aligned} \boldsymbol{\Gamma}_p &= \boldsymbol{\Gamma}_0 - \frac{\langle \boldsymbol{\Gamma}_0,\ \boldsymbol{B}\boldsymbol{\Phi} \rangle}{\langle \boldsymbol{\Psi},\ \boldsymbol{B}\boldsymbol{\Phi} \rangle}\boldsymbol{\Psi} \\ &= \boldsymbol{\Gamma}_0 - \frac{\langle \boldsymbol{B}^*\boldsymbol{\Gamma}_0,\ \boldsymbol{\Phi} \rangle}{\langle \boldsymbol{B}^*\boldsymbol{\Psi},\ \boldsymbol{\Phi} \rangle}\boldsymbol{\Psi} . \end{aligned} \tag{4.14}$$

Based on Eqs. (4.10), (4.7), (4.6) and (4.14), the following expression can be derived for the relative sensitivity of the response R with respect to a perturbation $\delta\boldsymbol{\sigma}$ [VI]:

$$\frac{\delta R(\hat{\boldsymbol{e}}, \boldsymbol{h})}{R} = \frac{R'_\sigma(\hat{\boldsymbol{e}})\,\delta\boldsymbol{\sigma}}{R} - \left\langle \boldsymbol{\Gamma}_p,\ \left(\boldsymbol{A}'_\sigma(\hat{\sigma})\boldsymbol{\Phi} - \frac{1}{k}\boldsymbol{B}'_\sigma(\hat{\sigma})\boldsymbol{\Phi}\right)\delta\boldsymbol{\sigma} \right\rangle_\Phi . \tag{4.15}$$

Sensitivity analysis based on this equation is known as *generalized perturbation theory* in reactor physics

4.2.1 Numerical computation

In practice, the criticality equation and the corresponding adjoint equations are solved numerically, which introduces some complications in the perturbation theory formalism. Ideally, the discretizations should be performed in a consistent manner,

so that the respective adjoint relations are satisfied at all stages of the computation [31]. However, as discussed in more detail in [V], this is usually infeasible in reactor physics calculations and therefore it is customary to take the eigenvalue problem discretized with respect to energy and direction as the starting point for sensitivity analysis.

Assuming isotropic scattering and the discrete ordinates approximation for angular dependence, the forward problem becomes

$$\begin{aligned}&\boldsymbol{\Omega}_m \cdot \nabla \Phi^g(\boldsymbol{r}, \boldsymbol{\Omega}_m) + \Sigma^g \, \Phi^g(\boldsymbol{r}, \boldsymbol{\Omega}_m) \\ &\quad = \frac{1}{4\pi} \sum_{h=1}^{G} \Sigma_{\mathrm{s}}^{h \to g} \, \phi^h(\boldsymbol{r}) + \frac{\chi_g}{4\pi k} \sum_{h=1}^{G} \overline{\nu} \, \Sigma_{\mathrm{f}}^h \, \phi^h(\boldsymbol{r}) \, , \quad g = 1, \ldots, G \, , \end{aligned} \tag{4.16}$$

where $\{\boldsymbol{\Omega}_m\}_{m=1}^M$ are the considered angular directions, and the scalar flux is approximated by the quadrature formula

$$\phi^h(\boldsymbol{r}) = \sum_{m=1}^{M} \omega_m \, \Phi^h(\boldsymbol{r}, \boldsymbol{\Omega}_m) \, . \tag{4.17}$$

Equation (4.16) follows from Eq. (2.6) after the discrete ordinates approximation. In fuel assembly calculations, the boundary conditions are usually assumed to be reflective to simulate an infinite lattice, i.e.

$$\Phi(\boldsymbol{r}, \boldsymbol{\Omega}_m, E) = \Phi(\boldsymbol{r}, \boldsymbol{\Omega}'_m, E) \, , \quad \boldsymbol{r} \in \Gamma \, , \quad \boldsymbol{\Omega}_m \cdot \boldsymbol{n} < 0 \, , \tag{4.18}$$

where $\boldsymbol{\Omega}_m = \boldsymbol{\Omega}'_m - 2(\boldsymbol{n} \cdot \boldsymbol{\Omega}'_m)\, \boldsymbol{n}$ is the reflection direction.

In order to form the adjoint system of Eq. (4.16), the corresponding inner product needs to be defined. As mentioned previously, the continuous energy eigenvalue problem is typically considered in the space L^2. The inner product corresponding to the discretization employed in Eq. (4.16) can be defined in a consistent manner as

$$\langle \boldsymbol{\Phi}, \, \boldsymbol{\Psi} \rangle = \sum_{g=1}^{G} \sum_{m=1}^{M} \omega_m \int_D d^3\boldsymbol{r} \; \Phi^g(\boldsymbol{r}, \boldsymbol{\Omega}_m) \, \Psi^g(\boldsymbol{r}, \boldsymbol{\Omega}_m) \, . \tag{4.19}$$

It is now straightforward to show that the following system

$$\begin{aligned}&-\boldsymbol{\Omega}_m \cdot \nabla \Psi^g(\boldsymbol{r}, \boldsymbol{\Omega}_m) + \Sigma^g \, \Psi^g(\boldsymbol{r}, \boldsymbol{\Omega}_m) \\ &\quad = \frac{1}{4\pi} \sum_{h=1}^{G} \Sigma_s^{g \to h} \, \psi^h(\boldsymbol{r}) + \frac{\overline{\nu} \, \Sigma_f^g}{4\pi k} \sum_{h=1}^{G} \chi_h \, \psi^h(\boldsymbol{r}) \, , \quad g = 1, \ldots, G \end{aligned} \tag{4.20}$$

with the boundary conditions

$$\Psi(\boldsymbol{r}, \boldsymbol{\Omega}_m, E) = \Psi(\boldsymbol{r}, \boldsymbol{\Omega}'_m, E) \, , \quad \boldsymbol{r} \in \Gamma \, , \; \boldsymbol{\Omega}_m \cdot \boldsymbol{n} > 0 \tag{4.21}$$

satisfies the adjoint relation of Eq. (4.7) with respect to the inner product defined by Eq. (4.19).

The generalized adjoint problem for a response of the form of Eq. (4.2) can be written, respectively

$$-\boldsymbol{\Omega}_m \cdot \nabla \Gamma^g(\boldsymbol{r}, \boldsymbol{\Omega}_m) + \Sigma^g \Gamma^g(\boldsymbol{r}, \boldsymbol{\Omega}_m) = \frac{1}{4\pi} \sum_{h=1}^{G} \Sigma_s^{g\to h} \gamma^h(\boldsymbol{r}) + \\ + \frac{\overline{\nu}\,\Sigma_f^g}{4\pi k} \sum_{h=1}^{G} \chi_h \gamma^h(\boldsymbol{r}) + \frac{\Sigma_1^g(\boldsymbol{r})}{\langle \boldsymbol{\Phi},\, \boldsymbol{\Sigma}_1 \rangle} - \frac{\Sigma_2^g(\boldsymbol{r})}{\langle \boldsymbol{\Phi},\, \boldsymbol{\Sigma}_2 \rangle}\ ,\ g = 1, \ldots, G\ , \tag{4.22}$$

where the generalized adjoint scalar flux in has been denoted by $\gamma^h(\boldsymbol{r})$.

The numerical solution of the fundamental adjoint from Eq. (4.20) has been considered in [V], and the computation of the generalized adjoint functions from Eq. (4.22) in [VI]. In both cases, it is advantageous that the adjoint systems are of the same form as the forward problem, which can be utilized in numerical computations. After computing the necessary adjoint functions, the sensitivities can be computed according to Eqs. (4.9) and (4.15). In this context, it is customary to further discretize the inner product of Eq. (4.19) as

$$\langle \boldsymbol{\Phi},\, \boldsymbol{\Psi} \rangle \approx \sum_{i=1}^{I} \sum_{g=1}^{G} \sum_{m=1}^{M} \omega_m V_i \overline{\Phi}^{g,i,m} \overline{\Psi}^{g,i,m}\ , \tag{4.23}$$

where i denotes the mesh index and $\overline{\Phi}^{g,i,m}$ and $\overline{\Psi}^{g,i,m}$ denote the average fluxes.

4.3 Application to CASMO-4

CASMO-4 is a two-dimensional fuel assembly burnup calculation program developed by Studsvik Scandpower [29]. It can be used for burnup calculations on boiling water reactor (BWR) and pressurized water reactor (PWR) pin cells or assemblies. The main purpose of fuel assembly transport calculations is to obtain the detailed neutron flux in the system, and to use this flux to compute homogenized parameters, which can then be passed on to the following full core computations. Because the properties of the fuel assemblies do not change sharply in the axial direction for the most part, it is generally sufficient to perform these computations in two dimensions. The boundary conditions of fuel assemblies are usually assumed to be reflective in order to represent the model as an infinite lattice.

In the 2-D transport calculation module of CASMO-4, Eq. (4.16) is solved with the method of characteristics [38]. The transport calculation is performed in the true heterogeneous geometry of the assembly, but the number of energy groups is typically reduced before the computation. The cross-section libraries of CASMO-4 contain 70 energy groups (14 fast groups, 13 resonance groups, and 43 thermal groups) and they include the following cross-sections: absorption, fission, production, scattering and total. After computing the macroscopic cross-sections based on microscopic cross-sections and the nuclide densities for the assembly under consideration, the cross-sections of the important resonance absorbers are self-shielded based on tabulated effective resonance integrals. In the following micro group calculation, the

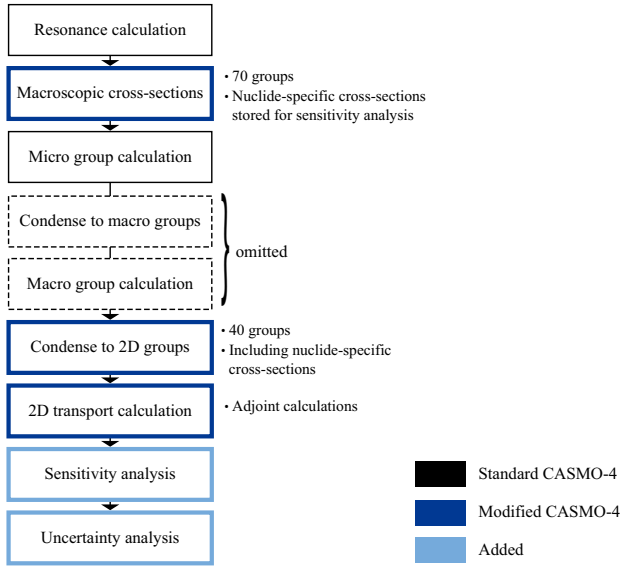

Figure 4.3. Outline of the CASMO-4 calculations.

detailed flux is solved for each pin cell type in the assembly by the method of collision probabilities, and the flux is used to homogenize the pin cells. These steps are followed by the macro group calculation, where the flux spectra is solved over the assembly using the homogenized pin cells and the response matrix method. The macro group calculation is performed using 40 energy groups by default. The flux spectra obtained from this computation are used to collapse the energy groups to the final group structure used in the 2-D transport calculation.

The implementation of perturbation theory according to the principles presented in Section 4.2.1 required modifications to several modules of CASMO-4. Figure 4.3 shows the flow diagram of the modified code. In order to be able to compute the sensitivities with respect to nuclide-specific cross-sections, they needed to be stored and collapsed to the energy group structure used in the 2-D transport calculation. It was decided to keep 40 energy groups in the transport calculation in order to obtain sufficiently detailed sensitivity profiles.

The solution of the fundamental adjoint and the generalized adjoint functions corresponding to the homogenized two-group cross-sections were implemented to the 2-D transport calculation module according to the guidelines presented in [V] and [VI]. After computing the necessary adjoint functions, the sensitivities of the multiplication factor and system responses are computed according to perturbation theory. The sensitivities are computed with respect to fission spectrum χ, the average number of fission neutrons $\overline{\nu}$, and the multi-group cross-sections present in the nuclear data library of CASMO-4.

In order to enable uncertainty analysis, the covariance matrices from `ZZ-SCALE6.0/COVA-44G` [39] were processed for compatibility with CASMO-4. The

Table 4.1. Parameters for which there exists covariance data in the SCALE library.

Parameter	MT number
σ_{t}	1
σ_{e}	2
σ_{i}	4
$\sigma_{n,2n}$	16
σ_{f}	18
σ_{γ}	102
$\sigma_{n,p}$	103
$\sigma_{n,d}$	104
$\sigma_{n,t}$	105
$\sigma_{n,He}$	106
$\sigma_{n,\alpha}$	107
$\overline{\nu}$	456
χ	1018

library is based on evaluations from various sources (including ENDF/B-VII, ENDF/B-VI, JENDL-3.1) and approximate covariance data. The covariances in the library are given in relative terms, and therefore the library is intended to be used with all cross-section libraries, including the ones that are inconsistent with the evaluations. While this is not strictly correct, it is considered to be acceptable due to the scarcity of comprehensive covariance data, among other reasons [40]. In the covariance library, the available covariance matrices are given in a 40-group structure for the parameters listed in Table 4.1. It should be emphasized that there is no covariance data for the group-to-group transfer cross-sections.

The covariance matrices from `ZZ-SCALE6.0/COVA-44G` were first transformed to the 40-group structure used in the 2-D transport calculation. The employed procedure, based on simple mathematical techniques, is described in detail in [V]. The use of the Sandwich rule for uncertainty analysis necessitates that the sensitivities and covariance matrices are formed with respect to the same parameters. Therefore, a problem was faced due to the covariance matrices being given for individual capture and scattering reactions, whereas the cross-section libraries of CASMO-4 only contain data for the total capture and scattering reactions. The cross-section model used in CASMO-4 is characteristic for several fuel assembly codes [41–43] and this issue affects the uncertainty analysis irrespective of the method used, whether deterministic or statistical. As a solution to this discrepancy, a technique for combining the covariance matrices of the individual subreactions was devised [V]. Since the relationships between the total and individual capture and scattering reactions are linear, the covariance matrices corresponding to the total capture and scattering reactions can be computed with the Sandwich rule without introducing any approximation. However, the sensitivity profiles with respect to the individual and the total scattering cross-sections cannot be defined in a consistent manner, and this produces some systematic differences to the results. This is explained in the following.

As mentioned previously, there is no cross-section data for the transfer cross-

sections $\sigma_{\mathrm{x}}^{h\to g,j}$ but only for $\sigma_{\mathrm{x}}^{g,j} = \sum_{h=1}^{G} \sigma_{\mathrm{x}}^{g\to h,j}$, where x refers to a scattering reaction (e.g., elastic, inelastic) and j is the nuclide index. Therefore, in order to use the scattering covariance data, the sensitivity profiles should be computed with respect to $\sigma_{\mathrm{x}}^{g,j}$. Because of the scattering source term in Eq. (4.16), however, the derivative with respect to $\sigma_{\mathrm{x}}^{g,j}$ is not mathematically well-defined without additional constraints. Typically it is assumed that the probabilities of transfers to various groups are fixed, i.e.

$$\sigma_{\mathrm{x}}^{g\to h,j} = \sigma_{\mathrm{x}}^{g,j}\, p_{\mathrm{x}}^{g\to h,j} \,, \tag{4.24}$$

where $p_{\mathrm{x}}^{g\to h}$ is the proportion of neutrons scattered from energy group g to energy group h, which is assumed to remain fixed, even if the scattering cross-section $\sigma_{\mathrm{x}}^{g,j}$ is perturbed [44]. Based on this assumption, the scattering source in Eq. (4.16) can be written

$$S^{g} = \frac{1}{4\pi} \sum_{h=1}^{G} \Sigma_{\mathrm{s}}^{h\to g}\, \phi^{h} = \frac{1}{4\pi} \sum_{\mathrm{x}} \sum_{j} N^{j} \sum_{h=1}^{G} \sigma_{\mathrm{x}}^{h,j}\, p_{\mathrm{x}}^{h\to g}\, \phi^{h} \,, \tag{4.25}$$

where the summations over x include all scattering reactions. After this assumption, the derivative with respect to $\sigma_{\mathrm{x}}^{g,j}$ is well-defined and can be computed as usual. However, the sensitivity with respect to the total scattering cross-section $\sigma_{\mathrm{s}}^{j} = \sum_{\mathrm{x}} \sigma_{\mathrm{x}}^{j}$ is not well-defined, if the constraint (4.24) is enforced. In order to define this sensitivity, fixed transfer rates must be assumed for the total scattering cross-section. Since the two assumptions required to compute the individual and total scattering sensitivities are inconsistent, the chain rule of derivation does not apply to them, and, for example, although $\sigma_{\mathrm{s}}^{g,j} = \sigma_{\mathrm{e}}^{g,j} + \sigma_{\mathrm{i}}^{g,j}$ holds, $\frac{dR}{d\sigma_{\mathrm{e}}^{g,j}} \neq \frac{dR}{d\sigma_{\mathrm{s}}^{g,j}} \frac{d\sigma_{\mathrm{s}}^{g,j}}{d\sigma_{\mathrm{e}}^{g,j}}$. Since the assumption of fixed transfer rates for the total scattering is clearly stricter than Eq. (4.24), the methodology employed in CASMO-4 typically produces smaller uncertainties, when multiple scattering reactions are present [V, VI]. However, it should be kept in mind that both of these approaches are in fact based on simplifications of the true problem, and are likely to underestimate the uncertainty related to scattering cross-sections.

5. Summary of the publications

This chapter summarizes the main results of the publications included in this thesis.

5.1 Publication I: Computing the matrix exponential in burnup calculations

Burnup equations describe the changes in the nuclide concentrations due to radioactive decay and neutron-induced transmutation reactions. They form a system of first order linear differential equations that can in principle be solved by computing the burnup matrix exponential. Due to the decay and transmutation constants of the nuclides varying extensively, the system is extremely stiff, which complicates the numerical computation of the matrix exponential solution. The short-lived nuclides are especially problematic, inducing eigenvalues of extremely large magnitude, and can lead to the burnup matrix norm being of the order of 10^{21}. These difficulties have traditionally been solved by using simplified burnup chains or by treating the most short-lived nuclides separately, when computing a matrix exponential solution.

In this paper, this problem is approached for the first time by studying the spectral properties of burnup matrices. Based on physical constraints related to the problem, the eigenvalues of burnup matrices can be deduced to be generally confined to a region near the negative real axis. The established matrix exponential methods for solving the burnup equations are introduced and their suitability is discussed from this perspective. Based on the eigenvalues being located near the negative real axis, the Chebyshev rational approximation method (CRAM) is proposed as a novel method for solving the burnup equations. CRAM can be characterized as the best rational approximation on the negative real axis and it is highly accurate in the region where the burnup matrix eigenvalues are located.

The introduced matrix exponential methods are applied to two test cases representing an infinite pressurized water reactor pin-cell lattice. In addition, the test cases are solved with the semi-analytical linear chain method, in which the complicated transmutation chains are resolved into a set of linear sub-chains that can be solved analytically. The first test case was designed to be well-behaved in terms of the burnup matrix size and norm, whereas the second test case corresponds to a full burnup system with over a thousand nuclides with rather extreme numerical

characteristics. In the first test case, all matrix exponential methods gave consistent results. In the second test case, however, all other matrix exponential methods suffered a breakdown, whereas the results obtained with CRAM remained consistent with those given by the linear chain method to the same degree as in the first test case. In terms of computational efficiency, CRAM clearly outperformed all the other methods. The results suggest that CRAM is a very promising method for solving the burnup equations with a low computational cost.

5.2 Publication II: Rational approximations to the matrix exponential in burnup calculations

The topic of the paper is solving the burnup equations using dedicated rational approximations accurate near the negative real axis. The burnup equations describe the changes in nuclide concentrations due to radioactive decay and neutron-induced transmutation reactions. They form a system of first order linear differential equations which is extremely stiff due to the decay constants of the nuclides varying extensively. In Publication [I], it was discovered that although the numerical properties of burnup matrices are otherwise rather difficult, their eigenvalues are generally confined to a region near the negative real axis. This observation prompted proposing the Chebyshev rational approximation method (CRAM) as a novel method for solving the burnup equations.

In this paper, two different types of rational approximation are considered for computing the exponential of a burnup matrix. The previously introduced CRAM, which can be characterized as the best rational approximation on the negative real axis, is analyzed in more detail. In addition, a method based on quadrature rules applied to a contour integral around the negative real axis is proposed. The motivation for introducing the latter method is that the computation of higher order CRAM approximations can become rather involved. In the quadrature-based approach, the approximation order can easily be adjusted to suit the needs for accuracy or efficiency. Furthermore, it was discovered that the previous literature values for coefficients of CRAM of order 14 contain errors, and result in relative accuracy two orders of magnitude poorer than expected by theory. To rectify this, new partial fraction decomposition coefficients for CRAM of order 14 and 16 were computed based on polynomial coefficients given in literature and provided in this paper.

The accuracy and convergence of both methods are studied and they are tested against highly accurate reference solutions computed with high-precision arithmetics. The sources of approximation error are analyzed and the previously observed difference in resulting accuracy for fresh and depleted fuel is explained. Based on the study, both methods appear to yield convergence rates close to the respective asymptotic convergence rates on the negative real axis when applied to burnup equations. In addition, the test cases indicate that both methods are capable of providing a very accurate and robust solution to the burnup equations.

5.3 Publication III: Correction to partial fraction decomposition coefficients for Chebyshev rational approximation on the negative real axis

The purpose of this note is to provide correct partial fraction decomposition (PFD) coefficients for the Chebyshev rational approximation method (CRAM) of order 14 and 16 on the negative real axis. The note was prompted by the observation that the literature values given previously for approximation order 14 by Gallopoulos and Saad in [22] are erroneous.

CRAM of order k can be characterized as the rational function yielding the smallest maximum deviation between the exponential function and any rational function of the same degree on the entire negative real axis. The asymptotic convergence rate of CRAM is remarkably fast, and it can be a viable method for computing the matrix exponential for matrices with eigenvalues in the vicinity of the negative real axis.

The main difficulty in using CRAM for computing the matrix exponential is determining the coefficients of the rational function for a given approximation order. For higher approximation orders the computation of the coefficients becomes rather involved and requires delicate algorithms combined with high-precision arithmetics. In addition, it is generally advantageous to employ the rational function in its PFD form which requires computing its poles, residues and limit at $\mathrm{Re}\, z \to -\infty$.

The PFD coefficients for CRAM of order 14 have been previously provided in literature, and therefore they have been used in several applications. In [II], these coefficients were discovered to contain errors that resulted in 10^2 times poorer accuracy than expected by theory. In this note, the correct PFD coefficients are provided for approximation orders 14 and 16. The correct coefficients were computed based on literature values for the polynomial coefficients of the respective rational functions. The theory for computing the PFD coefficients from the polynomial is reviewed and the employed computational procedure is described. The approximation accuracy resulting from erroneous poles and residues is analyzed.

5.4 Publication IV: Solving linear systems with sparse Gaussian elimination in the Chebyshev rational approximation method (CRAM)

The topic of this paper is the solving of the linear systems arising when computing the matrix exponential solution to burnup equations with the Chebyshev rational approximation method (CRAM). The burnup matrices have difficult numerical characteristics that may compromise the accuracy of some iterative methods used for solving the linear systems. In this paper, a direct method is considered to overcome this difficulty.

The numerical properties of burnup matrices are reviewed. The proposed direct method is based on sparse Gaussian elimination in which the sparsity pattern of the resulting upper triangular matrix is determined before the numerical elimination phase. The stability of Gaussian elimination is discussed and, based on the

properties of burnup matrices, it is shown that the proposed method is well-suited for solving the linear systems. Suitable algorithms are presented for computing the symbolic factorization and numerical elimination. The accuracy and efficiency of the described technique are demonstrated by computing the CRAM approximations for a large test case with over 1600 nuclides.

5.5 Publication V: Incorporating sensitivity and uncertainty analysis to a lattice physics code with application to CASMO-4

The topic of this paper is the implementation of classical perturbation theory based sensitivity and uncertainty analysis features to the fuel assembly burnup calculation program CASMO-4 in the context of the UAM benchmark [28], whose first stage aims at propagating the uncertainty related to nuclear data through fuel assembly calculations. The benchmark was prepared in 2006 to establish the current state and needs of sensitivity and uncertainty analysis, with the ultimate goal of being able to propagate uncertainty through all stages in a coupled neutronics/thermal hydraulics calculation. At that time, the generally employed reactor physics codes did not have uncertainty analysis capabilities, and the modified CASMO-4 was one of the first fuel assembly programs that enabled sensitivity and uncertainty analysis based on perturbation theory.

Classical perturbation theory studies the changes in the multiplication factor due to perturbations in system parameters. In this framework, the critical eigenvalue sensitivities to uncertain nuclear data parameters are computed efficiently by utilizing the adjoint system of the eigenvalue problem. After computing the sensitivities, the uncertainty related to these parameters can be propagated deterministically to the multiplication factor. Both the theoretical background as well as practical considerations for implementing classical perturbation theory to a reactor physics code are reviewed and discussed in detail in the paper.

In the process of modifying CASMO-4, a problem was faced due to the incompatibility of the cross-section models between the covariance libraries and the code itself. In this paper, a technique for overcoming this difficulty by combining the covariance matrices is proposed. The sensitivities can then be computed with respect to the combined reactions. The proposed technique accurately combines the capture reactions in a consistent manner, but results in systematic differences for the scattering reactions. The issue is analyzed and the difference is explained by incompatible constraints in the two calculation strategies.

Numerical results are presented for two of the benchmarks fuel pin-cell test problems representing a PWR and a GEN-III core with MOX fuel, and the results are compared against TSUNAMI-1D. The comparison supports the observations made on the developed methodology, i.e. the results are consistent except for scattering reactions, where systematic differences appear in cases with multiple scattering reactions.

5.6 Publication VI: Perturbation-theory-based sensitivity and uncertainty analysis with CASMO-4

This paper considers the implementation of generalized perturbation theory based sensitivity and uncertainty capability to the fuel assembly burnup calculation program CASMO-4. The motivation for the described work has been the participation in the UAM benchmark [28]. Initially, classical perturbation theory was implemented to CASMO-4, which allowed the sensitivity analysis with respect to the multiplication factor. This work was reported in [V].

Generalized perturbation theory studies the changes in responses that can be represented as reaction rate ratios. For each response, the computation of the sensitivity profiles with respect to all parameters of interest requires solving one generalized adjoint system. This is computationally efficient, when the number of parameters is large, as is the case in reactor physics applications. After computing the sensitivity profiles, the uncertainty related to nuclear data can be propagated deterministically to the response under consideration by approximating the relationship between the parameters and the response to be linear.

The mathematical background as well as the physical interpretation of the generalized adjoint solutions are reviewed in the paper, and practical guidelines are given for modifying a deterministic transport code to solve the generalized adjoint systems needed in sensitivity analysis. The theory for computing the sensitivity profiles is presented both from the perspective of function space analysis and numerical computations.

Numerical results are presented for a lattice physics test problem in the benchmark, and they are compared to the results given by the TSUNAMI-2D sequence in SCALE 6.1. Two-group homogenized cross-sections are considered as responses in the generalized perturbation theory framework. The results are in accordance with theoretical considerations. In particular, they are consistent for the thermal responses, whereas some systematic differences are observed for fast responses. These differences are explained by the incompatible constraints in defining the sensitivities, an issue which was analyzed in detail in [V].

6. Conclusions

The objective of burnup calculations is to simulate the changes in the composition of nuclear fuel over time. Due to safety considerations related to the target of application, it is important that the applied calculation methods are constantly improved. In addition, uncertainty analysis methods are needed for evaluating the reliability of the calculation results.

Burnup calculations are built upon solving the neutron transport criticality equation and burnup equations sequentially in a cyclic manner. This thesis focused on two areas essential for burnup calculations: the numerical solution of burnup equations based on computing the burnup matrix exponential and the uncertainty analysis of the criticality equation based on perturbation theory.

Matrix exponential solution of burnup equations

The burnup equations govern the changes in nuclide concentrations over time. They form a system of first order differential equations, which can be formally solved by computing the matrix exponential of the burnup matrix. Due to the dramatic variation in the half-lives of different nuclides, the system is extremely stiff, and the problem is complicated by the vast range of time steps used in burnup calculations. Because of these characteristics, the computation of the burnup matrix exponential has been previously considered impossible for the full burnup system. Instead, simplified burnup chains have been used, or the most short-lived nuclides have been treated separately when computing a matrix exponential solution.

In Publication [I], the spectral properties of burnup matrices were studied for the first time. It was reasoned that although the magnitudes of the eigenvalues of burnup matrices vary extensively, they are generally confined to a region near the negative real axis. The observation was based on considering the physical constraints related to burnup equations and studying the strongly connected components of the burnup matrix graph.

In Chapter 3.1 of this thesis, the mathematical properties of burnup matrices were further studied. Firstly, the negatives of burnup matrices were identified to belong to the class of Z-matrices, which guarantees the non-negativity of the burnup matrix exponential, for example. To further study the eigenvalues, burnup matrices were

categorized into conventional and augmented burnup matrices based on whether the production of by-product nuclides was taken into account when constructing them. The negatives of conventional burnup matrices were then recognized as M-matrices, which gave a wedge condition to their spectrum around the negative real axis. Augmented burnup matrices, on the other hand, can be permuted to block triangular form, with the eigenvalues of the matrix comprising of the eigenvalues of the diagonal blocks. Apart from the block corresponding to the by-product nuclides, the diagonal blocks were shown to be M-matrices. The block corresponding to the by-product nuclides was identified with the matrix class L_0^2, meaning that it has a single positive eigenvalue.

The observation about the burnup matrix eigenvalues being located near the negative real axis prompted proposing rational approximations that are accurate on the negative real axis for solving the burnup equations [I, II]. In Publication [I], the Chebyshev rational approximation method (CRAM), which can also be characterized as the best rational approximation on the negative real axis, was introduced with very promising results. In contrast to other matrix exponential methods considered previously, CRAM was demonstrated to be applicable to large burnup problems containing over a thousand nuclides and with a matrix norm of the order of 10^{21}. In addition, CRAM was shown to allow time steps of the order of 10^7 s, which can be considered the maximum feasible time step in burnup calculations. Based on these results, CRAM was implemented to the reactor physics code Serpent developed at VTT. In addition to CRAM, rational approximations based on quadrature rules applied to contour integrals around the negative real axis were suggested as an alternative solution method [II]. This approach has the advantage that the order of approximation can be easily adjusted.

The accuracy and convergence of CRAM were further studied in [II] by comparing the results against highly accurate reference solutions computed with high-precision accuracy. The results supported the assessment of CRAM being capable of providing a very accurate and robust solution to the burnup equations at a very low computational cost.

The application of CRAM requires determining the partial fraction decomposition coefficients (PFD) of the rational function for a given approximation order. Unfortunately, the computation of these coefficients is difficult and requires delicate algorithms combined with high-precision accuracy. The PFD coefficients for CRAM of order 14 have been previously provided in literature, and have therefore been used in several applications. In Publication [II], these coefficients were discovered to contain errors that resulted in 10^2 times poorer accuracy than expected by theory. The correct PFD coefficients for approximation order 14 and 16 were then computed based on literature values for the polynomial coefficients of the respective rational functions. These coefficients were first reported in [II] and later in [III] with a more detailed description and an analysis of the approximation accuracy deterioration resulting from the erroneous coefficients.

In practise, the application of CRAM to solving the burnup equations requires a linear solver in addition to the PFD coefficients. Due to the difficult numerical char-

acteristics of burnup matrices, the accuracy of some iterative solution methods may be compromised. In [IV] a direct method based on sparse Gaussian elimination was considered. It was demonstrated that the characteristics of burnup matrices allow using Gaussian elimination without pivoting, which enables computing the symbolic LU factorization of the matrix before starting the numerical elimination phase. Due to the sparsity pattern of burnup matrices, the linear systems arising during CRAM can be solved both efficiently and accurately with this approach [IV].

Uncertainty analysis of the criticality equation based on perturbation theory

When uncertain parameters are utilized in a computation, the calculation results also contain uncertainty. The imprecision of neutron interaction data is considered to be one of the most significant sources of uncertainty in all reactor physics calculations, including burnup calculations.

In this thesis, uncertainty analysis was applied to the criticality equation on a fuel assembly level. The motivation for this work was participating in the UAM benchmark [28] whose goal is to propagate the uncertainty in the nuclear data through a coupled neutronics/thermal-hydraulics calculation. The first phase of the benchmark aims at propagating uncertainty through fuel assembly calculations, which are used to produce homogenized data for the following coupled calculations. The objective of the first phase can be considered ambitious, since the generally used fuel assembly codes did not have uncertainty analysis capabilities when the benchmark was started.

Due to vast number of uncertain nuclear data in fuel assembly calculations, perturbation theory was chosen as the framework for the uncertainty analysis. The fuel assembly burnup calculation code CASMO-4 [29] was chosen as the development platform. Perturbation theory allows computing the sensitivity profiles of a response with respect to any number of parameters in an efficient manner by solving an adjoint system in addition to the original forward problem. The uncertainty related to these parameters can then be propagated deterministically by linearizing the response.

Initially, classical perturbation theory was implemented to CASMO-4, which enabled the uncertainty analysis of the multiplication factor [V]. In the process of modifying CASMO-4, a problem was faced due to the incompatibility of the cross-section models between the covariance libraries containing the neutron interaction uncertainty data and the code itself. In publication [V], a technique for overcoming this issue by combining the covariance matrices was devised. The proposed approach accurately combines the capture reactions whereas it results in systematic differences for the scattering reactions. The issue was analyzed and the difference was explained by the incompatible constraints implicitly assumed in the two calculation strategies [V]. The uncertainty analysis methodology was later extended to responses that can be represented as reaction rate ratios [VI]. This framework is called generalized perturbation theory and it was applied to two-group homogenized cross-sections.

Bibliography

[1] J. Leppänen and M. Pusa, "Burnup calculation capability in the PSG2/Serpent Monte Carlo reactor physics code," In Proc. of International Conference on Mathematics, Computational Methods & Reactor Physics (M&C 2009), on CD-ROM, 1662–1673, American Nuclear Society (2009).

[2] D. G. Cacuci, ed., *Handbook of Nuclear Engineering*, Vol. 2: Reactor Design, Springer (2010).

[3] A. Koning, R. Forrest, M. Kellett, R. Mills, H. Henriksson and Y. Rugama, "The JEFF-3.1 Nuclear Data Library", JEFF Report 21, NEA Data Bank (2006).

[4] A. Koning, S. Hilaire, and S. Goriely, "TALYS-1.4, a Nuclear Reaction Program, User Manual" (2011).

[5] H. Amann, *Ordinary Differential Equations, An Introduction to Nonlinear Analysis*, Walter de Gruyter (1990).

[6] A. Berman and R. J. Plemmons, *Nonnegative Matrices in the Mathematical Sciences*, SIAM (1994).

[7] R. B. Kellogg, "On complex eigenvalues of *M* and *P* matrices," *Numer. Math.*, **19**, 170–175 (1972).

[8] S. M. Fallat, C. R. Johnson, R. L. Smith, and P. van den Driessche, "Eigenvalue location for nonnegative and *Z*-matrices," *Linear Algebra and its Applications*, **277**, 187–198 (1998).

[9] R. Dreher, "Modified Bateman Solution for Identical Eigenvalues," *Ann. Nucl. Energy*, **53** (2013).

[10] L. N. Trefethen and M. Embree, *Spectra and Pseudospectra*, Princeton University Press (2005).

[11] T. G. Wright, "Eigtool," `http://www.comlab.ox.ac.uk/pseudospectra/eigtool/` (accessed February 13, 2013) (2005).

[12] N. J. Higham, *Functions of Matrices, Theory and Computation*, SIAM (2008).

[13] L. A. Zadeh and C. A. Desoer, *Linear System Theory: The State Space Approach*, McGraw-Hill Book Company, Inc. (1963).

[14] I. C. Gauld, O. W. Hermann, and R. M. Westfall, "Origen-S: Scale System Module to Calculate Fuel Depletion, Actinide Transmutation, Fission Product Buildup and Decay, and Associated Radiation Source Terms," in "SCALE: A Modular Code System for Performing Standardized Computer Analyses for Licensing Evaluation," Vol. II, Sec. F7, Oak Ridge National Library/U.S. Nuclear Regulatory Commission (Nov. 2006).

[15] A. Yamamoto, M. Tatsumi, and N. Sugimura, "Numerical Solution of Stiff Burnup Equations with Short Half Lived Nuclides by the Krylov Subspace Method," *J. Nucl. Sci. Technol.*, **44**, 2, 147–154 (2007).

[16] C. Moler and C. van Loan, "Nineteen Dubious Ways to Compute the Exponential of a Matrix, Twenty-Five Years Later," *SIAM Rev.*, **45** (2003).

[17] N. J. Higham, "The Scaling and Squaring Method for the Matrix Exponential Revisited," *SIAM J. Matrix Anal. & Appl.*, **26**, 4, 1179–1193 (2005).

[18] L. N. Trefethen, J. A. C. Weideman, and T. Schmelzer, "Talbot Quadratures and Rational Approximations," *BIT.*, **46**, 3, 653–670 (2006).

[19] A. A. Gonchar and E. A. Rakhmanov, "Equilibrium Distributions and Degree of Rational Approximation of Analytic Functions," *Math. USSR Sb.*, **62**, 2 (1989).

[20] H. Stahl and T. Schmelzer, "An Extension of the '1/9'-Problem," *Journal of Computational and Applied Mathematics*, **233**, 821–834 (2009).

[21] A. J. Carpenter, A. Ruttan, and R. S. Varga, "Extended Numerical Computations on the '1/9' Conjecture in Rational Approximation Theory," "Rational Approximation and Interpolation" in *Lecture Notes in Mathematics*, Vol. 1105, 383–411, P. R. Graves-Morris, E. B. Saff, and R. S. Varga, Eds., Springer-Verlag (1984).

[22] E. Gallopoulos and Y. Saad, "Efficient Solution of Parabolic Equations by Krylov Approximation Methods," *SIAM J. Sci. Stat. Comput.*, **13**, 5, 1236–1264 (1992).

[23] R. B. Sidje, "Expokit: a Software Package for Computing Matrix Exponentials," *ACM Trans. Math. Softw.*, **24**, 1, 130–156 (1998).

[24] A. Isotalo and P. A. Aarnio, "Comparison of depletion algorithms," *Ann. Nucl. Energy*, **38**, 2–3, 261–268 (2011).

[25] H. Bateman, "Solution of a system of differential equations occurring in the theory of radioactive transformations." *Proc. Cambridge Philos. Soc.*, **15**, 423–427 (1910).

[26] J. Cetnar, "General Solution of Bateman Equations for Nuclear Transmutations," *Ann. Nucl. Energy*, **33**, 640–645 (2006).

[27] J. Weideman and L. N. Trefethen, "Parabolic and Hyperbolic Contours for Computing the Bromwich Integral," *Math. Comp.*, **76**, 259, 1341–1356 (2007).

[28] K. Ivanov, M. Avramova, S. Kamerow, I. Kodeli, and E. Sartori, E. Ivanov, O. Cabellos, "Benchmark for Uncertainty Analysis in Modeling (UAM) for Design, Operation, and Safety Analysis of LWRs, Volume I: Specification and Support Data for the Neutronics Cases (Phase I)," NEA/NSC/DOC(2012)10 (2012).

[29] J. Rhodes and M. Edenius, "CASMO-4, A Fuel Assembly Burnup Program, User's Manual," (proprietary) Studsvik Scandpower, SSP-01/400 (2001).

[30] E. T. Jaynes, *Probability Theory: the Logic of Science*, Cambridge University Press (2003).

[31] D. G. Cacuci, *Sensitivity and Uncertainty Analysis*, vol. 1, Chapman & Hall/CRC (2003).

[32] E. P. Wigner, *Effects of Small Perturbations on Pile Period*, CP-3048, Manhattan Project Report (1945).

[33] L. N. Usachev, *Perturbation Theory for the Breeding Ratio and for Other Number Ratios Pertaining to Various Reactor Processes*, J. Nucl. Energy, Parts A/B, **18**, 571 (1964).

[34] B. G. Carlson and K. D. Lathrop, "Transport Theory—the Method of Discrete Ordinates," in H. Greenspan, C. N. Kelber, and D. Okrent, eds., "Computing Methods in Reactor Physics," Gordon and Breach Science Publishers (1968).

[35] E. E. Lewis and J. W. F. Miller, *Computational Methods of Neutron Transport*, John Wiley & Sons (1984).

[36] J. Lewins, *Importance: the Adjoint Function*, Pergamon Press, Oxford (1965).

[37] M. L. Williams, "Perturbation Theory for Nuclear Reactor Analysis," in Y. Ronen, Ed., "CRC Handbook of Nuclear Reactors Calculations," , Vol. 3, CRC Press (1986).

[38] J. R. Askew, "A Characteristics Formulation of the Neutron Transport Equation in Complicated Geometries," Tech. Rep. AAEW-M 1108 (1972).

[39] ZZ-SCALE6.0/COVA-44G, a 44-group cross section covariance matrix library retrieved from the SCALE-6.0 package, NEA Data Bank code package USCD1236/03 (2011).

[40] M. L. Williams, D. Wiarda, G. Arbanas, and B. L. Broadhead, "Scale Nuclear Data Covariance Library," in "SCALE: A Modular Code System for Performing Standardized Computer Analyses for Licensing Evaluation, Version 5," ORNL/TM-2005/39, Oak Ridge National Library/U.S. Nuclear Regulatory Commission (January 2009).

[41] "HELIOS Methods," Studsvik Scandpower (2000).

[42] "WIMS9A, NEW FEATURES, A Guide to the New Features of WIMS Version 9A," Serco Assurance, http://www.sercoassurance.com/answers/ (accessed February 13, 2013) (2005).

[43] G. Marleau, A. Hébert, and R. Roy, "A User Guide For Dragon Version 4," IGE294, http://www.polymtl.ca/nucleaire/DRAGON/ (accessed February 13, 2013) (2009).

[44] C. R. Weisbin and *et al*, "Application of FORSS Sensitivity and Uncertainty Methodology to Fast Reactor Benchmark Analysis," Tech. Rep. ORNL/TM-5563 (1976).

PUBLICATION I

Computing the matrix exponential in burnup calculations

In: Nuclear Science and Engineering,
164, 2, pp. 140–150.

NUCLEAR SCIENCE AND ENGINEERING: **164**, 140–150 (2010)

Computing the Matrix Exponential in Burnup Calculations

Maria Pusa* and Jaakko Leppänen

VTT Technical Research Centre of Finland, P.O. Box 1000, FI-02044 VTT, Finland

Received February 10, 2009
Accepted July 13, 2009

Abstract—*The topic of this paper is the computation of the matrix exponential in the context of burnup equations. The established matrix exponential methods are introduced briefly. The eigenvalues of the burnup matrix are important in choosing the matrix exponential method, and their characterization is considered. Based on the characteristics of the burnup matrix, the Chebyshev rational approximation method (CRAM) and its interpretation as a numeric contour integral are discussed in detail. The introduced matrix exponential methods are applied to two test cases representing an infinite pressurized water reactor pin-cell lattice, and the numerical results are presented. The results suggest that CRAM is capable of providing a robust and accurate solution to the burnup equations with a very short computation time.*

I. INTRODUCTION

The neutronic properties of a reactor fuel are strongly dependent on the isotopic compositions of the fissile materials. The changes in the material compositions must be taken into account in all reactor physics calculations. This is in practice handled by burnup calculation codes. An essential part of a burnup calculation is the solving of the burnup equations that describe the rates by which the concentrations of the various nuclides change. The burnup equations form a system of first-order linear differential equations that can be written

$$\frac{dN_j}{dt} = \sum_{i \neq j} \lambda_{ij} N_i - \lambda_j N_j \ , \quad N_j(0) = N_0 \ , \quad j = 1, \ldots, n \ , \tag{1}$$

where

N_j = concentration of nuclide j

n = total number of nuclides

λ_{ij} = coefficients characterizing the rates of neutron-induced reactions and spontaneous radioactive decay.

*E-mail: Maria.Pusa@vtt.fi

In this paper we consider the burnup system under the assumption that these coefficients are fixed constants. The burnup equations can then be written in matrix notation as

$$\boldsymbol{n}' = \boldsymbol{A}\boldsymbol{n} \ , \quad \boldsymbol{n}(0) = \boldsymbol{n}_0 \ , \tag{2}$$

where

$\boldsymbol{n}(t) \in \mathbb{R}^n$ = nuclide concentration vector

$\boldsymbol{A} \in \mathbb{R}^{n \times n}$ = burnup matrix containing the decay and transmutation coefficients of the nuclides under consideration.

Equation (2) can be formally solved by the matrix exponential method yielding the simple solution

$$\boldsymbol{n}(t) = e^{\boldsymbol{A}t}\boldsymbol{n}_0 \ , \tag{3}$$

where the exponential of the matrix $\boldsymbol{A}t$ is defined as the power series expression

$$e^{\boldsymbol{A}t} = \sum_{k=0}^{\infty} \frac{1}{k!} (\boldsymbol{A}t)^k \ , \tag{4}$$

with the additional definition $\boldsymbol{A}^0 = \boldsymbol{I}$.

There are numerous algorithms for computing the matrix exponential, but many of them are computationally expensive or of dubious numerical quality.[1] Because the decay constants and reaction rates of the nuclides vary extensively, the burnup matrix has a wide spectrum

of eigenvalues, making the approximation of the matrix exponential more difficult. Short-lived nuclides are especially problematic because they can induce eigenvalues of arbitrarily large magnitude. These difficulties have traditionally been solved by using simplified burnup chains or by treating the most short-lived nuclides separately when computing a matrix exponential solution. The selection of a suitable matrix exponential method depends substantially on the characteristics of the problem at hand. For example, the norm and eigenvalue spectrum of the burnup matrix as well as the length of the time step are the key aspects that should be taken into consideration when choosing the matrix exponential method. However, notably little interest and research effort have been shown toward this topic.

The focus of our study was to examine if it is possible to solve a detailed burnup system containing thousands of nuclides by a single matrix exponential method. The motivation for this was the development of the burnup calculation routines in the PSG2/Serpent Monte Carlo reactor physics code.[2] The current burnup calculation implementation in Serpent is based on the TTA method,[3] in which the complicated transmutation chains are resolved into a set of linear subchains that can be solved analytically. The main advantage of this method is that it can handle the extensive variations in the transmutation and decay coefficients and is relatively easy to implement in its basic form using a recursive loop. The most significant problem with the TTA method is that the computation time can easily become excessive if all chains are followed until a stable nuclide is encountered, and cutoffs have to be enforced to terminate insignificant chains. In addition, the current implementation of the method cannot treat chains that form a closed cycle, but the trajectory is terminated if the same nuclide is encountered twice in a single chain.

II. EIGENVALUES OF THE BURNUP MATRIX

In solving the burnup equations with the matrix exponential method, it is beneficial to estimate the character of the matrix eigenvalues, e.g., whether they are real-valued or complex-valued, and, in the latter case, the magnitude of the eigenvalues' imaginary parts.

II.A. Real Parts of Eigenvalues

It is known that the general solution of system (2) is a linear combination of functions of the form

$$t^k e^{\alpha t}\cos(\omega t)\boldsymbol{a}\ ,\quad t^l e^{\alpha t}\sin(\omega t)\boldsymbol{b}\ ,\quad \boldsymbol{a},\boldsymbol{b}\in\mathbb{R}^n\ , \tag{5}$$

where $\lambda = \alpha + i\omega$ runs through all the eigenvalues of $\boldsymbol{A}$ with $\omega \geq 0$ and $k, l \leq m(\lambda) - 1$, where $m(\lambda)$ denotes the algebraic multiplicity of eigenvalue λ (for proof, see Ref. 4). If all eigenvalues of the burnup matrix are real, the concentration of each nuclide is a linear combination of functions of the form $f(t) = t^k e^{\alpha t}$. In this case the eigenvalue determines the rate of exponential growth or decay of the function f. On the other hand, an eigenvalue with a nonzero imaginary part ω indicates that the solution has an oscillating component with period $T = 2\pi/\omega$.

Some understanding of the burnup eigenvalues can be gained by considering the physical constraints related to system (2). For example, it is evident that the concentration of each nuclide must remain bounded at all times. The following theorem (Ref. 4, p. 165) therefore gives a useful characterization of the real parts of the burnup eigenvalues.

Theorem: Every solution $\boldsymbol{n}$ of system (2) remains bounded as $t \to \infty$ if and only if the following hold:

(i) $\mathrm{Re}(\lambda) \leq 0\ \forall\ \lambda \in \Lambda(\boldsymbol{A})$;

(ii) Every $\lambda \in \Lambda(\boldsymbol{A})$ with $\mathrm{Re}(\lambda) = 0$ is a semisimple eigenvalue; i.e., the geometric and algebraic multiplicities agree.

Here, $\Lambda(\boldsymbol{A})$ denotes the set of the eigenvalues of $\boldsymbol{A}$.

The real parts of the eigenvalues of the burnup matrix must therefore all be nonpositive. A purely imaginary eigenvalue would correspond to a nondamped oscillation, which is physically unrealistic in the context of burnup calculation. It can thus be deduced that the real parts of the nonzero eigenvalues of the burnup matrix are always negative.

II.B. Imaginary Parts of Eigenvalues

The characterization of the imaginary parts of the burnup eigenvalues is more difficult. If the burnup chain does not contain any closed cycles—i.e., no paths from any vertex back to itself exist in the burnup matrix—the matrix can be permuted into a triangular form. In this case the eigenvalues are the diagonal elements, and hence, all are real-valued and negative. The nonreal eigenvalues result from closed transition cycles occurring in the burnup chain. However, not all closed transition cycles induce nonreal eigenvalues, and in practice only a fraction of the eigenvalues of the burnup matrix have nonzero imaginary parts.

A suitable mathematical method for establishing a link between the structure and eigenvalues of a matrix is the computation of the strongly connected components of the graph of the matrix.[5] A strongly connected component is defined as a set of vertices such that there exists a path from each vertex to every other vertex. If all of the strongly connected components of a matrix are sorted topologically, the corresponding systems of differential equations can be solved independently in this order. The different cyclic components of a burnup chain can therefore be studied conveniently by calculating its strongly connected components. If the burnup matrix does

not contain any closed cycles, the size of every strongly connected component is one, and the solution of system (2) can be calculated by solving n ordinary linear differential equations. The nonreal eigenvalues can therefore be identified with certain cyclic parts in the burnup transition chain.

We have computed the eigenvalues for a wide range of burnup matrices, and based on our experiments, it seems that they are generally confined to a region near the negative real axis. Based on our observations it appears that a prerequisite for a nonreal eigenvalue is that the majority of the reactions involved in a closed cycle have transition rates that are of the same order. In this scenario the slowest reactions appear to have the most significance for the period of the oscillation. This seems reasonable from a physical standpoint, as well. The cycle that is most likely to induce oscillations appears to consist of an alpha decay followed by successive (n,γ) and β^- reactions. An example of this kind of loop is the transition cycle resulting from the alpha decay of ^{242}Cm. The decay constant of this reaction is of order 10^{-8} 1/s (half-life 162 days), and in a thermal reactor operating at full power, the corresponding cycle typically induces three pairs of complex eigenvalues with imaginary parts of order $\leq 10^{-8}$.

The shortest half-lives encountered in reactor calculations are generally of the order of milliseconds, although there are some even more short-lived nuclides. The half-lives corresponding to neutron-induced reactions are considerably longer. In a thermal reactor operating at full power, most of the transmutation coefficients are of order $\leq 10^{-8}$ 1/s, and they are even smaller in a fast reactor. Therefore, it can be expected that the imaginary parts of the burnup eigenvalues are at most of this order. For every burnup matrix that we have considered, this has also been the case. When the power level is decreased, the transmutation coefficients become smaller. In this case the absolute values of the imaginary parts of the eigenvalues decrease as well. It seems that the oscillations are most likely to occur for reduced power cases where the greatest transmutation coefficients are of order $\leq 10^{-12}$. In general, the eigenvalues of the burnup matrix appear to remain bounded near the negative real axis in all conceivable burnup calculation cases. This observation is exploited in the construction of the matrix exponential method, whose framework is considered in Sec. IV.

III. ESTABLISHED METHODS

III.A. Approximation near Origin

The most obvious approach is to calculate the exponential directly from the definition (4) using a truncated Taylor series. This approximation is naturally most accurate near the origin, so it is ill-suited for burnup calculations, where the matrix norm $\|\boldsymbol{A}t\|$ can become arbitrarily large. In some cases even increasing the number of terms does not improve the approximation because of the accuracy limitations in the computer arithmetics.[1] The accuracy of the series method can be improved by using the method of scaling and squaring, which is based on the identity

$$e^{\boldsymbol{A}t} = (e^{\boldsymbol{A}t/m})^m \quad , \tag{6}$$

where m can be taken as a power of two, $m = 2^k$, so that the norm $\|\boldsymbol{A}/m\|$ becomes sufficiently small. The truncated series is then calculated for the scaled matrix, and the result is squared by repeated multiplications. The accuracy of this technique may be compromised, if the elements of $e^{\boldsymbol{A}t}$ grow before they decay, as t increases. Numerical problems are faced when this so-called "hump" is located between t/m and t (Ref. 1). The series method with scaling and squaring is implemented in the ORIGEN code[6] by excluding short-lived nuclides from the burnup matrix and treating them separately.

The most well-established method for calculating the matrix exponential is probably the rational Padé approximation with scaling and squaring. For example, the matrix exponential function `expm` in MATLAB is based on this approach. Although this method generally outperforms the truncated Taylor series approach, it shares the requirement of $\|\boldsymbol{A}t\|$ remaining relatively small.[1] Accordingly, numerical problems are faced when $\|\boldsymbol{A}\| \gg 1$ and $t \sim 10^6$ s, both of which are plausible values in the context of burnup calculation.

III.B. Krylov Subspace Approach

Various Krylov subspace algorithms are currently very popular, and they have also been recently applied to burnup calculations.[7] In this framework, the original large and sparse matrix $\boldsymbol{A}$ is projected to a lower-dimensional Krylov subspace, and the matrix exponential is then calculated using the series method or the Padé approximation. The projection can be carried out with the well-known Arnoldi iteration, which results in m iteration steps to the partial Hessenberg reduction

$$\boldsymbol{A}\boldsymbol{Q}_m = \boldsymbol{Q}_m\boldsymbol{H}_m + h_{m+1,m}\boldsymbol{q}_{m+1}\boldsymbol{e}_m^T \quad , \tag{7}$$

where $\boldsymbol{Q}_m \in \mathbb{R}^{n\times m}$ is orthogonal, $\boldsymbol{H}_m \in \mathbb{R}^{m\times m}$ is a Hessenberg matrix, and $m < n$. The matrix exponential solution can then be approximated as

$$e^{\boldsymbol{A}t}\boldsymbol{n}_0 \approx \|\boldsymbol{n}_0\|\boldsymbol{Q}_m e^{\boldsymbol{H}_m t}\boldsymbol{e}_1 \quad . \tag{8}$$

This approach appears to be suitable for burnup problems because Krylov subspace methods tend to approximate better the eigenvalues located in the outermost part of the spectrum. These eigenvalues related to the short-lived nuclides are the ones that cause difficulties in most algorithms. Yamamoto, Tatsumi, and Sugimura[7] calculated the matrix exponential using Krylov subspace techniques and

diagonal Padé approximation with EXPOKIT (Ref. 8). They reported promising results in the case where the shortest half-life is ~30 s (^{106}Rh). In this case the burnup matrix norm was approximately $\|\boldsymbol{A}\| \approx 2.3 \times 10^{-2}$.

The m-dimensional Krylov subspace approximation of the matrix exponential is mathematically equivalent to approximating $e^{\boldsymbol{A}t}\boldsymbol{n}_0$ with a polynomial of degree $m-1$ that interpolates the exponential function in the Hermite sense at the eigenvalues of the Hessenberg matrix according to their multiplicities.[9] Consequently, it is evident that the approximation does not work well if the eigenvalues lie far apart from each other, even if the dimension of the subspace is increased. Therefore, the burnup time step must usually be split into smaller substeps in order to keep the eigenvalues located closer to each other.

Selecting the time step is probably the most challenging issue in applying the Krylov subspace approach. Most error estimates are derived from those of truncated Taylor series,[9,10] which leads to highly pessimistic estimates and accordingly impractically short time steps when $\|\boldsymbol{A}\| \gg 1$ and $t \sim 10^6$ s. We found that in such cases error estimation based on the concept of generalized residual[11] gave the most realistic results. However, even when the time step is chosen to be as large as possible, the computation time can easily become prohibitively long. Based on our experiments, it seems that the Krylov subspace approximation alone is not practical for burnup calculations when $\|\boldsymbol{A}\| \gg 1$. However, if the nuclides with the shortest half-lives are excluded from the burnup matrix, this approximation could be a viable replacement for mere Padé approximation with scaling and squaring, for example. Numerical examples are presented in Sec. V.

IV. QUADRATURE FORMULAS AND RATIONAL APPROXIMATION

As mentioned in Sec. II, the eigenvalues of the burnup matrix appear to be generally confined to the vicinity of the negative real axis $\mathbb{R}^-$. This observation is exploited in the matrix exponential method that is described in detail in this section.

IV.A. Relation to Contour Integrals

By the Cauchy integral formula, the solution of system (2) can be represented as a contour integral,

$$\boldsymbol{n}(t) = e^{\boldsymbol{A}t}\boldsymbol{n}_0 = \frac{1}{2\pi i}\int_\Gamma e^z (z\boldsymbol{I} - \boldsymbol{A}t)^{-1}\boldsymbol{n}_0\, dz \ , \qquad (9)$$

where Γ is a closed contour winding once around the spectrum of $\boldsymbol{A}t$. The resolvent of the matrix $\boldsymbol{A}t$ can be written in the form

$$(z\boldsymbol{I} - \boldsymbol{A}t)^{-1} = \frac{\boldsymbol{B}(z)}{\det(z\boldsymbol{I} - \boldsymbol{A}t)} \ , \qquad (10)$$

where

$$\boldsymbol{B}(z) = z^{n-1}\boldsymbol{B}_0 + z^{n-2}\boldsymbol{B}_1 + \cdots + z\boldsymbol{B}_{n-2} + \boldsymbol{B}_{n-1} \qquad (11)$$

with $\boldsymbol{B}_0, \boldsymbol{B}_1, \ldots, \boldsymbol{B}_{n-1}$ matrices with constant elements.[12] It follows that every element of the resolvent is a proper rational function of z with the same denominator polynomial $\det(z\boldsymbol{I} - \boldsymbol{A}t)$. Hence, the poles of these rational functions are the eigenvalues of the matrix $\boldsymbol{A}t$, and calculating $\boldsymbol{n}(t)$ is essentially equivalent to evaluating contour integrals of the form

$$I = \frac{1}{2\pi i}\int_\Gamma e^z f(z)\, dz \ , \qquad (12)$$

where $f = \mathcal{O}(1)$ when $z \to -\infty$, and the singularities of f are the eigenvalues of $\boldsymbol{A}t$.

Integrals of this type are also encountered in the context of Laplace transforms, where they are usually written in the form

$$G(t) = \frac{1}{2\pi i}\int_\Gamma e^{st} g(s)\, ds = \frac{1}{2\pi i}\int_\Gamma e^z g(zt^{-1})t^{-1}\, dz \ . \qquad (13)$$

It should be noted that the solution of system (2) can also be written as an inverse Laplace transform of the form

$$\boldsymbol{n}(t) = \frac{1}{2\pi i}\int_B e^{st}(s\boldsymbol{I} - \boldsymbol{A})^{-1}\boldsymbol{n}_0\, ds = \frac{1}{2\pi i}\int_B e^z (zt^{-1}\boldsymbol{I} - \boldsymbol{A})^{-1}t^{-1}\boldsymbol{n}_0\, dz \ , \qquad (14)$$

where B denotes the Bromwich contour running from $-i\infty$ to $+i\infty$.

IV.B. Rational Approximation

When the contour Γ lies in the region of analyticity of f, integral (12) is independent of Γ under mild assumptions. When all of the singularities of function f are confined to a region near the negative real axis, Γ can be widened out to a parabolic or hyperbolic shape in the left complex plane. Because the integrand will decrease exponentially, these contour integrals can be efficiently approximated using numerical methods. These quadrature formulas can be associated with rational functions whose poles are the nodes and residues are the weights of the numerical integration formula. The proof can be found, e.g., in Ref. 13 and is repeated here.

Let $\phi(\theta)$ be an analytic function that maps the real line $\mathbb{R}$ onto the contour Γ that encloses the eigenvalues of matrix $\boldsymbol{A}t$. Integral (12) can then be written

$$I = \frac{1}{2\pi i} \int_{-\infty}^{\infty} e^{\phi(\theta)} f(\phi(\theta)) \phi'(\theta)\, d\theta \ . \tag{15}$$

This integral can be approximated by the trapezoid rule with N points θ_k spaced regularly on the interval $[-\pi, \pi]$ (chosen here for simplicity) yielding the approximation

$$I_N = (iN)^{-1} \sum_{k=1}^{N} e^{z_k} f(z_k) w_k = -\sum_{k=1}^{N} c_k f(z_k) \ , \tag{16}$$

where

$$z_k = \phi(\theta_k) \ ,$$

$$w_k = \phi'(\theta_k) \ ,$$

and

$$c_k = -(iN)^{-1} e^{z_k} w_k = iN^{-1} e^{z_k} w_k \ .$$

By the Cauchy integral formula, this sum can be written

$$I_N = \frac{1}{2\pi i} \int_C r(z) f(z)\, dz \ , \tag{17}$$

where $r(z)$ is a rational function of the form

$$r(z) = \sum_{k=1}^{N} \frac{c_k}{z - z_k} \tag{18}$$

and C is a negatively oriented closed contour that lies in the region of analyticity of f and encloses all the poles z_k.

Let Γ' denote the contour that has the same shape as Γ but lies between the contours C and Γ. Here, $f(z) = \mathcal{O}(1)$ so that $r(z)f(z) = \mathcal{O}(|z|^{-1})$ as $|z| \to \infty$. It follows that the contour C can be deformed to a contour consisting of the union of Γ' and a large circular arc with radius R so that

$$\lim_{R \to \infty} \int_{C_R} r(z) f(z)\, dz = 0 \ . \tag{19}$$

This gives the quadrature rule error estimate

$$I - I_N = \frac{1}{2\pi i} \int_{\Gamma'} (e^z - r(z)) f(z)\, dz \ , \tag{20}$$

which implies that $r(z)$ is a good approximation to e^z near $\mathbb{R}^-$. Therefore, any quadrature formula can be interpreted as a rational approximation. In the same way, every rational approximation can be viewed as a quadrature formula for a contour in the complex plane.

The selection of the contour and quadrature formula has been studied extensively in the context of inverse Laplace transforms. For the case where all of the singularities of f lie on the negative real axis, quite impressive convergence rates have been recently derived.[14] For example, for a cotangent contour originally suggested by Talbot,[15] a convergence rate $\mathcal{O}(3.89^{-N})$ can be achieved by using a trapezoid rule. Of course, it should be kept in mind that the selection of optimal contour and quadrature formula are related to the singularities of the function f.

IV.C. Best Rational Approximation

Another approach to rational approximation is to calculate the best approximation on some subset of the complex plane. This approach was made famous by Cody, Meinardus, and Varga[16] in 1969 in the context of rational approximation of e^{-x} in $[0,\infty)$. Let $\pi_{k,l}$ denote the collection of all real rational functions $r_{k,l}(x)$ of the form

$$r_{k,l} = \frac{p_k(x)}{p_l(x)} \ , \tag{21}$$

where p_j is a polynomial of degree j or less.

It is known from approximation theory that there exists a unique $\hat{r}_{k,l} \in \pi_{k,l}$ such that

$$\sup_{-\infty < x \le 0} |\hat{r}_{k,l}(-x) - e^x| = \inf_{r_{k,l} \in \pi_{k,l}} \left\{ \sup_{-\infty < x \le 0} |r_{k,l}(-x) - e^x| \right\} \ , \quad k \le l \ . \tag{22}$$

Establishing this approximation for given k and l is not easy, but it can be done with the Remes algorithm or the Carathéodory-Fejér method. It has been shown that this Chebyshev rational approximation $\hat{r}_{k,k}$ converges approximately at the rate 9.3^{-k} (Ref. 17). The contour plot of $|e^z - \hat{r}_{14,14}(-z)|$ is shown in Fig. 1, from which it can be seen that this approximation is remarkably accurate in a wide region in the left complex plane. From a computational point of view, it is advantageous that the poles $\{\theta_1, \ldots, \theta_k\}$ of the rational function $\hat{r}_{k,k}$ are distinct, so that it can be computed as a partial fraction expansion[10]

$$\hat{r}_{k,k}(z) = \alpha_0 + \sum_{i=1}^{k} \frac{\alpha_i}{z - \theta_i} \ , \tag{23}$$

where α_0 is the limit of the function at infinity and the scalars α_i are the residues at the poles θ_i. Therefore, the values of α_i and θ_i depend on k. Equation (23) can be derived by noting that $(\hat{r}_{k,k} - \alpha_0) \in \pi_{k-1,k}$ for which the result readily follows from the residue theorem. It should be noted that the poles of $\hat{r}_{k,k}$ come in conjugate pairs, so that for a real-valued variable $x \in \mathbb{R}$, the computational cost can be reduced to half:

$$\hat{r}_{k,k}(x) = \alpha_0 + \mathrm{Re}\left(\sum_{i=1}^{k/2} \frac{\alpha_i}{x - \theta_i} \right) \ . \tag{24}$$

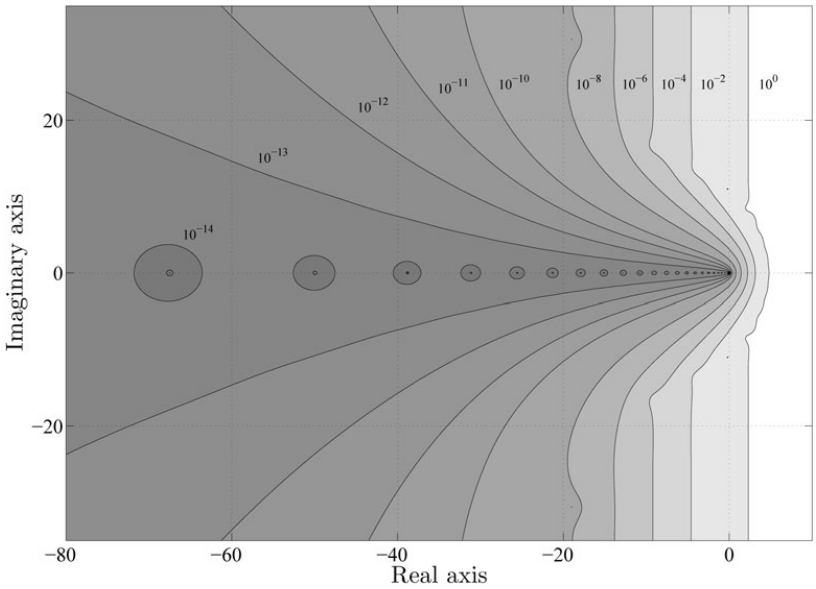

Fig. 1. Contour plot of $|e^z - \hat{r}_{14,14}(-z)|$.

The sets of coefficients for the Chebyshev rational function $\hat{r}_{k,k}$ have been reported for various approximation orders k, so the implementation of this method is relatively straightforward. For example, in Ref. 18 the polynomial coefficients are provided for $k \leq 30$. The partial fraction coefficients α_i and θ_i for each value of k can then be calculated from these polynomial coefficients with the help of a polynomial root finder. The partial fraction coefficients for the cases $k = 10$ and $k = 14$ have been directly given in Ref. 10. They can also be computed with the Carathéodory-Fejér method for $k \leq 14$ with good accuracy, and there is a MATLAB script provided for this purpose in Ref. 13.

Interestingly, the Chebyshev rational approximation $\hat{r}_{k,k}$ can also be interpreted as a quadrature formula for a contour integral of type (12), so the error estimate (20) remains valid.[13] This suggests that the rational approximation could be used for computing the matrix exponential $e^{\boldsymbol{A}t}$ when the eigenvalues of $\boldsymbol{A}t$ are located near the negative real axis. This has also been experimentally verified.[9] From this point of view, the accuracy of the approximation is affected by the magnitudes of the imaginary parts of the eigenvalues of $\boldsymbol{A}$ as long as the eigenvalues remain within the integration contour. However, if the eigenvalues fall outside the contour, Eq. (20) is no longer valid, and this method may yield poor results.

The Chebyshev rational approximation has previously been only occasionally used in scientific applications involving self-adjoint and negative semidefinite matrices.[8,16,19] Equation (20) implies, however, that this approximation is also applicable to non-Hermitian matrices with eigenvalues near $\mathbb{R}^-$. The formal convergence analysis of this special case forms an interesting future research topic.

For the burnup system (2), the matrix exponential solution based on the Chebyshev rational approximation $\hat{r}_{k,k}$ can be computed as

$$\boldsymbol{n}(t) = e^{\boldsymbol{A}t}\boldsymbol{n}_0 \approx \hat{r}_{k,k}(-\boldsymbol{A}t)\boldsymbol{n}_0 = \alpha_0\boldsymbol{n}_0 - \mathrm{Re}\left(\sum_{i=1}^{k/2}(\theta_i\boldsymbol{I} + \boldsymbol{A}t)^{-1}\alpha_i\boldsymbol{n}_0\right) , \quad (25)$$

where the last form follows directly from Eq. (24) by replacing x with $-\boldsymbol{A}t$. Using this formula, the concentration vector can be calculated simply by solving $k/2$ sparse linear systems. When the burnup matrix is formed by indexing the nuclides in ascending order with respect to their mass number, these systems can be solved efficiently by first calculating the symbolic lower-upper (LU) factorization of $\boldsymbol{A}$ (Ref. 20) and then performing a Gaussian elimination on this factorization.[21] The structure of a typical large burnup matrix generated in this manner is shown in Fig. 2.

It should be noted that this approximation is ideally suited for decay transmutation calculations, where the absence of closed cycles in the transition chains confines all eigenvalues of the decay matrix to lie strictly on the

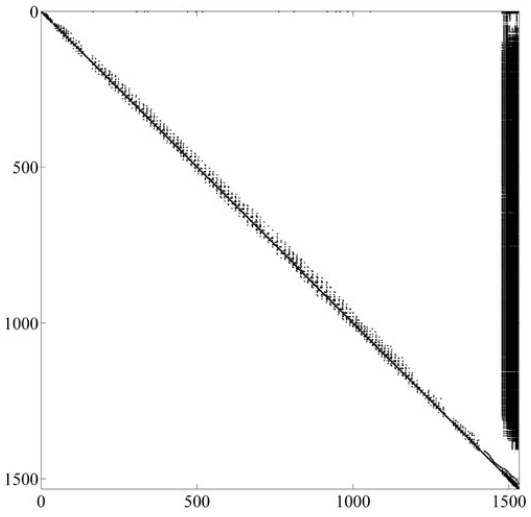

Fig. 2. The structure of the burnup matrix in test case 2 described in Sec. V. The nuclides have been indexed in ascending order with respect to their mass number. The result is that the nonzero elements are concentrated around the diagonal with fission product distributions on the right side.

negative real axis. Another fact worth noticing in Eq. (25) is that the order of the approximation can be adjusted according to needs for accuracy without significant impact on the computational cost as the amount $k/2$ of sparse matrix inversions is directly proportional to the order k of the approximation. However, it should be kept in mind that a rigorous mathematical analysis concerning the convergence properties of this approximation for other than self-adjoint negative semidefinite matrices has not been performed.

V. NUMERICAL RESULTS

The different matrix exponential methods and the TTA method were compared to each other by applying them to several burnup matrices. The two cases presented here can be thought to represent the extreme cases—in terms of matrix size and norm—that were encountered, and they were chosen for evaluating the performance of the different matrix exponential methods.

Both test cases represent an infinite pressurized water reactor (PWR) pin-cell lattice in which the fuel has been irradiated to 25 MWd/kg U burnup. Test case 1 was formed by selecting only the most important actinides and fission products in the calculation, totaling 219 nuclides (41 actinides, 178 fission products and light nuclides). For this case the matrix norm is sufficiently small, $\|\boldsymbol{A}\| \approx 7.3 \times 10^{-4}$, so that $\|\boldsymbol{A}t\| \approx 7.9 \times 10^{3}$. This case is a simplification of test case 2, which contains 1532 nuclides (75 actinides, 1457 fission products and light nuclides). The burnup matrix norm for this case is approximately $\|\boldsymbol{A}\| \approx 2.8 \times 10^{21}$ so that the norm of $\boldsymbol{A}t$ is of order 10^{28}. The time step in both test cases was 125 days corresponding to 5 MWd/kg U burnup.

The TTA results were obtained directly from the Serpent code, and the Chebyshev rational approximation method (CRAM) of order $k = 14$ was implemented as a separate C code that was later added to Serpent. This order for the Chebyshev approximation was chosen because it is generally considered sufficiently accurate[22] and because the partial fraction coefficients for this case are conveniently listed in Ref. 10. The Krylov subspace approximation with adaptive time step and subspace dimension selection was implemented as a MATLAB script. Finally, the standard MATLAB function `expm` was used for the Padé approximation with scaling and squaring.

The numerical results for test case 1 are shown in Fig. 3, from which it can be seen that all results are in good accordance with each other. In particular, the Padé approximation, the Krylov subspace method, and CRAM give almost identical results for this case, as can be seen from Fig. 4, where the absolute values of the relative differences are plotted. For example, the largest relative difference between the Chebyshev and Padé approximation solutions is ~0.00068% for the concentration of ^{252}Cf, for which $N \approx 2.17 \times 10^{-19}$ (b cm)$^{-1}$.

The nuclide concentrations in test case 2 are shown in Fig. 5. The Krylov subspace method could not be applied to this case because the time step selection based on local error estimation became practically impossible. The Padé approximation also faced severe numerical problems producing completely unrealistic results, as can be seen from Fig. 5. On the other hand, the solutions calculated with the TTA method and CRAM are consistent to the same degree as in test case 1. The comparison between these numerical results for the most important nuclides is presented in Table I.

The small differences between the TTA and the CRAM solutions can be attributed to the fact that the closed cycles are terminated in the current implementation of the TTA method. This is supported by the fact that all the concentrations calculated with CRAM are slightly greater, as can be physically expected considering that the feedback transitions are ignored in the TTA calculation. Also, the largest differences occur for nuclides for which the closed transition cycles are significant. In test case 1, for example, the largest relative difference, 0.84%, occurs for the hydrogen isotope ^{3}H, which forms one strongly connected component with the nuclides ^{1}H, ^{2}H, and ^{3}He.

As is pointed out in Sec. IV, the accuracy of CRAM depends on the magnitudes of the imaginary parts of the eigenvalues of $\boldsymbol{A}t$. In this test case the power density in the fuel was 40 kW/kg U, which results in a neutron flux

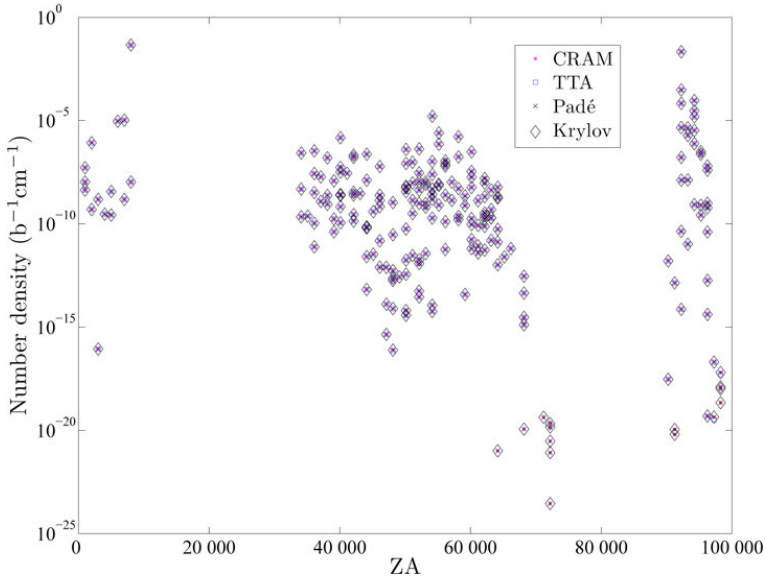

Fig. 3. Nuclide number densities for test case 1. Number densities smaller than 10^{-30} $(\mathrm{b\,cm})^{-1}$ have been omitted. ZA = $1000Z + A$, where Z is the atomic number and A is the mass number of the nuclide.

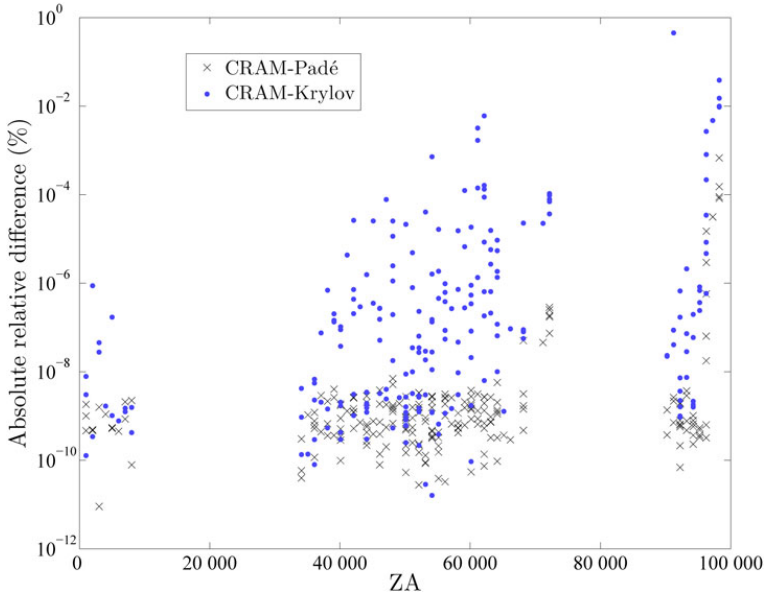

Fig. 4. Absolute values of the relative differences between the results calculated by CRAM, Padé approximation, and the Krylov subspace method. ZA = $1000Z + A$, where Z is the atomic number and A is the mass number of the nuclide.

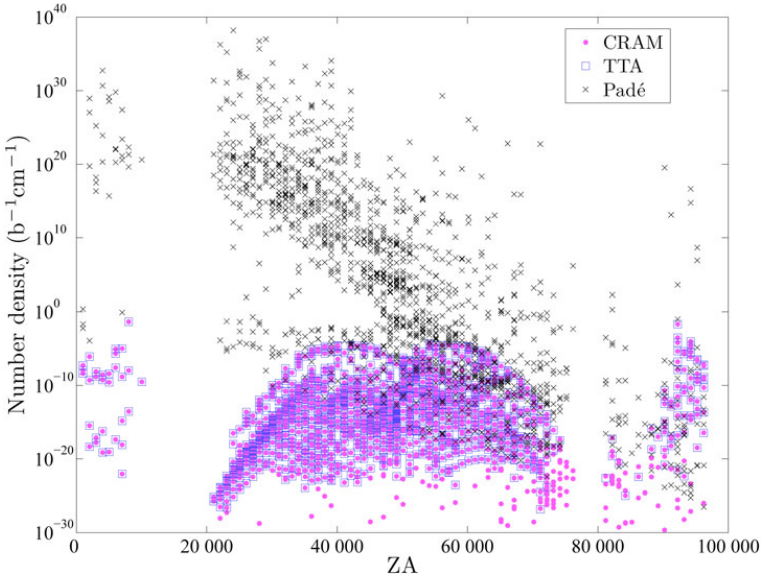

Fig. 5. Nuclide number densities in test case 2. Number densities smaller than 10^{-30} b^{-1} cm^{-1} have been omitted. ZA = $1000Z + A$, where Z is the atomic number and A is the mass number of the nuclide.

of 1.5×10^{14} 1/(cm^2 s) producing transmutation coefficients, most of which are of order $\leq 10^{-8}$ 1/s. The imaginary parts of the eigenvalues were correspondingly of the same order. The time steps in the burnup calculation generally vary from a few days at the beginning of the irradiation cycle to a few hundred days at the end. The time step used here was 125 days, which is of the same order as the practical maximum time step. Time steps greater than this would significantly violate the assumption of constant transmutation coefficients during each step. Therefore, even better convergence can be expected for shorter time steps.

Based on these observations, it seems that the CRAM method is capable of providing robust and accurate solutions regardless of the burnup matrix size or norm. The method is also computationally remarkably effective. The computation time for test case 2 involving a 1532 × 1532 matrix was only 0.1 s on a 2.6-GHz AMD Opteron CPU. The corresponding computation time for the TTA calculation was ~26 s. To further illustrate the efficiency of the CRAM method, it was compared to the TTA solution method using Serpent in a burnup calculation for a PWR fuel assembly with burnable absorber. The total number of depleted materials was 65, the irradiation history was divided into 42 steps with predictor-corrector calculation, and a total of 3 million neutron histories were run for each Monte Carlo simulation. The overall running time with TTA was 18.5 h, and using CRAM this was reduced to just over 13 h, which can be considered a significant improvement.

When computing the CRAM solution, most of the computation time is spent inverting the sparse matrices of Eq. (25). As pointed out in Sec. IV, the structure of the burnup matrix is crucial to the effectiveness of the solution scheme. In comparison to a random nuclide order, indexing the nuclides according to their mass number led to a computational speedup factor of 40 in test case 2. The corresponding ordered matrix is illustrated in Fig. 2. In this case, the sparse systems can be solved accurately and effectively by first calculating the symbolic LU factorization and then performing a Gaussian elimination on this factorization.

VI. CONCLUSIONS

The magnitude of the transmutation and decay constants of different nuclides vary extensively, which makes calculating the matrix exponential challenging in the context of burnup calculations. Short-lived nuclides are especially problematic because they can increase the matrix norm and induce eigenvalues with absolute values up to order 10^{21}.

We approached this problem by examining the characteristics of the eigenvalues of the burnup matrix. Based

TABLE I

A Comparison of the Numerical Results Computed Using CRAM and the TTA Method for the Most Important Nuclides

Nuclide	Case 1		Case 2	
	Concentration, CRAM ($b^{-1}\,cm^{-1}$)	Relative Difference to TTA (%)	Concentration, CRAM ($b^{-1}\,cm^{-1}$)	Relative Difference to TTA (%)
Actinides				
^{234}U	4.5718×10^{-6}	5.4633×10^{-5}	4.5632×10^{-6}	5.5873×10^{-5}
^{235}U	3.0456×10^{-4}	7.3299×10^{-5}	3.0738×10^{-4}	8.0322×10^{-5}
^{236}U	6.7457×10^{-5}	2.4295×10^{-5}	6.7627×10^{-5}	2.6525×10^{-5}
^{238}U	2.1423×10^{-2}	2.5090×10^{-5}	2.1413×10^{-2}	2.7600×10^{-5}
^{239}U	1.2933×10^{-8}	2.5083×10^{-5}	1.3510×10^{-8}	2.7595×10^{-5}
^{237}Np	4.3857×10^{-6}	3.2838×10^{-5}	4.4366×10^{-6}	4.2891×10^{-5}
^{239}Np	1.8656×10^{-6}	2.4399×10^{-5}	1.9488×10^{-6}	2.6853×10^{-5}
^{238}Pu	7.5350×10^{-7}	2.8311×10^{-5}	7.8289×10^{-7}	4.7964×10^{-5}
^{239}Pu	9.1938×10^{-5}	6.6197×10^{-5}	9.5985×10^{-5}	7.0639×10^{-5}
^{240}Pu	2.9316×10^{-5}	3.9718×10^{-4}	2.9007×10^{-5}	4.6375×10^{-4}
^{241}Pu	1.5002×10^{-5}	3.9580×10^{-4}	1.6400×10^{-5}	4.5646×10^{-4}
^{242}Pu	3.2839×10^{-6}	1.3219×10^{-4}	3.5014×10^{-6}	1.5190×10^{-4}
^{241}Am	2.3450×10^{-7}	1.2989×10^{-4}	2.5499×10^{-7}	1.6080×10^{-4}
^{242}Am	7.9173×10^{-10}	1.3073×10^{-4}	8.6280×10^{-10}	1.6164×10^{-4}
^{243}Am	3.1046×10^{-7}	4.7632×10^{-5}	3.4995×10^{-7}	5.4590×10^{-5}
^{242}Cm	6.2763×10^{-8}	4.7059×10^{-5}	6.8238×10^{-8}	6.1609×10^{-5}
^{244}Cm	3.9601×10^{-8}	9.7363×10^{-5}	4.8298×10^{-8}	1.0704×10^{-4}
Fission products and light nuclides				
^{3}H	5.2271×10^{-8}	8.4335×10^{-1}	5.2535×10^{-8}	8.2818×10^{-1}
^{95}Mo	1.6225×10^{-7}	7.4205×10^{-6}	1.9623×10^{-5}	8.6482×10^{-6}
^{99}Tc	2.9344×10^{-9}	1.0370×10^{-5}	2.5379×10^{-5}	2.1573×10^{-5}
^{103}Ru	6.2905×10^{-11}	5.7469×10^{-5}	2.3941×10^{-6}	8.4875×10^{-5}
^{109}Ag	7.7335×10^{-13}	1.1614×10^{-3}	1.8199×10^{-6}	1.3940×10^{-4}
^{135}Xe	2.7013×10^{-9}	4.9536×10^{-4}	7.2419×10^{-9}	5.6080×10^{-4}
^{133}Cs	8.2702×10^{-9}	3.2331×10^{-5}	2.6399×10^{-5}	6.5866×10^{-5}
^{143}Nd	3.4130×10^{-8}	4.3039×10^{-5}	1.9255×10^{-5}	6.6319×10^{-5}
^{145}Nd	1.7186×10^{-11}	2.3102×10^{-4}	1.6098×10^{-5}	1.2200×10^{-4}
^{147}Sm	1.7783×10^{-10}	1.6831×10^{-5}	1.0618×10^{-6}	1.3204×10^{-5}
^{149}Sm	5.2676×10^{-12}	2.0827×10^{-4}	6.6335×10^{-8}	4.3958×10^{-3}
^{150}Sm	3.2992×10^{-10}	8.6619×10^{-5}	5.3727×10^{-6}	3.4225×10^{-4}
^{151}Sm	2.0391×10^{-9}	4.2694×10^{-4}	3.1044×10^{-7}	5.6033×10^{-3}
^{152}Sm	9.3582×10^{-9}	3.3607×10^{-4}	2.5405×10^{-6}	8.8872×10^{-4}
^{153}Eu	4.3027×10^{-9}	1.2505×10^{-4}	1.8654×10^{-6}	3.8255×10^{-3}
^{155}Gd	1.0272×10^{-12}	1.0841×10^{-1}	6.4533×10^{-10}	1.4526×10^{-2}

on our experiments and physical reasoning, it seems that these eigenvalues are generally confined to a region near the negative real axis. The somewhat obscure fact that the CRAM technique can be interpreted as a numerical contour integral in the left complex plane led us to conduct further experiments with very promising results. We compared this approach with more established matrix exponential methods and the TTA method in solving the burnup equations. Our results imply that the CRAM solution scheme is well-suited for burnup calculation, where it outperformed the more conventional matrix exponential methods in terms of computational accuracy and efficiency. Unlike the previously applied matrix exponential methods, CRAM can readily treat the short-lived nuclides simultaneously with the long-lived nuclides. In addition, the practical maximum time step value can be used in CRAM without compromising the computational accuracy.

For evaluating the matrix exponential methods, we constructed two representative test cases. Test case 1 was designed to be well-behaved in terms of the burnup matrix size and norm ($[\boldsymbol{A}] \approx 200 \times 200$, $\|\boldsymbol{A}\| \sim 10^{-4}$), and test case 2 was designed to be pathologically difficult ($[\boldsymbol{A}] \approx 1500 \times 1500$, $\|\boldsymbol{A}\| \sim 10^{21}$). In test case 1, which

was well within the applicability domain of each tested method, the Padé approximation and CRAM gave virtually identical results. The results obtained with the Krylov subspace matrix exponential method were close, as well. The system was also solved using the TTA method, which gave coherent results. In test case 2, however, all other matrix exponential methods suffered a breakdown, but the results obtained with CRAM remained consistent with those given by the TTA method to the same degree as in the first test case.

Our motivation for the research was the prospect of incorporating a matrix exponential method in the burnup calculation routine of the Serpent code. Based on our positive results, CRAM was added to the code with computational speedup as one of the key improvements.

REFERENCES

1. C. MOLER and C. VAN LOAN, "Nineteen Dubious Ways to Compute the Exponential of a Matrix, Twenty-Five Years Later," *SIAM Rev.*, **45** (2003).

2. J. LEPPÄNEN, "PSG2/Serpent—A Continuous-Energy Monte Carlo Reactor Physics Burnup Calculation Code," VTT Technical Research Centre of Finland; available on the Internet at http://montecarlo.vtt.fi (Nov. 2008).

3. J. CETNAR, "General Solution of Bateman Equations for Nuclear Transmutations," *Ann. Nucl. Energy*, **33**, 640 (2006).

4. H. AMANN, *Ordinary Differential Equations, An Introduction to Nonlinear Analysis*, Walter de Gruyter, Berlin (1990).

5. R. E. TARJAN, "Depth-First Search and Linear Graph Algorithms," *SIAM J. Comput.*, **1**, *2*, 146 (1972).

6. I. C. GAULD, O. W. HERMANN, and R. M. WESTFALL, "Origen-S: Scale System Module to Calculate Fuel Depletion, Actinide Transmutation, Fission Product Buildup and Decay, and Associated Radiation Source Terms," in "SCALE: A Modular Code System for Performing Standardized Computer Analyses for Licensing Evaluation," Vol. II, Sec. F7, Oak Ridge National Laboratory/U.S. Nuclear Regulatory Commission (Nov. 2006).

7. A. YAMAMOTO, M. TATSUMI, and N. SUGIMURA, "Numerical Solution of Stiff Burnup Equations with Short Half Lived Nuclides by the Krylov Subspace Method," *J. Nucl. Sci. Technol.*, **44**, *2*, 147 (2007).

8. R. B. SIDJE, "Expokit: A Software Package for Computing Matrix Exponentials," *ACM Trans. Math. Software*, **24**, *1*, 130 (1998).

9. Y. SAAD, "Analysis of Some Krylov Subspace Approximations to the Matrix Exponential Operator," *SIAM J. Numer. Anal.*, **29**, *1*, 209 (1992).

10. E. GALLOPOULOS and Y. SAAD, "Efficient Solution of Parabolic Equations by Krylov Approximation Methods," *SIAM J. Sci. Stat. Comput.*, **13**, *5*, 1236 (1992).

11. M. HOCHBRUCK, C. LUBICH, and H. SELHOFER, "Exponential Integrators for Large Systems of Differential Equations," *SIAM J. Sci. Comput.*, **19**, *5*, 1552 (1998).

12. L. A. ZADEH and C. A. DESOER, *Linear System Theory: The State Space Approach*, McGraw-Hill Book Company (1963).

13. L. N. TREFETHEN, J. A. C. WEIDEMAN, and T. SCHMELZER, "Talbot Quadratures and Rational Approximations," *BIT Numer. Math.*, **46**, *3*, 653 (2006).

14. J. WEIDEMAN and L. N. TREFETHEN, "Parabolic and Hyperbolic Contours for Computing the Bromwich Integral," *Math. Comp.*, **76**, *259*, 1341 (2007).

15. A. TALBOT, "The Accurate Numerical Inversion of Laplace Transforms," *J. Instrum. Math. Appl.*, **23**, 97 (1979).

16. W. J. CODY, G. MEINARDUS, and R. S. VARGA, "Chebyshev Rational Approximations to e^{-x} in $[0,\infty)$ and Applications to Heat-Conduction Problems," *J. Approx. Theory*, **2**, 50 (1969).

17. A. A. GONCHAR and E. A. RAKHMANOV, "Equilibrium Distributions and Degree of Rational Approximation of Analytic Functions," *Mat. Sb.*, **134**, 306 (1987); see also *Math. USSR Sb.*, **62**, *2*, 305 (1989) (translation).

18. A. J. CARPENTER, A. RUTTAN, and R. S. VARGA, "Extended Numerical Computations on the 1/9 Conjecture in Rational Approximation Theory," in "Rational Approximation and Interpolation," *Lecture Notes in Mathematics*, Vol. 1105, pp. 383–411, P. R. GRAVES-MORRIS, E. B. SAFF, and R. S. VARGA, Eds., Springer-Verlag (1984).

19. T. SCHMELZER and L. N. TREFETHEN, "Evaluating Matrix Functions for Exponential Integrators via Carathéodory-Fejér Approximation and Contour Integrals," *Electron. Trans. Numer. Anal.*, **28**, 1 (2007).

20. D. J. ROSE and R. E. TARJAN, "Algorithmic Aspects of Vertex Elimination on Directed Graphs," *SIAM J. Appl. Math*, **40**, 176 (1978).

21. R. E. TARJAN, "Graph Theory and Gaussian Elimination," CS-TR-75-526, Stanford University, Department of Computer Science (1975).

22. L. LOPEZ and V. SIMONCINI, "Analysis of Projection Methods for Rational Function Approximation to the Matrix Exponential," *SIAM J. Numer. Anal.*, **44**, *2*, 613 (2007).

PUBLICATION II

Rational approximations to the matrix exponential in burnup calculations

In: Nuclear Science and Engineering,
169, 2, pp. 155–167.

NUCLEAR SCIENCE AND ENGINEERING: **169**, 155–167 (2011)

Rational Approximations to the Matrix Exponential in Burnup Calculations

Maria Pusa*

VTT Technical Research Centre of Finland
P.O. Box 1000, FI-02044 VTT, Finland

Received October 26, 2010
Accepted February 28, 2011

Abstract—*The topic of this paper is solving the burnup equations using dedicated matrix exponential methods that are based on two different types of rational approximation near the negative real axis. The previously introduced Chebyshev Rational Approximation Method (CRAM) is now analyzed in detail for its accuracy and convergence, and correct partial fraction coefficients for approximation orders 14 and 16 are given to facilitate its implementation and improve the accuracy. As a new approach, rational approximation based on quadrature formulas derived from complex contour integrals is proposed, which forms an attractive alternative to CRAM, as its coefficients are easy to compute for any order of approximation. This gives the user the option to routinely choose between computational efficiency and accuracy all the way up to the level permitted by the available arithmetic precision. The presented results for two test cases are validated against reference solutions computed using high-precision arithmetics. The observed behavior of the methods confirms the previous conclusions of CRAM's excellent suitability for burnup calculations and establishes the quadrature-based approximation as a viable and flexible alternative that, like CRAM, has its foundation in the specific eigenvalue properties of burnup matrices.*

I. INTRODUCTION

The topic of this paper is solving the burnup equations using matrix exponential methods based on rational approximation near the negative real axis. Solving the burnup equations is an essential part of the burnup calculations that are necessary to predict the changes in the material compositions in a nuclear reactor.

The burnup equations form a system of first-order linear differential equations that can be written in matrix notation as

$$\boldsymbol{n}' = \boldsymbol{A}\boldsymbol{n} \ , \quad \boldsymbol{n}(0) = \boldsymbol{n}_0 \ , \tag{1}$$

where

$\boldsymbol{n}(t) \in \mathbb{R}^n$ = nuclide concentration vector

$\boldsymbol{A} \in \mathbb{R}^{n \times n}$ = burnup matrix containing the decay and transmutation coefficients of the nuclides under consideration.

*Email: Maria.Pusa@vtt.fi

The matrix elements A_{ij} characterize the rates of neutron-induced reactions and spontaneous radioactive decay by which nuclide j is transformed to nuclide i. In this paper these coefficients are assumed to be fixed constants.

The burnup equations can be formally solved by the matrix exponential method yielding the simple solution

$$\boldsymbol{n}(t) = e^{\boldsymbol{A}t}\boldsymbol{n}_0 \ , \tag{2}$$

where the exponential of the matrix $\boldsymbol{A}t$ is defined as the power series expression

$$e^{\boldsymbol{A}t} = \sum_{k=0}^{\infty} \frac{1}{k!} (\boldsymbol{A}t)^k \ , \tag{3}$$

with the additional definition $\boldsymbol{A}^0 = \boldsymbol{I}$. There are numerous algorithms for computing the matrix exponential, but unfortunately, most of them are not well-suited for solving the burnup equations. Because the decay constants of the nuclides vary extensively, the burnup matrix has a wide spectrum of eigenvalues. Short-lived

nuclides are especially problematic since they can induce eigenvalues with absolute values up to an order of 10^{21}, consequently making the differential system extremely stiff. Furthermore, the time steps used in burnup calculations can typically vary from a few days (10^5 s) to several months (10^7 s), and even to thousands of years, if only decay reactions are considered. Most of the established matrix exponential methods, such as the truncated Taylor series approach or rational Padé approximation, are based on approximation near the origin and work well only when the matrix norm $\|\boldsymbol{A}t\|$ is sufficiently small. Consequently, these algorithms are prone to severe numerical problems when applied to the burnup equations, where this norm can be of the order of 10^{27} (Ref. 1).

These difficulties have traditionally been solved by using simplified burnup chains or by treating the most short-lived nuclides separately when computing a matrix exponential solution. For example, in the ORIGEN code,[2] the matrix exponential is computed with the truncated Taylor series method with scaling and squaring after excluding short-lived nuclides from the burnup matrix to be treated separately. In the AEGIS code, a Krylov subspace method is applied to a simplified burnup chain with 221 nuclides, in which case the burnup matrix norm is of the order of 10^{-2} (Ref. 3). However, it was recently discovered by the author that the eigenvalues of the burnup matrix are generally confined to a region near the negative real axis.[1] This observation led to applying the Chebyshev Rational Approximation Method (CRAM) to solve the burnup equations. This method can be interpreted as the best rational approximation on the negative real axis, and it was shown to give a robust and accurate solution to the burnup equations with a very short computation time. For further information on established matrix exponential methods and their applicability to solving burnup equations, see, e.g., Refs. 1 and 4. For a comparison between CRAM and ORIGEN, see Ref. 5.

The main challenge in using CRAM is determining the coefficients of the Chebyshev rational approximation. The computation of higher-order CRAM coefficients especially can be rather involved. Motivated by these challenges in implementing CRAM, an alternative and easier-to-implement method is presented in Sec. II.B. This method is based on constructing rational approximations from trapezoidal quadrature rules applied to contour integrals in the left complex plane. Although these approximations do not converge as fast as CRAM, they have the advantage that the order of the approximation can easily be adjusted. These approximations are accurate near the negative real axis, so they are well-suited to solving the burnup equations and can be used to obtain extremely high solution accuracy. The convergence and accuracy of the different rational approximations applied to burnup equations are discussed in Sec. III.

II. RATIONAL APPROXIMATION OF THE MATRIX EXPONENTIAL NEAR THE NEGATIVE REAL AXIS

The matrix exponential can be computed based on a rational function $r(z)$ that is known to be a good approximation to the function e^z in some region in the complex plane $\mathbb{C}$. The matrix exponential and the approximating matrix rational function can be defined in various ways. The approach based on the Cauchy integral formula is considered here. Based on this formula, the matrix exponential can be written as a complex contour integral of the form

$$e^{\boldsymbol{A}t} = \frac{1}{2\pi i}\int_{\Gamma} e^z (z\boldsymbol{I} - \boldsymbol{A}t)^{-1}\, dz \ , \tag{4}$$

where Γ is a closed contour winding once around the spectrum of $\boldsymbol{A}t$. The resolvent of the matrix $\boldsymbol{A}t$ can be written in the form

$$(z\boldsymbol{I} - \boldsymbol{A}t)^{-1} = \frac{\boldsymbol{B}(z)}{\det(z\boldsymbol{I} - \boldsymbol{A}t)} \ , \tag{5}$$

where

$$\boldsymbol{B}(z) = z^{n-1}\boldsymbol{B}_0 + z^{n-2}\boldsymbol{B}_1 + \cdots + z\boldsymbol{B}_{n-2} + \boldsymbol{B}_{n-1} \tag{6}$$

with $\boldsymbol{B}_0, \boldsymbol{B}_1, \ldots, \boldsymbol{B}_{n-1}$ matrices with constant elements.[6] It follows that every element of the resolvent is a proper rational function of z with the same denominator polynomial $\det(z\boldsymbol{I} - \boldsymbol{A}t)$. Hence, the poles of these rational functions are the eigenvalues of the matrix $\boldsymbol{A}t$, and calculating $e^{\boldsymbol{A}t}$ is essentially equivalent to evaluating contour integrals of the form

$$(e^{\boldsymbol{A}t})_{kl} = \frac{1}{2\pi i}\int_{\Gamma} e^z R_{kl}(z)\, dz \ , \tag{7}$$

where $\boldsymbol{R} = (z\boldsymbol{I} - \boldsymbol{A}t)^{-1}$, $R_{kl} = \mathcal{O}(1)$ when $z \to -\infty$, and the singularities of R_{kl} are the eigenvalues of $\boldsymbol{A}t$. It follows that when the eigenvalues of $\boldsymbol{A}t$ are confined to a region near the negative real axis, Γ can be extended to a parabolic or hyperbolic shape in the left complex plane. Because the integrand will decrease exponentially, these contour integrals can be approximated efficiently using quadrature formulas. These quadrature formulas can be associated with rational functions, whose poles and residues are the nodes and weights of the numerical integration formula, respectively. In addition, every rational function can be correspondingly interpreted as a quadrature formula applied to a contour integral in the left complex plane (for proof, see Ref. 7).

It is usually advantageous to employ the rational approximation in the partial fraction decomposition (PFD) form. For a rational function $r_{k,k}(z) = p_k(z)/q_k(z)$ with simple poles, and p_k and q_k being polynomials of order k, the decomposition takes the form

$$r_{k,k}(z) = \alpha_0 + \sum_{j=1}^{k} \frac{\alpha_j}{z - \theta_j} \ , \tag{8}$$

where

α_0 = limit of the function $r_{k,k}$ at infinity

α_j = residues at the poles θ_j.

Also rational functions $r_{k-1,k}$ can be written in this form with $\alpha_0 = 0$. The poles of a rational function with real-valued coefficients form conjugate pairs, so the computational cost can be reduced to half for a real variable x:

$$r_{k,k}(x) = \alpha_0 + 2\mathrm{Re}\left(\sum_{j=1}^{k/2} \frac{\alpha_j}{x - \theta_j} \right) \ . \tag{9}$$

The rational approximation to Eq. (2) can then be written

$$\boldsymbol{n} = \alpha_0 \boldsymbol{n}_0 + 2\mathrm{Re}\left(\sum_{j=1}^{k/2} \alpha_j (\boldsymbol{A}t - \theta_j \boldsymbol{I})^{-1} \boldsymbol{n}_0 \right) \ , \tag{10}$$

which requires solving $k/2$ sparse linear systems. It is worth noting that the linear systems in Eq. (10) are independent, so they can be solved in parallel. Notice that Eq. (10) can be used to apply any rational approximation $r_{k,k}$ or $r_{k-1,k}$ to Eq. (2). A MATLAB code implementing this equation is shown in Fig. 1 to further illustrate how these approximations are computed in practice.

II.A. Chebyshev Rational Approximation Method

In CRAM the rational function $r(z)$ is chosen as the best rational approximation of the exponential function on the negative real axis $\mathbb{R}_-$. Let $\pi_{k,k}$ denote the set of rational functions $r_{k,k}(x) = p_k(x)/q_k(x)$, where p_k and q_k are polynomials of order k. The CRAM approximation of order k is defined as the unique rational function $\hat{r}_{k,k} = \hat{p}_k(x)/\hat{q}_k(x)$ satisfying

$$\sup_{x \in \mathbb{R}_-} |\hat{r}_{k,k}(x) - e^x| = \inf_{r_{k,k} \in \pi_{k,k}} \left\{ \sup_{x \in \mathbb{R}_-} |r_{k,k}(x) - e^x| \right\} \ . \tag{11}$$

The asymptotic convergence of this approximation on the negative real axis is remarkably fast. Let us define

$$\delta_k = \sup_{x \in \mathbb{R}_-} |\hat{r}_{k,k}(x) - e^x| \ . \tag{12}$$

It has been proven that

$$\lim_{k \to \infty} \delta_k^{1/k} = \frac{1}{9.289\,025\,49\ldots} = H \ , \tag{13}$$

where H is the Halphen constant that can be represented in closed form using certain elliptic integrals.[8] It follows that for sufficiently large approximation orders k, roughly k correct digits may be expected. Surprisingly, it was recently discovered by Stahl and Schmelzer[9] that this convergence extends to compact subsets on the complex plane and also to Hankel contours in $\mathbb{C} \setminus \mathbb{R}_-$, i.e.,

$$\lim_{k \to \infty} \left(\sup_{z \in K} |\hat{r}_{k,k}(z) - e^z| \right)^{1/k} = \lim_{k \to \infty} \left(\sup_{z \in \Gamma} |\hat{r}_{k,k}(z) - e^z| \right)^{1/k} = H \tag{14}$$

```
function n = rat_apprx(theta, alpha, alpha_0, A, t, n_0)

    % theta   = poles of the rational function r
    % alpha   = residues at these poles
    % alpha_0 = limit of r at infinity

    s = length(theta);
    A = A * t;
    n = 0 * n_0;

    for j = 1 : s
        n = n + (A - theta(j) * eye(size(A))) \ (alpha(j) * n_0);
    end
    n = 2 * real(n);
    n = n + alpha_0 * n_0;

end
```

Fig. 1. MATLAB code illustrating how a rational function $r_{k,k}$ or $r_{k-1,1}$ is applied to Eq. (1) to approximate the matrix exponential solution `n`. The input arguments are the partial fraction coefficients corresponding to the rational function, burnup matrix `A`, time step `t`, and initial composition vector `n_0`.

for any compact $K \subset \mathbb{C}$ and for any Hankel contour $\Gamma \subset \mathbb{C}\backslash\mathbb{R}_-$. However, it is worth noticing that this convergence is related to the asymptotic properties of the sequence $\{\delta_k\}$, and the accuracy of the approximation of order k is still dependent on the choice of the subset and the contour under consideration.

As previously stated, the main difficulty in using CRAM is determining the coefficients of the rational function for a given k. In principle the polynomial coefficients of $\hat{p}_k$ and $\hat{q}_k$ can be computed with Remez-type methods, but this requires delicate algorithms combined with high-precision arithmetics. Fortunately, these coefficients have been computed to a high accuracy by Carpenter, Ruttan, and Varga for approximation orders $k = 0, 1, \ldots, 30$, and they are provided in Ref. 10. In practical applications, however, CRAM approximation is usually needed in the PFD form. Although the PFD coefficients can in principle be computed from the polynomial coefficients, the computation of the polynomial roots is ill-conditioned and requires great care. The only reference providing the PFD coefficients (for approximation orders 10 and 14) is presumably Ref. 11, and the coefficients for approximation of order $k = 14$ have therefore been used in several applications including the EXPOKIT matrix exponential computing package[12] and Serpent reactor physics code.[13] However, it seems that these coefficients suffer from round-off errors and hence do not correspond to the true best approximation. Figure 2 shows the error of order 14 approximation on the negative real axis computed using two different sets of coefficients: the polynomial coefficients from Ref. 10 and the partial fraction coefficients from Ref. 11. According to theory, a necessary and sufficient condition for the best approximation is that the corresponding error function equioscillates; i.e., there exists a set of points where it attains its maximum absolute value with alternating signs. Notice that the approximation computed with the coefficients from Ref. 11 does not exhibit this behavior. In addition, these coefficients result in 10^2 times poorer accuracy than expected by theory.

To provide better accuracy, new sets of partial fraction coefficients for approximation orders $k = 14$ and $k = 16$ were computed from the polynomial coefficients provided in Ref. 10, and these coefficients are listed in Tables I and II. The computations were performed with MATLAB's Symbolic Toolbox using high-precision arithmetics with 200 digits to ensure sufficient accuracy. In Tables I and II the coefficients have been rounded off to

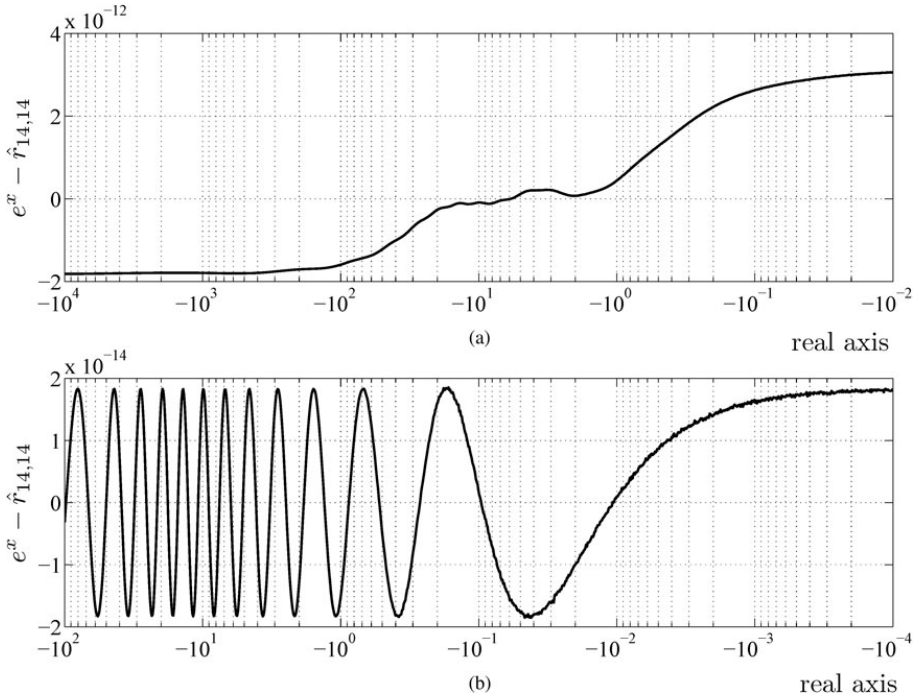

Fig. 2. Plot of $e^x - \hat{r}_{14,14}(x)$ on the negative real axis. In (a) $\hat{r}_{14,14}$ was computed based on the partial fraction coefficients from Ref. 11 and in (b) based on the polynomial coefficients from Ref. 10.

TABLE I

Partial Fraction Decomposition Coefficients for CRAM Approximation of Order 14

Coefficient	Real Part	Imaginary Part
θ_1	$-8.897\,773\,186\,468\,888\,819\,9 \times 10^{0}$	$+1.663\,098\,261\,990\,208\,530\,4 \times 10^{1}$
θ_2	$-3.703\,275\,049\,423\,448\,060\,3 \times 10^{0}$	$+1.365\,637\,187\,148\,326\,817\,1 \times 10^{1}$
θ_3	$-0.208\,758\,638\,250\,130\,125\,1 \times 10^{0}$	$+1.099\,126\,056\,190\,126\,091\,3 \times 10^{1}$
θ_4	$+3.993\,369\,710\,578\,568\,519\,4 \times 10^{0}$	$+6.004\,831\,642\,235\,037\,317\,8 \times 10^{0}$
θ_5	$+5.089\,345\,060\,580\,624\,506\,6 \times 10^{0}$	$+3.588\,824\,029\,027\,006\,510\,2 \times 10^{0}$
θ_6	$+5.623\,142\,572\,745\,977\,124\,8 \times 10^{0}$	$+1.194\,069\,046\,343\,966\,976\,6 \times 10^{0}$
θ_7	$+2.269\,783\,829\,231\,112\,709\,7 \times 10^{0}$	$+8.461\,737\,973\,040\,221\,401\,9 \times 10^{0}$
α_1	$-7.154\,288\,063\,589\,067\,285\,3 \times 10^{-5}$	$+1.436\,104\,334\,954\,130\,011\,1 \times 10^{-4}$
α_2	$+9.439\,025\,310\,736\,168\,877\,9 \times 10^{-3}$	$-1.718\,479\,195\,848\,301\,751\,1 \times 10^{-2}$
α_3	$-3.763\,600\,387\,822\,696\,871\,7 \times 10^{-1}$	$+3.351\,834\,702\,945\,010\,421\,4 \times 10^{-1}$
α_4	$-2.349\,823\,209\,108\,270\,119\,1 \times 10^{1}$	$-5.808\,359\,129\,714\,207\,400\,4 \times 10^{0}$
α_5	$+4.693\,327\,448\,883\,129\,304\,7 \times 10^{1}$	$+4.564\,364\,976\,882\,776\,079\,1 \times 10^{1}$
α_6	$-2.787\,516\,194\,014\,564\,646\,8 \times 10^{1}$	$-1.021\,473\,399\,905\,645\,143\,4 \times 10^{2}$
α_7	$+4.807\,112\,098\,832\,508\,890\,7 \times 10^{0}$	$-1.320\,979\,383\,742\,872\,388\,1 \times 10^{0}$
α_0	$+1.832\,174\,378\,254\,041\,275\,1 \times 10^{-14}$	$+0.000\,000\,000\,000\,000\,000\,0 \times 10^{0}$

TABLE II

Partial Fraction Decomposition Coefficients for CRAM Approximation of Order 16

Coefficient	Real Part	Imaginary Part
θ_1	$-1.084\,391\,707\,869\,698\,802\,6 \times 10^{1}$	$+1.927\,744\,616\,718\,165\,228\,4 \times 10^{1}$
θ_2	$-5.264\,971\,343\,442\,646\,889\,5 \times 10^{0}$	$+1.622\,022\,147\,316\,792\,730\,5 \times 10^{1}$
θ_3	$+5.948\,152\,268\,951\,177\,480\,8 \times 10^{0}$	$+3.587\,457\,362\,018\,322\,282\,9 \times 10^{0}$
θ_4	$+3.509\,103\,608\,414\,918\,097\,4 \times 10^{0}$	$+8.436\,198\,985\,884\,375\,082\,6 \times 10^{0}$
θ_5	$+6.416\,177\,699\,099\,434\,192\,3 \times 10^{0}$	$+1.194\,122\,393\,370\,138\,687\,4 \times 10^{0}$
θ_6	$+1.419\,375\,897\,185\,665\,978\,6 \times 10^{0}$	$+1.092\,536\,348\,449\,672\,258\,5 \times 10^{1}$
θ_7	$+4.993\,174\,737\,717\,996\,399\,1 \times 10^{0}$	$+5.996\,881\,713\,603\,942\,226\,0 \times 10^{0}$
θ_8	$-1.413\,928\,462\,488\,886\,211\,4 \times 10^{0}$	$+1.349\,772\,569\,889\,274\,538\,9 \times 10^{1}$
α_1	$-5.090\,152\,186\,522\,491\,565\,0 \times 10^{-7}$	$-2.422\,001\,765\,285\,228\,797\,0 \times 10^{-5}$
α_2	$+2.115\,174\,218\,246\,603\,090\,7 \times 10^{-4}$	$+4.389\,296\,964\,738\,067\,391\,8 \times 10^{-3}$
α_3	$+1.133\,977\,517\,848\,393\,052\,7 \times 10^{2}$	$+1.019\,472\,170\,421\,585\,645\,0 \times 10^{2}$
α_4	$+1.505\,958\,527\,002\,346\,752\,8 \times 10^{1}$	$-5.751\,405\,277\,642\,181\,997\,9 \times 10^{0}$
α_5	$-6.450\,087\,802\,553\,964\,659\,5 \times 10^{1}$	$-2.245\,944\,076\,265\,209\,605\,6 \times 10^{2}$
α_6	$-1.479\,300\,711\,355\,799\,971\,8 \times 10^{0}$	$+1.768\,658\,832\,378\,293\,790\,6 \times 10^{0}$
α_7	$-6.251\,839\,246\,320\,791\,889\,2 \times 10^{1}$	$-1.119\,039\,109\,428\,322\,848\,0 \times 10^{1}$
α_8	$+4.102\,313\,683\,541\,002\,127\,3 \times 10^{-2}$	$-1.574\,346\,617\,345\,546\,819\,1 \times 10^{-1}$
α_0	$+2.124\,853\,710\,495\,223\,748\,8 \times 10^{-16}$	$+0.000\,000\,000\,000\,000\,000\,0 \times 10^{0}$

20 digits. Some of the newly computed coefficients differ significantly from the ones in Ref. 11. The PFD coefficients for approximation orders $1 \leq k \leq 13$ can be computed with high accuracy by using the approximative Carathéodory–Fejér method. A MATLAB script is provided for this purpose in Ref. 14. With the help of these coefficients, the implementation of the CRAM matrix exponential method for approximation orders $k \leq 16$ is extremely straightforward; as can be seen from Eq. (10), only solving a set of linear equations is required in addition to the coefficients. In order to implement CRAM in MATLAB, only the code from Fig. 1 is needed in addition to these coefficients. CRAM is therefore a very attractive method for solving the burnup equations in reactor physics codes.

However, if higher-order approximations are desired, complications ensue. Based on our experiments, the accuracy of the polynomial coefficients provided in

Ref. 10 is not sufficient for computing the partial fraction coefficients for approximation orders higher than 16. For this reason, an alternative and easier-to-implement method is presented in Sec. II.B. This approach is based on deriving the rational approximation from quadrature formulas applied to a contour integral in the left complex plane. Although these approximations do not converge as fast as CRAM, they have the advantage that the computation of the coefficients can be done on the fly, and therefore, the accuracy of the approximation can be easily adjusted.

II.B. Rational Approximations from Contour Integrals

When the eigenvalues of the matrix $\boldsymbol{At}$ are confined to a region near the negative real axis, the computation of the matrix exponential is effectively equivalent to evaluating contour integrals of the form represented by Eq. (7). Because of the exponential factor in the integrand, the contribution to the integral decays rapidly as $\mathrm{Re}(z) \to -\infty$, and the integral can be approximated efficiently using quadrature rules. These quadrature formulas can furthermore be interpreted as rational approximations that can be used to approximate the matrix exponential.

The idea of constructing rational approximations to the exponential function from quadrature rules was recently resurfaced by Trefethen, Weideman, and Schmelzer[7] and Weideman and Trefethen.[15] In Ref. 15, two types of contours, namely, hyperbolas and parabolas, have been analyzed, and asymptotically optimal parameters for these contours have been derived by balancing the error terms related to the approximation of the contour integrals by quadrature rules. Of these contours the parabola is the simpler one, so it is considered in this paper to illustrate the method. For integrands of type (7) with singularities on the negative real axis, Weideman has proposed the parabola:

$$\phi : \mathbb{R} \to \mathbb{C} \ ,$$

$$\phi(x) = N(0.1309 - 0.1149x^2 + i0.2500x) \ , \qquad (15)$$

which yields the convergence rate $O(2.85^{-N}) = O(e^{-1.05N})$ (Ref. 7). A rational approximation obtained from this contour is applied to solving the burnup equations in Sec. III.B.

The rational approximation of the exponential function based on a contour integral can be simply constructed as

$$r(z) = \sum_{k=1}^{N} \frac{\alpha_k}{z - \theta_k} \ , \qquad (16)$$

where $\theta_k = \phi(x_k)$ are the quadrature points from the contour, and

$$\alpha_k = -\frac{h}{2\pi i} e^{\phi(x_k)} \phi'(x_k) \qquad (17)$$

are the weights of the quadrature rule, where h denotes the interval length used in the quadrature scheme. For a detailed derivation, see Refs. 1 or 7. Figure 3 shows a MATLAB code illustrating how the coefficients corresponding to the contour of Eq. (15) may be computed in practice. After obtaining the coefficients, the code shown in Fig. 1 can be used to apply the approximation to Eq. (1).

The type of convergence analysis applied in Ref. 15 is based on mathematical theorems that characterize the convergence of quadrature rules on the real line $\mathbb{R}$. For integrands that decay sufficiently fast when $x \to \pm\infty$, the rate of convergence is determined by the integrand function's region of analyticity in the vicinity of the real axis. These convergence results can then be extended to contour integrals with the help of conformal functions that map the real axis $\mathbb{R}$ onto the contour Γ under consideration (for details and further information see, e.g., Ref. 16). When the decay of the integrand is exponential, the truncation error can also be assumed to be exponential, and the quadrature scheme can be chosen to give an asymptotic convergence rate with respect to the total error.

```
function [theta, alpha, alpha_0] = quad_coeffs(k)

    x       = pi * (1 : 2 : k - 1) / k;
    theta   = k * (0.1309 - 0.1194 * x .^ 2 + 0.2500 * x * 1i);
    w_j     = k * (-2 * 0.1194 * x + 0.2500 * 1i);
    alpha   = 1i * 1 / k * exp(theta) .* w_j;
    alpha_0 = 0;

end
```

Fig. 3. MATLAB code illustrating how the partial fraction coefficients may be computed for a rational approximation derived from a quadrature formula applied to the contour of Eq. (15). The input argument `k` is the degree of approximation, and it must be an even number.

TABLE III

Accuracy of CRAM Approximation Applied to Test Case 1*

Approximation Order	Mean Error	Maximum Error	Mean Relative Error	Maximum Relative Error
2	3.3901×10^{-7}	3.3110×10^{-4}	8.3015×10^{-2}	1.9561×10^{0}
4	4.0252×10^{-9}	3.8736×10^{-6}	5.6140×10^{-3}	6.3820×10^{-1}
6	4.7339×10^{-11}	4.5163×10^{-8}	2.2452×10^{-4}	3.8184×10^{-2}
8	5.5808×10^{-13}	5.2486×10^{-10}	7.1664×10^{-6}	1.5762×10^{-3}
10	6.5685×10^{-15}	6.0944×10^{-12}	1.9529×10^{-7}	5.1640×10^{-5}
12	7.6474×10^{-17}	6.9690×10^{-14}	4.7280×10^{-9}	1.4323×10^{-6}
14	9.5452×10^{-19}	9.5339×10^{-16}	1.0384×10^{-10}	3.4990×10^{-8}
16	2.0748×10^{-19}	1.6377×10^{-16}	2.1196×10^{-12}	7.7286×10^{-10}

*The errors were computed against a reference solution calculated with high-precision arithmetics.

III. APPLICATION TO BURNUP EQUATIONS

To evaluate the accuracy and study the convergence of the rational approximations, they were applied to two large burnup systems, and the solutions were compared to highly accurate reference solutions that were computed using MATLAB's Symbolic Toolbox and high-precision arithmetics. Both test cases represented an infinite pressurized water reactor pin-cell lattice. The time step used in the computations was 125 days, which is of the same order as the practical maximum time step. In the first test case, the fuel was irradiated to 25 MWd/kg U burnup, and the number of nuclides was 1532.[a] The second test case contained 1290 nuclides, and the burnup system was formed for both fresh fuel and fuel irradiated to 20 MWd/kg U burnup. In the first test case, the burnup matrix norm was of the order of 10^{21}, and in the second test case, it was of the order of 10^{16}.

III.A. Chebyshev Rational Approximation Method

The CRAM approximations of orders $k \leq 12$ were computed using the Carathéodory–Fejér method implemented as a MATLAB script in Ref. 14, and approximations of orders 14 and 16 were formed using the newly computed coefficients provided in Tables I and II. The numerical results for the first test case are shown in Table III and Fig. 4. Note that no nuclides were excluded from these results; i.e., even the nuclides with extremely small number densities have been included in the mean and maximum relative errors. The improvement in accuracy gained by recomputing the CRAM coefficients for approximation order 14 is illustrated in Fig. 5, which shows that the relative error is roughly 10^2 times smaller with the new coefficients provided in Sec. II.A.

[a]This is the same system as test case 1 in Ref. 1.

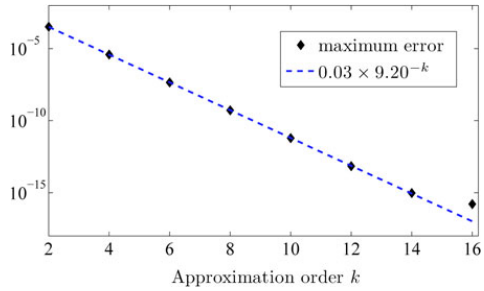

Fig. 4. Convergence of CRAM approximation applied to the first test case with 1532 nuclides.

Overall, it can be seen from the results that even relatively small CRAM approximation orders give remarkably accurate solutions to the first test case. From a practical point of view, orders of approximation as small as $k = 2$ or $k = 4$ could be used for solving the burnup equations for this test case without compromising the accuracy of the entire burnup calculation. For comparison, arguably the most established matrix exponential method, the Padé approximation (with scaling and squaring) suffered a total breakdown when applied to the same test case,[1] which serves well to illustrate the special characteristics of the burnup equations.

To study the convergence rate of CRAM, the error of the nuclide concentrations in the maximum norm was plotted against the approximation order, and the results are shown in Fig. 4. It can be seen that the convergence of the method is clearly geometric. The actual convergence rate can be estimated by performing a least-squares fit to the points, suggesting that the convergence is of the order of $O(9.20^{-N})$ for $k = 2, \ldots, 14$. Notice that this is very close to the theoretical asymptotic convergence rate, giving further proof of this method's

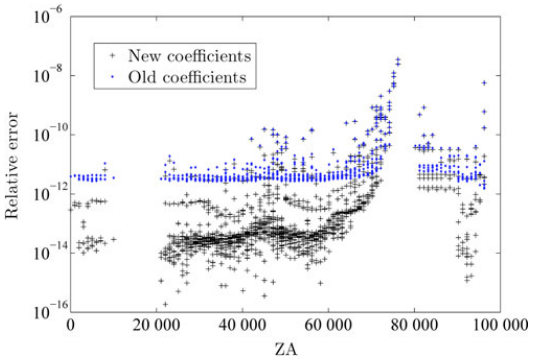

Fig. 5. Absolute values of the errors computed with CRAM approximation of order 14 using the PFD coefficients from Ref. 11 (dots) and using the recently computed coefficients (crosses). $ZA = 1000 \times Z + A$, where Z is the atomic number and A is the mass number of the nuclide.

suitability in the context of burnup equations. For $k = 16$, the round-off error began to affect the result, and hence, the convergence was slightly slower. It should be noted that as an approximation of order k requires $k/2$ linear solves, Fig. 4 also illustrates the computational cost of CRAM versus the maximum error.

It has been observed that the accuracy of CRAM depends relatively little on the fuel composition or neutron spectrum corresponding to the burnup matrix.[1,5] However, it has been noticed that CRAM generally produces less accurate results for fresh fuel than for depleted fuel.[5] When the fuel is fresh, only a few elements of $\boldsymbol{n}_0$ in Eq. (1) are nonzero, and all the nuclides are produced solely from these initial nuclides. For a large part of nuclides, this means both long and complex transmutation chains. It has been suggested that the observed reduction in accuracy is due to this and that the errors might be averaged out in depleted cases, where there are more initial nuclides.[5] To further quantify this effect, CRAM was applied to fresh fuel and fuel irradiated to 20 MWd/kg U burnup. This setup is referred to as test case 2 in this paper, and the numerical results are shown in Table IV. It can be seen from these results that although the absolute errors for both cases are very similar, the relative errors related to the fresh fuel computation are roughly 10^2 times greater than the ones corresponding to the depleted fuel case.

To further investigate this issue, a CRAM approximation of order 16 was explicitly computed for the burnup matrices representing fresh and depleted fuel in test case 2, and the elements of the approximation matrices $\hat{\boldsymbol{E}} = \hat{r}_{16,16}(\boldsymbol{A}t)$ were compared to the reference matrix exponentials $\boldsymbol{E} = e^{\boldsymbol{A}t}$ computed using MATLAB's Symbolic toolbox with high-precision arithmetics. This comparison showed that the accuracy of the approximation is of

TABLE IV

Accuracy of CRAM Approximation Applied to Test Case 2*

Approximation Order	Mean Error	Maximum Error	Mean Relative Error	Maximum Relative Error
Fresh fuel				
2	4.0451×10^{-7}	3.3117×10^{-4}	4.2189×10^{0}	2.3900×10^{3}
4	4.8034×10^{-9}	3.8747×10^{-6}	4.4645×10^{-1}	1.5813×10^{2}
6	5.6347×10^{-11}	4.5181×10^{-8}	4.0548×10^{-2}	1.9953×10^{1}
8	6.5984×10^{-13}	5.2511×10^{-10}	4.5634×10^{-3}	3.9451×10^{0}
10	7.6769×10^{-15}	6.0979×10^{-12}	5.5147×10^{-5}	5.3277×10^{-2}
12	8.9182×10^{-17}	6.9653×10^{-14}	1.6627×10^{-6}	1.7515×10^{-3}
14	1.0448×10^{-18}	8.1185×10^{-16}	4.2531×10^{-8}	4.7451×10^{-5}
16	3.0297×10^{-19}	2.6715×10^{-16}	9.5605×10^{-10}	1.1091×10^{-6}
Depleted fuel				
2	4.0231×10^{-7}	3.3113×10^{-4}	4.7487×10^{-2}	1.7192×10^{0}
4	4.7767×10^{-9}	3.8741×10^{-6}	1.4957×10^{-3}	8.8440×10^{-2}
6	5.6312×10^{-11}	4.5172×10^{-8}	1.3526×10^{-3}	1.6976×10^{0}
8	6.6458×10^{-13}	5.2498×10^{-10}	1.1667×10^{-3}	1.5040×10^{0}
10	7.8380×10^{-15}	6.0962×10^{-12}	1.2991×10^{-6}	1.6558×10^{-3}
12	9.1377×10^{-17}	6.9757×10^{-14}	2.7517×10^{-10}	5.9628×10^{-8}
14	9.7118×10^{-19}	6.7307×10^{-16}	4.6712×10^{-12}	1.1744×10^{-9}
16	3.3790×10^{-19}	3.6082×10^{-16}	2.5916×10^{-13}	2.2667×10^{-10}

*The errors were computed against a reference solution calculated with high-precision arithmetics.

the same order for burnup matrices representing fresh and depleted fuel; i.e., the reduced accuracy is not related to the properties of the burnup matrix. However, a closer examination showed a clear trend between the importance of particular nuclide chains and the relative accuracy of the corresponding matrix elements. That is, the matrix elements corresponding to less important chains are also computed with poorer relative accuracy with CRAM. This is mathematically reasonable since the relative accuracy of CRAM approximation $\hat{r}(x)$ diminishes as $x \to -\infty$.[b]

It follows that the reduced relative accuracy observed in fresh fuel cases is indeed related to the less important nuclide chains. The approximation error for nuclide concentration n_i may be written

$$\varepsilon_i = \left| \sum_{j=1}^{n} (E_{ij} - \hat{E}_{ij}) n_{0j} \right| \quad . \tag{18}$$

When the fuel is fresh, most of the initial concentrations are zero, and hence, the error ε_i is determined by the accuracy of the few matrix elements $\hat{E}_{ij}$ that correspond to the chains originating from these nuclides. As an example, consider the curium isotope ^{246}Cm, which causes the maximum relative error 1.1091×10^{-6} in CRAM approximation of order 16 in test case 2. There are 61 nuclides ranging from ^{232}Th to ^{245}Cm that may contribute to the concentration of this nuclide, and in terms of the burnup matrix alone, nuclides corresponding to simple and short nuclide chains are the most significant ones. The theoretical contribution attributable to such chains is as much as 10^8 to 10^{26} times greater than the contribution originating from uranium isotopes. When the fuel is fresh, however, the uranium isotopes are the only nuclides having nonzero initial concentrations. The reduced relative accuracy is a direct consequence of this. In this example case, the only relevant chain actually originates from ^{238}U, and the relative error corresponding to this chain is of the order of 10^{-6}, which is in accordance with the relative error of the result. For comparison, the relative error for this nuclide is 6.2857×10^{-11} in the depleted fuel case.

As no nuclides were excluded from the results shown in Table IV, the relative maximum errors may reflect individual concentrations corresponding to exotic nuclides or concentrations arbitrarily close to zero. In the depleted case, for example, all relative errors of order 10^0 occur for the unstable dysprosium isotope ^{155}Dy, whose atomic fraction is $\sim 10^{-24}$. The relative errors corresponding to CRAM approximation of order 6 are shown in Fig. 6. It can be seen from Fig. 6 that all other nuclides have relative errors that are several orders of magnitude smaller. The least unlikely nuclide chains for ^{155}Dy originate from fission product nuclides, and hence, the reduced relative accuracy is observed in depleted fuel cases with small approximation orders. Notice that for higher approximation orders the relative errors are also consistently extremely small.

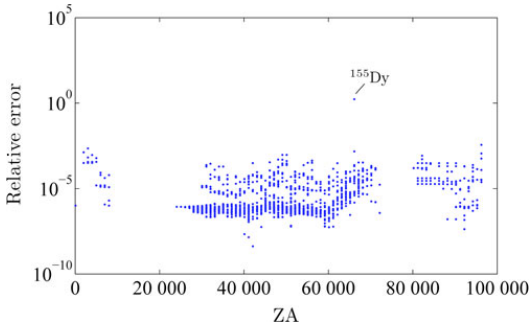

Fig. 6. Relative errors related to CRAM approximation of order 6 applied to the depleted fuel burnup equations in test case 2. The errors were computed against a reference solution calculated with high-precision arithmetics.

From a practical point of view, the results computed with CRAM approximation are remarkably accurate in both test cases. The cross-section uncertainties related to the transmutation reaction rates (i.e., burnup matrix elements) usually range from 10^{-2} to 10^{-1} in typical reactor physics calculations. When Monte Carlo methods are used, the statistical error also reduces the accuracy of the burnup matrix elements. With all this taken into consideration, even approximation orders as low as $k = 6$ could be used without compromising the total accuracy of a burnup calculation.

In addition to accuracy, another advantage of CRAM is its low computational cost. The order of approximation can be easily adjusted to suit needs for accuracy or speed. As can be seen from Eq. (10), the computation time is directly proportional to the approximation order k. If the sparsity pattern of the burnup matrix is properly exploited, the approximations can be computed with remarkably short calculation times. For example, the computation of an approximation of order $k = 14$ for a test case with about 1500 nuclides takes less than a tenth of a second in the Serpent reactor physics code.[1,5]

III.B. Rational Approximation from Quadrature Formula

As explained in Sec. II.B, rational approximations to the matrix exponential can be derived from quadrature rules applied to contour integrals. Here, this technique is illustrated by using the contour of Eq. (15), which is of the form

$$\phi(x) = k(\alpha - \beta x^2 + i\gamma x) \quad , \tag{19}$$

[b]Notice that it is impossible to derive best approximations with respect to the relative error.

where $\alpha, \beta, \gamma > 0$ and $x \in \mathbb{R}$. In the context of burnup equations, the integral under consideration is of the form of Eq. (7) and can be written

$$(e^{At})_{kl} = \frac{1}{2\pi i} \int_{\Gamma} e^{z} R_{kl}(z)\, dz \ ,$$

$$= \frac{1}{2\pi i} \int_{-\infty}^{\infty} e^{\phi(x)} R_{kl}(\phi(x))\phi'(x)\, dx \ . \quad (20)$$

The numerical results for test cases 1 and 2 are shown in Tables V and VI, respectively. By comparing these results to those obtained with CRAM, it can be seen that this approach is well-suited for solving the burnup equations. Notice that although the convergence of this method is much slower than the convergence of CRAM, the results are qualitatively very similar. The results for test case 1 are again more accurate, and the large overall relative errors in the depleted case of test case 2 result from the single dysprosium isotope ^{155}Dy.

The total error in the results consists of the theoretical approximation error and the round-off error related to the finite precision arithmetics used in the computations. When the approximation order is greater than 36, the round-off errors begin to contribute to the accuracy, after which the maximum error does not significantly diminish. However, it can be seen from the results that with sufficiently high quadrature orders, it is possible to obtain at least ten correct digits for all nuclide concentrations, which can be considered quite remarkable. This is a sufficient accuracy for all considerable burnup calculations, and hence, this approach could be suitable for computing reference solutions for other numerical methods.

Another advantage related to rational approximations derived from quadrature formulas is that it is possible to derive conservative convergence estimates for different eigenvalue distributions. Because of the exponential factor in the integral, the convergence of quadrature rules applied to the computation of this integral is determined by the region of analyticity of the integrand function continued to the complex plane. If the integrand function is analytic in the infinite strip

$$D_S = \{z \in \mathbb{C} \,|\, z = x + iy, -d < y < c\} \ , \quad (21)$$

the convergence with respect to the interval length h is of order $O(e^{-2\pi c/h} + e^{-2\pi d/h})$ as $h \to 0$. In addition, the truncation error can be estimated to be of order $O(|g(hN)|)$ as $N \to \infty$ (Ref. 15). The integrand in Eq. (20) can be written

$$g(x + i\omega) = e^{\phi(x+i\omega)} R_{kl}(\phi(x + i\omega))\phi'(x + i\omega) \ . \quad (22)$$

Because the only singularities of the function g are the poles of the rational function R_{kl}, the singularity distribution of g consists of points that are mapped onto the eigenvalues of $\boldsymbol{A}t$. Since the eigenvalues of burnup matrices are all confined to a region near the negative real axis, the convergence rate should be dominated by the factor $O(e^{2\pi c/h})$, where the constant c depends directly on the magnitudes of the imaginary parts of the eigenvalues.

TABLE V

Accuracy of Quadrature Approximation Applied to Test Case 1*

Approximation Order	Mean Error	Maximum Error	Mean Relative Error	Maximum Relative Error
4	1.4726×10^{-6}	1.4526×10^{-3}	2.4786×10^{-1}	1.4951×10^{1}
8	2.2621×10^{-8}	2.1925×10^{-5}	3.5720×10^{-2}	4.7308×10^{0}
12	3.3657×10^{-10}	3.2264×10^{-7}	2.0632×10^{-3}	4.1914×10^{-1}
16	5.0968×10^{-12}	4.8108×10^{-9}	8.8273×10^{-5}	2.2515×10^{-2}
20	7.6246×10^{-14}	7.0702×10^{-11}	3.1568×10^{-6}	9.4284×10^{-4}
24	1.1477×10^{-15}	1.0443×10^{-12}	9.9082×10^{-8}	3.3211×10^{-5}
28	1.7191×10^{-17}	1.5314×10^{-14}	2.8082×10^{-9}	1.0277×10^{-6}
32	3.3333×10^{-19}	2.7756×10^{-16}	7.4740×10^{-11}	2.8729×10^{-8}
36	1.2452×10^{-19}	1.5266×10^{-16}	1.7969×10^{-12}	7.3949×10^{-10}
40	3.2204×10^{-20}	2.4286×10^{-17}	4.4542×10^{-14}	1.7772×10^{-11}
44	2.6421×10^{-19}	3.6082×10^{-16}	5.9574×10^{-15}	4.0187×10^{-13}
48	7.0675×10^{-19}	8.8124×10^{-16}	1.2903×10^{-14}	2.3370×10^{-13}
52	6.5418×10^{-19}	4.9266×10^{-16}	1.6877×10^{-14}	2.4932×10^{-13}
56	2.8871×10^{-18}	3.0947×10^{-15}	5.1656×10^{-14}	1.4797×10^{-13}
60	3.7784×10^{-18}	4.7531×10^{-15}	6.2409×10^{-14}	2.2402×10^{-13}

*The errors were computed against a reference solution calculated with high-precision arithmetics.

TABLE VI

Accuracy of Quadrature Approximation Applied to Test Case 2*

Approximation Order	Mean Error	Maximum Error	Mean Relative Error	Maximum Relative Error
Fresh fuel				
4	1.7504×10^{-6}	1.4528×10^{-3}	3.0494×10^{1}	1.5087×10^{4}
8	2.6904×10^{-8}	2.1931×10^{-5}	3.5070×10^{0}	1.5082×10^{3}
12	3.9894×10^{-10}	3.2276×10^{-7}	4.1829×10^{-1}	3.1038×10^{2}
16	5.9978×10^{-12}	4.8131×10^{-9}	2.7340×10^{-2}	2.2658×10^{1}
20	8.9027×10^{-14}	7.0744×10^{-11}	3.7238×10^{-2}	4.6645×10^{1}
24	1.3364×10^{-15}	1.0451×10^{-12}	9.4550×10^{-4}	1.1684×10^{0}
28	1.9949×10^{-17}	1.5307×10^{-14}	1.2510×10^{-6}	1.4528×10^{-3}
32	3.5814×10^{-19}	2.8449×10^{-16}	3.4718×10^{-8}	4.1451×10^{-5}
36	1.7146×10^{-19}	1.8735×10^{-16}	8.7330×10^{-10}	1.0632×10^{-6}
40	8.0602×10^{-20}	8.3267×10^{-17}	2.0294×10^{-11}	2.5030×10^{-8}
44	2.9928×10^{-19}	3.6776×10^{-16}	5.1227×10^{-13}	5.4906×10^{-10}
48	6.8488×10^{-19}	5.3429×10^{-16}	2.8378×10^{-13}	3.4522×10^{-10}
52	2.0623×10^{-19}	2.3592×10^{-16}	1.2807×10^{-13}	1.5392×10^{-10}
56	4.3947×10^{-18}	3.8441×10^{-15}	4.3086×10^{-13}	5.2005×10^{-10}
60	2.8439×10^{-18}	1.8804×10^{-15}	1.9729×10^{-13}	1.8854×10^{-10}
Depleted fuel				
4	1.7491×10^{-6}	1.4527×10^{-3}	1.5504×10^{-1}	2.2859×10^{0}
8	2.6863×10^{-8}	2.1928×10^{-5}	8.1883×10^{-3}	5.7021×10^{-1}
12	4.0052×10^{-10}	3.2270×10^{-7}	9.2944×10^{-4}	8.4914×10^{-1}
16	6.0748×10^{-12}	4.8119×10^{-9}	1.7091×10^{-4}	2.1048×10^{-1}
20	9.0998×10^{-14}	7.0723×10^{-11}	3.0635×10^{-4}	3.9490×10^{-1}
24	1.3717×10^{-15}	1.0447×10^{-12}	5.3881×10^{-3}	6.9504×10^{0}
28	2.0572×10^{-17}	1.5314×10^{-14}	5.8635×10^{-7}	7.5604×10^{-4}
32	4.2531×10^{-19}	2.8449×10^{-16}	2.1854×10^{-12}	6.4981×10^{-10}
36	1.6180×10^{-19}	1.4572×10^{-16}	5.2742×10^{-14}	1.3987×10^{-11}
40	2.0604×10^{-19}	1.9429×10^{-16}	2.3263×10^{-14}	2.4936×10^{-11}
44	3.9955×10^{-19}	4.1633×10^{-16}	8.4011×10^{-15}	3.8230×10^{-12}
48	9.5099×10^{-19}	7.3552×10^{-16}	6.8619×10^{-14}	6.7985×10^{-11}
52	1.2022×10^{-18}	1.0270×10^{-15}	1.1006×10^{-13}	1.1291×10^{-10}
56	3.7045×10^{-18}	3.0531×10^{-15}	3.8593×10^{-13}	4.0835×10^{-10}
60	4.3363×10^{-18}	3.2127×10^{-15}	1.7439×10^{-13}	1.3113×10^{-10}

*The errors were computed against a reference solution calculated with high-precision arithmetics.

As the value of c is increased from zero, the contour $\phi(x + ic)$ narrows down, and it approaches the negative real axis when c reaches the value $c = \gamma/(2\beta)$. By choosing $h = 2\pi/k$ the convergence of order

$$O(e^{-ck}) = O(e^{-1.0469k}) = O(2.85^{-k})$$

is achieved for the case, where all the eigenvalues lie on the negative real axis. This result can be generalized for burnup matrices having eigenvalues near the negative real axis. It seems to be sufficient to require that $\mathrm{Im}\,\phi(x + ic) > 0.1$ at the origin. From this requirement it is straightforward to derive the following equation for c:

$$k^2\beta^{-1}(\alpha + \beta c^2 - \gamma c)(\gamma - 2\beta)^2 = 0.1 \quad . \qquad (23)$$

In practice, the convergence of the quadrature scheme can be estimated by solving this equation for sufficiently small k with respect to the number of nodes used in the calculations. For quadrature order $k = 4$, Eq. (23) gives $c = 0.93$, and thus, the convergence should be at least of the order of $O(2.53^{-N})$ for this singularity distribution. Note that this estimate corresponds to the worst-case scenario, where practically all the singularities are located on the contour $\phi(x + ic)$. In practice, however, only a fraction of the eigenvalues of $\boldsymbol{A}t$ lie off the real axis, and the majority of them have imaginary parts smaller than 10^{-1}.

The maximum norm error in test case 1 is plotted against the quadrature order in Fig. 7. As in the case of CRAM, the computational cost is directly proportional to the approximation order k, and consequently, Fig. 7 also illustrates the computational cost of the quadrature scheme versus the maximum error. A least-squares fit to the points $k \leq 32$ suggests that the convergence is

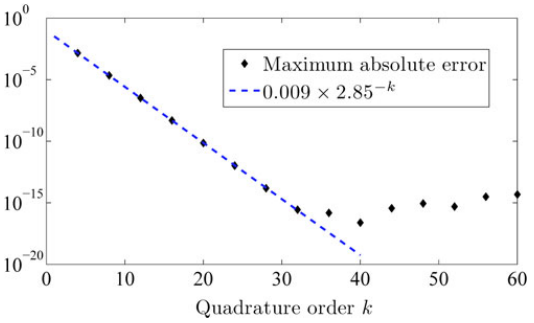

Fig. 7. Convergence of the quadrature approximation applied to the first test case with 1532 nuclides.

actually of the order of 2.85^{-k} until round-off errors begin to dominate the error. Judging by this, the few non-real eigenvalues having small imaginary parts are not relevant when using rational approximations that are accurate near the negative real axis. This gives further credibility to the suitability of this type of approximation in the context of burnup equations.

IV. SUMMARY AND CONCLUSIONS

The computation of the matrix exponential has been considered challenging in the context of burnup equations because the magnitudes of the transmutation and decay constants vary extensively, making the problem extremely stiff. Traditionally, these difficulties have been avoided by using simplified models or by excluding the short-lived nuclides from the computation and treating them separately. However, it was recently discovered by the author that the eigenvalues of burnup matrices are confined to a region near the negative real axis, and this property can be exploited by using rational approximations that are highly accurate there.[1] This allows for simultaneously solving the entire system containing thousands of nuclides in an accurate and efficient manner.

In this paper, two different types of rational approximation were considered for computing the exponential of a burnup matrix—the previously introduced CRAM approximation, which can be characterized as the best rational approximation on the negative real axis, and an approximation method based on quadrature rules applied to a contour integral around the negative real axis. Both methods are very straightforward to implement because only a few lines of program code and a function for solving a set of linear equations are required.

The motivation for introducing the latter method was that although CRAM appears to be the most efficient method for computing the matrix exponential of a burnup matrix, its higher-order partial fraction coefficients are difficult to obtain. In addition, the previous literature values[11] for order-14 coefficients were discovered to contain round-off errors that resulted in relative accuracy two orders of magnitude poorer than expected by theory. To rectify this, new partial fraction coefficients were computed and reported for CRAM approximation orders 14 and 16. Although the accuracy of order-16 CRAM is more than sufficient for most thinkable burnup applications, and it can be readily implemented using the coefficients provided in this paper, the proposed quadrature approach is an attractive alternative. Its benefits include flexibility in terms of balancing efficiency and accuracy for routine burnup calculations with geometric convergence properties as well as the possibility of computing reference results with extremely high accuracy, limited only by the available arithmetic precision. Such reference results offer a distinct benchmark that other matrix exponential methods can be compared against in the future. In this paper, the reference solutions for the two test cases were painstakingly computed using high-precision arithmetics, and they confirmed the accuracy of the high-order quadrature approximations.

Regarding CRAM, this paper is the first to discuss approximation orders other than 14 and to study the convergence properties of the method in the context of burnup equations. In addition, the sources of approximation error were analyzed, and the observed differences in resulting accuracy for fresh and depleted fuel were explained. The new discoveries and observations fully support our previous assessment of CRAM being capable of providing a very accurate and robust solution to the burnup equations with a very low computational cost.

The main motivation and context for the presented work is the Serpent reactor physics code,[13] which was the first of its kind to implement CRAM specifically for solving the burnup equations. As previously mentioned, the literature values for the order-14 CRAM coefficients, on which the implementation of CRAM in the current release version of Serpent is also based, are inaccurate, and future development plans for Serpent include implementing CRAM of orders 2 through 16 using the correct coefficients.

REFERENCES

1. M. PUSA and J. LEPPÄNEN, "Computing the Matrix Exponential in Burnup Calculations," *Nucl. Sci. Eng.*, **164**, 140 (2010).

2. I. C. GAULD, O. W. HERMANN, and R. M. WESTFALL, "Origen-S: Scale System Module to Calculate Fuel Depletion, Actinide Transmutation, Fission Product Buildup and Decay, and Associated Radiation Source Terms," in "SCALE: A Modular Code System for Performing Standardized

Computer Analyses for Licensing Evaluations," Vol. II, Sec. F7, ORNL/TM-2005/39, Oak Ridge National Laboratory/U.S. Nuclear Regulatory Commission (Nov. 2006).

3. A. YAMAMOTO, M. TATSUMI, and N. SUGIMURA, "Numerical Solution of Stiff Burnup Equations with Short Half Lived Nuclides by the Krylov Subspace Method," *J. Nucl. Sci. Technol.*, **44**, *2*, 147 (2007).

4. C. MOLER and C. VAN LOAN, "Nineteen Dubious Ways to Compute the Exponential of a Matrix, Twenty-Five Years Later," *SIAM Rev.*, **45**, 3 (2003).

5. A. ISOTALO and P. A. AARNIO, "Comparison of Depletion Algorithms," *Ann. Nucl. Energy*, **38**, *2–3*, 261 (2011).

6. L. A. ZADEH and C. A. DESOER, *Linear System Theory: The State Space Approach*, McGraw-Hill Books Company, Inc. (1963).

7. L. N. TREFETHEN, J. A. C. WEIDEMAN, and T. SCHMELZER, "Talbot Quadratures and Rational Approximations," *BIT.*, **46**, *3*, 653 (2006).

8. A. A. GONCHAR and E. A. RAKHMANOV, "Equilibrium Distributions and Degree of Rational Approximation of Analytic Functions," *Math. USSR Sb.*, **62**, 2 (1989).

9. H. STAHL and T. SCHMELZER, "An Extension of the 1/9-Problem," *J. Comput. Appl. Math.*, **233**, 821 (2009).

10. A. J. CARPENTER, A. RUTTAN, and R. S. VARGA, "Extended Numerical Computations on the 1/9 Conjecture in Rational Approximation Theory," "Rational Approximation and Interpolation" in *Lecture Notes in Mathematics*, Vol. 1105, pp. 383–411, P. R. GRAVES-MORRIS, E. B. SAFF, and R. S. VARGA, Eds., Springer-Verlag (1984).

11. E. GALLOPOULOS and Y. SAAD, "Efficient Solution of Parabolic Equations by Krylov Approximation Methods," *SIAM J. Sci. Stat. Comput.*, **13**, *5*, 1236 (1992).

12. R. B. SIDJE, "Expokit: a Software Package for Computing Matrix Exponentials," *ACM Trans. Math. Softw.*, **24**, *1*, 130 (1998).

13. J. LEPPÄNEN, "PSG2/Serpent—a Continuous-Energy Monte Carlo Reactor Physics Burnup Calculation Code," VTT Technical Research Centre of Finland (Nov. 2008); http://montecarlo.vtt.fi (current as of October 26, 2010).

14. T. SCHMELZER, "Carathéodory–Fejér Approximation," Matlab Central (Nov. 2008); http://www.mathworks.com/matlabcentral (current as of October 26, 2010).

15. J. WEIDEMAN and L. N. TREFETHEN, "Parabolic and Hyperbolic Contours for Computing the Bromwich Integral," *Math. Comput.*, **76**, *259*, 1341 (2007).

16. J. LUND and K. L. BOWERS, *Sinc Methods for Quadrature and Differential Equations*, Society for Industrial and Applied Mathematics (1992).

PUBLICATION III

Correction to partial fraction decomposition coefficients for Chebyshev rational approximation on the negative real axis

arXiv:1206.2880v1 [math.NA] (2012).

CORRECTION TO PARTIAL FRACTION DECOMPOSITION COEFFICIENTS FOR CHEBYSHEV RATIONAL APPROXIMATION ON THE NEGATIVE REAL AXIS

MARIA PUSA

ABSTRACT. Chebyshev rational approximation can be a viable method to compute the exponential of matrices with eigenvalues in the vicinity of the negative real axis, and it was recently applied successfully to solving nuclear fuel burnup equations. Determining the partial fraction decomposition (PFD) coefficients of this approximation can be difficult and they have been provided (for approximation orders 10 and 14) by Gallopoulos and Saad in "Efficient solution of parabolic equations by Krylov approximation methods", SIAM J. Sci. Stat. Comput., 13(1992). It was recently discovered that the order 14 coefficients contain errors and result in 10^2 times poorer accuracy than expected by theory. The purpose of this note is to provide the correct PFD coefficients for approximation orders 14 and 16 and to briefly discuss the approximation accuracy resulting from the erroneous coefficients.

1. Chebyshev rational approximation

This note concerns the computation of matrix exponential based on the Chebyshev rational approximation method (abbreviated CRAM in [7]) on the negative real axis. In this approach, the matrix exponential $e^{\boldsymbol{A}t}$ is approximated by a rational matrix function $\hat{r}(\boldsymbol{A}t)$, where the rational function $\hat{r}(z)$ is chosen as the best rational approximation of the exponential function on the negative real axis $\mathbb{R}_-$. Let $\pi_{k,k}$ denote the set of rational functions $r_{k,k}(x) = p_k(x)/q_k(x)$ where p_k and q_k are polynomials of order k. The CRAM approximation of order k is defined as the unique rational function $\hat{r}_{k,k} = \hat{p}_k(x)/\hat{q}_k(x)$ satisfying

$$\sup_{x\in\mathbb{R}_-} |\hat{r}_{k,k}(x) - e^x| = \inf_{r_{k,k}\in\pi_{k,k}} \left\{ \sup_{x\in\mathbb{R}_-} |r_{k,k}(x) - e^x| \right\} . \tag{1}$$

The asymptotic convergence of this approximation on the negative real axis is remarkably fast with the convergence rate $O(H^{-k})$, where $H = 9.289\,025\,49\ldots$ is called the Halphen constant [4]. It was recently discovered by Stahl and Schmelzer [11] that this convergence extends to compact subsets on the complex plane and also to Hankel contours in $\mathbb{C}\setminus\mathbb{R}_-$. The application of this approximation to computing the matrix exponential was originally made famous by Cody, Meinardus, and Varga in 1969 in the context of rational approximation of e^{-x} on $[0,\infty)$ and it was recently resurfaced by Trefethen, Weideman, and Schmelzer [12]. For self-adjoint and negative semi-definite matrices, the method is

Date: 12 June 2012.

2000 *Mathematics Subject Classification.* 41-04, 65F60.

Key words and phrases. best rational approximation, CRAM, partial fraction decomposition, matrix exponential.

guaranteed to yield an error bound in 2-norm that corresponds to the maximum error of the rational approximation on the negative real axis. This has also been the main context for scientific applications [2, 9, 10]. Recently, the method has also been successfully applied to non-self-adjoint matrices with eigenvalues near the negative real axis [7, 6]. These specific matrices arise from a reactor physics application, where the changes in nuclide concentrations due to radioactive decay and neutron-induced reactions are governed by a linear system $\boldsymbol{x}' = \boldsymbol{A}\boldsymbol{x}$ known as the burnup equations.

2. Partial fraction decomposition form

The main difficulty in using CRAM for computing the matrix exponential is determining the coefficients of the rational function for a given k. In principle, the polynomial coefficients of $\hat{p}_k$ and $\hat{q}_k$ can be computed with Remez-type methods but this requires delicate algorithms combined with high-precision arithmetics. Fortunately, these coefficients have been computed to a high accuracy by Carpenter et al. for approximation orders $k = 0, 1, \ldots, 30$ and they are provided in [1]. In practical applications, however, it is usually advantageous to employ CRAM in the partial fraction decomposition (PFD) form. For simple poles, this composition takes the form

$$\hat{r}_{k,k}(z) = \alpha_0 + \sum_{j=1}^{k} \frac{\alpha_j}{z - \theta_j} \ , \tag{2}$$

where α_0 is the limit of the function $\hat{r}_{k,k}$ at infinity, and α_j are the residues at the poles θ_j:

$$\alpha_j = \frac{\hat{p}_k(\theta_j)}{\hat{q}_k'(\theta_j)} \ . \tag{3}$$

Since the coefficients of $\hat{r}_{k,k}$ are real, its poles form conjugate pairs, so the computational cost can be reduced to half for a real variable x

$$\hat{r}_{k,k}(x) = \alpha_0 + 2\,\mathrm{Re}\left(\sum_{j=1}^{k/2} \frac{\alpha_j}{x - \theta_j} \right) \tag{4}$$

and the matrix exponential solution may be approximated as

$$\boldsymbol{x} = \alpha_0 \boldsymbol{x}_0 + 2\,\mathrm{Re}\left(\sum_{j=1}^{k/2} \alpha_j (\boldsymbol{A}t - \theta_j \boldsymbol{I})^{-1} \boldsymbol{x}_0 \right) \tag{5}$$

for a real matrix $\boldsymbol{A} \in \mathbb{R}^{n \times n}$.

Although the PFD coefficients can in principle be computed from the polynomial coefficients, the computation of the polynomial roots may be ill-conditioned and requires great care. The PFD coefficients for approximation orders 10 and 14 have been provided in [3], and the given coefficients for $k = 14$ have been used in several applications including the matrix exponential computing package EXPOKIT [10] and the reactor physics code Serpent [5]. However, in the latter context, it was recently observed that these reported coefficients contain errors and do not correspond to the true best approximation [6]. To illustrate this, Figure 1 shows the error of order 14 approximation on the negative real axis computed using two different sets of coefficients: the partial fraction coefficients from [3], with the corresponding

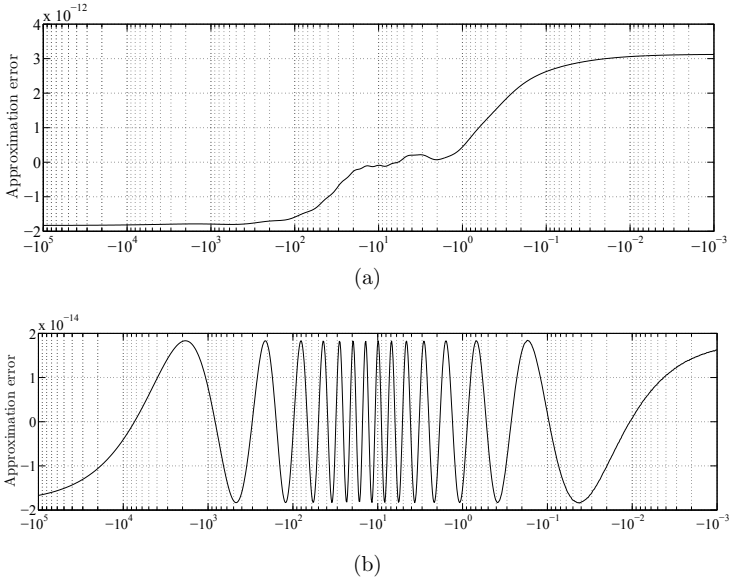

FIGURE 1. (a) Plot of $e^x - \check{r}_{14,14}(x)$ on the negative real axis with $\check{r}_{14,14}$ computed based on the partial fraction coefficients from [3], (b) Plot of $e^x - \hat{r}_{14,14}(x)$ based on the polynomial coefficients from [1]. The plots were computed using high-precision arithmetics with 32 digits.

approximation denoted by $\check{r}_{14,14}$, and the polynomial coefficients from [1], with the corresponding approximation denoted by $\hat{r}_{14,14}$. According to theory, a necessary and sufficient condition for the best approximation is that the corresponding error function equioscillates, i.e. there exists a set of points where it attains its maximum absolute value with alternating signs. Notice that the approximation computed with the coefficients from [3] does not exhibit this behavior and in addition results in a 10^2 times poorer accuracy than expected by theory.

After discovering the erroneous behavior induced by the coefficients from [3], partial fraction coefficients for approximation orders $k = 14$ and $k = 16$ were computed from the polynomial coefficients provided in [1] and subsequently reported in [6]. The computed PFD coefficients are repeated here in Tables 1 and 2. The computations were performed with MATLAB's Symbolic Toolbox using high precision arithmetics with 200 digits to ensure a sufficient accuracy. In Tables 1 and 2 the coefficients have been rounded off to 20 digits. The coefficients in [1] have been also given with 20 digits' accuracy, and based on our experience, the approximation order $k = 16$ is the highest for which this accuracy is sufficient for computing the PFD coefficients. For lower approximation orders, $1 \le k \le 13$, the PFD coefficients can be accurately computed with the approximative Carathéodory–Fejér method and a MATLAB script is provided for this purpose in [8].

TABLE 1. Recomputed values for the partial fraction decomposition coefficients for CRAM approximation of order 14.

Coefficient	Real part	Imaginary part
θ_1	$-8.897\,773\,186\,468\,888\,819\,9 \times 10^{0}$	$+1.663\,098\,261\,990\,208\,530\,4 \times 10^{1}$
θ_2	$-3.703\,275\,049\,423\,448\,060\,3 \times 10^{0}$	$+1.365\,637\,187\,148\,326\,817\,1 \times 10^{1}$
θ_3	$-0.208\,758\,638\,250\,130\,125\,1 \times 10^{0}$	$+1.099\,126\,056\,190\,126\,091\,3 \times 10^{1}$
θ_4	$+3.993\,369\,710\,578\,568\,519\,4 \times 10^{0}$	$+6.004\,831\,642\,235\,037\,317\,8 \times 10^{0}$
θ_5	$+5.089\,345\,060\,580\,624\,506\,6 \times 10^{0}$	$+3.588\,824\,029\,027\,006\,510\,2 \times 10^{0}$
θ_6	$+5.623\,142\,572\,745\,977\,124\,8 \times 10^{0}$	$+1.194\,069\,046\,343\,966\,976\,6 \times 10^{0}$
θ_7	$+2.269\,783\,829\,231\,112\,709\,7 \times 10^{0}$	$+8.461\,737\,973\,040\,221\,401\,9 \times 10^{0}$
α_1	$-7.154\,288\,063\,589\,067\,285\,3 \times 10^{-5}$	$+1.436\,104\,334\,954\,130\,011\,1 \times 10^{-4}$
α_2	$+9.439\,025\,310\,736\,168\,877\,9 \times 10^{-3}$	$-1.718\,479\,195\,848\,301\,751\,1 \times 10^{-2}$
α_3	$-3.763\,600\,387\,822\,696\,871\,7 \times 10^{-1}$	$+3.351\,834\,702\,945\,010\,421\,4 \times 10^{-1}$
α_4	$-2.349\,823\,209\,108\,270\,119\,1 \times 10^{1}$	$-5.808\,359\,129\,714\,207\,400\,4 \times 10^{0}$
α_5	$+4.693\,327\,448\,883\,129\,304\,7 \times 10^{1}$	$+4.564\,364\,976\,882\,776\,079\,1 \times 10^{1}$
α_6	$-2.787\,516\,194\,014\,564\,646\,8 \times 10^{1}$	$-1.021\,473\,399\,905\,645\,143\,4 \times 10^{2}$
α_7	$+4.807\,112\,098\,832\,508\,890\,7 \times 10^{0}$	$-1.320\,979\,383\,742\,872\,388\,1 \times 10^{0}$
α_0	$+1.832\,174\,378\,254\,041\,275\,1 \times 10^{-14}$	$+0.000\,000\,000\,000\,000\,000\,0 \times 10^{0}$

TABLE 2. Computed values for the partial fraction decomposition coefficients for CRAM approximation of order 16.

Coefficient	Real part	Imaginary part
θ_1	$-1.084\,391\,707\,869\,698\,802\,6 \times 10^{1}$	$+1.927\,744\,616\,718\,165\,228\,4 \times 10^{1}$
θ_2	$-5.264\,971\,343\,442\,646\,889\,5 \times 10^{0}$	$+1.622\,022\,147\,316\,792\,730\,5 \times 10^{1}$
θ_3	$+5.948\,152\,268\,951\,177\,480\,8 \times 10^{0}$	$+3.587\,457\,362\,018\,322\,282\,9 \times 10^{0}$
θ_4	$+3.509\,103\,608\,414\,918\,097\,4 \times 10^{0}$	$+8.436\,198\,985\,884\,375\,082\,6 \times 10^{0}$
θ_5	$+6.416\,177\,699\,099\,434\,192\,3 \times 10^{0}$	$+1.194\,122\,393\,370\,138\,687\,4 \times 10^{0}$
θ_6	$+1.419\,375\,897\,185\,665\,978\,6 \times 10^{0}$	$+1.092\,536\,348\,449\,672\,258\,5 \times 10^{1}$
θ_7	$+4.993\,174\,737\,717\,996\,399\,1 \times 10^{0}$	$+5.996\,881\,713\,603\,942\,226\,0 \times 10^{0}$
θ_8	$-1.413\,928\,462\,488\,886\,211\,4 \times 10^{0}$	$+1.349\,772\,569\,889\,274\,538\,9 \times 10^{1}$
α_1	$-5.090\,152\,186\,522\,491\,565\,0 \times 10^{-7}$	$-2.422\,001\,765\,285\,228\,797\,0 \times 10^{-5}$
α_2	$+2.115\,174\,218\,246\,603\,090\,7 \times 10^{-4}$	$+4.389\,296\,964\,738\,067\,391\,8 \times 10^{-3}$
α_3	$+1.133\,977\,517\,848\,393\,052\,7 \times 10^{2}$	$+1.019\,472\,170\,421\,585\,645\,0 \times 10^{2}$
α_4	$+1.505\,958\,527\,002\,346\,752\,8 \times 10^{1}$	$-5.751\,405\,277\,642\,181\,997\,9 \times 10^{0}$
α_5	$-6.450\,087\,802\,553\,964\,659\,5 \times 10^{1}$	$-2.245\,944\,076\,265\,209\,605\,6 \times 10^{2}$
α_6	$-1.479\,300\,711\,355\,799\,971\,8 \times 10^{0}$	$+1.768\,658\,832\,378\,293\,790\,6 \times 10^{0}$
α_7	$-6.251\,839\,246\,320\,791\,889\,2 \times 10^{1}$	$-1.119\,039\,109\,428\,322\,848\,0 \times 10^{1}$
α_8	$+4.102\,313\,683\,541\,002\,127\,3 \times 10^{-2}$	$-1.574\,346\,617\,345\,546\,819\,1 \times 10^{-1}$
α_0	$+2.124\,853\,710\,495\,223\,748\,8 \times 10^{-16}$	$+0.000\,000\,000\,000\,000\,000\,0 \times 10^{0}$

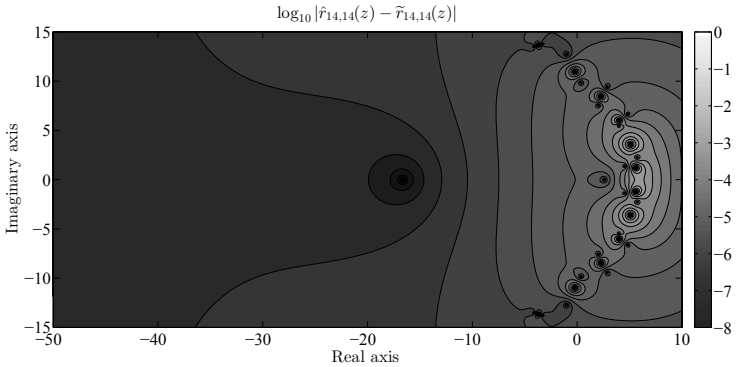

FIGURE 2. Plot of $\log_{10}|\hat{r}_{14,14}(z) - \widetilde{r}_{14,14}(z)|$ in the complex plane. $\hat{r}_{14,14}$ was computed based on the partial fraction coefficients from Table 1 and $\widetilde{r}_{14,14}$ was formed by truncating these coefficients to 6 significant digits. The poles of $\hat{r}_{14,14}$ have been marked to the plot with asterisks.

3. Analysis of inaccurate PFD coefficients for $k = 14$

To analyze the effect of inaccurate PFD coefficients denoted by $\{\widetilde{\theta_j}\}$ and $\{\widetilde{\alpha}_j\}$, let $\widetilde{r}$ denote the corresponding rational approximation. The error caused by the inaccuracies in the PFD coefficients may be estimated

$$|\hat{r}_{k,k}(z) - \widetilde{r}_{k,k}(z)| \lesssim |\alpha_0 - \widetilde{\alpha}_0| + \sum_{j=1}^{k} \frac{|\alpha_j|}{|z-\theta_j|^2}\,|\theta_j - \widetilde{\theta}_j| + \frac{1}{|z-\theta_j|}\,|\alpha_j - \widetilde{\alpha}_j|\ , \tag{6}$$

indicating that the error is the greatest in the vicinity of the poles. It can also be seen from Eq. (6) that the inaccuracy related to the poles has a greater impact near the poles, whereas the error related to the residues should begin to dominate the total error farther away from the poles. By comparing the old and the recomputed PFD coefficients for $k = 14$, it can be seen that the poles all agree to about 6 digits whereas the residues agree to about 5 digits.[1] The most dramatic discrepancy occurs for the coefficient α_0 for which the significands agree to 5 digits but the exponent value given in [3] is -12, although the correct value is -14.

On the grounds of Eq. (6), it can be estimated that coefficients with 6 correct digits should produce a rational function whose deviation from $\hat{r}_{14,14}(z)$ is at most of the order of 10^{-3} on the negative real axis. Figure 2 shows the difference between $\hat{r}_{14,14}(z)$ and a rational function $\widetilde{r}_{14,14}(z)$ that was formed by truncating the PFD coefficients of $\hat{r}_{14,14}$ to 6 significant digits. Interestingly, as can be seen from Fig. 1a, the approximation $\hat{r}_{14,14}(x)$, corresponding to the PFD coefficients from [3], yields a significantly better accuracy of order 10^{-12} than is expected based on the accuracy of the coefficients alone.

[1]Notice that the PFD coefficients in [3] are given for the rational approximation of e^{-x} on $[0,\infty)$ and that they have been multiplied by a factor of two making Eq. (37) in [3] equivalent to Eq. (5).

To investigate the matter further, let us now take the poles $\{\check{\theta}_j\}$ reported in [3] as a starting point for constructing a rational approximation of order 14. The poles $\{\check{\theta}_j\}$ define a polynomial

$$\check{q}_{14}(x) = \prod_{j=1}^{14}(x - \check{\theta}_j) \tag{7}$$

whose values agree to about 6 digits with the values of the correct polynomial $\hat{q}_{14}(x)$ on the negative real axis. The residues at the poles $\{\check{\theta}_j\}$ cannot be computed in a fully consistent manner, since the poles do not correspond to the true zeros of $\hat{q}_{14}$. However, two alternative approaches for computing the residues can be considered. One possibility is to use the correct rational function $\hat{r}_{14,14}$ and Eq. (3) to compute the residues, but this is inconsistent as Eq. (3) only holds at the true poles. Another option is to define a new rational function using $\check{q}_{14}$ as the denominator and the correct polynomial $\hat{p}_{14}$ as the numerator, after which the residues can be computed exactly using symbolic arithmetics. With both of these approaches we obtain a rational approximation, whose accuracy is of the order of 10^{-6} on the negative real axis. It is also worth mentioning that forming the rational function based on the poles $\{\check{\theta}_j\}$ and the correct residues $\{\alpha_j\}$ from Table 1 yields an approximation whose accuracy is of the order of 10^{-7} on the negative real axis.

The article [3] by Gallopoulos and Saad does not indicate, how the reported PFD coefficients were computed, but based on the observations regarding the accuracy of the resulting approximation, it is evident that the values given for the residues somehow compensate for the inaccuracies in the poles $\{\check{\theta}_j\}$ and it seems likely that they have been optimized to minimize the deviation from $\hat{r}_{14,14}$ on the negative real axis. In fact, using the poles $\{\check{\theta}_j\}$ and standard least squares optimization in MATLAB with 10^7 points chosen from the interval $[-10^3, -10^{-10}]$, we were able to produce residues yielding only a slightly worse accuracy of order 10^{-11}. In any case, it should be noted that optimizing the residues properly in the Chebyshev sense would essentially form a problem of comparable difficulty as the original problem of determining $\hat{r}_{14,14}$.

References

[1] A. J. Carpenter, A. Ruttan, and R. S. Varga, *Extended numerical computations on the 1/9 conjecture in rational approximation theory*, in Rational Approximation and Interpolation, P. R. Graves-Morris, E. B. Saff, and R. S. Varga, eds., vol. 1105 of Lecture Notes in Mathematics, Springer-Verlag, 1984, pp. 383–411.

[2] W. J. Cody, G. Meinardus, and R. S. Varga, *Chebyshev rational approximations to e^{-x} in $[0, \infty)$ and applications to heat-conduction problems*, J. Approx. Theory, 2 (1969), pp. 50–65.

[3] E. Gallopoulos and Y. Saad, *Efficient solution of parabolic equations by Krylov approximation methods*, SIAM J. Sci. Stat. Comput., 13 (1992), pp. 1236–1264.

[4] A. A. Gonchar and E. A. Rakhmanov, *Equilibrium distributions and degree of rational approximation of analytic functions*, Math. USSR Sb., 62 (1989).

[5] J. Leppänen, Serpent, a Continuous-energy Monte Carlo Reactor Physics Burnup Calculation Code, URL: `http://montecarlo.vtt.fi`, VTT Technical Research Centre of Finland, 2012.

[6] M. Pusa, *Rational approximations to the matrix exponential in burnup calculations*, Nucl. Sci. Eng., 169 (2011), pp. 155–167.

[7] M. Pusa and J. Leppänen, *Computing the matrix exponential in burnup calculations*, Nucl. Sci. Eng., 164 (2010), pp. 140–150.

[8] T. Schmelzer, *Carathéodory–Fejér approximation*, Matlab Central, 2008.

[9] T. Schmelzer and L. N. Trefethen, *Evaluating matrix functions for exponential integrators via Carathéodory–Fejér approximation and contour integrals*, Electron. Trans. Numer. Anal., 28 (2007), pp. 1–18.
[10] R. B. Sidje, *Expokit: a software package for computing matrix exponentials*, ACM Trans. Math. Softw., 24 (1998), pp. 130–156.
[11] H. Stahl and T. Schmelzer, *An extension of the '1/9'-problem*, Journal of Computational and Applied Mathematics, 233 (2009), pp. 821–834.
[12] L. N. Trefethen, J. A. C. Weideman, and T. Schmelzer, *Talbot quadratures and rational approximations*, BIT., 46 (2006), pp. 653–670.

VTT Technical Research Centre of Finland, Nuclear Energy, P.O. Box 1000, FI-02044 VTT, Finland
E-mail address: maria.pusa@vtt.fi

PUBLICATION IV

Solving linear systems with sparse Gaussian elimination in the Chebyshev Rational Approximation Method (CRAM)

Accepted for publication in Nuclear Science and Engineering.

SOLVING LINEAR SYSTEMS WITH SPARSE GAUSSIAN ELIMINATION IN THE CHEBYSHEV RATIONAL APPROXIMATION METHOD (CRAM)

MARIA PUSA AND JAAKKO LEPPÄNEN

ABSTRACT. The Chebyshev Rational Approximation Method (CRAM) has been recently introduced by the authors for solving the burnup equations with excellent results. This method has been shown to be capable of simultaneously solving an entire burnup system with thousands of nuclides both accurately and efficiently. The method was prompted by an analysis of the spectral properties of burnup matrices, and it can be characterized as the best rational approximation on the negative real axis. The coefficients of the rational approximation are fixed and have been reported for various approximation orders. In addition to these coefficients, implementing the method only requires a linear solver. This paper describes an efficient method for solving the linear systems associated with the CRAM approximation. The introduced direct method is based on sparse Gaussian elimination, where the sparsity pattern of the resulting upper triangular matrix is determined before the numerical elimination phase. The stability of the proposed Gaussian elimination method is discussed based on considering the numerical properties of burnup matrices. Suitable algorithms are presented for computing the symbolic factorization and numerical elimination in order to facilitate the implementation of CRAM and its adoption into routine use. The accuracy and efficiency of the described technique are demonstrated by computing the CRAM approximations for a large test case with over 1600 nuclides.

1. INTRODUCTION

The changes in material compositions of a reactor fuel must be taken into account in all reactor physics calculations, which is in practice handled by burnup calculation codes. An essential part of a burnup calculation is the solving of the burnup equations that describe the rates by which the concentrations of the various nuclides change. The burnup equations form a system of first-order linear differential equations that can be written in matrix notation as

$$\boldsymbol{n}' = \boldsymbol{A}\boldsymbol{n} \ , \quad \boldsymbol{n}(0) = \boldsymbol{n}_0 \ , \tag{1}$$

where $\boldsymbol{n}(t) \in \mathbb{R}^n$ is the nuclide concentration vector and $\boldsymbol{A} \in \mathbb{R}^{n \times n}$ is the burnup matrix containing the decay and transmutation coefficients of the nuclides under consideration. The matrix elements A_{ij} characterize the rates of neutron-induced reactions and spontaneous radioactive decay by which nuclide j is transformed to nuclide i, and they are assumed to be fixed constants.

The burnup equations can be formally solved by the matrix exponential method yielding the simple solution

$$\boldsymbol{n}(t) = e^{\boldsymbol{A}t}\boldsymbol{n}_0 \ , \tag{2}$$

Accepted for publication in the November 2013 issue of *Nuclear Science and Engineering*.

where the exponential of the matrix $\boldsymbol{A}t$ is defined as the power series expression

$$e^{\boldsymbol{A}t} = \sum_{k=0}^{\infty} \frac{1}{k!} (\boldsymbol{A}t)^k \ , \tag{3}$$

with the additional definition $\boldsymbol{A}^0 = \boldsymbol{I}$.

There are numerous algorithms for computing the matrix exponential, but because of the numerical properties of burnup matrices, most of them are ill-suited for solving the burnup equations. The decay constants of the nuclides vary extensively, which induces elements with both extremely small and large absolute values to the burnup matrix. Short-lived nuclides—corresponding to elements with the largest magnitude—are especially problematic since they increase the matrix norm and induce eigenvalues with absolute values up to the order of 10^{21}. Furthermore, the time steps used in burnup calculations can typically vary from a few days (10^5 seconds) to several months (10^7 seconds), and to even thousands of years, if only decay reactions are considered. Most of the established matrix exponential methods, such as the truncated Taylor series approach or the rational Padé approximation, are based on approximation near the origin and work well only when the matrix norm $\|\boldsymbol{A}t\|$ is sufficiently small. Consequently, these algorithms are prone to severe numerical problems when applied to the burnup equations, where this norm can be of the order of 10^{28} [1].

These difficulties have traditionally been solved by using simplified burnup chains or by treating the most short-lived nuclides separately when computing a matrix exponential solution. However, it was recently discovered by the authors that the eigenvalues of the burnup matrix are generally confined to a region near the negative real axis [1]. This observation combined with the fact that in the Chebyshev Rational Approximation Method (CRAM) the rational function $r(z)$ is chosen as the best rational approximation of the exponential function on the negative real axis $\mathbb{R}_-$, led to applying CRAM to solving the burnup equations. The rational approximation in CRAM can be formally defined as the unique rational function $\hat{r}_{k,k} = \hat{p}_k(x)/\hat{q}_k(x)$ satisfying

$$\sup_{x\in\mathbb{R}_-} |\hat{r}_{k,k}(x) - e^x| = \inf_{r_{k,k}\in\pi_{k,k}} \left\{ \sup_{x\in\mathbb{R}_-} |r_{k,k}(x) - e^x| \right\} \ , \tag{4}$$

where $\pi_{k,k}$ denotes the set of rational functions $r_{k,k}(x) = p_k(x)/q_k(x)$, where p_k and q_k are polynomials of order k. CRAM has been shown to give a robust and accurate solution to the burnup equations with a very short computation time [1, 2, 3].

For numerical reasons, it is generally advantageous to compute the matrix rational function in the partial fraction decomposition form. For a rational function $r_{k,k}(x)$ with simple poles, the decomposition takes the form

$$r_{k,k}(z) = \alpha_0 + \sum_{j=1}^{k} \frac{\alpha_j}{z - \theta_j} \ , \tag{5}$$

where α_0 is the limit of the function $r_{k,k}$ at infinity and α_j are the residues at the poles θ_j. The poles of a rational function with real-valued coefficients form conjugate pairs, so the computational cost can be reduced to half

for a real variable x:

$$r_{k,k}(x) = \alpha_0 + 2\,\mathrm{Re}\left(\sum_{j=1}^{k/2} \frac{\alpha_j}{x - \theta_j}\right) \quad . \tag{6}$$

The rational approximation to Eq. (2) can then be written

$$\boldsymbol{n} = \alpha_0 \boldsymbol{n}_0 + 2\,\mathrm{Re}\left(\sum_{j=1}^{k/2} \alpha_j (\boldsymbol{A}t - \theta_j \boldsymbol{I})^{-1} \boldsymbol{n}_0\right) \quad . \tag{7}$$

Therefore, the computation of a CRAM approximation of order k requires solving $k/2$ linear systems of the form

$$(\boldsymbol{A}t - \theta_j \boldsymbol{I})\, \boldsymbol{x}_j = \alpha_j\, \boldsymbol{n}_0 \ . \tag{8}$$

Notice that the partial fraction coefficients for each CRAM approximation order are fixed. Therefore, implementing CRAM only requires a linear solver in addition to these coefficients. The approximation orders $1 \leq k \leq 13$ can be computed with high accuracy by using the approximative Carathéodory–Fejér method. A MATLAB script is provided for this purpose in [4]. In addition, revised sets of partial fraction coefficients for approximation orders $k = 14$ and $k = 16$ have been recently computed and reported [3, 5]. The development version of Serpent 2 features CRAM approximation of orders 6, 8, 10, 12, 14 and 16.

When no nuclides are excluded from the computation, the linear systems are large—the dimensions of the burnup matrix being in the order of a thousand—which complicates the computation of the CRAM approximation. Also, the numerical characteristics of burnup matrices may compromise the accuracy of widely used iterative solvers. The objective of this paper is to describe a method that can be used to solve these linear systems in order to compute the CRAM approximation in a burnup code. The proposed method is based on sparse Gaussian elimination and it has been implemented to the reactor physics code Serpent [6]. This paper is organized as follows. In Section 2, we briefly discuss the numerical properties of burnup matrices that are essential when selecting a numerical method for solving the linear systems according to Eq. (8). In Section 3 we review the theoretical background for sparse Gaussian elimination and introduce suitable algorithms for implementing the method. Finally, numerical results are presented in Section 4 and the accuracy and efficiency of the proposed method is demonstrated.

2. Numerical Properties of Burnup Matrices

In order to select a well-suited method for solving the linear systems of Eq. (8), it is necessary to consider the numerical characteristics of burnup matrices. First of all, they are both large and sparse. Depending on the nuclear data libraries used in the computation, the number of nuclides is generally between 1200 and 1600, if no nuclides are excluded from the computation. The density of the burnup matrix is a few percent, which corresponds to some tens of thousands of non-zero elements in a single matrix. The nuclides can naturally be indexed arbitrarily, which can be exploited when constructing the matrix. Fortunately, the burnup matrix becomes nearly upper triangular if the nuclides are indexed in ascending order with respect to their ZAI index, defined as $\mathrm{ZAI} = 10\,000Z + 10A + I$, where Z is the atomic number, A is the mass number and I is the isomeric state number. Due to the

size of the problem, the method used to solve systems of Eq. (8) should either be iterative or exploit the sparsity pattern of the matrices.

The diagonal elements of a burnup matrix are non-positive and the element a_{jj} characterizes the total rate by which nuclide j is transformed to other nuclides. The off-diagonal elements, on the other hand, are non-negative and the element a_{ij} describes the rate by which nuclide j is transformed to nuclide i. When forming the burnup equations, it is possible to take into account the production of by-product nuclides. In this case, for example, the reaction rate for each (n, p) reaction contributes to the production rate of $^{1}\mathrm{H}$. Traditionally, the production of nuclides as by-products has been ignored in the burnup matrix [7, 8]. Therefore, we will use the term *augmented burnup matrix* to refer to the case, where the production of by-product nuclides has been taken into account when constructing the burnup matrix. In the development version of Serpent 2, the augmented burnup equations are solved by default.

The augmented burnup matrix elements satisfy the following relation:

$$-d_j \, a_{jj} = \sum_{i \neq j} a_{ij} \ , \quad j = 1, \ldots, n \ , \tag{9}$$

where d_j is the *average* number of nuclides produced in the transmutation and decay reactions of nuclide j, consisting of the daughter nuclide and the reaction by-products. Since at most four nuclides can result from a single transmutation or decay reaction, e.g., from the $(\mathrm{n}, 3\alpha)$ reaction, it holds $1 \leq d_j \leq 4$. Apart from fission, the reactions producing two or more nuclides are relatively improbable, however, and hence it generally holds $1 \leq d_j \leq 2$.

The half-lives of nuclides vary significantly, and as a result, the absolute values of burnup matrix elements can range from zero even up to the order of 10^{21}. As mentioned in Section 1, the extensive variations in the half-lives induce eigenvalues with extremely small and large magnitudes. The respective eigensystem is generally poorly conditioned with many nearly confluent eigenvalues. Many of the popular iterative methods, such as biconjugate gradient and generalized minimum residual method, are based on Krylov subspace techniques and their convergence is ultimately related to the spectral properties of the matrix at hand. In this context, it is particularly disadvantageous, if the matrix eigenvalues lie far apart from each other, which is the case for burnup matrices. Therefore, the numerical characteristics of burnup matrices may cause both convergence and round-off problems in these algorithms. For these reasons it was decided to implement a direct method to Serpent.

3. Sparse Gaussian Elimination

In order to avoid introducing any additional error to the matrix exponential solution, it would be favorable to solve the systems of Eq. (8) with a direct method instead of an iterative one. The sparsity pattern of burnup matrices makes Gaussian elimination a prominent candidate for this task and therefore the application of this method is considered in detail in this section.

As is well-known, the main complication in basic Gaussian elimination is related to round-off errors. It is easy to demonstrate that in the presence of finite precision arithmetics, this method may lead to totally erroneous results due to its instability. In addition, the triangular matrices (i.e., LU decomposition) generated during the

process may be more ill-conditioned than the original matrix, which can in turn grow the round-off error in the forward and back substitution phases of the solution. This may be demonstrated by the following classical example matrix [9]

$$\boldsymbol{A} = \begin{bmatrix} 10^{-20} & 1 \\ 1 & 1 \end{bmatrix} , \tag{10}$$

which has the LU decomposition

$$\boldsymbol{L} = \begin{bmatrix} 1 & 0 \\ 10^{20} & 1 \end{bmatrix} , \qquad \boldsymbol{U} = \begin{bmatrix} 10^{-20} & 1 \\ 0 & 1 - 10^{20} \end{bmatrix} . \tag{11}$$

In floating point arithmetics the number $u_{22} = 1 - 10^{20}$ will be rounded off to roughly $\tilde{u}_{22} = -10^{20}$. Consequently, for respective floating point matrices $\widetilde{\boldsymbol{L}}$ and $\widetilde{\boldsymbol{U}}$ produced by the algorithm, we get the following result

$$\widetilde{\boldsymbol{L}}\widetilde{\boldsymbol{U}} = \begin{bmatrix} 10^{-20} & 1 \\ 1 & 0 \end{bmatrix} , \tag{12}$$

which is substantially different from $\boldsymbol{A} = \boldsymbol{L}\boldsymbol{U}$. Also, if we solve the system $\widetilde{\boldsymbol{L}}\widetilde{\boldsymbol{U}}\boldsymbol{x} = \boldsymbol{b}$, the solution will differ drastically from the true solution of $\boldsymbol{A}\boldsymbol{x} = \boldsymbol{b}$.

The instability demonstrated in the previous example arises when the intermediate quantities computed during the algorithm are large relative to the elements of $\boldsymbol{A}$. In order to control this instability, Gaussian elimination is nearly always implemented with *partial pivoting*. In partial pivoting, the rows of the matrix are permuted in such manner that in each column the largest element of the lower triangular part of the matrix is chosen as the pivot element. This guarantees that the elements of the lower triangular matrix $\boldsymbol{L}$ fulfill $|L_{ij}| \leq 1$. In this case the algorithm is stable if the elements of $\boldsymbol{U}$ are of the same order as the elements of $\boldsymbol{A}$. This stability can be monitored based on a quantity called the *growth factor*, defined as

$$\rho = \frac{\max_{i,j} |u_{ij}|}{\max_{i,j} |a_{ij}|} . \tag{13}$$

When ρ is of order 1, we can expect Gaussian elimination with partial pivoting to be stable. Gaussian elimination with partial pivoting is considered to be extremely stable in practice, although it is possible to construct matrices with large growth factors. When using partial pivoting, the elements of $\boldsymbol{U}$ can become large (compared to the elements of $\boldsymbol{A}$) only through the subtraction of rows in the Gaussian elimination. Therefore, it is relatively easy to show that the maximum value for the growth factor is $\rho_{\max} = 2^{n-1}$. In practice, however, for the growth factor to attain the value $\rho_{\max}$ would require very special matrices that never seem to arise in real applications [9].

Therefore, Gaussian elimination with partial pivoting is considered to be a reliable method for solving linear systems. There are, however, some difficulties in applying it efficiently to sparse systems. First of all, it would be sensible to utilize the sparsity pattern of the matrix under consideration and perform the elimination solely on the non-zero elements of the matrix. This requires employing a sparse matrix format where only the non-zero entries are stored together with their row and column information. During the Gaussian elimination phase, however, new

non-zero elements are introduced in the matrix. Unfortunately, putting on new non-zero elements to the sparse matrix structure during the elimination may easily begin to dominate the computational cost. For this reason, an efficient implementation of a sparse Gaussian elimination requires that the non-zero structure of the resulting decomposition is determined in advance. This allows allocating storage for all non-zero entries before beginning the numerical elimination. Determining this sparsity pattern is called computing the *symbolic LU factorization* and the matrix containing the non-zero structure is called the fill-in matrix. It is noteworthy that when computing a CRAM approximation of order k, this sparsity pattern is similar for all $k/2$ matrix equations of Eq. (8) and it is therefore sufficient to compute the symbolic factorization only once for each CRAM approximation.

Unfortunately, this strategy fails if we wish to implement Gaussian elimination with partial pivoting. In this case the sparsity pattern of $\boldsymbol{U}$ depends on the employed permutations, which are determined during the numerical elimination. Hence, partial pivoting inhibits computing the symbolic LU factorization before the numerical elimination phase, which deteriorates the computational efficiency of this approach. Luckily, the special characteristics of burnup matrices actually allow using Gaussian elimination without partial pivoting. This is explained in Section 3.2

3.1. **Symbolic factorization.** This section describes an algorithm that can be used to compute the sparsity pattern of the fill-in matrix $\boldsymbol{F}$ resulting from the Gaussian elimination. The method presented here is essentially the algorithm FILL2 from [10] but we attempt to introduce it without the unnecessary use of graph-theoretical notation in order to facilitate its comprehensibility and implementation.

The column and row indices of $\boldsymbol{A}$ are referred to as nodes. When $a_{ij} \neq 0$, the notation $i \to j$ is used. We say that there is a *path* of length m from node i to node k, if there exists a sequence of non-zero nodes $[i = i_1, i_2, i_3 \ldots, i_m, i_{m+1} = k]$ such that $i_n \to i_{n+1}$ for $n = 1, \ldots, m+1$. The physical interpretation for this is that there exists a transmutation path of length m from nuclide k to nuclide i.

The sparsity pattern of the matrix $\boldsymbol{F}$ can be computed efficiently by studying the various paths related to the graph of $\boldsymbol{A}$. This is a direct consequence from Lemma 1 in [10], which states that $F_{ij} \neq 0$ if and only if there exists a path from node i to node j such that

$$i_n < \min(i, j) \qquad \text{for} \quad 2 \leq n \leq m \ . \tag{14}$$

Algorithm 1 can be used to compute the non-zero structure of $\boldsymbol{F}$ based on Lemma 1 from [10]. As a first step, the sparsity pattern of $\boldsymbol{F}$ is initialized with the sparsity pattern of $\boldsymbol{A}$. The algorithm then proceeds column-wise through the matrix. In each column, the upper triangular part of $\boldsymbol{F}$ is studied. If a non-zero element F_{ij} with $i < j$ is found, node i is added to the set of nodes Ω_j to be considered later. After examining the non-zero pattern of column j, the algorithm continues by deleting nodes one by one from the set Ω_j. After deleting node i from Ω_j, the respective column of matrix $\boldsymbol{F}$ is examined. If a non-zero element a_{ki} with $k > i$ is found, there exists a path $k \to i \to j$ such that $i < \min(k, j)$, and according to Lemma 1, it follows that F_{kj} is non-zero in the fill-in matrix. In addition, if $i < k < j$, there is a prospect for a longer path to node j through nodes

Algorithm 1 Symbolic factorization

```
Initialize F with the sparsity pattern of A
for j = 2, ..., n do
  Ω_j = ∅
  a = 0
  for each non-zero F_ij in column j do
    a_i = 1
    if i < j then
      add i to Ω_j
    end if
  end for
  while Ω_j ≠ ∅ do
    Delete some node i from Ω_j
    for each non-zero F_ki in column i do
      if k > i and a_k = 0 then
        add F_kj to the non-zero structure of F
        a_k = 1
        if k < j then
          add k to Ω_j
        end if
      end if
    end for
  end while
end for
```

i and k, and therefore node k is added to the set Ω_j. Notice that since the matrix $\boldsymbol{F}$ is studied column-wise starting from the second column, the non-zeros F_{kj} with $k < i$ and $k < j$ can be ignored at this stage, since the columns with indices smaller than j have already been taken into account. The calculation continues this way until the set Ω_j is empty. The auxiliary vector $\boldsymbol{a}$ is used to keep track of the non-zero elements that have already been added to the sparsity structure of $\boldsymbol{F}$ in each column.

It is straightforward to estimate the computational cost of Algorithm 1. The first step in the algorithm is proportional to the number of non-zeros in the column j of $\boldsymbol{F}$. Then, for each non-zero F_{ij} in the upper triangular part of column j, the lower triangular part of column i is studied. We'll use the notation $|\cdot|$ to denote the number of non-zero entries in a matrix or a vector, and write the fill-in matrix in the following form:

$$\boldsymbol{F} = \boldsymbol{F}^L + \boldsymbol{D} + \boldsymbol{F}^U \ , \tag{15}$$

where $\boldsymbol{F}^L$ contains the lower triangular part, $\boldsymbol{D}$ the diagonal, and $\boldsymbol{F}^U$ the upper triangular part of the matrix. Using this notation, we can state that the computational cost of Algorithm 1 is proportional to

$$|\boldsymbol{F}| + \sum_{j=1}^{n} |\boldsymbol{F}_j^U||\boldsymbol{F}_j^L| \ .$$

This is computationally affordable, especially considering that the computational cost of basic Gaussian elimination is proportional to $\frac{2}{3}n^3$. The number of non-zero

entries is generally of the order of $\frac{1}{100}n^2$ in burnup matrices. As already mentioned, it is also advantageous that we only need to compute this symbolic factorization once when computing a CRAM approximation.

It should be mentioned that Algorithm 1 can also be executed row-wise. The implementation in the current release of Serpent is row-based, whereas the column-based version, considered here, has been adopted to the development version of Serpent 2.

3.2. **Diagonal Dominance.** It was previously stated that the special characteristics of burnup matrices allow using Gaussian elimination without partial pivoting. This matter is explained in the following.

In Gaussian elimination, a matrix $\boldsymbol{A} \in \mathbb{R}^{n\times n}$ is transformed to lower triangular form by a series of updates, which corresponds to multiplying the matrix by a sequence of lower-triangular matrices $\boldsymbol{L}_j$ from the left. Let $\boldsymbol{A}^{(j)}$ denote the matrix obtained after j updates, i.e. $\boldsymbol{A}^{(j)} = \boldsymbol{L}_j \cdots \boldsymbol{L}_2\boldsymbol{L}_1\boldsymbol{A}$. After $n-1$ updates, the matrix becomes upper-triangular:

$$\boldsymbol{L}_{n-1}\boldsymbol{L}_{n-2}\cdots\boldsymbol{L}_2\boldsymbol{L}_1\boldsymbol{A} = \boldsymbol{U} \ , \tag{16}$$

after which setting $\boldsymbol{L} = \boldsymbol{L}_1^{-1}\boldsymbol{L}_2^{-1}\cdots\boldsymbol{L}_{n-2}^{-1}\boldsymbol{L}_{n-1}^{-1}$ gives the decomposition $\boldsymbol{A} = \boldsymbol{L}\boldsymbol{U}$. During the elimination, the elements of $\boldsymbol{L}$ are computed according to

$$L_{ij} = -\frac{a_{ij}^{(j-1)}}{a_{jj}^{(j-1)}} \ , \qquad i > j \ . \tag{17}$$

Therefore, $|L_{ij}| \leq 1$, if the absolute values of the diagonal elements remain greater than the absolute values of the elements below the diagonal during the updates. It is well-known that for column diagonally dominant matrices, diagonal dominance is preserved during Gaussian elimination. However, as mentioned in Section 2, due to reactions that produce two or more nuclides, burnup matrices are not generally diagonally dominant.

According to Lemma 1 in[10], the element a_{ij} is *updated* during Gaussian elimination, if there exists a path from $i \to j$ satisfying Eq. (14) with length $m \geq 2$. Physically this means that there exists a transmutation path from nuclide j to nuclide i through nuclides whose ZAI index is smaller than the indices of i and j. In particular, the element a_{lj} affects the element a_{ij} through the updates if $l \in \{i_n\}$.

In burnup matrices, diagonal dominance is violated by reactions that produce two or more nuclides. Let k denote the index of the first fissionable nuclide. Aside from fission, the only nuclides emitted as by-products are the hydrogen isotopes ^{1}H, ^{2}H and ^{3}H and the helium isotopes ^{3}He and ^{4}He. According to the previous Lemma, for the corresponding rows to affect other rows during Gaussian elimination would require the existence of transmutation paths originating from the by-product nuclides. However, this is generally impossible, since all these nuclides are stable aside from ^{3}H (which decays into ^{3}He) and they do not elicit neutron reactions that would produce nuclides outside this group. The violation of diagonal dominance in the submatrix $\boldsymbol{A}(k:n, k:n)$, on the other hand, would require a transmutation path from a fissile nuclide to another fissile nuclide through a fission product nuclide, which is extremely unlikely in reactor conditions.[1]

[1]Interestingly, paths from fission product nuclides to fissile nuclides are theoretically possible if data based on nuclear models rather than measurements is considered. For example, the nuclear data library `TENDL-2011` [11] produced with the nuclear reaction program Talys [12] contains data

Algorithm 2 Numerical elimination

```
v = 0
for i = 1, 2, ..., n − 1 do
  for j ∈ F(i) do
    v_j = a_ij
  end for
  for j ∈ F(i) do
    if i > j then
      c_i = c_i − (F_ij / F_jj) c_j
      for k ∈ F(j) do
        v_k = v_k − (F_ij / F_jj) F_jk
      end for
    end if
  end for
  for j ∈ F(i) do
    F_ij = v_j
  end for
end for
```

3.3. **Numerical Elimination.** After computing the non-zero structure of the fill-in matrix $\boldsymbol{F}$, the numerical elimination can be efficiently performed on this symbolic factorization using Algorithm 2. It has been derived from the method CELIMINATE in [13]. CELIMINATE considers a system of the form of $\boldsymbol{x}\boldsymbol{M} = \boldsymbol{c}$, where $\boldsymbol{x} \in \mathbb{R}^{1\times n}$, $\boldsymbol{M} \in \mathbb{R}^{n\times n}$ and $\boldsymbol{x} \in \mathbb{R}^{1\times n}$, whereas we consider a system of the form of Eq. (8).

When using a sparse matrix format, it is most efficient to store the matrices and implement the numerical elimination row-wise. The notation $F(i)$ is used to denote the set of column indices of the non-zero entries on the i^{th} row of the fill-in matrix $\boldsymbol{F}$, i.e. $j \in F(i)$ if $F_{ij} \neq 0$. These column indices need to sorted in ascending order. Algorithm 2 proceeds row by row by introducing zeros to the left of the matrix diagonal. Since the non-zero structure of the resulting matrix has been determined before starting the numerical elimination, the actual elimination phase can be performed with a minimal computational cost. An auxiliary vector $\boldsymbol{v}$ is employed in order to make the subtracting of the matrix rows more efficient. Notice that the elements in each row need to be accessible in order by their column indices. In practice, this requires sorting the matrix structure after computing the fill-in by Algorithm 1. In Serpent, insertion sort is used for this purpose. It is also convenient to store the diagonal elements of the matrix to an auxiliary vector in order to allow for an easy access to them during the computation.

that enables these paths. However, since these transmutation paths are extremely unlikely, they are not further considered here.

TABLE 1. CPU time required for computing the CRAM approximation of different orders for the test case with 1606 nuclides.

Approximation order	CPU time (s)
16	0.108
14	0.094
12	0.086
10	0.079
8	0.070
6	0.063

4. Numerical Results

To evaluate the efficiency and accuracy of the described technique, it was applied to a burnup system that can be considered to represent the extreme case in terms of the matrix size. The test case represents a PWR pin-cell with fuel irradiated to 0.1 MWd/kgU burnup with the time step of 12.5 days. The number of nuclides present in the calculation is 1606, which is representative of the practical maximum encountered in burnup calculations. The absolute values of the matrix elements range from zero to the order of 10^{21}, the largest entries corresponding to the decay of ^{7}B whose half-life is $\sim 10^{-24}$ s.

The burnup matrix was formed by indexing the nuclides according to their ZAI index. The sparsity pattern of the resulting matrix is shown in Figure 1. The burnup matrix has 59 668 non-zero entries, which corresponds to a density of approximately 2.3%. Rows $2, \ldots, 6$ correspond to hydrogen and helium isotopes. These rows are relatively dense because these nuclides are emitted as by-products in some neutron and decay reactions. The dense columns in the right part of the matrix result from fission reactions. The non-zero elements below the diagonal correspond to beta negative decay and the (n, γ) reaction.

The CRAM approximations of orders 6, 8, 10, 12, 14 and 16 were computed for this burnup system. The calculations were performed with the development version of Serpent 2 on a quad-core 3.00 GHz Intel Xeon X5450 CPU. The respective calculation times are shown in Table 1. These calculation times support the previous observation that in terms of computational efficiency, CRAM either matches or outperforms other established methods used in the context of burnup equations [2]. For each approximation order, the total calculation time is dominated by the numerical elimination phase. For the approximation of order 16, the numerical elimination takes about 60% of the total CPU time, as opposed to about 40% for the approximation of order 6. According to Eq. (7), the computational cost of this phase for approximation order k is proportional to $k/2$. The proportion of the total calculation time for performing the symbolic factorization phase, including the sorting of the row indices, increases from 13% to 23% when the approximation order is reduced from 16 to 6. The number of fill-in elements is 7 449 for this test case matrix.

In order to evaluate the accuracy and to study the stability of the chosen approach, a reference solution was computed with MATLAB's Symbolic Toolbox using

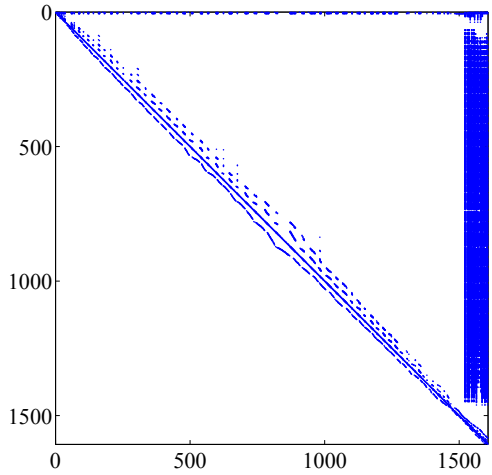

FIGURE 1. The non-zero structure of the test case burnup matrix.

high-precision arithmetics for approximation order 16. As round-off errors are accumulated with an increasing CRAM approximation order, the highest considered approximation order should provide the most conservative error estimate for the presented test case. The relative difference between the reference solution and the solution computed with Gaussian elimination using double precision is plotted in Figure 2. Recalling that we can expect about 15 correct digits with double precision arithmetics, it can be seen from the figure that, apart from ^{1}H, not many digits have been lost to round-off errors. As explained in Section 3, Gaussian elimination is stable, if the matrix growth factor ρ defined according to Eq. (13) is of the order of 1. For this test case, the growth factor is exactly one for each linear system, indicating that no amplification of the matrix entries takes place during the numerical elimination. However, the practicality of this observation is hindered by the fact that $\boldsymbol{A}$ contains entries of very large magnitude. Interestingly, the poorest relative accuracy, corresponding to about 12 correct digits, is obtained for the nuclide ^{1}H. In the burnup matrix, this nuclide corresponds to the first row, which does not change during the numerical elimination. Therefore, the round-off error in the result is solely attributable to the back substitution phase in the algorithm and reflects the characteristics of the original matrix. In particular, due to the decay of ^{7}B by proton emission, this first row in the matrix contains the largest element of the matrix.

To further illustrate the numerical characteristics of the linear systems encountered in CRAM, the same test case was solved with some standard iterative solvers available in MATLAB. The considered iterative methods were the generalized minimum residual (GMRES) method and the biconjugate gradient (BCG) method, and they were used to compute the CRAM approximation of order 16. Figure 3 shows the relative difference between the solutions obtained with these iterative techniques

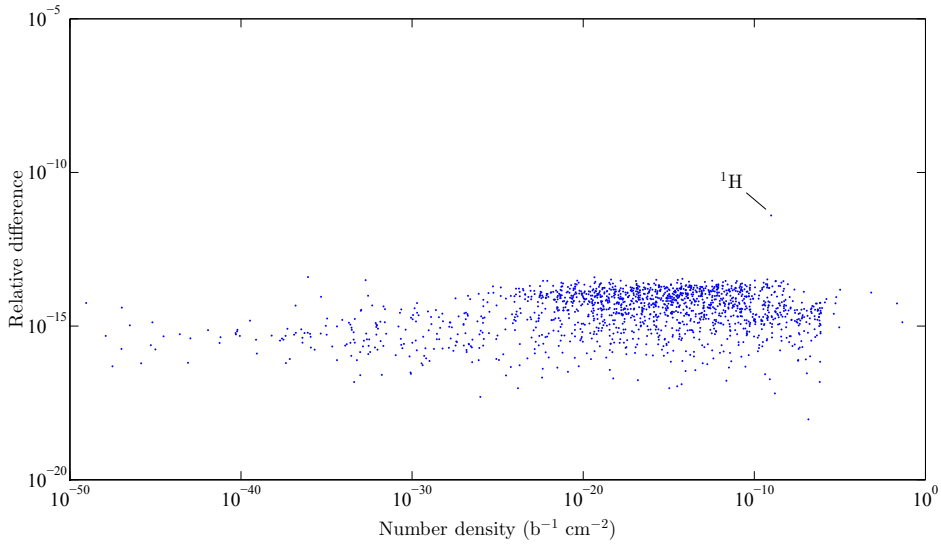

FIGURE 2. The relative difference between the test case solutions obtained using double and high-precision arithmetics for CRAM approximation of order 16.

and the reference solution based on Gaussian elimination with high-precision arithmetics. As can be seen from the figure, the accuracy of both iterative methods is questionable for this test case. This can be attributed to the methods stagnating before a reasonable accuracy was reached. With the GMRES method, the stagnation occurred between 23 and 42 iterations, with the norm of the relative residual being in the order of 10^{-4}. The BCG method converged slightly faster, with all relative residuals being in the order of 10^{-5} after less than 10 iterations when the method stagnated.

Both of these iterative methods are based on projecting the original problem to a lower dimensional Krylov subspace. Therefore, the observed convergence problems can ultimately be traced back to the spectral properties of the burnup matrix. In the GMRES method, the iteration is based on minimizing the 2-norm of the residual in a Krylov subspace, whose dimension increases with each iteration. In the BCG method, on the other hand, the same residual is forced orthogonal to another Krylov subspace. (For further details, see e.g., [9].) However, it should be kept in mind that these basic iterative methods can be substantially improved by preconditioning techniques. Therefore, this study does not imply that all Krylov-based iterative methods are ill-suited for solving these linear systems. However, it is clear that the numerical method for this purpose should be carefully selected and tested.

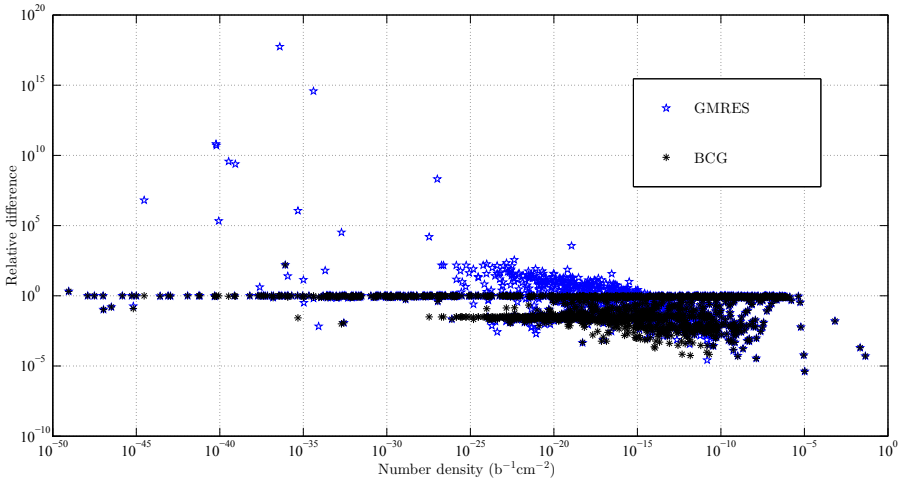

FIGURE 3. The relative difference between the reference solution and solutions obtained with the generalized minimum residual (GMRES) method and the biconjugate gradient (BCG) method for a CRAM approximation of order 16.

5. CONCLUSIONS

The computation of the matrix exponential in burnup calculations has been traditionally challenging due to the extreme stiffness of the problem resulting from the extensively varying magnitudes of the transmutation and decay constants. Based on the discovery that the eigenvalues of burnup matrices are generally confined to the vicinity of the negative real axis, the Chebyshev Rational Approximation Method (CRAM) was successfully proposed and applied to solving the burnup equations by the authors, effectively eliminating all previously encountered computational problems. The method can be described as the best rational approximation on the negative real axis, and it has been shown [1, 3] to give a robust and accurate solution to the burnup equations combined with high computational efficiency.

For numerical reasons it is generally advantageous to compute the CRAM approximation in its partial fraction form. Since these partial fraction coefficients are fixed for each approximation order, implementing CRAM in a burnup code is extremely straightforward—only a linear solver is required in addition to these coefficients. Unfortunately, the difficult numerical properties of burnup matrices may compromise the accuracy of some numerical methods used for solving the linear systems. In this paper, a direct method was considered. The introduced technique is based on sparse Gaussian elimination, where the non-zero structure of the resulting upper triangular matrix is determined before beginning the numerical elimination phase. The numerical properties of burnup matrices and the stability of Gaussian elimination were considered. The efficiency and accuracy of this approach were

demonstrated by applying it to a large test case with over 1600 nuclides. This paper's contribution together with the recently reported, more accurate CRAM partial fraction coefficients [3, 5] are hoped to further facilitate the implementation of CRAM for burnup calculations.

Acknowledgment

This work was funded through the Finnish National Research Programme on Nuclear Power Plant Safety 2011–2014, SAFIR2014.

References

[1] M. Pusa and J. Leppänen, "Computing the Matrix Exponential in Burnup Calculations," *Nucl. Sci. Eng.*, **164**, 2, 140–150 (2010).
[2] A. Isotalo and P. A. Aarnio, "Comparison of depletion algorithms," *Ann. Nucl. Energy*, **38**, 2–3, 261–268 (2011).
[3] M. Pusa, "Rational Approximations to the Matrix Exponential in Burnup Calculations," *Nucl. Sci. Eng.*, **169**, 2, 155–167 (2011).
[4] T. Schmelzer, "Carathéodory–Fejér approximation", `http://www.mathworks.com/matlabcentral`, Matlab Central (Nov. 2008).
[5] M. Pusa, "Correction to Partial Fraction Decomposition Coefficients for Chebyshev Rational Approximation on the Negative Real Axis," `arXiv:1206.2880v1 [math.NA]` (2012).
[6] "PSG2/Serpent Monte Carlo Reactor Physics Burnup Calculation Code", `http://montecarlo.vtt.fi`, VTT Technical Research Centre of Finland (2012).
[7] J. Leppänen and M. Pusa, "Burnup calculation capability in the PSG2/Serpent Monte Carlo Reactor Physics Code," International Conference on Mathematics, Computational Methods & Reactor Physics (M&C 2009), Springer-Verlag, Saratoga Springs, New York (2009), CD-ROM, 1662 - 1673, American Nuclear Society, LaGrange Park, IL.
[8] D. G. Cacuci, ed., *Handbook of Nuclear Engineering*, Vol. 2: Reactor Design, Springer (2010).
[9] L. N. Trefethen and D. Bau, *Numerical Linear Algebra*, SIAM (1997).
[10] D. J. Rose and R. E. Tarjan, "Algorithmic Aspects of Vertex Elimination on Directed Graphs," *SIAM J. Appl. Math*, **34**, 176–197 (1978).
[11] A. J. Koning and D. Rochman, "tendl-2011, talys-based Evaluated Nuclear Data Library", Nuclear Research and Consultancy Group (NRG) (2011).
[12] A. Koning, S. Hilaire and S. Goriely, "talys-1.4, a Nuclear Reaction Program, User Manual", Nuclear Research and Consultancy Group (NRG) (2011).
[13] R. E. Tarjan, "Graph Theory and Gaussian Elimination." Tech. Rep. CS-TR-75-526, Stanford University, Department of Computer Science, Stanford, CA, USA (1975).

VTT Technical Research Centre of Finland, Nuclear Energy, P.O. Box 1000, FI-02044 VTT, Finland
E-mail address: `maria.pusa@vtt.fi`

PUBLICATION V

Incorporating sensitivity and uncertainty analysis to a lattice physics code with application to CASMO-4

In: Annals of Nuclear Energy,
40, 1, pp. 153–162.

Annals of Nuclear Energy 40 (2012) 153–162

Contents lists available at SciVerse ScienceDirect

Annals of Nuclear Energy

journal homepage: www.elsevier.com/locate/anucene

Incorporating sensitivity and uncertainty analysis to a lattice physics code with application to CASMO-4

Maria Pusa *

VTT Technical Research Centre of Finland, Nuclear Energy, P.O. Box 1000, FI-02044 VTT, Finland

ARTICLE INFO

Article history:
Received 20 May 2011
Received in revised form 17 October 2011
Accepted 18 October 2011
Available online 1 December 2011

Keywords:
Sensitivity analysis
Uncertainty analysis
Perturbation theory

ABSTRACT

This paper describes the implementation of classical perturbation theory based sensitivity and uncertainty analysis to the reactor physics code CASMO-4 in the context of the UAM (Uncertainty Analysis in Best-Estimate Modelling for Design, Operation and Safety Analysis of LWRS) benchmark. The theoretical background as well as practical guidelines for similar work are reviewed and the developed methodology is described in detail. A technique is proposed for handling a discrepancy between the code and covariance libraries regarding the amount of reactions present in the cross-section model. Numerical results for PWR and GEN-III MOX pin-cell test problems are presented and compared to TSUNAMI-1D. The results are in accordance with theoretical considerations and reflect the characteristics of the developed methodology.

1. Introduction

In recent years the interest towards sensitivity and uncertainty (S&U) analysis has increased notably in the field of nuclear engineering. In 2006, the OECD/NEA expert group on Uncertainty Analysis in Modelling decided to prepare a benchmark titled *Uncertainty Analysis in Best-Estimate Modelling (UAM) for Design, Operation and Safety Analysis of LWRs* (Ivanov et al., 2011) to establish the current state and needs of S&U analysis. The goal of the benchmark is to propagate uncertainty through all stages of coupled neutronics/thermal hydraulics calculations. The imprecision of neutron cross-sections is likely one of the most significant sources of uncertainty in these calculations, and therefore the propagation of this uncertainty is the main priority in the benchmark at the moment. As a first step, this requires developing S&U analysis methods for reactor physics codes that are used to produce homogenized data for coupled neutronics/thermal-hydraulics calculations.

The objective of the benchmark is fairly ambitious as the commonly used reactor physics codes, such as CASMO (Rhodes and Edenius, 2001), HELIOS (HELIOS, 2000), and NEWT (DeHart, 2009), do not have S&U analysis capabilities. In addition, incorporating S&U features to such codes can be quite involved, if the code was not designed from this perspective in the first place. In particular, if a lattice physics code is based on a cross-section model, where the individual capture and scattering reactions have been combined to total scattering and capture reactions, respectively, this will cause complications because the covariance matrices are always reported for the individual reactions. This applies to both statistical and deterministic uncertainty analysis. For example, the lattice physics codes CASMO, HELIOS, WIMS (WIMS9A, 2005), and DRAGON (Marleau et al., 2009) all have a similar cross-section model that is based on combining the individual capture and scattering cross-sections.

At VTT, the UAM benchmark was recognized as an opportunity to start developing an S&U analysis calculation system. Since CASMO-4 is the standard tool for lattice physics calculations at VTT, it was decided to begin developing S&U analysis capability to it. As a first step, classical perturbation theory (CPT) has been implemented to enable the computation of critical eigenvalue sensitivities with respect to cross-sections. In addition, a methodology was developed for processing the covariance matrices from SCALE 6 (NEA Data Bank, 2011) to become compatible with the cross-section model of CASMO-4 to enable uncertainty analysis. This processing methodology has since been adopted by other participants in the UAM benchmark (Wieselquist et al., 2011). In addition to describing the developed methodology, the purpose of this paper is to review the theoretical background and practical guidelines for implementing S&U methods to lattice physics codes. Emphasis is put on dealing with the cross-section model of CASMO-4.

2. Theoretical background

The purpose of sensitivity analysis is to study how sensitive a mathematical model is to perturbations in its uncertain parameters. The objective of uncertainty analysis is to estimate how the uncertainty in these parameters is propagated to a response

* Tel.: +358 40 756 8257; fax: +358 20 722 5000.
E-mail address: Maria.Pusa@vtt.fi

0306-4549/$ - see front matter © 2011 Elsevier Ltd. All rights reserved.
doi:10.1016/j.anucene.2011.10.013

dependent on the mathematical model under consideration. In this work the mathematical model is the neutron transport criticality equation, which is an eigenvalue problem that can be written in operator form as

$$\boldsymbol{A}\boldsymbol{\Phi} = \frac{1}{k}\boldsymbol{B}\boldsymbol{\Phi}, \tag{1}$$

where $\boldsymbol{\Phi} \in H_\Phi$ is the neutron flux, H_Φ is a Hilbert space and k is the multiplication factor. It should be noted that both the continuous-energy criticality equation and the various systems derived from it in numerical computations can be written in the form of Eq. (1). The uncertain parameters are the neutron cross-sections and they are denoted by $\boldsymbol{\sigma} \in E_\sigma$, where E_σ is a normed space. The response R under consideration is the critical eigenvalue k, which forms a special case in terms of sensitivity analysis and can be treated with classical perturbation theory as described in the following section.

2.1. Sensitivity analysis

The object of local sensitivity analysis is to determine how the multiplication factor k depends on the cross-sections near their evaluated value $\hat{\boldsymbol{\sigma}}$. This dependence is characterized by the directional derivative of the response in the direction of the perturbation $\delta\boldsymbol{\sigma}$. When considering the continuous-energy criticality equation, the cross-sections are functions of energy and location, and the appropriate derivative is the functional directional derivative called the Gâteaux-variation (Cacuci, 2003). It follows that the sensitivity of R with respect to the perturbation $\boldsymbol{h} = [\delta\boldsymbol{\Phi}, \delta\boldsymbol{\sigma}] \in D = H_\Phi \times E_\sigma$ at the point $\hat{\boldsymbol{e}} = [\boldsymbol{\Phi}, \hat{\boldsymbol{\sigma}}] \in D$ may be defined as:

$$\delta R(\hat{\boldsymbol{e}}; \boldsymbol{h}) = \lim_{t\to 0} \frac{R(\hat{\boldsymbol{e}} + t\boldsymbol{h}) - R(\hat{\boldsymbol{e}})}{t}. \tag{2}$$

When the cross-sections are perturbed, also the solution $\boldsymbol{\Phi}$ is affected and therefore the computation of the sensitivity $\delta R(\hat{\boldsymbol{e}}; \boldsymbol{h})$ requires that the perturbation $\delta\boldsymbol{\Phi}$ is known. In principle, $\delta\boldsymbol{\Phi}$ can be computed from the following *forward sensitivity system*:

$$\delta k(\hat{\boldsymbol{e}}; \boldsymbol{h})\boldsymbol{A}\boldsymbol{\Phi} + k\delta\boldsymbol{A}(\hat{\boldsymbol{e}}; \boldsymbol{h}) = \delta\boldsymbol{B}(\hat{\boldsymbol{e}}; \boldsymbol{h}), \tag{3}$$

which can be derived by taking the Gâteaux-variation of system (1) with respect to a perturbation $\boldsymbol{h}$ on both sides. However, when computing several sensitivities, this approach would require the repetitive solving of Eq. (3).

Fortunately, the sensitivities can be computed more efficiently by exploiting the adjoint of Eq. (1), which is defined as the system that satisfies the following relation[1]:

$$\left\langle \boldsymbol{A}\boldsymbol{\Phi} - \frac{1}{k}\boldsymbol{B}\boldsymbol{\Phi}, \boldsymbol{\Psi} \right\rangle = \left\langle \boldsymbol{\Phi}, \boldsymbol{A}^*\boldsymbol{\Psi} - \frac{1}{k}\boldsymbol{B}^*\boldsymbol{\Psi} \right\rangle \tag{4}$$

where the brackets $\langle \cdot, \cdot \rangle$ denote an inner product. When considering the continuous-energy criticality equation, it is customary to employ the L^2 inner product (Carlson and Lathrop, 1968; Lewis and Miller, 1984). The expression for the sensitivity (3) can now be written utilizing this adjoint relation. Since the operators $\boldsymbol{A}$ and $\boldsymbol{B}$ are linear with respect to $\boldsymbol{\Phi}$, they are also Fréchet-differentiable with respect to $\boldsymbol{\Phi}$ with $\boldsymbol{A}'_\Phi = \boldsymbol{A}$ and $\boldsymbol{B}'_\Phi = \boldsymbol{B}$. Eq. (3) can thus be written in the form:

$$\delta k(\hat{\boldsymbol{e}}; \boldsymbol{h})\boldsymbol{A}\boldsymbol{\Phi} + k\boldsymbol{A}'_\sigma(\hat{\boldsymbol{e}})\ \delta\boldsymbol{\sigma} + k\boldsymbol{A}(\hat{\boldsymbol{e}})\ \delta\boldsymbol{\Phi} = \boldsymbol{B}'_\sigma(\hat{\boldsymbol{e}})\ \delta\boldsymbol{\sigma} + \boldsymbol{B}(\hat{\boldsymbol{e}})\ \delta\boldsymbol{\Phi}. \tag{5}$$

For any $\boldsymbol{\Psi} \in H_\Phi$ not orthogonal with $\boldsymbol{A}\boldsymbol{\Phi}$ or $\boldsymbol{B}\boldsymbol{\Phi}$, it now holds:

$$\begin{aligned}
\delta k(\hat{\boldsymbol{e}}; \boldsymbol{h}) &= \frac{\left\langle (-k\boldsymbol{A}'_\sigma + \boldsymbol{B}'_\sigma)\delta\boldsymbol{\sigma}, \boldsymbol{\Psi} \right\rangle + \left\langle (-k\boldsymbol{A} + \boldsymbol{B})\delta\boldsymbol{\Phi}, \boldsymbol{\Psi} \right\rangle}{\langle \boldsymbol{A}\boldsymbol{\Phi}, \boldsymbol{\Psi} \rangle} \\
&= -\frac{\left\langle (\boldsymbol{A}'_\sigma - \frac{1}{k}\boldsymbol{B}'_\sigma)\delta\boldsymbol{\sigma}, \boldsymbol{\Psi} \right\rangle + \left\langle (\boldsymbol{A} - \frac{1}{k}\boldsymbol{B})\delta\boldsymbol{\Phi}, \boldsymbol{\Psi} \right\rangle}{\left\langle \frac{1}{k^2}\boldsymbol{B}\boldsymbol{\Phi}, \boldsymbol{\Psi} \right\rangle} \\
&= -\frac{\left\langle (\boldsymbol{A}'_\sigma - \frac{1}{k}\boldsymbol{B}'_\sigma)\delta\boldsymbol{\sigma}, \boldsymbol{\Psi} \right\rangle + \left\langle \delta\boldsymbol{\Phi}, (\boldsymbol{A}^* - \frac{1}{k}\boldsymbol{B}^*)\boldsymbol{\Psi} \right\rangle}{\left\langle \frac{1}{k^2}\boldsymbol{B}\boldsymbol{\Phi}, \boldsymbol{\Psi} \right\rangle}.
\end{aligned} \tag{6}$$

If the function $\boldsymbol{\Psi}$ is chosen as the solution of the adjoint system

$$\left(\boldsymbol{A}^* - \frac{1}{k}\boldsymbol{B}^*\right)\boldsymbol{\Psi} = 0 \tag{7}$$

the response sensitivity may be computed as

$$\delta k(\hat{\boldsymbol{e}}; \boldsymbol{h}) = -\frac{\left\langle (\boldsymbol{A}'_\sigma - \frac{1}{k}\boldsymbol{B}'_\sigma)\delta\boldsymbol{\sigma}, \boldsymbol{\Psi} \right\rangle}{\left\langle \frac{1}{k^2}\boldsymbol{B}\boldsymbol{\Phi}, \boldsymbol{\Psi} \right\rangle} \tag{8}$$

which is known as classical perturbation theory in reactor physics.

In practice the criticality equation and the corresponding adjoint equation are solved numerically, which gives rise to some complications in the CPT formalism. Ideally, the numerical method applied to computing the sensitivities should fulfill two conditions. Firstly, the discretized forward and adjoint systems and the discretized operators corresponding to the functional derivatives A'_σ and B'_σ should be consistent with the analytical equations (Cacuci, 2003). Secondly, the inner product in (8) should be discretized in a manner consistent with the discretized operators thereby bringing the operators into a Hilbert-space, where the discretized operators are adjoints with respect to the discretized inner product (Cacuci, 2003).

However, this type of consistent sensitivity analysis is usually infeasible in reactor physics calculations. For example, if the multi-group approximation is applied to the continuous-energy forward and adjoint systems, this leads to two sets of multi-group cross-sections—one weighted with the energy spectrum corresponding to the forward system and one weighted with the energy spectrum corresponding to the adjoint system. For this reason, it is customary to take the multi-group criticality equation as the starting point and apply CPT to it. Another common approach is to apply the discrete ordinates approximation before formulating the CPT setup. As previously noted, after these approximations the criticality equation can still be written as a system of the form of Eq. (1), where $\boldsymbol{\Phi}$ is now a vector. The inner product corresponding to this system can be defined in a consistent manner as

$$\langle \boldsymbol{\Phi}, \boldsymbol{\Psi} \rangle = \sum_{g=1}^{G} \sum_{m=1}^{M} \omega_m \int_D d^3\boldsymbol{r}\, \Phi^g(\boldsymbol{r}, \boldsymbol{\Omega}_m)\Psi^g(\boldsymbol{r}, \boldsymbol{\Omega}_m) \tag{9}$$

where $\{\boldsymbol{\Omega}_m\}$ are the considered directions in the discrete ordinates approximation and ω_m are the associated quadrature weights. After fixing the boundary conditions for the forward problem, the adjoint system and its boundary conditions can be determined based on Eq. (4).

2.2. Uncertainty analysis

The uncertainty of the cross-sections $\boldsymbol{\sigma}$ should be understood in terms of the Bayesian probability interpretation. In this framework, all knowledge about a parameter σ is presented as a probability distribution and the spread of this distribution characterizes the uncertainty related to σ. Typically, the variance of the distribution is chosen to give a numerical value to this uncertainty. When several parameters are considered simultaneously, the probability distribution under consideration is their joint distribution $p(\boldsymbol{\sigma})$, and the covariance matrix of this distribution may be chosen as the

[1] In some cases it is more convenient to write the adjoint relation in the form $\langle \boldsymbol{A}\boldsymbol{\Phi} + \frac{1}{k}\boldsymbol{B}\boldsymbol{\Phi}, \boldsymbol{\Psi} \rangle = \langle \Phi, \boldsymbol{A}^*\boldsymbol{\Psi} + \frac{1}{k}\boldsymbol{B}^*\boldsymbol{\Psi} \rangle + [\boldsymbol{P}(\boldsymbol{\Psi}, \boldsymbol{\Phi})]_{\boldsymbol{x}\in\partial\Omega}$ where $[\boldsymbol{P}(\boldsymbol{\Psi}, \boldsymbol{\Phi})]_{\boldsymbol{x}\in\partial\Omega}$ is a bilinear form associated with the system. We will only consider cases where it is straightforward to force this term to vanish.

descriptive statistic for the uncertainty. The uncertainty related to cross-sections is generally reported as covariance matrices.

In the Bayesian formalism, the outcome of the uncertainty analysis should ideally be the posterior distribution $p(R)$ containing all knowledge about the response R under consideration. However, determining $p(R)$ is usually extremely challenging and can often only be done based on a simulation. Therefore, a common practice is to compute estimates for the mean and variance of $p(R)$ and assume the distribution to be Gaussian. Typically the estimate for $\mathrm{Var}[R]$ is obtained by linearizing $R \approx \boldsymbol{s}\boldsymbol{\sigma}$, where $\boldsymbol{s} \in \mathbb{R}^{1\times K}$, and using the identity

$$\mathrm{Var}[R] \approx \mathrm{Var}[\boldsymbol{s}\boldsymbol{\sigma}] = \boldsymbol{s}\mathrm{Cov}[\boldsymbol{\sigma}]\boldsymbol{s}^T \tag{10}$$

known as the *Sandwich rule*. Eq. (10) can be generalized to several responses $\boldsymbol{R} \in \mathbb{R}^J$ as:

$$\mathrm{Cov}[\boldsymbol{R}] = \boldsymbol{S}\mathrm{Cov}[\boldsymbol{\sigma}]\boldsymbol{S}^T \tag{11}$$

where $\boldsymbol{S} \in \mathbb{R}^{J\times K}$. This procedure is exact when $\boldsymbol{R}$ depends linearly on the parameters and $p(\boldsymbol{\sigma})$ is a Gaussian distribution. If $\boldsymbol{\sigma}$ obeys a Gaussian distribution with mean $\hat{\boldsymbol{\sigma}}$ and covariance matrix $\mathrm{Cov}[\boldsymbol{\sigma}]$, i.e. $\boldsymbol{\sigma} \sim \mathrm{N}(\hat{\boldsymbol{\sigma}}, \mathrm{Cov}[\boldsymbol{\sigma}])$, it follows that

$$\boldsymbol{\eta} = \boldsymbol{c} + \boldsymbol{S}\boldsymbol{\sigma} \sim \mathrm{N}(\boldsymbol{c} + \boldsymbol{S}\hat{\boldsymbol{\sigma}}, \boldsymbol{S}\mathrm{Cov}[\boldsymbol{\sigma}]\boldsymbol{S}^T) \tag{12}$$

where $\boldsymbol{c} \in \mathbb{R}^K$ is a constant vector and $\boldsymbol{S}$ is a constant matrix. Therefore, in this special case, the Sandwich rule yields the exact posterior distribution for the response $\boldsymbol{\eta}$.

3. Implementation

3.1. Computation of adjoint flux

It is generally quite straightforward to modify a deterministic transport solver to also run in adjoint mode. This section reviews the guidelines for this procedure and describes the methodology used in implementing an adjoint solver to CASMO-4.

In CASMO-4, the multi-group criticality equation is solved by the method of characteristics assuming isotropic scattering. Therefore, the following system of equations may be taken as the forward problem:

$$\begin{aligned}&\boldsymbol{\Omega}_m \cdot \nabla \Phi^g(\boldsymbol{r}, \boldsymbol{\Omega}_m) + \Sigma^g \Phi^g(\boldsymbol{r}, \boldsymbol{\Omega}_m)\\ &\quad = \frac{1}{4\pi}\sum_{h=1}^{G} \Sigma_s^{h\to g}\phi^h(\boldsymbol{r}) + \frac{\chi_g}{4\pi k}\sum_{h=1}^{G} \bar{\nu}\Sigma_f^h \phi^h(\boldsymbol{r}), \quad g = 1,\ldots,G.\end{aligned} \tag{13}$$

In Eq. (13) the scalar flux is approximated by the quadrature formula

$$\phi^h(\boldsymbol{r}) = \sum_{m=1}^{M} \omega_m \Phi^h(\boldsymbol{r}, \boldsymbol{\Omega}_m). \tag{14}$$

In order to simulate an infinite lattice, the boundary conditions are often assumed to be reflective, i.e.

$$\boldsymbol{\Phi}(\boldsymbol{r}, \boldsymbol{\Omega}_m, E) = \boldsymbol{\Phi}(\boldsymbol{r}, \boldsymbol{\Omega}'_m, E) \quad \boldsymbol{r} \in \Gamma,\ \boldsymbol{\Omega}_m \cdot \boldsymbol{n} < 0 \tag{15}$$

where $\boldsymbol{\Omega}_m = \boldsymbol{\Omega}'_m - 2(\boldsymbol{n}\cdot\boldsymbol{\Omega}'_m)\,\boldsymbol{n}$ is the reflection direction. The adjoint system corresponding to the inner product defined by Eq. (9) can now be written

$$\begin{aligned}&-\boldsymbol{\Omega}_m \cdot \nabla \Psi^g(\boldsymbol{r}, \boldsymbol{\Omega}_m) + \Sigma^g \Psi^g(\boldsymbol{r}, \boldsymbol{\Omega}_m)\\ &\quad = \frac{1}{4\pi}\sum_{h=1}^{G} \Sigma_s^{g\to h}\psi^h(\boldsymbol{r}) + \frac{\bar{\nu}\Sigma_f^g}{4\pi k}\sum_{h=1}^{G} \chi_h \psi^h(\boldsymbol{r}), \quad g = 1,\ldots,G\end{aligned} \tag{16}$$

with the boundary conditions

$$\boldsymbol{\Psi}(\boldsymbol{r}, \boldsymbol{\Omega}_m, E) = \boldsymbol{\Psi}(\boldsymbol{r}, \boldsymbol{\Omega}'_m, E) \quad \boldsymbol{r} \in \Gamma,\ \boldsymbol{\Omega}_m \cdot \boldsymbol{n} > 0. \tag{17}$$

It is straightforward to check that systems (13) and (16) with their respective boundary conditions satisfy Eq. (4) with respect to the inner product defined by Eq. (9).

When solving the system of Eq. (13) numerically, the eigenvalue and flux are iterated in turns. The iteration step for the flux can typically be written

$$\boldsymbol{A}\boldsymbol{\Phi}^{n+1} = \frac{1}{k^n}\boldsymbol{B}\boldsymbol{\Phi}^n. \tag{18}$$

After solving $\boldsymbol{\Phi}^{n+1}$ from this equation, a new estimate is obtained for the multiplication factor according to

$$k^{n+1} = \frac{\langle \boldsymbol{w}, \boldsymbol{B}\boldsymbol{\Phi}^{n+1}\rangle}{\langle \boldsymbol{w}, \boldsymbol{A}\boldsymbol{\Phi}^{n+1}\rangle} = k^n \frac{\langle \boldsymbol{w}, \boldsymbol{B}\boldsymbol{\Phi}^{n+1}\rangle}{\langle \boldsymbol{w}, \boldsymbol{B}\boldsymbol{\Phi}^{n}\rangle} \tag{19}$$

where $\boldsymbol{w}$ is a weighting function. This approach is also well-suited for solving the adjoint system. In CASMO-4, however, the eigenvalue iteration is based on physical considerations, and therefore it was replaced by the conventional power iteration based on Eq. (19) before adding the adjoint mode to the code.

Solving Eq. (18) forms an essential part of the iteration. By comparing the forward system (13) to the adjoint system (16), it can be seen that the systems are of the same form, but the adjoint system has a different source and it is solved in the opposite direction. This property may be exploited by using the inner iterations solver with a modified input for the adjoint system (Williams, 1986). This can be achieved by performing the following operations before the adjoint calculation:

1. Transpose the scattering matrix
2. Interchange the vectors $\bar{\nu}\boldsymbol{\sigma}_f$ and $\boldsymbol{\chi}$
3. Invert the group indices as follows: $G \leftrightarrow 1$, $(G-1) \leftrightarrow 2, \ldots$

The solution given by the forward solver must then be interpreted so that $\Phi_i^g(\boldsymbol{r}_k, \boldsymbol{\Omega}_m)$ corresponds to $\Psi_i^{G+1-g}(\boldsymbol{r}_k, -\boldsymbol{\Omega}_m)$. Notice that these operations automatically convert the forward boundary conditions to the adjoint boundary conditions. Therefore, only minor modifications are often needed to solve the adjoint flux with a transport code.

The so far described methodology does not ensure that the consistency objectives discussed in Section 2.1 are met. As previously mentioned, the numerical method used in the inner iterations should ideally produce discretized systems that are adjoints with respect to the discretized inner product. When an iteration based on Eqs. (18) and (19) is used, it is guaranteed that both systems converge to the same eigenvalue. Unfortunately, many of the established numerical methods do not enable this type of consistency. For example, the very popular diamond difference method does not guarantee adjointness in curved geometries (Greenspan, 1982). The method of characteristics used in CASMO-4, on the other hand, is not well-suited for this type of formal analysis, since it does not directly provide a discretization scheme that could be used to check if Eq. (4) holds. For these reasons, the inner product of Eq. (9) was approximated as

$$\langle \boldsymbol{\Phi}, \boldsymbol{\Psi}\rangle \approx \sum_{i=1}^{I}\sum_{g=1}^{G}\sum_{m=1}^{M} \omega_m\, V_i\, \overline{\Phi}^{g,i,m}\overline{\Psi}^{g,i,m} \tag{20}$$

where i denotes the mesh index and $\overline{\Phi}^{g,i,m}$ and $\overline{\Psi}^{g,i,m}$ denote the average fluxes. Notice that this discretization can be used with any type of numerical method including multi-group Monte Carlo techniques (Rearden, 2009).

3.2. Computation of sensitivity and uncertainty profiles

After obtaining the adjoint solution, the sensitivities with respect to the multi-group cross-sections and other parameters

of interest can be computed according to Eq. (8). Notice that even after the multi-group approximation, these parameters are still spatial functions and therefore the derivatives in Eq. (8) refer to functional derivatives. After obtaining expressions for all derivatives $\boldsymbol{A}'_\sigma$ and $\boldsymbol{B}'_\sigma$ of interest, the respective sensitivities may be computed simply by applying the discretization scheme of Eq. (9) to Eq. (8).

In order to compute the uncertainties using the Sandwich rule, the sensitivities and covariance matrices need to be based on similar cross-section models. However, as mentioned in Section 1, lattice physics codes such as CASMO, HELIOS, WIMS and DRAGON, have cross-section models different from the one used in the covariance files. More specifically, their cross-section models only contain the total capture and scattering cross-sections, whereas the covariance data is reported for the individual capture and scattering subreactions. This greatly complicates the implementation of uncertainty analysis with both deterministic and statistical methods, since the prerequisite for uncertainty analysis is that the probability distributions for the parameters used in the calculation are known.

Naturally, this difficulty can be overcome by creating new nuclear data libraries and modifying the cross-section model in the code, but this requires extensive work. Another option, suitable for deterministic analysis, is to not use problem-dependent cross-sections in the sensitivity analysis. In this case, the sensitivity coefficients can be computed outside the code based on the forward and adjoint fluxes and any set of cross-sections. This was the idea, for example, behind connecting DRAGON with the sensitivity and uncertainty analysis code SUSD3D After a generalized adjoint mode was implemented to DRAGON (Bidaud et al., 2009).

In this work, this complication was solved by the novel approach of creating a covariance library that is consistent with the cross-section model of CASMO-4. In practice this requires combining the covariance matrices of the individual capture and scattering reactions. Interestingly, this treatment of covariance matrices draws attention to the significance of some basic assumptions made in sensitivity analysis. This approach is explained next by first describing the procedure used to process the covariance matrices to the energy-group structure of CASMO-4, and then considering the methodology for combining the capture and scattering reactions.

3.2.1. Modifying the energy-group structure of covariance matrices

Applying the Sandwich rule requires a covariance library in the same energy-group structure as the sensitivity profiles used in the uncertainty computation. When the starting point is a multi-group covariance library, the matrices can in principle be transformed to another multi-group structure by simple mathematical techniques. The applicability of this approach depends on the differences between the group-structures. In particular, the widths of the energy groups should not be drastically different. In this work, the covariance data was taken from the multi-group covariance library ZZ-SCALE6.0/COVA-44G (NEA Data Bank, 2011) and the code Angelo 2.3 (Kodeli, 2010) was used for transforming the matrices to the energy-group structure used in the sensitivity calculations with CASMO-4.

The transformation procedure in Angelo 2.3 is based on a flat-flux approximation, i.e. no weighting is used in the process. Covariance matrices are treated as correlation matrices and relative standard deviations, whose values are computed separately on the new energy grid. The resampled values on the new grid are computed as lethargy overlap weighted averages. This guarantees that the integrals over the new energy groups remain constant in the resampling process. When the new energy groups extend outside the region spanned by the original energy groups, a complete correlation is assumed with the group from which the extrapolation is carried out (Kodeli and Sartori, 1990).

Because the fission spectrum always satisfies the normalization condition

$$\sum_{g=1}^{G} \chi_g = 1 \tag{21}$$

it follows that the corresponding covariance matrix $\boldsymbol{C}_\chi$ should satisfy the constraint that the sum of the elements on any row of the matrix equals zero, which is also stated in the manual for the ENDF-6 format (Herman and Trkov, 2009). When the energy group structure of $\boldsymbol{C}_\chi$ is modified, there is no guarantee that this constraint is satisfied, which may in turn lead to an erroneously large fission spectrum uncertainty in a criticality calculation (Kodeli et al., 2008). If this zero-sum rule is not too severely violated, there is a suggested correction procedure for the matrix in the ENDF-6 manual.

However, it is often more practical to apply the correction directly to the sensitivity coefficients. In this case the coefficients are called *constrained*. The absolute constrained sensitivities are defined as

$$\boldsymbol{s}_{\text{constr.}} = (\boldsymbol{I} - \boldsymbol{u}\boldsymbol{\chi}^T)\boldsymbol{s}_\chi \tag{22}$$

where $\boldsymbol{I} \in \mathbb{R}^{G\times G}$ is an identity matrix, $\boldsymbol{u} = [1, 1, \ldots, 1]^T$ and vector $\boldsymbol{s}_\chi$ contains the unconstrained sensitivities. In case of a small deviation from the zero-sum rule, applying this correction to the sensitivities is identical to the correction scheme suggested in the ENDF-6 manual. It is easy to see that if the matrix $\boldsymbol{C}_\chi$ already satisfies the zero-sum rule, constraining the sensitivities has no effect on the results (Kodeli et al., 2008). This approach was also applied in this work.

3.2.2. S&U analysis of capture cross-section

Generally, the total capture cross-section is defined as the sum of the individual capture cross-sections (ENDF/MT 102–107). In CASMO-4, however, also the (n,2n) cross-section (ENDF/MT 16) has been added to the capture cross-section with a negative sign in the highest energy group. The expression for a capture cross-section used in the code can therefore be written in matrix form as

$$\boldsymbol{\sigma}_{\text{capt}} = \sum_{\text{MT}=102}^{107} \boldsymbol{\sigma}_{\text{MT}} + \boldsymbol{E}\boldsymbol{\sigma}_{16} = \boldsymbol{S}\boldsymbol{\sigma} \tag{23}$$

where $\boldsymbol{E} \in \mathbb{R}^{G\times G} : E_{11} = 1,\ E_{ij} = 0$ otherwise; $\boldsymbol{S} \in \mathbb{R}^{G\times 7G}$ and the vector $\boldsymbol{\sigma}$ contains the concatenated reaction-specific cross-sections. Since the relationship between $\boldsymbol{\sigma}_{\text{capt}}$ and $\boldsymbol{\sigma}$ is linear, the absolute covariance matrix corresponding to $\boldsymbol{\sigma}_{\text{capt}}$ can be accurately computed with the Sandwich rule:

$$\text{Cov}[\boldsymbol{\sigma}_{\text{capt}}] = \boldsymbol{S}\text{Cov}[\boldsymbol{\sigma}]\boldsymbol{S}^T. \tag{24}$$

Notice that this treatment does not involve any approximation in the Bayesian framework, if all the probability distributions are assumed to be Gaussian, which is a standard practice in nuclear data uncertainty analysis. The corresponding relative covariance matrix can then be easily calculated by dividing the covariance matrix elements C_{ij} by $\sigma_i\sigma_j$, i.e. by dividing the covariance matrix element-wise by the matrix $\boldsymbol{\sigma} \otimes \boldsymbol{\sigma}$. Fig. 1 shows an example of this treatment for the capture reactions of ^{16}O.

After forming the covariance matrices for the capture cross-sections, they can be used in both deterministic and statistical uncertainty analysis. In the deterministic case, the sensitivities with respect to the capture cross-sections can be computed in the usual manner according to Eq. (8). Notice that apart from the (n,2n) reaction, this approach should give results that are consistent with those obtained by computing the sensitivities with respect to the individual capture reactions.

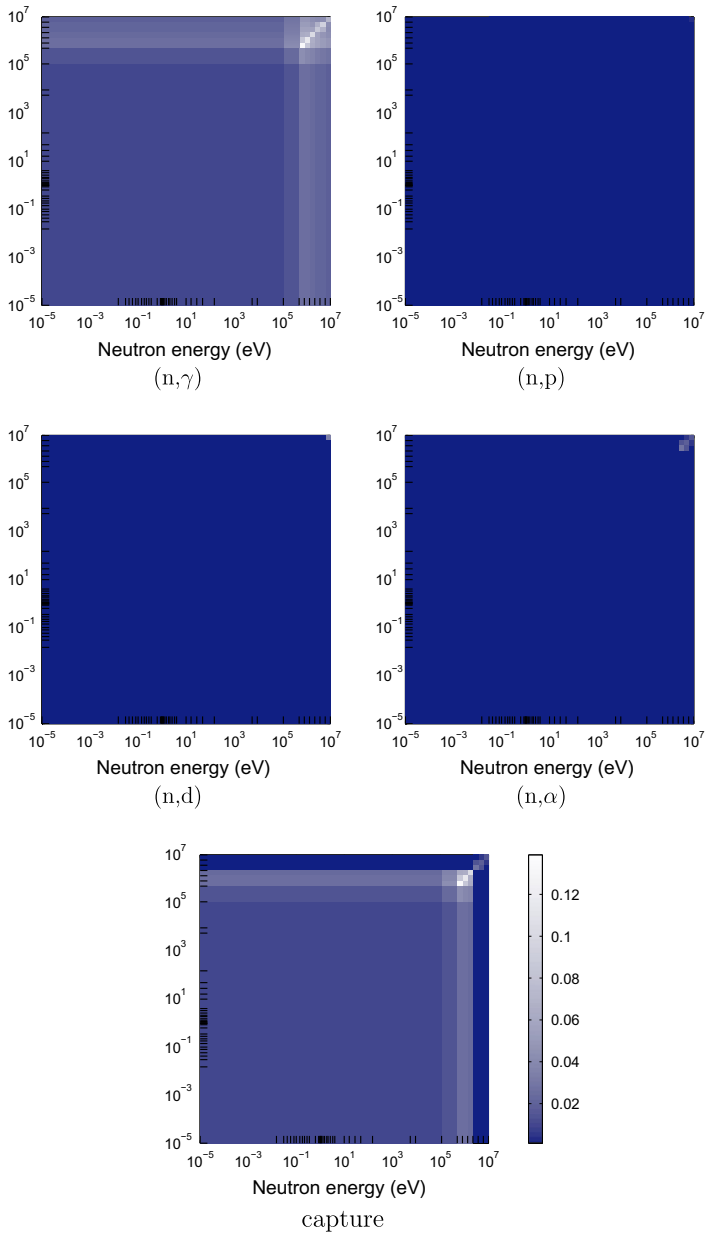

Fig. 1. Covariance matrices corresponding to the individual capture cross-sections and the total capture cross-section of ^{16}O. The covariance matrices in this example are from the SCALE 5.1 covariance library `44groupv6rec` and they have been processed to conform to the energy-group structure of CASMO-4.

3.2.3. S&U analysis of scattering cross-section

Dealing with scattering cross-sections is more complicated. In general, there are no covariance data available for transfer cross-sections $\sigma_x^{h\to g,j}$ but only for $\sigma_x^{g,j}=\sum_{h=1}^{G}\sigma_x^{g\to h,j}$, where x refers to a scattering reaction (e.g. elastic, inelastic) and j is the nuclide index. However, because of the scattering source term in Eq. (13), the derivative with respect to $\sigma_x{}^{g,j}$ is not mathematically well-defined without additional constraints. Typically it is assumed that the probabilities of transfers to various groups are fixed, i.e.

$$\sigma_x^{g\to h,j}=\sigma_x^{g,j}p_x^{g\to h,j} \tag{25}$$

where $p_x^{g\to h}$ is the proportion of neutrons scattered from energy group g to energy group h, which is assumed to remain fixed even if the scattering cross-section $\sigma_x^{g,j}$ is perturbed (Weisbin et al., 1976). Based on this assumption, the scattering source in Eq. (13) can be written

$$S^g=\frac{1}{4\pi}\sum_{h=1}^{G}\Sigma_s^{h\to g}\phi^h=\frac{1}{4\pi}\sum_x\sum_j N^j\sum_{h=1}^{G}\sigma_x^{h,j}p_x^{h\to g}\phi^h \tag{26}$$

where the summations over x include all scattering reactions. After this assumption, the derivative with respect to $\sigma_x^{g,j}$ is well-defined and can be computed as usual. It is straightforward to show that this approach corresponds to computing the sensitivity coefficients with respect to the transfer cross-sections $\sigma_x^{g\to h,j}$ and summing them over h.

Unfortunately, the sensitivity with respect to the total scattering cross-section $\sigma_s^j = \sum_x \sigma_x^j$ is not well-defined if the constraint (25) is enforced. Instead, fixed transfer rates must be assumed for the total scattering cross-section, which is clearly a stricter assumption than Eq. (25). Mathematically, this approach corresponds to computing the relative sensitivities with respect to the individual scattering reactions and adding them up. It should be emphasized that because the sensitivity coefficients corresponding to the total and individual scattering reactions are based on inconsistent assumptions, the chain rule of derivation is not applicable to these sensitivities. Therefore, it is not possible to perform S&U analysis with respect to the total scattering cross-section in a manner that would produce results consistent with the approach where the sensitivities are computed with respect to the individual scattering reactions. Nonetheless, the covariance matrices for the individual scattering reactions can be combined in a similar manner as the capture reactions. However, it should be kept in mind that both these approaches are in fact based on simplifications of the true problem and are likely to underestimate the uncertainty related to scattering cross-sections.

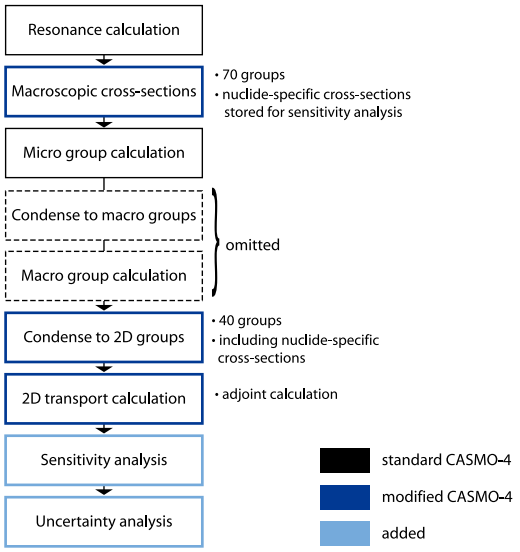

Fig. 2. Outline of the CASMO-4 calculations.

4. Results

The calculation framework was applied to two test cases from the UAM benchmark Exercise 1.1 (Ivanov et al., 2011). The first test problem represents TMI-1 under hot zero power conditions and the second one is a GEN-III MOX pin-cell test case with 9.8% of plutonium. These test problems were chosen to be presented here because they can also be modeled in one dimension and therefore the results can be compared against TSUNAMI-1D (Rearden, 2009) In addition, based on experiments with other pin-cell test cases included in the UAM benchmark specification, the chosen test cases are highly representative and characteristic in terms of comparison to TSUNAMI-1D. The developed CASMO-4 calculation system is naturally also well-suited for fuel assembly calculations, but because the S&U results for pin-cell and lattice problems are essentially very similar, only the 1D results were chosen to be presented here due to the possibility to validate them by comparison to TSUNAMI-1D.

The outline of the CASMO-4 calculations is presented in Fig. 2. The calculations were carried out using the cross-section library E60200 that contains 70 energy groups and is based on ENDF/B-VI data (Rhodes, 2005). The covariance data were taken from the SCALE 6 library ZZ-SCALE6.0/COVA-44G (NEA Data Bank, 2011), which is the most comprehensive covariance library available at the time of writing. The library is based on true evaluations from various sources (including ENDF/B-VII, ENDF/B-VI, JENDL-3.1) and approximate covariance data. The covariances in the library are given in relative terms and therefore the library is intended to be used with all cross-section libraries including the ones that are inconsistent with the evaluations. While this is not strictly correct, it is considered to be acceptable due to the scarcity of comprehensive covariance data among other reasons (Williams et al., 2009).

The list of the nuclides present in these test cases can be found in the benchmark specification (Ivanov et al., 2011). Apart from the isotopes of Cr and Fe, all available covariance data in the library was included in the uncertainty computations. The reason for excluding these isotopes is that the employed cross-section library E60200 does not contain isotope-specific cross-sections for these materials. For this same reason, the given nuclide composition could not be specified for the zircalloy-4 cladding in the MOX test case, but was instead replaced by the zircalloy-4 composition given for the PWR test case.

The covariance matrices from ZZ-SCALE6.0/COVA-44G were processed for compatibility with CASMO-4. The sensitivity profiles in CASMO-4 were computed using the 40-group structure option that was the closest match to the amount of groups in the covariance data and, as mentioned in Section 3.2, the code Angelo 2.3 (Kodeli, 2010) was used to process the covariance matrices to this energy-group structure. Next, the nuclear data processing code NJOY (MacFarlane and Muir, 1994) was used to transform the 40-group covariance files to the BOXR format. Auxiliary FORTRAN programs were written for combining the covariance matrices according to the principles described in Section 3.2.

The TSUNAMI-1D calculations were performed using the ENDF/B-VI-based cross-section library V6-238 containing 238 energy groups. The module CENTRM was used for self-shielding. Implicit sensitivity analysis (Williams et al., 2001) was omitted in the TSUNAMI calculations in order to facilitate the comparison of the results given by CASMO-4 and TSUNAMI-1D. The boundary conditions for the 1D models were assumed to be white, whereas reflective boundary conditions were used for the 2D-calculations with CASMO-4.

4.1. PWR pin-cell

A summary of the numerical results for the PWR pin-cell representing TMI-1 is presented in Table 1. The relative difference between the multiplication factors computed with CASMO-4 and TSUNAMI-1D is 0.1763% in the forward case and 0.1768% in the

Table 1
Summary of the results for the PWR pin-cell test case.

Code	Forward k	Adjoint k	Rel. uncertainty, $\frac{\Delta k}{k}$ (%)
CASMO-4	1.421684	1.421686	0.5120
TSUNAMI-1D	1.419177	1.419172	0.4888

Table 2
The ten most significant sources of uncertainty in the PWR pin-cell test case and the corresponding energy-and region-integrated relative sensitivity coefficients. The sensitivity coefficients with respect to the parameter χ have been constrained according to Eq. (22).

Nuclide	Parameter pair	Sensitivity, CASMO	Sensitivity, TSUNAMI	Contribution to $\frac{\Delta k}{k}$ (%), CASMO	Contribution to $\frac{\Delta k}{k}$ (%), TSUNAMI
^{238}U	σ_c, σ_c	-2.609×10^{-1}	-2.219×10^{-1}	3.253×10^{-1}	2.836×10^{-1}
^{235}U	$\bar{\nu}$, $\bar{\nu}$	9.379×10^{-1}	9.392×10^{-1}	2.641×10^{-1}	2.643×10^{-1}
^{235}U	σ_c, σ_c	-1.549×10^{-1}	-1.539×10^{-1}	2.225×10^{-1}	2.098×10^{-1}
^{235}U	σ_c, σ_f			1.087×10^{-1}	1.039×10^{-1}
^{235}U	χ, χ	2.166×10^{-6}	-3.581×10^{-9}	8.345×10^{-2}	8.774×10^{-2}
^{235}U	σ_f, σ_f	2.559×10^{-1}	2.538×10^{-1}	7.838×10^{-2}	7.652×10^{-2}
^{238}U	$\bar{\nu}$, $\bar{\nu}$	6.210×10^{-2}	6.076×10^{-2}	7.225×10^{-2}	7.122×10^{-2}
Zr	σ_c, σ_c	-9.403×10^{-3}	-8.315×10^{-3}	6.195×10^{-2}	5.070×10^{-2}
^{238}U	σ_s, σ_s	-5.858×10^{-3}	-6.178×10^{-3}	3.941×10^{-2}	1.058×10^{-1}
^{1}H	σ_s, σ_s	1.952×10^{-1}	1.866×10^{-1}	2.739×10^{-2}	2.581×10^{-2}

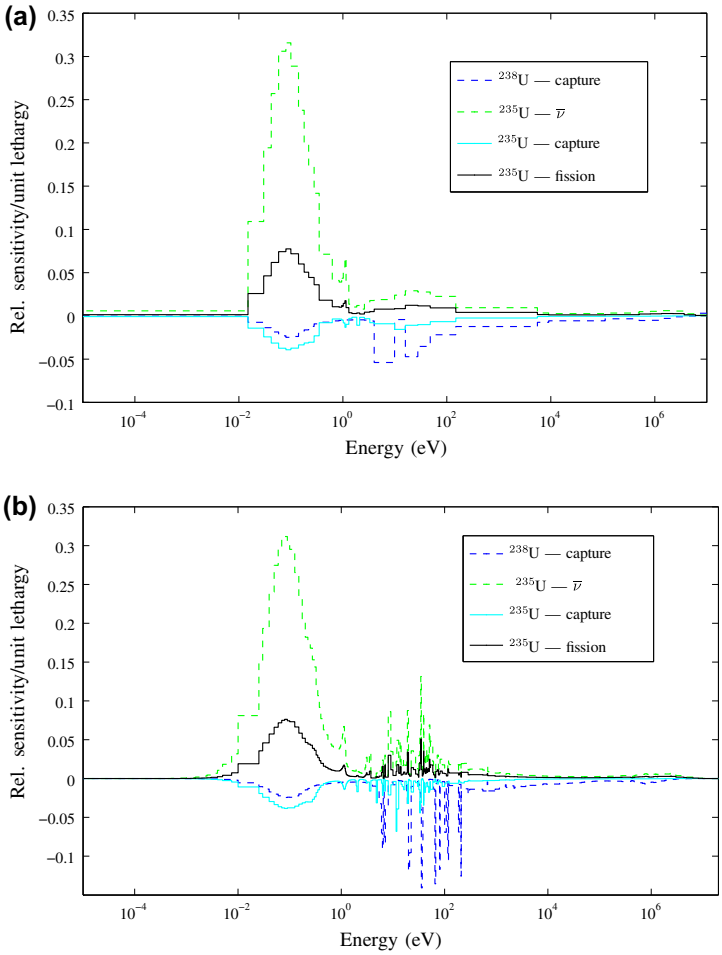

Fig. 3. Sensitivity profiles for the PWR pin-cell test case computed with (a) CASMO-4 and (b) TSUNAMI-1D.

adjoint case. For the total uncertainty, on the other hand, the value given by CASMO is 4.531% greater. Table 2 shows the ten most significant sources of uncertainty together with the corresponding energy-and region-integrated sensitivity coefficients. It can be seen from this Table that in both calculations the main contribution to the total uncertainty comes from the capture cross-section of ^{238}U, which is characteristic of LWR calculations with UOX. Also, the difference in the total uncertainties is mainly attributable to the fact that the CASMO calculation yields greater sensitivities for this cross-section. This appears to originate from the differences in the cross-section libraries. In particular, the cross-section library `E60200` used in the CASMO calculation has not been

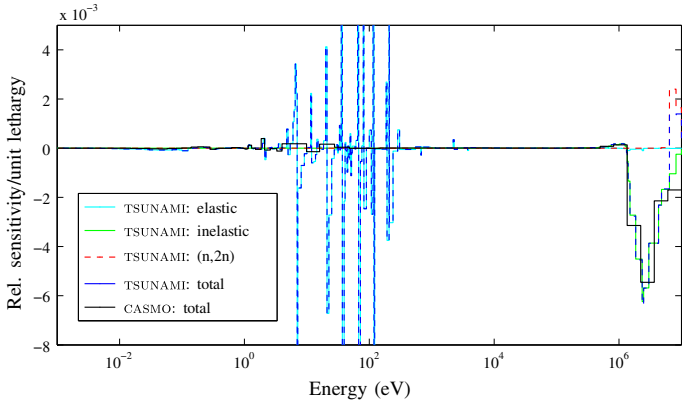

Fig. 4. Closeup of scattering sensitivity profiles of ^{238}U in the PWR pin-cell test case.

Table 3
Summary of the results for the MOX pin-cell test case.

Code	Forward k	Adjoint k	Rel. uncertainty, $\frac{\Delta k}{k}$ (%)
CASMO-4	1.09964	1.09964	0.9156
TSUNAMI-1D	1.09493	1.09495	0.9338

reduced in terms of the ^{238}U resonance integral, which is known to be overestimated in the ENDF/B-VI data (Rhodes, 2005). The ^{238}U capture sensitivity profile and some other sensitivity plots of interest are shown in Fig. 3.

From Fig. 3 and Table 2, it can be seen that, overall, the results between CASMO-4 and TSUNAMI-1D are in good accordance. It should be noticed that the ^{235}U fission spectrum sensitivities in Table 2 have been constrained according to Eq. (22). Therefore these values should theoretically vanish and the non-zero values result from round-off errors. In particular, the single-precision arithmetics used in CASMO-4 produces a greater deviation. Other than this, the only notable difference in the uncertainty results occurs for the scattering cross-section of ^{238}U, which is due to the inconsistency in defining the sensitivities, as discussed in Section 3.2. The corresponding scattering sensitivities are plotted in Fig. 4. Notice that in some energy groups the reaction-specific scattering sensitivities have opposite signs, which is in clear contradiction with the chain rule of derivation.

4.2. MOX pin-cell

The results for the MOX pin-cell test case are summarized in Table 3. In the forward case, the relative difference between the multiplication factors computed with CASMO-4 and TSUNAMI-1D is 0.4283%. In the adjoint case, the respective relative difference is 0.4265%. For this test case, TSUNAMI-1D gives a greater uncertainty with a relative difference of 1.988%. The ten covariance matrices that contributed the most to the multiplication factor uncertainty are shown in Table 4 together with the corresponding energy-and region-integrated sensitivity coefficients. In addition, the sensitivity profiles of the five most significant sources of uncertainty are plotted in Figs. 5 and 6.

It can be seen from Table 4 that the main contribution to the total uncertainty in both CASMO-4 and TSUNAMI-1D calculations comes from the parameter $\bar{\nu}$ of ^{239}Pu. The capture cross-section of ^{238}U is another significant contributor to the total uncertainty. Similarly to the PWR pin-cell calculation, CASMO-4 yields a greater sensitivity for this cross-section, causing a greater contribution to the total uncertainty. The most notable difference in the results occurs for the capture reaction of ^{242}Pu, for which CASMO-4 yields a significantly greater sensitivity, and consequently a greater uncertainty. The respective sensitivity profiles, as computed with both codes, are shown in Fig. 6. Although the integrated value of TSUNAMI-1D is about 33% smaller, it can be seen from this figure that qualitatively the sensitivity profiles are very similar. The cause of the inconsistency in the sensitivities is not evident, but it may be related to differences in both the cross-section libraries as well as the self-shielding treatment of ^{242}Pu. As an example of the latter's effect on the sensitivity, computing the same test case using SCALE 5.1 with the module NITAWL for self-shielding, resulted in a 6.493% greater sensitivity value than the one given by SCALE 6 with the module CENTRM.

Another relevant difference in the results occurs again for the scattering cross-section of ^{238}U, which is due to the discussed inconsistency in defining the sensitivities. It is noteworthy that

Table 4
The ten most significant sources of uncertainty in the MOX pin-cell test case and the corresponding energy-and region-integrated relative sensitivity coefficients. The sensitivity coefficients with respect to the parameter χ have been constrained according to Eq. (22).

Nuclide	Parameter pair	Sensitivity, CASMO	Sensitivity, TSUNAMI	Contribution to $\frac{\Delta k}{k}$ (%), CASMO	Contribution to $\frac{\Delta k}{k}$ (%), TSUNAMI
^{239}Pu	$\bar{\nu},\bar{\nu}$	7.212×10^{-1}	7.251×10^{-1}	7.273×10^{-1}	7.311×10^{-1}
^{238}U	σ_c,σ_c	-1.963×10^{-1}	-1.611×10^{-1}	2.457×10^{-1}	2.078×10^{-1}
^{242}Pu	σ_c,σ_c	-2.339×10^{-2}	-1.557×10^{-2}	2.339×10^{-1}	1.359×10^{-1}
^{239}Pu	σ_f,σ_f	3.619×10^{-1}	3.596×10^{-1}	2.236×10^{-1}	2.204×10^{-1}
^{239}Pu	σ_c,σ_c	-1.974×10^{-1}	-2.004×10^{-1}	1.960×10^{-1}	1.928×10^{-1}
^{239}Pu	χ,χ	-5.462×10^{-7}	5.672×10^{-9}	1.640×10^{-1}	1.997×10^{-1}
^{239}Pu	σ_c,σ_f			1.555×10^{-1}	1.582×10^{-1}
^{240}Pu	σ_c,σ_c	-1.104×10^{-1}	-1.052×10^{-1}	1.549×10^{-1}	1.459×10^{-1}
^{238}U	σ_s,σ_s	-1.591×10^{-2}	-1.494×10^{-2}	9.952×10^{-2}	2.721×10^{-1}
^{238}U	$\bar{\nu},\bar{\nu}$	8.333×10^{-2}	8.165×10^{-2}	9.668×10^{-2}	9.534×10^{-2}

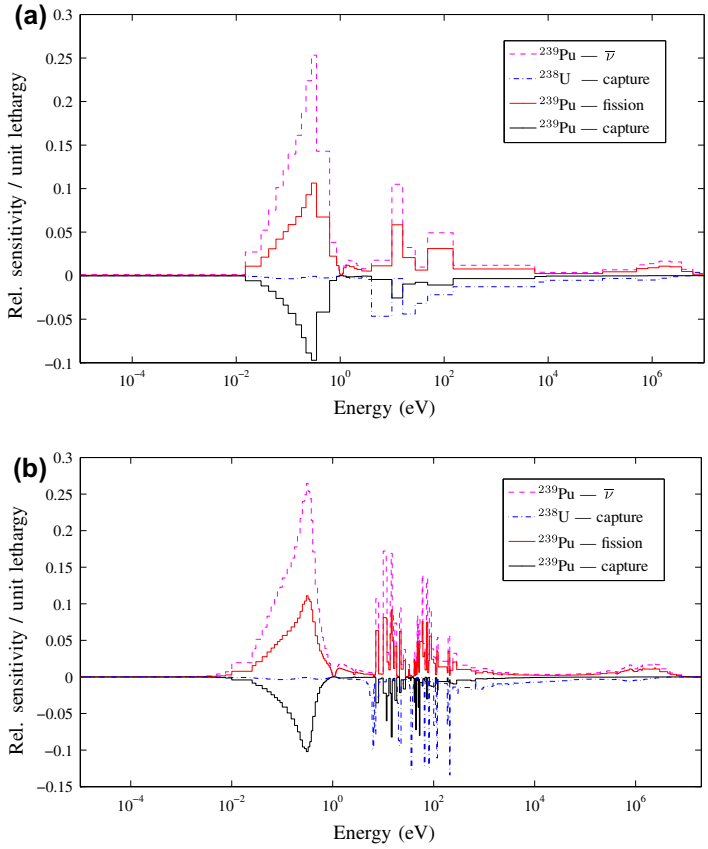

Fig. 5. Sensitivity profiles for the MOX pin-cell test case computed with (a) CASMO-4 and (b) TSUNAMI-1D.

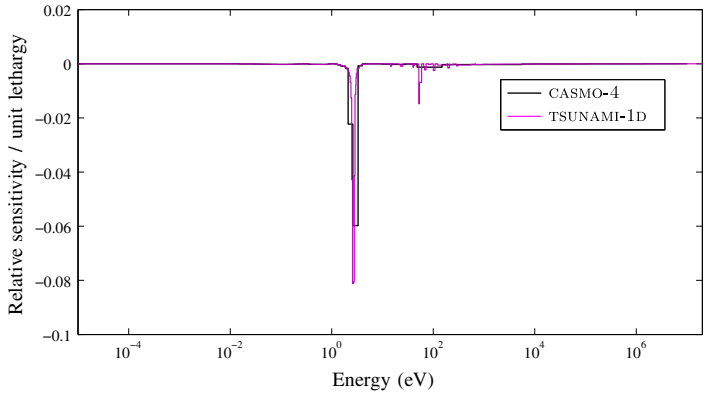

Fig. 6. Sensitivity profiles for the total capture cross-section of ^{242}Pu in the MOX pin-cell test case.

in this test case this inconsistency has a more pronounced effect on the overall results compared to the PWR test case. This is due to the harder neutron spectrum of MOX fuel, which increases the sensitivity of the multiplication factor to the inelastic scattering of ^{238}U. In the TSUNAMI-1D computation, this parameter is actually the second most significant source of uncertainty, contributing 2.703×10^{-1}% to the total uncertainty, whereas the contribution from the respective total scattering is only 9.952×10^{-2}% in the

CASMO-4 calculation. The fact that TSUNAMI-1D gives a greater total uncertainty for the multiplication factor is mainly attributable to this.

5. Summary and conclusions

The motivation of the presented work has been participating in the UAM benchmark, whose first stage aims at propagating the uncertainty related to neutron cross-sections through a reactor physics calculation. CASMO-4 was chosen as the development platform due to its role as the standard code at VTT Technical Research Centre of Finland.

As a first development, classical perturbation theory has been implemented to CASMO-4, which has enabled performing sensitivity analysis of the multiplication factor. In the process of modifying CASMO-4, a problem was faced due to the incompatibility of the cross-section models between the covariance libraries and the code itself because in CASMO-4, the individual capture and scattering cross-sections have been combined into total capture and scattering cross-sections. This issue affects all similar reactor physics codes irrespective of the method used for S&U analysis, whether deterministic or statistical. As a solution to this discrepancy, a technique for combining the covariance matrices of the individual subreactions and computing the sensitivities with respect to the combined reactions was devised and applied with success. The technique accurately combines the capture reactions in a consistent manner, but the combination of the scattering reactions resulted in some systematic differences in comparison to TSUNAMI-1D. This observation drew attention to the basic assumptions that must be made in dealing with scattering reactions. The observed differences were eventually explained by the incompatible constraints in the calculation process, which in turn caused the chain rule of derivation not being applicable.

Inspired by the experiences gained in the process, the theoretical background of S&U was reviewed and presented in detail, and practical considerations were also discussed to benefit readers interested in implementing perturbation analysis capabilities to reactor physics codes. Numerical results were presented for fuel pin-cell test problems representing a PWR and a GEN-III core with MOX fuel, and the results were compared against TSUNAMI-1D. The comparison supported the observations made on the developed methodology, i.e. the results were consistent except for scattering reactions, where systematic differences appeared in cases where multiple scattering reactions were present.

At the time of writing, the work in the benchmark has continued by implementing generalized perturbation theory to CASMO-4, which enables performing S&U analysis on other responses in addition to the multiplication factor. Future work includes the refinement and validation of the implementation. When this has been accomplished, the developed S&U calculation system enables producing uncertainty estimates for homogenized assembly data, which can in turn be propagated to coupled neutronics/thermal hydraulics calculations.

Acknowledgment

The author wishes to express her gratitude to Dr. Ivan Kodeli (Institute Jozef Stefan, Slovenia) for his invaluable help regarding the code Angelo 2.3 and the covariance libraries used in this work.

References

Bidaud, A., Marleau, G., Noblat, E., 2009. Nuclear data uncertainty analysis using the coupling of DRAGON with SUSD3D. In: International Conference on Mathematics, Computational Methods & Reactor Physics (M& C 2009).

Cacuci, D.G., 2003. Sensitivity and Uncertainty Analysis, vol. 1. Chapman & Hall/CRC.

Carlson, B.G., Lathrop, K.D., 1968. Transport theory—the method of discrete ordinates. In: Greenspan, H., Kelber, C.N., Okrent, D. (Eds.), Computing Methods in Reactor Physics. Gordon and Breach Science Publishers.

DeHart, M.D., 2009. NEWT: a new transport algorithm for two-dimensional discrete ordinates analysis in non-orthogonal geometries. In: SCALE: A Modular Code System for Performing Standardized Computer Analyses for Licencing Evaluation, Version 6. No. ORNL/TM-2005/39. Oak Ridge National Library/US Nuclear Regulatory Commission.

Greenspan, E., 1982. Sensitivity functions for uncertainty analysis. In: Lewins, J., Becker, M. (Eds.), Advances in Nuclear Science and Technology, Vol. 14. Plenum Press, New York and London.

HELIOS, 2000. Methods, Studsvik Scandpower.

Herman, M., Trkov, A. (Eds.), 2009. ENDF-6 formats manual: data formats and procedures for the evaluated nuclear data file ENDF/B-VI and ENDF/B-VII. Document ENDF-102. Report BNL-90365-2009. Brookhaven National Laboratory.

Ivanov, K., Avramova, M., Kamerow, S., Kodeli, I., Sartori, E., 2011. Benchmark for Uncertainty Analysis in Modeling (UAM) for Design, Operation, and Safety Analysis of LWRs. vol. I: Specification and Support Data for the Neutronics Cases (Phase I). Version 2.0 (NEA/NSC/DOC(2011)).

Kodeli, I., Sartori, E., 1990. Neutron cross-section covariance data in multigroup form and procedure for interpolation to users' group structures for uncertainty analysis applications. In: International Conference on the Physics of Reactors: Operation, Design and Computation (PHYSOR 1990).

Kodeli, I., Ishikawa, M., Aliberti, G., 2008. Evaluation of fission spectra uncertainty and their propagation, Appendix C In: OECD/NEA WPEC Subgroup 26 final report: Uncertainty and target accuracy assessment for innovative systems using recent covariance data evaluations. OECD.

Kodeli, I., 2010. Manual for ANGELO2 and LAMBDA Codes. NEA-1798/03 Package.

Lewis, E.E., Miller Jr., W.F., 1984. Computational Methods of Neutron Transport. John Wiley & Sons.

MacFarlane, R.E., Muir, D.W., 1994. The NJOY Nuclear Data Processing System, Version 91, Manual. Los Alamos National Laboratory (LA-12740-M).

Marleau, G., Hébert, A., Roy, R., 2009. A User Guide for DRAGON Version 4. (IGE294) <http://www.polymtl.ca/nucleaire/DRAGON/>.

NEA Data Bank, 2011. ZZ-SCALE6.0/COVA-44G, a 44-group cross section covariance matrix library retrieved from the SCALE 6.0 package. (USCD1236/03).

Rearden, B.T., 2009. TSUNAMI-1D: Control module for one-dimensional cross-section sensitivity and uncertainty analysis for criticality. In: SCALE: A Modular Code System for Performing Standardized Computer Analyses for Licencing Evaluation, Version 6. No. ORNL/TM-2005/39. Oak Ridge National Library/US Nuclear Regulatory Commission.

Rearden, B.T., 2009. TSUNAMI-3D: control module for three-dimensional cross-section sensitivity and uncertainty analysis for criticality. In: SCALE: A Modular Code System for Performing Standardized Computer Analyses for Licencing Evaluation, Version 6. No. ORNL/TM-2005/39. Oak Ridge National Library/US Nuclear Regulatory Commission.

Rhodes, J., Edenius, M., 2001. CASMO-4, a fuel assembly burnup program, users manual. Studsvik of America (SSP-01/400 Rev 4, proprietary).

Rhodes, J., 2005. JEF 2.2 and ENDF/B-VI 70 group neutron data libraries. Studsvik Scandpower (SSP-04/454 Rev 2, proprietary).

Weisbin, C.R., et al., 1976. Application of FORSS sensitivity and uncertainty methodology to fast reactor benchmark analysis. Tech. Rep. (ORNL/TM-5563).

Wieselquist, W.A., Vasiliev, A., Ferroukhi, H., 2011. Towards an uncertainty quantification methodology with casmo-5. In: The International Conference on Mathematics and Computational Methods applied to Nuclear Science and Engineering (M& C 2011).

Williams, M.L., 1986. Perturbation theory for nuclear reactor analysis. In: Ronen, Y. (Ed.), CRC Handbook of Nuclear Reactors Calculations, vol. 3. CRC Press.

Williams, M.L., Broadhead, B.L., Parks, C.V., 2001. Eigenvalue sensitivity theory for resonance-shielded cross sections. Nuclear Science and Engineering 138, 177–191.

Williams, M.L., Wiarda, D., Arbanas, G., Broadhead, B.L., 2009. Scale nuclear data covariance library. In: SCALE: A Modular Code System for Performing Standardized Computer Analyses for Licencing Evaluation, Version 6. No. ORNL/TM-2005/39. Oak Ridge National Library/U.S. Nuclear Regulatory Commission.

WIMS9A, 2005. New Features, A Guide to the New Features of WIMS Version 9A <http://www.sercoassurance.com/answers/>.

PUBLICATION VI

Perturbation-theory-based sensitivity and uncertainty analysis with CASMO-4

In: Science and Technology of Nuclear Installations, **2012**, Article ID 157029.

Hindawi Publishing Corporation
Science and Technology of Nuclear Installations
Volume 2012, Article ID 157029, 11 pages
doi:10.1155/2012/157029

Research Article

Perturbation-Theory-Based Sensitivity and Uncertainty Analysis with CASMO-4

Maria Pusa

VTT Technical Research Centre of Finland, P.O. Box 1000, VTT 02044, Finland

Correspondence should be addressed to Maria Pusa, maria.pusa@vtt.fi

Received 25 June 2012; Accepted 5 October 2012

Academic Editor: Kostadin Ivanov

The topic of this paper is the development of sensitivity and uncertainty analysis capability to the reactor physics code CASMO-4 in the context of the UAM (Uncertainty Analysis in Best-Estimate Modelling for Design, Operation, and Safety Analysis of LWRs) benchmark. The sensitivity analysis implementation is based on generalized perturbation theory, which enables computing the sensitivity profiles of reaction rate ratios efficiently by solving one generalized adjoint system for each response. Both the theoretical background and the practical guidelines for modifying a deterministic transport code to compute the generalized adjoint solutions and sensitivity coefficients are reviewed. The implementation to CASMO-4 is described in detail. The developed uncertainty analysis methodology is deterministic, meaning that the uncertainties are computed based on the sensitivity profiles and covariance matrices for the uncertain nuclear data parameters. The main conclusions related to the approach used for creating a covariance library compatible with the cross-section libraries of CASMO-4 are presented. Numerical results are given for a lattice physics test problem representing a BWR, and the results are compared to the TSUNAMI-2D sequence in SCALE 6.1.

1. Introduction

The topic of this paper is the development of sensitivity and uncertainty analysis capability to the reactor physics code CASMO-4 [1] in the context of the UAM (Uncertainty Analysis in Best-Estimate Modelling for Design, Operation and Safety Analysis of LWRs) benchmark [2]. At VTT, CASMO-4 is the standard tool for lattice physics calculations, and therefore it was a natural choice as the development platform for a sensitivity and uncertainty calculation system for the pin cell and fuel assembly exercises in the benchmark.

Sensitivities with respect to uncertain parameters can be computed efficiently by utilizing the adjoint system of the criticality equation. The propagated parameter uncertainty can then be calculated deterministically by the Sandwich rule by combining the sensitivity profiles with the covariance matrices of the parameters. As a first step, classical perturbation theory (CPT) was implemented to CASMO-4 to enable the computation of critical eigenvalue sensitivities with respect to nuclear data parameters. In this context, a methodology was devised for processing the covariance matrices from SCALE 6 [3] to become compatible with the cross-section libraries of CASMO-4 to enable uncertainty analysis. This work has been reported in detail in [4]. Recently, generalized perturbation theory (GPT) has been added to the code as a new feature. This enables performing sensitivity analysis for responses that can be presented as reaction rate ratios. In this framework, one generalized adjoint system needs to be solved for each response, after which the response sensitivity profiles for all parameters of interest can be computed in an efficient manner.

This paper is organized as follows. Section 2 reviews the theoretical background for sensitivity and uncertainty analysis based on generalized perturbation theory, and Section 3 focuses on the implementation to CASMO-4. In Section 3.1, the computation of generalized adjoint solutions is considered and practical guidelines are presented for modifying a deterministic transport code to solve the adjoint problems needed in sensitivity analysis. Section 3.2 concerns the computation of sensitivity and uncertainty profiles. Finally, in Section 4, numerical results are presented for a lattice physics test problem representing a BWR, and they are compared to the TSUNAMI-2D sequence in SCALE 6.1.

2. Theoretical Background

The purpose of sensitivity analysis is to study how sensitive a mathematical model is to perturbations in its uncertain parameters. The target of uncertainty analysis is to estimate how the uncertainty in these parameters is propagated to a response dependent on the mathematical model under consideration. In this work the mathematical model is the neutron transport eigenvalue problem, which can be written in operator form as

$$\mathbf{A}\boldsymbol{\Phi} = \frac{1}{k}\mathbf{B}\boldsymbol{\Phi}, \tag{1}$$

where $\boldsymbol{\Phi} \in H_\Phi$ is the neutron flux, H_Φ is a Hilbert space, and k is the multiplication factor. The uncertain parameters consist of nuclear data parameters and they are denoted by the vector $\boldsymbol{\sigma} \in E_\sigma$. It should be noted that both the continuous-energy criticality equation and the various systems derived from it in numerical computations can be written in the form of (1).

2.1. Sensitivity Analysis. The object of local sensitivity analysis is to determine how the response R depends on the uncertain parameters in the vicinity of their best-estimate values. In this work, the responses under consideration include homogenized assembly parameters and the multiplication factor, whereas the uncertain parameters are neutron cross-sections. When considering the continuous-energy eigenvalue problem, the cross-sections are functions of energy and location, and the appropriate derivative is the functional directional derivative called the Gâteaux variation [5]. It follows that the sensitivity of R with respect to the perturbation $\mathbf{h} = [\delta\boldsymbol{\Phi}, \delta\boldsymbol{\sigma}] \in D = H_\Phi \times E_\sigma$ at the point $\hat{\mathbf{e}} = [\hat{\boldsymbol{\Phi}}, \hat{\boldsymbol{\sigma}}] \in D$ may be defined as

$$\delta R(\hat{\mathbf{e}}; \mathbf{h}) = \lim_{t \to 0} \frac{R(\hat{\mathbf{e}} + t\mathbf{h}) - R(\hat{\mathbf{e}})}{t}. \tag{2}$$

When the parameters $\boldsymbol{\sigma}$ are perturbed, also the solution $\boldsymbol{\Phi}$ is affected and therefore the computation of the sensitivity $\delta R(\hat{\mathbf{e}}; \mathbf{h})$ requires that the perturbation $\delta\boldsymbol{\Phi}$ is known. In principle, $\delta\boldsymbol{\Phi}$ can be computed to first order from the following *forward sensitivity system*:

$$\begin{aligned}\delta\mathbf{A}(\hat{\mathbf{e}}; \mathbf{h}) &= -\frac{1}{k^2}\delta k(\hat{\mathbf{e}}; \mathbf{h})\mathbf{B}\boldsymbol{\Phi} + \frac{1}{k}\delta\mathbf{B}(\hat{\mathbf{e}}; \mathbf{h}) \\ \Longleftrightarrow\ \mathbf{A}'_\sigma(\hat{\mathbf{e}})\delta\boldsymbol{\sigma} + \mathbf{A}(\hat{\mathbf{e}})\delta\boldsymbol{\Phi} &= -\frac{1}{k^2}\delta k(\hat{\mathbf{e}}; \mathbf{h})\mathbf{B}\boldsymbol{\Phi} \\ &\quad + \frac{1}{k}\mathbf{B}'_\sigma(\hat{\mathbf{e}})\delta\boldsymbol{\sigma} + \frac{1}{k}\mathbf{B}(\hat{\mathbf{e}})\delta\boldsymbol{\Phi},\end{aligned} \tag{3}$$

which can be derived by taking the Gâteaux variation of system (1) with respect to a perturbation $\mathbf{h}$ on both sides. However, when computing several sensitivities, this approach would require the repetitive solving of (3).

Fortunately, the sensitivities can be computed more efficiently by exploiting the adjoint of (1), which is defined as the system that satisfies the following relation: (In some cases the adjoint relation needs to be written in the form $\langle \mathbf{A}\boldsymbol{\Phi} + (1/k)\mathbf{B}\boldsymbol{\Phi}, \boldsymbol{\Psi}\rangle = \langle \Phi, \mathbf{A}^*\boldsymbol{\Psi} + (1/k)\mathbf{B}^*\boldsymbol{\Psi}\rangle + [\mathbf{P}(\boldsymbol{\Psi}, \boldsymbol{\Phi})]_{\mathbf{x}\in\partial\Omega}$, where $[\mathbf{P}(\boldsymbol{\Psi}, \boldsymbol{\Phi})]_{\mathbf{x}\in\partial\Omega}$ is a bilinear form associated with the system. We will only consider cases where it is straightforward to force this term to vanish.)

$$\left\langle \mathbf{A}\boldsymbol{\Phi} - \frac{1}{k}\mathbf{B}\boldsymbol{\Phi}, \boldsymbol{\Psi} \right\rangle = \left\langle \boldsymbol{\Phi}, \mathbf{A}^*\boldsymbol{\Psi} - \frac{1}{k}\mathbf{B}^*\boldsymbol{\Psi} \right\rangle, \tag{4}$$

where the brackets $\langle \cdot, \cdot \rangle$ denote an inner product. When considering the continuous-energy criticality equation, it is customary to employ the L^2 inner product [6, 7]. The solution to the adjoint problem

$$\left(\mathbf{A}^* - \frac{1}{k}\mathbf{B}^*\right)\boldsymbol{\Psi} = 0 \tag{5}$$

is called the *fundamental adjoint*. Physically, the solution to this system can be interpreted to represent the average contribution, that is, importance of a neutron to the multiplication factor. Interestingly, the adjoint system of (5) can be derived solely based on this physical interpretation [8]. Like the neutron flux, the fundamental adjoint has an arbitrary normalization, and the concept of importance should be understood in relative terms. Therefore, the value $\boldsymbol{\Psi}(\mathbf{r}, \boldsymbol{\Omega}, E)$ represents the importance of a neutron located at the point $[\mathbf{r}, \boldsymbol{\Omega}, E]$ compared to the importance of neutrons elsewhere in the phase space [9]. Based on this physical reasoning, it can be deduced that the fundamental adjoint must always be nonnegative.

By utilizing (4) and (5), it is straightforward to obtain the following expression for the relative sensitivity of the multiplication factor with respect to a perturbation $\delta\boldsymbol{\sigma}$ (For derivation, see for example, [4, 10]):

$$\frac{\delta k(\hat{\mathbf{e}}; \mathbf{h})}{k} = -\frac{\langle (\mathbf{A}'_\sigma(\hat{\mathbf{e}}) - (1/k)\mathbf{B}'_\sigma(\hat{\mathbf{e}}))\delta\boldsymbol{\sigma}, \boldsymbol{\Psi}\rangle}{\langle (1/k)\mathbf{B}\boldsymbol{\Phi}, \boldsymbol{\Psi}\rangle}. \tag{6}$$

This equation is known in reactor physics as *classical perturbation theory*. In addition, the adjoint system can be utilized in the sensitivity analysis of the eigenvalue problem for other responses fulfilling the following properties. Firstly, the response R must be Fréchet-differentiable with respect to $\boldsymbol{\Phi}$, in which case we can write

$$\delta R(\hat{\mathbf{e}}; \mathbf{h}) = R'_\sigma(\hat{\mathbf{e}})\delta\boldsymbol{\sigma} + \langle \nabla_\Phi R(\hat{\mathbf{e}}), \delta\boldsymbol{\Phi}\rangle_\Phi. \tag{7}$$

In addition, the response's Fréchet derivative $\nabla_\Phi R$ (also called gradient) must be orthogonal to the forward solution

$$\langle \nabla_\Phi R, \boldsymbol{\Phi}\rangle = 0. \tag{8}$$

When these assumptions are fulfilled, the *generalized adjoint* corresponding to the response R can be defined as the solution to the following inhomogeneous system:

$$\left(\mathbf{A}^* + \frac{1}{k}\mathbf{B}^*\right)\boldsymbol{\Gamma} = \frac{\nabla_\Phi R}{R}. \tag{9}$$

Notice that in the previous equation the eigenvalue k is fixed to correspond to the solution of (1) and therefore the operator $\mathbf{A}^* + (1/k)\mathbf{B}^*$ is singular, which necessitates (8) in

order for the solution $\boldsymbol{\Gamma}$ to exist. Also, when a solution $\boldsymbol{\Gamma}_0$ to (9) exists, there exists an infinite amount of solutions of the form

$$\boldsymbol{\Gamma} = \boldsymbol{\Gamma}_0 + a\boldsymbol{\Psi}, \quad a \in \mathbb{R}. \tag{10}$$

In this case, it is possible to choose a solution that is orthogonal to the (forward) fission source. This particular solution can be written as

$$\begin{aligned}\boldsymbol{\Gamma}_p &= \boldsymbol{\Gamma}_0 - \frac{\langle \boldsymbol{\Gamma}_0, \mathbf{B}\boldsymbol{\Phi}\rangle}{\langle \boldsymbol{\Psi}, \mathbf{B}\boldsymbol{\Phi}\rangle}\boldsymbol{\Psi} \\ &= \boldsymbol{\Gamma}_0 - \frac{\langle \mathbf{B}^*\boldsymbol{\Gamma}_0, \boldsymbol{\Phi}\rangle}{\langle \mathbf{B}^*\boldsymbol{\Psi}, \boldsymbol{\Phi}\rangle}\boldsymbol{\Psi}.\end{aligned} \tag{11}$$

We can now derive a practical expression for the response sensitivity with respect to a perturbation $\delta\boldsymbol{\sigma}$:

$$\begin{aligned}\frac{\delta R(\hat{\mathbf{e}}, \mathbf{h})}{R} &= \frac{R'_\sigma(\hat{\mathbf{e}})\delta\boldsymbol{\sigma}}{R} + \left\langle \frac{\nabla_\Phi R(\hat{\mathbf{e}})}{R}, \delta\boldsymbol{\Phi} \right\rangle_\Phi \\ &\overset{(9)}{=} \frac{R'_\sigma(\hat{\mathbf{e}})\delta\boldsymbol{\sigma}}{R} + \left\langle (\mathbf{A}^* + \frac{1}{k}\mathbf{B}^*)\boldsymbol{\Gamma}, \delta\boldsymbol{\Phi} \right\rangle_\Phi \\ &\overset{(4)}{=} \frac{R'_\sigma(\hat{\mathbf{e}})\delta\boldsymbol{\sigma}}{R} + \left\langle \boldsymbol{\Gamma}, \left(\mathbf{A} + \frac{1}{k}\mathbf{B}\right)\delta\boldsymbol{\Phi} \right\rangle_\Phi \\ &\overset{(3)}{=} \frac{R'_\sigma(\hat{\mathbf{e}})\delta\boldsymbol{\sigma}}{R} - \left\langle \boldsymbol{\Gamma}, \left(\mathbf{A}'_\sigma(\hat{\mathbf{e}}) - \frac{1}{k}\mathbf{B}'_\sigma(\hat{\mathbf{e}})\right)\delta\boldsymbol{\sigma} \right\rangle_\Phi \\ &\quad - \frac{\delta k(\hat{\mathbf{e}}; \mathbf{h})}{k^2}\langle \boldsymbol{\Gamma}, \mathbf{B}\boldsymbol{\Phi}\rangle_\Phi \\ &= \frac{R'_\sigma(\hat{\mathbf{e}})\delta\boldsymbol{\sigma}}{R} - \left\langle \boldsymbol{\Gamma}_p, \left(\mathbf{A}'_\sigma(\hat{\mathbf{e}}) - \frac{1}{k}\mathbf{B}'_\sigma(\hat{\mathbf{e}})\right)\delta\boldsymbol{\sigma} \right\rangle_\Phi.\end{aligned} \tag{12}$$

This framework is often referred to as *generalized perturbation theory* when the response R is of the form:

$$R(\mathbf{e}) = \frac{\langle \boldsymbol{\Phi}, \boldsymbol{\Sigma}_1\rangle}{\langle \boldsymbol{\Phi}, \boldsymbol{\Sigma}_2\rangle}. \tag{13}$$

In this case, it is straightforward to show that (8) is satisfied and that R is Fréchet-differentiable, the relative gradient being

$$\frac{\nabla_\Phi R}{R} = \frac{\boldsymbol{\Sigma}_1}{\langle \boldsymbol{\Phi}, \boldsymbol{\Sigma}_1\rangle} - \frac{\boldsymbol{\Sigma}_2}{\langle \boldsymbol{\Phi}, \boldsymbol{\Sigma}_2\rangle}. \tag{14}$$

The generalized adjoint $\boldsymbol{\Gamma}(\mathbf{r}, \boldsymbol{\Omega}, E)$ can be physically interpreted as the average contribution of an additional neutron at the phase space point $[\mathbf{r}, \boldsymbol{\Omega}, E]$ to the response under consideration. The generalized adjoint is normalized according to the value of the response. It should also be noticed that since an additional neutron may also reduce the value of the response, generalized adjoints can also have negative values. The gradient of the response may also be negative in some parts of the phase space.

In practice, the eigenvalue problem and the corresponding adjoint equations are solved numerically, which gives rise to some complications in the perturbation theory formalism. Ideally, the discretizations should be performed in a consistent manner so that the respective adjoint relations are satisfied at all stages of the computation [5]. However, this is usually infeasible in reactor physics calculations, and therefore it is customary to take the eigenvalue problem discretized with respect to energy and direction as the starting point for sensitivity analysis. This issue is discussed in more detail in [4].

2.2. Uncertainty Analysis. The uncertainty of the uncertain parameters $\boldsymbol{\sigma}$ should be understood in terms of the Bayesian probability interpretation. In this framework, probability is defined as a subjective measure that characterizes the plausibility of various hypotheses. When estimating parameters, all knowledge about a parameter σ_j is assumed to be incorporated into its marginal probability distribution $p(\sigma_j)$. This distribution is defined so that the integral $\int_a^b p(\sigma_j)\, d\sigma_j$ corresponds to the (Bayesian) probability that the value of σ_j belongs to the interval $[a, b]$. The distribution $p(\boldsymbol{\sigma})$ can then be used to form an estimate for the parameters and their associated uncertainties. Usually, the mean value or the mode is chosen as the estimate for the parameters, whereas the covariance matrix of the distribution is chosen as the descriptive statistic for the uncertainty.

In the Bayesian formalism, the outcome of the uncertainty analysis should ideally be the full posterior distribution $p(\mathbf{R})$. However, determining $p(\mathbf{R})$ analytically is usually extremely challenging and the distribution can only be estimated pointwise based on a simulation. In deterministic uncertainty analysis, the objective is not to form the entire distribution $p(\mathbf{R})$, but to compute an estimate for the covariance matrix $\mathrm{Cov}[\mathbf{R}]$ by linearizing the response $\mathbf{R} \approx \mathbf{S}\boldsymbol{\sigma}$. Here $\mathbf{S} \in \mathbb{R}^{J\times K}$ is the response vector sensitivity matrix, J is the number of responses, and K is the number of uncertain parameters. After linearizing the response, the covariance matrix can be computed simply using the identity

$$\mathrm{Cov}[\mathbf{R}] \approx \mathrm{Cov}[\mathbf{S}\boldsymbol{\sigma}] = \mathbf{S}\,\mathrm{Cov}[\boldsymbol{\sigma}]\mathbf{S}^T, \tag{15}$$

known as the first-order uncertainty propagation formula or the *Sandwich rule*.

3. Implementation

3.1. Computation of Generalized Adjoint Fluxes. This section reviews the guidelines for modifying a deterministic transport solver to compute the adjoint solutions needed in generalized perturbation theory and describes the methodology used in the implementation to CASMO-4. As mentioned previously, the description on the implementation of classical perturbation theory to CASMO-4 has been recently published in [4], and therefore, in this paper, the emphasis is placed on the GPT-specific features.

As explained in Section 2.1, it is customary to take the energy- and direction-discretized system as the starting point for perturbation theory. In CASMO-4, the multigroup criticality equation is solved by the method of characteristics

assuming isotropic scattering. Therefore, the following system of equations may be taken as the forward problem:

$$\begin{aligned}&\boldsymbol{\Omega}_m \cdot \nabla \Phi^g(\mathbf{r}, \boldsymbol{\Omega}_m) + \Sigma^g \Phi^g(\mathbf{r}, \boldsymbol{\Omega}_m)\\ &\quad = \frac{1}{4\pi} \sum_{h=1}^{G} \Sigma_{\mathrm{s}}^{h \to g}\ \phi^h(\mathbf{r}) + \frac{\chi_g}{4\pi k} \sum_{h=1}^{G} \overline{\nu}\ \Sigma_{\mathrm{f}}^h \phi^h(\mathbf{r}), \qquad (16)\\ &\qquad\qquad g = 1, \ldots, G.\end{aligned}$$

In (16) the scalar flux is approximated by the quadrature formula

$$\phi^h(\mathbf{r}) = \sum_{m=1}^{M} \omega_m \Phi^h(\mathbf{r}, \boldsymbol{\Omega}_m). \qquad (17)$$

In order to simulate an infinite lattice, the boundary conditions are often assumed to be reflective, that is,

$$\Phi(\mathbf{r}, \boldsymbol{\Omega}_m, E) = \Phi(\mathbf{r}, \boldsymbol{\Omega}'_m, E), \quad \mathbf{r} \in \Gamma,\ \boldsymbol{\Omega}_m \cdot \mathbf{n} < 0, \qquad (18)$$

where $\boldsymbol{\Omega}_m = \boldsymbol{\Omega}'_m - 2(\mathbf{n} \cdot \boldsymbol{\Omega}'_m)\mathbf{n}$ is the reflection direction. The inner product corresponding to this discretization can be defined in a consistent manner as

$$\langle \boldsymbol{\Phi}, \boldsymbol{\Psi} \rangle = \sum_{g=1}^{G} \sum_{m=1}^{M} \omega_m \int_D d^3\mathbf{r} \Phi^g(\mathbf{r}, \boldsymbol{\Omega}_m) \Psi^g(\mathbf{r}, \boldsymbol{\Omega}_m). \qquad (19)$$

The adjoint system can now be written

$$\begin{aligned}&-\boldsymbol{\Omega}_m \cdot \nabla \Psi^g(\mathbf{r}, \boldsymbol{\Omega}_m) + \Sigma^g\ \Psi^g(\mathbf{r}, \boldsymbol{\Omega}_m)\\ &\quad = \frac{1}{4\pi} \sum_{h=1}^{G} \Sigma_{\mathrm{s}}^{g \to h} \psi^h(\mathbf{r}) + \frac{\overline{\nu}\ \Sigma_{\mathrm{f}}^g}{4\pi k} \sum_{h=1}^{G} \chi_h \psi^h(\mathbf{r}), \quad g = 1, \ldots, G,\end{aligned} \qquad (20)$$

with the boundary conditions

$$\Psi(\mathbf{r}, \boldsymbol{\Omega}_m, E) = \Psi(\mathbf{r}, \boldsymbol{\Omega}'_m, E), \quad \mathbf{r} \in \Gamma,\ \boldsymbol{\Omega}_m \cdot \mathbf{n} > 0. \qquad (21)$$

It is straightforward to check that the systems (16) and (20) with their respective boundary conditions satisfy (4) with respect to the inner product defined by (19).

The generalized adjoint problem for a response of the form of (13) can now be written

$$\begin{aligned}&-\boldsymbol{\Omega}_m \cdot \nabla \Gamma^g(\mathbf{r}, \boldsymbol{\Omega}_m) + \Sigma^g\ \Gamma^g(\mathbf{r}, \boldsymbol{\Omega}_m)\\ &\quad = \frac{1}{4\pi} \sum_{h=1}^{G} \Sigma_{\mathrm{s}}^{g \to h} \gamma^h(\mathbf{r}) + \frac{\overline{\nu}\ \Sigma_{\mathrm{f}}^g}{4\pi k} \sum_{h=1}^{G} \chi_h \gamma^h(\mathbf{r}) \qquad (22)\\ &\qquad + \frac{\Sigma_1^g(\mathbf{r})}{\langle \boldsymbol{\Phi}, \boldsymbol{\Sigma}_1 \rangle} - \frac{\Sigma_2^g(\mathbf{r})}{\langle \boldsymbol{\Phi}, \boldsymbol{\Sigma}_2 \rangle}, \quad g = 1, \ldots, G,\end{aligned}$$

where the generalized adjoint of the scalar flux has been denoted by $\gamma^h(\mathbf{r})$. As explained in Section 2.1, this system may have an infinite number of solutions, of which we wish to solve the one that satisfies

$$\left\langle \mathbf{B}^* \boldsymbol{\Gamma}_p, \boldsymbol{\Phi} \right\rangle = 0. \qquad (23)$$

In deterministic transport solvers, the iteration for fixed source calculations is generally of the form

$$\mathbf{A}\boldsymbol{\Phi}^{n+1} = \mathbf{B}\boldsymbol{\Phi}^n + \mathbf{S}, \qquad (24)$$

where $\mathbf{S}$ is an external source. This iteration scheme with a fixed eigenvalue is also well suited for solving the generalized adjoint problem of (22), in which case the iteration takes the form

$$\mathbf{A}^* \boldsymbol{\Gamma}^{n+1} = \frac{1}{k} \mathbf{B}^* \boldsymbol{\Gamma}^n + \frac{\nabla_\Phi R}{R}. \qquad (25)$$

During the iteration, however, the convergence to the particular solution that is orthogonal to the fission source must be ensured. It is straightforward to show that if the initial guess for the generalized adjoint flux satisfies (23), this orthogonality property is preserved during the iteration. Firstly,

$$\begin{aligned}\left\langle \mathbf{A}^* \boldsymbol{\Gamma}^{n+1}, \boldsymbol{\Phi} \right\rangle &\overset{(25)}{=} \frac{1}{k} \langle \mathbf{B}^* \boldsymbol{\Gamma}^n, \boldsymbol{\Phi} \rangle + \left\langle \frac{\nabla_\Phi R}{R}, \boldsymbol{\Phi} \right\rangle\\ &\overset{(8)}{=} \frac{1}{k} \langle \mathbf{B}^* \boldsymbol{\Gamma}^n, \boldsymbol{\Phi} \rangle.\end{aligned} \qquad (26)$$

On the other hand,

$$\begin{aligned}\left\langle \mathbf{A}^* \boldsymbol{\Gamma}^{n+1}, \boldsymbol{\Phi} \right\rangle &= \left\langle \boldsymbol{\Gamma}^{n+1}, \mathbf{A}\boldsymbol{\Phi} \right\rangle \overset{(1)}{=} \frac{1}{k} \left\langle \boldsymbol{\Gamma}^{n+1}, \mathbf{B}\boldsymbol{\Phi} \right\rangle\\ &= \frac{1}{k} \left\langle \mathbf{B}^* \boldsymbol{\Gamma}^{n+1}, \boldsymbol{\Phi} \right\rangle.\end{aligned} \qquad (27)$$

Therefore, for each iteration n,

$$\left\langle \mathbf{B}^* \boldsymbol{\Gamma}^{n+1}, \boldsymbol{\Phi} \right\rangle = \langle \mathbf{B}^* \boldsymbol{\Gamma}^n, \boldsymbol{\Phi} \rangle, \qquad (28)$$

from which the result follows. In practice, however, due to round-off errors and the unavoidable inconsistencies in formulating the discretizations and adjoint relations, a refinement of the iteration scheme is necessary to guarantee that (23) remains satisfied [11]. A suitable procedure is to force the orthogonality of the solution with each outer iteration. In this case, in accordance with (11), the iteration takes the form

$$\mathbf{A}^* \boldsymbol{\Gamma}^{n+1} = \frac{1}{k} \mathbf{B}^* \left(\boldsymbol{\Gamma}^n - \frac{\langle \mathbf{B}^* \boldsymbol{\Gamma}^n, \boldsymbol{\Phi} \rangle}{\langle \mathbf{B}^* \boldsymbol{\Psi}, \boldsymbol{\Phi} \rangle} \boldsymbol{\Psi} \right) + \frac{\nabla_\Phi R}{R}. \qquad (29)$$

Notice that this iteration scheme requires that the forward solution and the fundamental adjoint solution have been previously computed and that they are accessible during the iteration.

By comparing (29) with the forward problem of (16), it can be seen that if the forward system had an external source, the systems would be of the same form with the exception that the adjoint system is solved in the opposite direction. Therefore, if the transport solver does not rely on the assumption of the nonnegativity of the flux or the sources, relatively few modifications are needed to transform the solver to also compute the generalized adjoint functions. For example, the method of characteristics, used in CASMO-4, does not require that the solution or the sources are nonnegative. In this case, the following operations need to be performed *before* the adjoint calculation [10].

(1) Transpose the scattering matrix.

(2) Interchange the vectors $\overline{\nu}\boldsymbol{\sigma}_{\mathrm{f}}$ and $\boldsymbol{\chi}$.

(3) Invert the group indices for all variables as follows: $G \leftrightarrow 1, (G-1) \leftrightarrow 2, \ldots$.

After these operations, the transport solver can be used to compute the fundamental adjoint solution. Notice also that these operations automatically convert the forward boundary conditions to the adjoint boundary conditions. When solving a generalized adjoint problem, the following changes need to be additionally implemented *within* the (forward) transport solver.

(1) Add the response gradient $\nabla_{\Phi} R/R$ to the variable for an external source.

(2) Modify the fission source F_g to the form

$$F_g = \frac{\chi_g}{4\pi k} \sum_{h=1}^{G} \overline{\nu}\, \Sigma_{\mathrm{f}}^{h} \left(\phi^{h}(\mathbf{r}) - \frac{\langle \mathbf{B}\boldsymbol{\Phi}, \boldsymbol{\Phi}_{\mathrm{F}} \rangle}{\langle \mathbf{B}\boldsymbol{\Psi}, \boldsymbol{\Phi}_{\mathrm{F}} \rangle} \Psi^{g} \right), \tag{30}$$

where $\boldsymbol{\Phi}_{\mathrm{F}}$ denotes the forward solution of (16) and $\boldsymbol{\Psi}$ the adjoint solution of (20).

The multigroup solution $\boldsymbol{\Phi}$ given by the solver must then be interpreted so that, for example, $\Phi^{g}(\mathbf{r}, \boldsymbol{\Omega})$ corresponds to $\boldsymbol{\Gamma}^{G+1-g}(\mathbf{r}, -\boldsymbol{\Omega})$. Notice that if the transport solver is based on a numerical scheme that relies on the nonnegativity of the flux or the sources, some additional modifications are necessary in addition to the ones described above. For further details, see for example, [11].

3.2. Computation of Sensitivity and Uncertainty Profiles. After obtaining the adjoint solutions, the sensitivities with respect to the multigroup nuclear data parameters can be computed according to (6) and (12). Notice that even after the multigroup approximation, these parameters are still spatial functions and therefore the derivatives in the equations refer to functional derivatives. The inner product in the sensitivity expressions can be discretized as

$$\langle \boldsymbol{\Phi}, \boldsymbol{\Psi} \rangle \approx \sum_{i=1}^{I} \sum_{g=1}^{G} \sum_{m=1}^{M} \omega_m V_i\, \overline{\Phi}^{g,i,m}\, \overline{\Psi}^{g,i,m}, \tag{31}$$

where i denotes the mesh index and $\overline{\Phi}^{g,i,m}$ and $\overline{\Psi}^{g,i,m}$ denote the average fluxes.

In order to compute the uncertainties using the Sandwich rule, the sensitivities and covariance matrices need to be formed with respect to the same parameters using the same energy group structure. In the SCALE 6 covariance library [3], the available covariance matrices are given in a 40-group structure for the parameters listed in Table 1. Most of these covariance matrices are nuclide specific. It should be emphasized that there is no covariance data for the group-to-group transfer cross-sections.

Multigroup covariance matrices can in principle be transformed to another multigroup structure by simple mathematical techniques. The applicability of this approach depends on the differences between the group structures.

Table 1: Parameters for which there exists covariance data in the SCALE library.

Parameter	MT number
σ_{t}	1
σ_{e}	2
σ_{i}	4
$\sigma_{\mathrm{n,2n}}$	16
σ_{f}	18
σ_{γ}	102
$\sigma_{\mathrm{n,p}}$	103
$\sigma_{\mathrm{n,d}}$	104
$\sigma_{\mathrm{n,t}}$	105
$\sigma_{\mathrm{n,He}}$	106
$\sigma_{\mathrm{n},\alpha}$	107
$\overline{\nu}$	456
χ	1018

In particular, the widths of the energy groups should not dramatically change. In this work, the code Angelo 2.3 [12] was used to transform the matrices to the energy group structure used in the sensitivity calculations with CASMO-4. The transformation procedure used in the code is based on flat-flux approximation, where the resampled values on the new grid are computed as lethargy overlap weighted averages. For further details, see [13]. When modifying the energy group structure of fission spectrum covariance matrices, further correction procedures are necessary in order to guarantee that the covariance matrices are in accordance with the normalization condition $\sum_g \chi^g = 1$ [14]. The correction can also be applied to the fission spectrum sensitivities in which case the sensitivities are called *constrained* [14]. This was the approach chosen in this work.

In order to utilize the covariance data given for the parameters in Table 1, sensitivity profiles should be computed with respect to the same parameters. However, many lattice physics codes such as CASMO, HELIOS [15], WIMS [16], and DRAGON [17] employ nuclear data libraries that do not contain cross-section data for the individual capture and scattering reactions, but only for the total capture and scattering cross-section. There are generally three different approaches to overcome this difficulty. The most natural approach is perhaps to add the missing cross-sections to the code, either by creating a new cross-section library or by modifying the cross-sections inside the code [18]. Another option, suitable for deterministic analysis, is not to use problem-dependent cross-sections in the sensitivity analysis. In this case, the sensitivity coefficients can be computed outside the code based on the forward and adjoint fluxes and any set of cross-sections. This was the idea, for example, behind connecting DRAGON with the sensitivity and uncertainty analysis code SUSD3D after a generalized adjoint mode was implemented to DRAGON [19]. The third option is to form the covariance matrices corresponding to the total capture and scattering cross-sections [4]. This is the approach that was chosen in this work.

Since the relationships between the total and individual capture and scattering reactions are linear, the covariance matrices corresponding to the total capture and scattering reactions can be computed with the Sandwich rule without introducing any approximation. The method used for combining the covariance matrices has been recently described in detail in [4]. Therefore, only the most important conclusions related to the methodology are repeated here.

Firstly, in the context of the capture reactions, the results are expected to be fully consistent with the case where the sensitivities are computed with respect to the individual capture reactions. In the case of the scattering reactions, however, the sensitivity profiles with respect to the individual and the total scattering cross-sections cannot be defined in a consistent manner and this affects the uncertainty results. In this context, it should be emphasized that the treatment of the covariance matrices involves no approximations and the inconsistency is solely related to the computation of the sensitivities. As mentioned previously, there is no cross-section data for the transfer cross-sections $\sigma_{\mathrm{x}}^{h\to g,j}$ but only for $\sigma_{\mathrm{x}}^{g,j}=\sum_{h=1}^{G}\sigma_{\mathrm{x}}^{g\to h,j}$, where x refers to a scattering reaction (e.g., elastic, inelastic) and j is the nuclide index. Therefore, in order to use the scattering covariance data, the sensitivity profiles should be computed with respect to $\sigma_{\mathrm{x}}^{g,j}$. Because of the scattering source term in (16), however, the derivative with respect to $\sigma_{\mathrm{x}}^{g,j}$ is not mathematically well defined without additional constraints. Typically it is assumed that the probabilities of transfers to various groups are fixed, that is,

$$\sigma_{\mathrm{x}}^{g\to h,j}=\sigma_{\mathrm{x}}^{g,j}\,p_{\mathrm{x}}^{g\to h,j}, \tag{32}$$

where $p_{\mathrm{x}}^{g\to h}$ is the proportion of neutrons scattered from energy group g to energy group h, which is assumed to remain fixed even if the scattering cross-section $\sigma_{\mathrm{x}}^{g,j}$ is perturbed [20]. Based on this assumption, the scattering source in (16) can be written as

$$S^{g}=\frac{1}{4\pi}\sum_{h=1}^{G}\Sigma_{\mathrm{s}}^{h\to g}\phi^{h}=\frac{1}{4\pi}\sum_{\mathrm{x}}\sum_{j}N^{j}\sum_{h=1}^{G}\sigma_{\mathrm{x}}^{h,j}\,p_{\mathrm{x}}^{h\to g}\phi^{h}, \tag{33}$$

where the summations over x include all scattering reactions. After this assumption, the derivative with respect to $\sigma_{\mathrm{x}}^{g,j}$ is well defined and can be computed as usual. It is straightforward to show that this approach corresponds to computing the sensitivity coefficients with respect to the transfer cross-sections $\sigma_{\mathrm{x}}^{g\to h,j}$ and summing them over h.

However, the sensitivity with respect to the total scattering cross-section $\sigma_{\mathrm{s}}^{j}=\sum_{x}\sigma_{\mathrm{x}}^{j}$ is not well defined if the constraint (32) is enforced. In order to define this sensitivity, fixed transfer rates must be assumed for the total scattering cross-section. Also, computing the total scattering sensitivity as the sum of the individual scattering sensitivities implicitly enforces this constraint. Since the two assumptions required to compute the individual and total scattering sensitivities are inconsistent, the chain rule of derivation does not apply to them, and, for example, although $\sigma_{\mathrm{s}}^{g,j}=\sigma_{\mathrm{e}}^{g,j}+\sigma_{\mathrm{i}}^{g,j}$ holds, $dR/d\sigma_{\mathrm{e}}^{g,j}\neq(dR/d\sigma_{\mathrm{s}}^{g,j})(d\sigma_{\mathrm{s}}^{g,j}/d\sigma_{\mathrm{e}}^{g,j})$.

4. Numerical Results for PB-2 Lattice Physics Exercise

The calculation framework was applied to the BWR test case from the UAM benchmark lattice physics Exercise 1.2 considering a single fuel assembly with reflective boundary conditions [2], and the results were compared against the TSUNAMI-2D sequence in SCALE 6.1 [21]. The test problem represents Peach Bottom 2 (PB-2) under hot zero power conditions. Two-group homogenized cross-sections have been considered as responses in the GPT framework.

The outline of the CASMO-4 calculations is presented in Figure 1. The calculations were carried out using the cross-section library E60200 that contains 70 energy groups and is based on ENDF/B-VI data [22]. The covariance data were taken from the SCALE 6 library ZZ-SCALE6.0/COVA-44G [3] according to the guidelines of the benchmark. The library is based on evaluations from various sources (including ENDF/B-VII, ENDF/B-VI, JENDL-3.1) and approximate covariance data. The covariances in the library are given in relative terms, and therefore the library is intended to be used with all cross-section libraries including the ones that are inconsistent with the evaluations. While this is not strictly correct, it is considered to be acceptable due to the scarcity of comprehensive covariance data among other reasons [23].

The list of the nuclides present in these test cases can be found in the benchmark specification [2]. Apart from the isotopes of chromium and iron, all available covariance data in the library was included in the uncertainty computations. The reason for excluding these isotopes is that the employed cross-section library E60200 does not contain isotope-specific cross-sections for these materials but only cross-sections for natural chromium and iron.

The covariance matrices from ZZ-SCALE6.0/COVA-44G were processed for compatibility with CASMO-4. The sensitivity profiles in CASMO-4 were computed using the 40-group structure option that was the closest match to the amount of groups in the covariance data and, as mentioned in Section 3.2, the code Angelo 2.3 [12] was used to process the covariance matrices to this energy group structure. Next, the nuclear data processing code NJOY [24] was used to transform the 40-group covariance files to the BOXR format. Auxiliary FORTRAN programs were written for combining the covariance matrices according to the principles described in Section 3.2.

The TSUNAMI-2D calculations were performed using the ENDF/B-VI-based cross-section library V6-238 containing 238 energy groups. The module CENTRM was used for self-shielding. Implicit sensitivity analysis [9] was omitted in the TSUNAMI calculations in order to facilitate the comparison of the results given by CASMO-4 and TSUNAMI-2D.

4.1. Results Based on Classical Perturbation Theory. A summary of the results based on classical perturbation theory for the multiplication factor is presented in Table 2. The relative difference between the multiplication factors computed with CASMO-4 and TSUNAMI-2D is 52 pcm in both forward and adjoint cases. For the total uncertainty, the

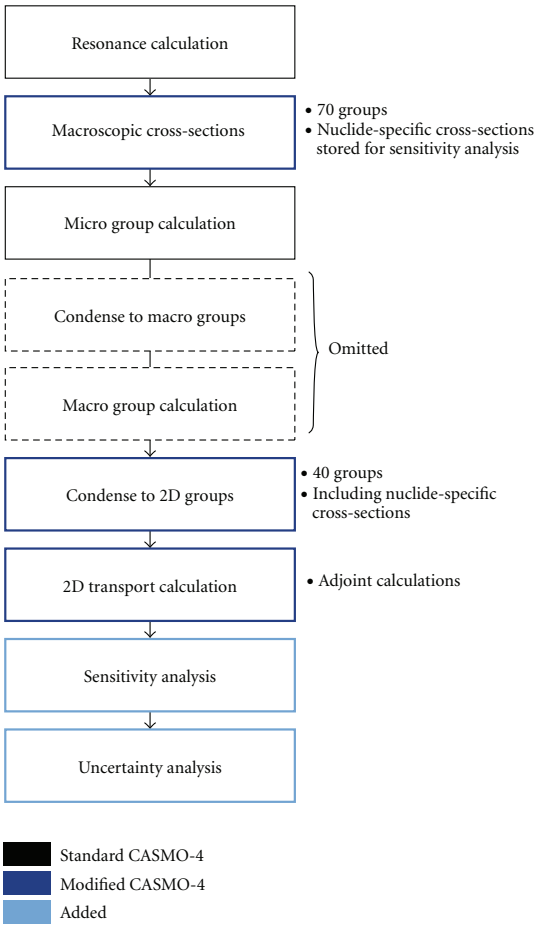

Figure 1: Outline of the CASMO-4 calculations.

values given by CASMO-4 and TSUNAMI-2D are also very consistent. Table 3 shows the five most significant sources of uncertainty together with the corresponding energy- and region-integrated sensitivity coefficients. As can be seen from this table, both the sensitivity and the uncertainty results are in good accordance. The greatest difference occurs for the capture cross-section of ^{238}U, for which CASMO-4 yields a greater sensitivity. This appears to originate from the differences in the cross-section libraries. In particular, the cross-section library E60200 used in the CASMO-4 calculation has not been reduced in terms of the ^{238}U resonance integral, which is known to be overestimated in the ENDF/B-VI data [22].

Figure 2 shows the volume-averaged forward flux and the volume-averaged fundamental adjoint $\overline{\Psi}$ corresponding to this test case. As explained in Section 2.1, the value $\overline{\Psi}^g$ represents the average importance of neutrons in the energy group g to the multiplication factor in comparison to neutrons

Table 2: Summary of the results for the multiplication factor.

Code	Forward k	Adjoint k	Rel. uncertainty, $\Delta k/k$ (%)
CASMO-4	1.10548	1.10546	0.508
TSUNAMI-2d	1.10490	1.10490	0.506

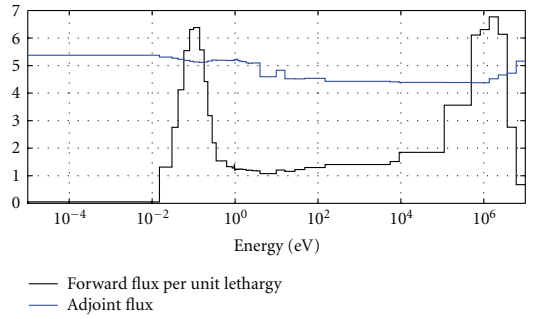

Figure 2: Volume-averaged forward flux and fundamental adjoint flux.

in other energy groups. The plot can be interpreted from this point of view. For example, it can easily be seen from the figure how the ^{238}U capture cross-section resonances reduce the importance of neutrons in the corresponding energy groups. This phenomenon is particularly clear in the energy group E_{14} = [4.00 eV, 9.88 eV], where the multigroup capture cross-section attains its maximum value. It can also be clearly distinguished from the plot how the adjoint function has a higher value in the energy groups corresponding to the peaks in the fission cross-section of ^{235}U. To further demonstrate this, Figure 3 shows a plot of the problem-dependent ^{235}U fission and ^{238}U capture cross-sections in the same 40-group structure. The increase in the adjoint values in the highest energy groups corresponds mainly to the increase in the value of $\bar{\nu}$ at these energies.

Figure 4 shows the multiplication factor sensitivity profiles for the parameters, whose integrated sensitivity coefficients have the greatest absolute values, excluding the sensitivity profile with respect to the fission spectrum of ^{235}U, which was constrained in the computation. As can be seen from the figure, the multiplication factor is the most sensitive to the fission parameters of ^{235}U, the capture cross-section of ^{238}U, and the scattering cross-section of ^{1}H. The positive sensitivity to the capture of ^{238}U in the highest energy group follows from the fact that in CASMO-4 the (n, 2n) reaction cross-section has been included in the capture cross-section with a negative sign in this group. It is instructive to compare the sensitivity profiles with the forward and adjoint fluxes plotted in Figure 2. Notice that the peaks in the sensitivity profiles of ^{235}U coincide with the thermal peak of the neutron flux, where most of the fissions occur. In general, perturbing a nuclear parameter has a greater impact on the results in the energy groups, where the flux is higher. On the contrary, the values of the fundamental adjoint represent the *average* importance

Table 3: The five most significant sources of uncertainty for the multiplication factor and the corresponding energy- and region-integrated relative sensitivity coefficients.

Nuclide	Parameter pair	Sensitivity		Contribution to $\Delta k/k$ (%)	
		CASMO	TSUNAMI	CASMO	TSUNAMI
^{238}U	σ_c, σ_c	-2.434×10^{-1}	-2.143×10^{-1}	3.198×10^{-1}	2.902×10^{-1}
^{235}U	$\bar{\nu}, \bar{\nu}$	9.160×10^{-1}	9.370×10^{-1}	2.720×10^{-1}	2.773×10^{-1}
^{235}U	σ_c, σ_c	-1.027×10^{-1}	-1.025×10^{-1}	1.454×10^{-1}	1.422×10^{-1}
^{235}U	σ_f, σ_f	4.038×10^{-1}	4.212×10^{-1}	1.372×10^{-1}	1.409×10^{-1}
^{235}U	σ_f, σ_c	4.038×10^{-1}	4.212×10^{-1}	1.238×10^{-1}	1.245×10^{-1}
		-1.027×10^{-1}	-1.025×10^{-1}		

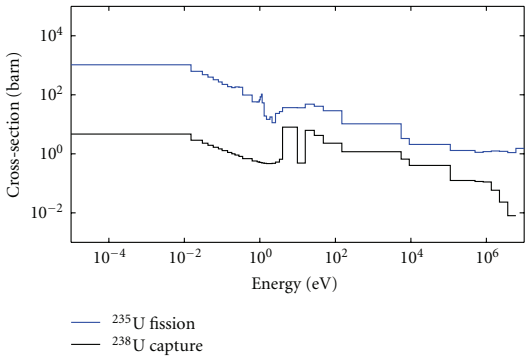

Figure 3: Self-shielded multigroup cross-sections corresponding to the test problem.

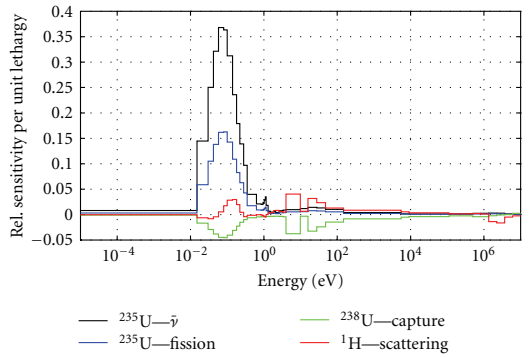

Figure 4: Multiplication factor sensitivity profiles.

of neutrons in different energy groups. In particular, the lowest energy group has the highest importance, but this is not manifested in the sensitivity profiles, as the flux is very close to zero in this group. The negative sensitivities to the scattering reaction of ^{1}H in the four lowest energy groups can be attributed to the fact that in these groups upscattering is more likely than downscattering. Therefore, neutrons are scattered to energy groups with a lower importance. The same reasoning applies to the scattering sensitivity of ^{1}H in the highest energy groups, where neutrons are scattered downwards and the values of the adjoint function decrease rapidly with energy.

4.2. Results Based on Generalized Perturbation Theory. Table 4 presents the values and the total uncertainties of the homogenized two-group cross-sections that were considered as responses in the GPT-based sensitivity and uncertainty analysis. In computing the responses, the thermal cut-off was set at 0.625 eV. It can be seen from the table that all total uncertainty values are in good agreement with the thermal responses, whereas for the fast responses the uncertainties given by TSUNAMI-2D are consistently greater.

Tables 5 and 6 show more detailed sensitivity and uncertainty results for the two-group homogenized production cross-sections $\nu\Sigma_{f,1}$ and $\nu\Sigma_{f,2}$. As can be seen from Table 6, in the case of $\nu\Sigma_{f,1}$, the difference in the total uncertainty values given by CASMO-4 and TSUNAMI-2D is attributable to the scattering of ^{238}U, for which TSUNAMI-2D yields a significantly greater uncertainty value, although the total scattering sensitivity coefficients given by both codes are very close. As explained in Section 3.2, the sensitivity with respect to the total scattering cross-section can only be defined if the group-to-group transfer probabilities are assumed to be fixed for the total scattering. Also, defining the total scattering sensitivity as the sum of the individual scattering sensitivities implicitly enforces this assumption. However, in the TSUNAMI-2D computation, the total scattering uncertainty is computed based on the individual scattering sensitivities, which rely on the assumption of fixed transfer rates for each scattering reaction. The difference in the total scattering uncertainties is hence explained by incompatible constraints in the two uncertainty calculations. This phenomenon is more evident for the fast group responses since they are more sensitive to the inelastic scattering of ^{238}U.

Figure 5 shows the volume-averaged generalized adjoint solutions for the responses $\nu\Sigma_{f,1}$ and $\nu\Sigma_{f,2}$, denoted by $\overline{\Gamma}_{f,1}$ and $\overline{\Gamma}_{f,2}$, respectively. As previously explained, the adjoint values in each energy group can be interpreted to represent the average importance of neutrons in that group to the response under consideration. Therefore, it is not surprising that thermal neutrons are more important to the response $\nu\Sigma_{f,2}$, whereas fast neutrons are more important to the response $\nu\Sigma_{f,1}$. The positive values of $\overline{\Gamma}_{f,2}$ in the fast groups result

Table 4: Values and uncertainties of the responses considered in the GPT framework.

Response R	Value		Relative uncertainty $\Delta R/R$ (%)	
	CASMO	TSUNAMI	CASMO	TSUNAMI
$\nu\Sigma_{f,1}$	4.976×10^{-3}	4.951×10^{-3}	8.399×10^{-1}	9.754×10^{-1}
$\nu\Sigma_{f,2}$	6.922×10^{-2}	6.938×10^{-2}	4.490×10^{-1}	4.478×10^{-1}
$\Sigma_{c,1}$	5.348×10^{-3}	5.380×10^{-3}	1.098×10^{0}	1.168×10^{0}
$\Sigma_{c,2}$	2.653×10^{-2}	2.672×10^{-2}	5.066×10^{-1}	5.040×10^{-1}
$\Sigma_{f,1}$	1.935×10^{-3}	1.927×10^{-3}	5.563×10^{-1}	6.820×10^{-1}
$\Sigma_{f,2}$	2.841×10^{-2}	2.847×10^{-2}	3.244×10^{-1}	3.226×10^{-1}

Table 5: The five most significant sources of uncertainty for the response $\nu\Sigma_{f,2}$ and the corresponding energy- and region-integrated relative sensitivity coefficients.

Nuclide	Param. pair	Sensitivity		Contribution to $\Delta R/R$ (%)	
		CASMO	TSUNAMI	CASMO	TSUNAMI
^{235}U	$\overline{\nu}, \overline{\nu}$	9.996×10^{-1}	9.998×10^{-1}	3.105×10^{-1}	3.106×10^{-1}
^{235}U	σ_f, σ_f	7.985×10^{-1}	7.941×10^{-1}	2.893×10^{-1}	2.869×10^{-1}
^{235}U	σ_f, σ_c	7.985×10^{-1}	7.941×10^{-1}	1.134×10^{-1}	1.139×10^{-1}
		-3.599×10^{-2}	-3.667×10^{-2}		
^{238}U	σ_c, σ_c	-4.406×10^{-2}	-4.255×10^{-2}	7.257×10^{-2}	7.222×10^{-2}
^{235}U	σ_c, σ_c	-3.599×10^{-2}	-3.667×10^{-2}	5.613×10^{-2}	5.672×10^{-2}

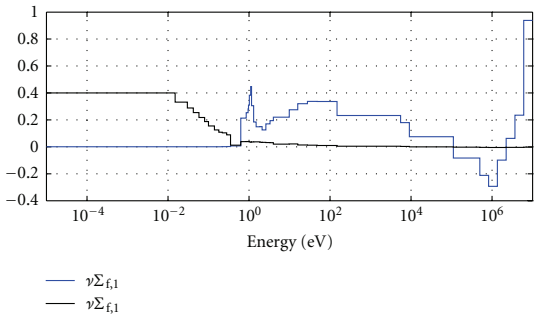

Figure 5: Volume-averaged generalized adjoints corresponding to the responses $\nu\Sigma_{f,1}$ and $\nu\Sigma_{f,2}$.

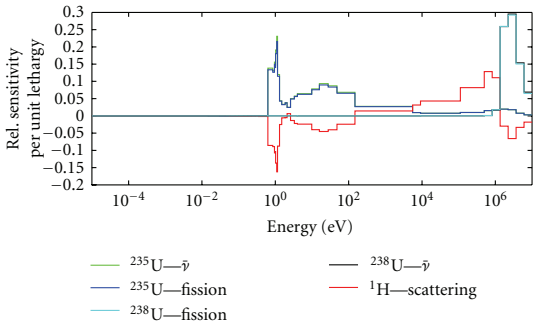

Figure 6: Sensitivity profiles of the response $\nu\Sigma_{f,1}$.

from the downscattering of neutrons. Notice that $\overline{\Gamma}_{f,1}$ also has a small positive value in the first thermal group, which corresponds to the possibility of upscattering. For the most part, both adjoint fluxes qualitatively follow the fission cross-section of ^{235}U plotted in Figure 3. In the highest energy groups, the values of $\overline{\Gamma}_{f,1}$ increase rapidly due to the increase in the values of $\overline{\nu}$. The negative values of $\overline{\Gamma}_{f,1}$ between 0.111 MeV and 2.231 MeV signify that additional neutrons in those energy groups would on average contribute more to the denominator $\langle \mathbf{\Phi}, \mathbf{1} \rangle_1$ than to the numerator $\langle \mathbf{\Phi}, \boldsymbol{\nu\Sigma}_f \rangle_1$. This in accordance with the fact that fission is unlikely to occur in this energy region.

Figure 6 shows the sensitivity profiles of $\nu\Sigma_{f,1}$ with respect to the parameters, whose integrated sensitivity coefficients have the greatest absolute values. As can be anticipated, the response is the most sensitive to the fission parameters of ^{235}U and ^{238}U and in addition to the scattering of ^{1}H. It is interesting to compare these profiles with the plot of the generalized adjoint $\overline{\Gamma}_{f,1}$ in Figure 5. The sensitivity to the scattering of ^{1}H has the smallest values in the groups with the highest importance, as this reaction transfers neutrons to energy groups with a lower importance. Since fast neutrons mostly scatter downwards, the scattering sensitivity has positive values in the groups between 149 eV and 1.35 MeV, where the importance decreases with increasing energy. This trend is reversed at 1.35 MeV, where the importance of the energy groups begins to increase with energy, mainly due to the increase in the values of $\overline{\nu}$ at these energies.

The sensitivity profiles corresponding to the response $\nu\Sigma_{f,2}$ are plotted in Figure 7. It is noteworthy that the profiles qualitatively resemble the respective profiles of the multiplication factor in the thermal region, whereas they quickly fall to nearly zero in the fast region. From the perspective of the GPT framework, it is again enlightening

Table 6: The five most significant sources of uncertainty for the response $\nu\Sigma_{f,1}$ and the corresponding energy- and region-integrated relative sensitivity coefficients. The sensitivity coefficients with respect to the parameter χ have been constrained.

Nuclide	Param. pair	Sensitivity		Contribution to $\Delta R/R$ (%)	
		CASMO	TSUNAMI	CASMO	TSUNAMI
^{235}U	χ,χ	4.657×10^{-9}	-2.757×10^{-10}	5.934×10^{-1}	6.150×10^{-1}
^{238}U	$\overline{\nu},\overline{\nu}$	3.975×10^{-1}	3.879×10^{-1}	4.623×10^{-1}	4.544×10^{-1}
^{238}U	σ_f,σ_f	3.931×10^{-1}	3.834×10^{-1}	2.084×10^{-1}	1.994×10^{-1}
^{238}U	σ_s,σ_s	-2.743×10^{-2}	-2.718×10^{-2}	2.015×10^{-1}	5.148×10^{-1}
^{235}U	σ_f,σ_f	5.826×10^{-1}	5.866×10^{-1}	1.588×10^{-1}	1.466×10^{-1}

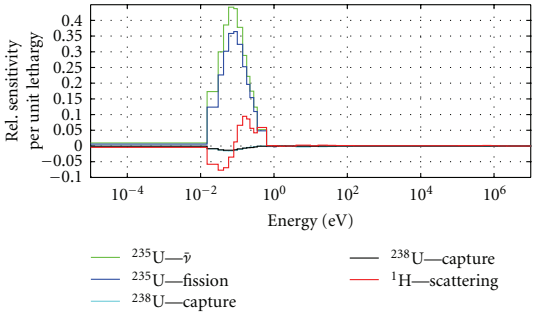

Figure 7: Sensitivity profiles of the response $\nu\Sigma_{f,2}$.

to compare the sensitivity plots with the adjoint function $\overline{\Gamma}_{f,2}$ plotted in Figure 5 and the flux $\overline{\Phi}$ shown in Figure 2. In the case of this response, the average importance of neutrons increases steadily with decreasing energy. Therefore, it is reasonable that the scattering sensitivities are again negative in the groups where upscattering is more likely than downscattering. Also, the sensitivities peak in the energy region coinciding with the thermal peak of the forward flux.

5. Summary and Conclusions

Sensitivity and uncertainty analysis capability has been developed to the reactor physics code CASMO-4 in the context of the UAM benchmark. Sensitivities with respect to nuclear data parameters can be computed efficiently by utilizing the adjoint system of the criticality equation. The propagated nuclear data uncertainty can then be calculated deterministically by the Sandwich rule.

Initially, classical perturbation theory was implemented to the code, which enabled sensitivity analysis of the critical eigenvalue. In this context, covariance matrices from scale 6 were transformed to become compatible with CASMO-4, and the resulting covariance library was connected with the code. Since the cross-section libraries of CASMO-4 do not contain data for the individual capture and scattering reactions, the covariance matrices of the individual subreactions were combined in the covariance library. This work has been reported in detail in [4], and the main conclusions related to the methodology were summarized in this paper. In particular, the sensitivities with respect to total scattering and individual scattering cross-sections cannot be defined in a consistent manner, which leads to some systematic differences in the uncertainty results.

Recently, generalized perturbation theory was added to the code as a new feature, which enables performing sensitivity analysis for responses that can be represented as reaction rate ratios. For each response, the computation of sensitivity profiles with respect to all parameters of interest requires solving one generalized adjoint system. The mathematical background as well as the physical interpretation of the generalized adjoint solutions were reviewed, and practical guidelines were given for modifying a deterministic transport code to solve the generalized adjoint systems needed in sensitivity analysis. The theory for computing the sensitivity profiles was presented both from the perspective of function space analysis and numerical computations.

Numerical results were presented for a lattice physics test problem representing a BWR in hot zero power conditions, and they were compared to the results given by the TSUNAMI-2D sequence in SCALE 6.1. Two-group homogenized cross-sections were considered as responses in the generalized perturbation theory framework. The results were in very good agreement with the thermal responses, whereas in the case of fast responses, the uncertainties given by TSUNAMI-2D were consistently greater. Detailed sensitivity and uncertainty results were presented and analyzed for the homogenized fast and thermal production cross-sections. The differences in the uncertainty results for the fast responses were explained by the incompatible constraints used in computing the scattering uncertainties.

In the future, the work will continue by extending the GPT framework to other responses in addition to two-group homogenized cross-sections with the eventual goal of modifying CASMO-4 to provide uncertainty estimates for all homogenized assembly data, which can then be propagated to coupled neutronics/thermal hydraulics calculations.

Acknowledgment

This work was funded through the Finnish National Research Programme on Nuclear Power Plant Safety 2011–2014, SAFIR2014.

References

[1] J. Rhodes and M. Edenius, *CASMO-4, A Fuel Assembly Burnup Program, Users Manual*, 2001.

[2] K. Ivanov, M. Avramova, I. Kodeli, and E. Sartori, "Benchmark for uncertainty analysis in modeling (UAM) for design, operation, and safety analysis of LWRs," NEA/NSC/DOC(2007) 23, 2007.

[3] ZZ-SCALE6.0/COVA44G, "A 44-group cross section covariance matrix library retrieved from the scale-6.0 package," NEA Data Bank Code Package USCD1236/03, 2011.

[4] M. Pusa, "Incorporating sensitivity and uncertainty analysis to a lattice physics code with application to CASMO-4," *Annals of Nuclear Energy*, vol. 40, no. 1, pp. 153–162, 2012.

[5] D. G. Cacuci, *Sensitivity and Uncertainty Analysis*, vol. 1, Chapman & Hall/CRC, Boca Raton, Fla, USA, 2003.

[6] B. G. Carlson and K. D. Lathrop, "Transport theory-the method of discrete ordinates," in *Computing Methods in Reactor Physics*, H. Greenspan, C. N. Kelber, and D. Okrent, Eds., Gordon and Breach Science Publishers, New York, NY, USA, 1968.

[7] E. E. Lewis and J. W. F. Miller, *Computational Methods of Neutron Transport*, John Wiley & Sons, New York, NY, USA, 1984.

[8] J. Lewins, *Importance: The Adjoint Function*, Pergamon Press, Oxford, UK, 1965.

[9] M. L. Williams, B. L. Broadhead, and C. V. Parks, "Eigenvalue sensitivity theory for resonance-shielded cross sections," *Nuclear Science and Engineering*, vol. 138, no. 2, pp. 177–191, 2001.

[10] M. L. Williams, "Perturbation theory for nuclear reactor analysis," in *CRC Handbook of Nuclear Reactors Calculations*, Y. Ronen, Ed., vol. 3, CRC Press, Boca Raton, Fla, USA, 1986.

[11] R. L. Childs, "Generalized perturbation theory using two-dimensional, discrete ordinates transport theory," Tech. Rep. ORNL/CSD/TM-127, Oak Ridge National Laboratory, Oak Ridge, Tenn, USA, 1980.

[12] I. Kodeli, "Manual for ANGELO2 and LAMBDA codes," NEA-1798/03 Package, 2010.

[13] I. Kodeli and E. Sartori, "Neutron cross-section covariance data in multigroup form and procedure for interpolation to users' group structures for uncertainty analysis applications," in *Proceedings of the PHYSOR International Conference on the Physics of Reactors: Operation, Design and Computation*, Marseille, France, 1990.

[14] I. Kodeli, M. Ishikawa, and G. Aliberti, "Evaluation of fission spectra uncertainty and their propagation," in *OECD/NEA WPEC Subgroup 26 Final Report: Uncertainty and Target Accuracy Assessment for Innovative Systems Using Recent Covariance Data Evaluations*, C. Appendix, Ed., OECD, Paris, France, 2008.

[15] "HELIOS Methods," Studsvik Scanpower, 2000.

[16] WIMS9A, "NEW FEATURES, A Guide to the New Features of WIMS Version 9A," Serco Assurance, http://www.sercoassurance.com/answers/, 2005.

[17] G. Marleau, A. Hébert, and R. Roy, "A User Guide For Dragon Version 4," IGE294, http://www.polymtl.ca/nucleaire/DRAGON/, 2009.

[18] W. Wieselquist, A. Vasiliev, and H. Ferroukhi, *Nuclear Data Uncertainty Propagation in a Lattice Physics Code Using Stochastic Sampling*, ANS Physics of Reactors (PHYSOR 2012): Advances of Reactor Physics, Knoxville, Tenn, USA, 2012.

[19] A. Bidaud, G. Marleau, and E. Noblat, "Nuclear data uncertainty analysis using the coupling of DRAGON with SUSD3D," in *Proceedings of the International Conference on Mathematics, Computational Methods & Reactor Physics (M&C '09)*, May 2009.

[20] C. R. Weisbin, J. H. Marable, J. L. Lucius et al., "Application of FORSS sensitivity and uncertainty methodology to fast reactor benchmark analysis," Tech. Rep. ORNL/TM-5563, 1976.

[21] "SCALE: a modular code system for performing standardized computer analyses for licensing evaluation," Tech. Rep. ORNL/TM-2005/39, Radiation Safety Information Computational Center at Oak Ridge National Laboratory as CCC-725, Oak Ridge, Tenn, USA, 2009, Version 6, Vols. I–III.

[22] J. Rhodes, *JEF 2.2 and ENDF/B-VI 70 Group Neutron Data Libraries*, Studsvik, Nykoping, Sweden, 2005.

[23] M. L. Williams, D. Wiarda, G. Arbanas, and B. L. Broadhead, "Scale nuclear data covariance library," in *SCALE: A Modular Code System for Performing Standardized Computer Analyses for Licencing Evaluation, Version 5*, ORNL/TM-2005/39, Oak Ridge National Library/U.S. Nuclear Regulatory Commission, Oak Ridge, Tenn, USA, 20052009.

[24] R. E. MacFarlane and D. W. Muir, "The NJOY Nuclear Data Processing System, Version 91," Manual LA-12740-M, Los Alamos National Laboratory, Los Alamos, NM, USA, 1994.

Series title and number
VTT Science 32

Title	**Numerical methods for nuclear fuel burnup calculations**
Author	Maria Pusa
Abstract	The material composition of nuclear fuel changes constantly due to nuclides transforming to other nuclides via neutron-induced transmutation reactions and spontaneous radioactive decay. The objective of burnup calculations is to simulate these changes over time. This thesis considers two essential topics of burnup calculations: the numerical solution of burnup equations based on computing the burnup matrix exponential, and the uncertainty analysis of neutron transport criticality equation based on perturbation theory. The burnup equations govern the changes in nuclide concentrations over time. They form a system of first order differential equations that can be formally solved by computing the matrix exponential of the burnup matrix. Due to the dramatic variation in the half-lives of different nuclides, the system is extremely stiff and the problem is complicated by vast variations in the time steps used in burnup calculations. In this thesis, the mathematical properties of burnup matrices are studied. It is deduced that their eigenvalues are generally confined to a region near the negative real axis. Rational approximations that are accurate near the negative real axis, and the Chebyshev rational approximation method (CRAM) in particular, are proposed as a novel method for solving the burnup equations. The results suggest that the proposed approach is capable of providing a robust and accurate solution to the burnup equations with a very short computation time. When a mathematical model contains uncertain parameters, this uncertainty is propagated to responses dependent on the model. This thesis studies the propagation of neutron interaction data uncertainty through the criticality equation on a fuel assembly level. The considered approach is based on perturbation theory, which allows computing the sensitivity profiles of a response with respect to any number of parameters in an efficient manner by solving an adjoint system in addition to the original forward problem. The uncertainty related to these parameters can then be propagated deterministically to the response by linearizing the response.
ISBN, ISSN	ISBN 978-951-38-7999-0 (Soft back ed.) ISBN 978-951-38-8000-2 (URL: http://www.vtt.fi/publications/index.jsp) ISSN-L 2242-119X ISSN 2242-119X (Print) ISSN 2242-1203 (Online)
Date	May 2013
Language	English
Pages	86 p. + app. 78 p.
Keywords	Burnup equations, Chebyshev rational approximation, CRAM, matrix exponential, sensitivity analysis, uncertainty analysis
Publisher	VTT Technical Research Centre of Finland P.O. Box 1000, FI-02044 VTT, Finland, Tel. +358 20 722 111

VTT Technical Research Centre of Finland is a globally networked multitechnological contract research organization. VTT provides high-end technology solutions, research and innovation services. We enhance our customers' competitiveness, thereby creating prerequisites for society's sustainable development, employment, and wellbeing.

Turnover: EUR 300 million
Personnel: 3,200

VTT publications

VTT employees publish their research results in Finnish and foreign scientific journals, trade periodicals and publication series, in books, in conference papers, in patents and in VTT's own publication series. The VTT publication series are VTT Visions, VTT Science, VTT Technology and VTT Research Highlights. About 100 high-quality scientific and professional publications are released in these series each year. All the publications are released in electronic format and most of them also in print.

VTT Visions

This series contains future visions and foresights on technological, societal and business topics that VTT considers important. It is aimed primarily at decision-makers and experts in companies and in public administration.

VTT Science

This series showcases VTT's scientific expertise and features doctoral dissertations and other peer-reviewed publications. It is aimed primarily at researchers and the scientific community.

VTT Technology

This series features the outcomes of public research projects, technology and market reviews, literature reviews, manuals and papers from conferences organised by VTT. It is aimed at professionals, developers and practical users.

VTT Research Highlights

This series presents summaries of recent research results, solutions and impacts in selected VTT research areas. Its target group consists of customers, decision-makers and collaborators.

Numerical methods for nuclear fuel burnup calculations

The material composition of nuclear fuel changes constantly due to nuclides transforming to other nuclides via neutron-induced transmutation reactions and spontaneous radioactive decay. The objective of burnup calculations is to simulate these changes over time. They are formulated around two basic equations in reactor physics: neutron transport criticality equation and burnup equations. This thesis considers the numerical solution of burnup equations based on computing the burnup matrix exponential, and the uncertainty analysis of neutron transport criticality equation based on perturbation theory.

In this thesis, the mathematical properties of burnup matrices are studied and the Chebyshev rational approximation method (CRAM) is proposed as a novel method for solving the burnup equations. The results suggest that the proposed approach is capable of providing a robust and accurate solution to the burnup equations with a very short computation time. Secondly, the propagation of neutron interaction data uncertainty through the criticality equation is studied on a fuel assembly level. The considered approach is deterministic and utilizes the adjoint system of the criticality equation, which allows propagating these uncertainties in an efficient manner.

ISBN 978-951-38-7999-0 (soft back ed.)
ISBN 978-951-38-8000-2 (URL: http://www.vtt.fi/publications/index.jsp)
ISSN-L 2242-119X
ISSN 2242-119X (Print)
ISSN 2242-1203 (Online)